TESE DE DOUTORAMENTO

COVALENT AND SUPRAMOLECULAR HELICAL POLYMERS: THE DAWN OF MATRYOSHKA MATERIALS

Zulema Fernández Villar

ESCUELA DE DOUTORAMENTO INTERNACIONAL

PROGRAMA DE DOUTORAMENTO EN CIENCIA E TECNOLOXÍA QUÍMICA

SANTIAGO DE COMPOSTELA

2020

USC
UNIVERSIDADE
DE SANTIAGO
DE COMPOSTELA

Abbreviations and Acronyms

°C	Celsius Degree
1,2-DCE	1,2-Dichloroethene
[α]	Standardized Specific Rotation
α	Optical Rotation
α_{obs}	Observed Optical Rotation
α_{agg}	Degree of Aggregation
Å	Angstrom
Aib	α-Aminoisobutiric Acid
AFM	Atomic Force Microscopy
ap	Antiperiplanar
BTA	Benzene-1,3,5-tricarboxamide
c	Concentration
c-c	*cis-cisoid*
c-t	*cis-transoid*
ca.	Latin expression "*circa*"; around
calcd	Calculated
CBT	Carbonyl-Bridged Triarylamine
CD	Circular Dichroism
cod	*cis*,*cis*-1,5-cyclooctadiene
CSP	Chiral Stationary Phase
CyD	Cyclodextrin
δ	Chemical Shift
d	Distance
DCM	Dicholomethane
DFT	Density Functional Theory
ΔH_{elo}	Elongation Enthalpy
ΔH_{np}	Nucleation Penalty
ΔH_{nuc}	Nucleation Enthalpy
DIPEA	*N*, *N*-Diisopropylethylamine
DMF	Dimethylformamide
DMSO	Dimethyl Sulfoxide
DNA	Deoxyribonucleic Acid
DSC	Differential Scanning Calorimetry
ΔS_{elo}	Elongation Entropy
ΔS_{nuc}	Nucleation Entropy
Δ^{Z}Bip	(Z)-β-(4,4'-biphenyl)- α,β-didehydropalanine
Δ^{Z}Phe	(Z)-α,β-didehydrophenylalanine

ε	Dielectric Constant
e.e.	Enantiomeric Excess
ECD	Electronic Circular Dichroism; a.k.a. CD
EDC	*N*-(3-dimethylaminopropyl)-*N*′-ethylcarbodiimide hydrochloride
e.g.	Latin expression "*exempli gratia*"; for example
equiv.	Equivalents
ESI	Electrospray Ionization
FT-IR ATR	Fourier Transform Infrared Spectroscopy Attenuated Total Reflectance; a.k.a. IR
FWHM	Full Width at Half-Maximum
g	Grams
GPC	Gel Performance Chromatography
HATU	2-(7-aza-1H-benzotriazole-1-yl)-1,1,3,3-tetramethyluronium
HBC	*peri*-hexabenzenecoronene
HOAT	1-Hydroxy-7-azabenzotriazole
HOPG	Highly Oriented Pyrolitic Graphite
HPLC	High-performance Liquid Chromatography
HPMC	Helical Polymer-Metal Complex
HRMS	High Resolution Mass Spectrometry
Θ	Tilting Degree
i.e.	Latin expression "*id est*"; it is
IR	Infrared Spectroscopy
it-PMMA	Isotactic Poly(methylmethacrylate)
K	Kelvin Degree
K_{elo}	Elongation Constant
K_{nuc}	Nucleation Constant
λ	Wavelength
l	Cell Length
LB	Langmuir-Blodget
L-CD	Left-handed Cicularly Polarized Light
LS	Langmuir-Schaefer
LSP	Living Supramolecular Polymerization
M	Molar
M	Minus; Counterclockwise Helix
M^+	Monovalent Metal Ion
M^{2+}	Divalent Metal Ion
m	Multiplet
MB	Mass-Balance
MCH	Methylcyclohexane

MeOH	Methanol
mg	Miligrams
MHz	Megahertz
mL	Mililiters
MM	Molecular Mechanics
μM	Micromolar
mM	Milimolar
mmol	Milimol
Mn	Number Average Molecular Weight
MOF	Metal-Organic Framework
MPA	α-Methoxyphenylacetic acid
m.r.u.	Monomeric Repeating Unit
MTPA	α-Methoxy-α-trifluoromethylphenylacetic acid
Mw	Weight Average Molecular Weight
Mz	Z Average
ν	Wavenumber
nbd	2,5-norbadiene
NMR	Nuclear Magnetic Resonance
nm	Nanometer
ODCB	*Ortho*-dichlorobenzene
OPE	Oligo(phenyleneethynylene)
OPV	Oligo(phenylenevinylene)
P	Plus; Clockwise Helix
PA	Poly(acetylene)
PBI	Perylenebisimide
PDI	Polydispersity
PLA	Poly(lactic)
PMMA	Poly(methylmethacrylate)
PPA	Poly(phenylacetylene)
ppm	Parts Per Million
POM	Polarized Optical Microscopy
POPEPA	Poly[oligo(phenyleneethynylene)phenylacetylene]
R	Gas Constant
R-CD	Right-handed Circularly Polarized Light
ROA	Raman Optical Activity
r.t.	Room Temperature
σ	Cooperativity Factor
s	Singlet

SC	Stereocomplex
SCF	Self-consistent Field
SEM	Scanning Electron Microscopy
SP	Supramolecular Polymer
sp	Synperiplanar
st-PMMA	Syndiotactic Poly(methylmethacrylate)
STM	Scanning Tunneling Microscopy
T	Temperature
t	Triplet
T_c	Conflict Temperature
T_e	Elongation Temperature Disassembly Process
T_e'	Elongation Temperature Assembly Process
t-c	*trans-cisoid*
t-t	*trans-transoid*
TBAF	Tetrabutylammonium Fluoride
TD-DFT	Time-Dependent Density Functional Theory
TEM	Transmission Electronic Microscopy
TGA	Thermogravimetric Analysis
THF	Tetrahydrofuran
TMS	Tetramethylsilyl
Tol	Toluene
TrMA	Triphenylmethyl Metacrylate
UV-Vis	Ultraviolet-Visible
VCD	Vibrational Circular Dichroism
VT-CD	Variable Temperature-Circular Dichroism
VT-UV-Vis	Variable Temperature-Ultraviolet-Visible
ω	Dihedral Angle
ZINDO/S	ZenerQs Intermediate Neglect of Differential Ovelap
ZnP	Zinc Porphyrin

Contents

Introduction

USC
UNIVERSIDADE
DE SANTIAGO
DE COMPOSTELA

Introduction

Helices are inherently chiral, thus right- and left-handed scaffolds cannot be overlapped. This structural motif is one of the most repeated in nature and plays a crucial role. The helical structure adopted by biological polymers that assemble into macromolecules in living organisms (coiled-coil helix bundle proteins, DNA superhelices or protein-DNA hybrid superstructures), is responsible for vital functions such as genetic information storage, replication, ion transport, recognition processes or asymmetric chemical transformations among others.[1] The discovery of the α-helix of proteins[2] and the structure proposed for the DNA double helix[3] (Figure 1) in the early 50's produced a milestone in molecular biology. It is important to mention that the helicity of these biomolecules is imposed by the homochiral nature of the constitutive *L*-aminoacids (proteins) or *D*-carbohydrates (DNA).[4]

Inspired by these findings, scientists have made a great effort to mimic the structures of the biological helices. However, during the last decades this endeavour was focused on developing new synthetic helical systems, which show unique properties and functionalities not observed in natural systems.[5]

At the same time of these biological findings, in 1955, Nata described the first synthetic helical structure, an isotactic poly(propylene) (poly-**1**, Figure 1).[6] In the solid state this polymer presented equal populations of right-handed and left-handed helices but, once the polymer was dissolved, this helical structure disappeared and became random. In the 1960's Pino *et al.* revealed the helical conformation of isotactic poly(vinyl) polymers (poly-**2**, Figure 1) for the first time.[7] The introduction of a chiral centre in the monomeric unit promoted the adoption of a preferred helical sense on the polymer, which was determined by optical rotation.

The major breakthrough was produced in the 70's, when many research groups started to work in the helical polymer area. In 1974 Nolte and Drenth resolved the structure of poly(tert-butyl isocyanide) (poly-**3**, Figure 1) by using chiral chromatography, observing right-handed and left-handed helices —*P* (plus) and *M* (minus) helices—.[8] Later, in 1979, Okamoto

1 (a) Alberts, B.; Johnson, A.; Lewis, J.; Morgan, D.; Raff, M.; Roberts, K.; Walter, P. *Molecular Biology of the Cell*, 6th ed.; Garland Science: New York, 2014. (b) Saenger, W. *Principles of Nucleic Acid Structure*, 1st ed.; Springer-Verlag: New York, 1984, p 556. (c) Schulz, G. E., Schrimer, R. H. *Principles of Protein Structure*, 1st ed.; Springer-Verlag: New York, 1979.

2 Pauling, L.; Corey, R. B.; Branson, H. R. *Proc. Natl. Acad. Sci. U.S.A.* **1951**, *37*, 205-211.

3 Watson, J. D.; Crick, F. H. C. *Nature* **1953**, *171*, 737-738.

4 Dorca, Y.; Greciano, E. E.; Valera, J. S.; Gómez, R.; Sánchez, L, *Chem. Eur. J.* **2019**, *25*, 5848-5864.

5 (a) Yashima, E.; Ousaka, N.; Taura, D.; Shimomura, K.; Ikai, K.; Maeda, K. *Chem. Rev.* **2016**, *116*, 13752-13990. (b) Schwartz, E.; Koepf, M.; Kitto, H. J.; Nolte, R. J. M.; Rowan, E. *Polym. Chem.* **2011**, *2*, 33-47. (c) Guichard, G.; Huc, I. *Chem. Commun.* **2011**, *47*, 5933-5941. (d) Yashima, E.; Maeda, K.; Iida, H.; Furusho, Y.; Nagai, K. *Chem. Rev.* **2009**, *109*, 6102-6211. (e) Liu, J.; Lam, J. W. Y.; Tang, B. Z. *Chem. Rev.* **2009**, *109*, 5799-5867. (f) Rosen, B. M.; Wilson, C. J.; Wilson, D. A.; Peterca, M.; Imam, M. R.; Percec, V. *Chem. Rev.* **2009**, *109*, 6275-6540. (g) Yashima, E.; Maeda,K.; Furusho, Y.; *Acc. Chem. Res.* **2008**, *41*, 1166-1180. (h) Yashima, E.; Maeda, K. *Macromolecules* **2008**, *41*, 3-12. (i) Rudick, J. G.; Percec, V. *Acc. Chem. Res.* **2008**, *41*, 1641-1652. (j) Horne, W. S.; Gellman, S. H. *Acc. Chem. Res.* **2008**, *41*, 1399-1408. (k) Maeda, K.; Yashima, E. *Top. Curr. Chem.* **2006**, *265*, 47-88. (l) Nakano, T.; Okamoto, Y. *Chem. Rev.* **2001**, *101*, 4013-4038. (m) Cornelissen, J. J. L. M.; Rowan, A. E.; Nolte, R. J. M.; Sommerdijk, N. A. J. M. *Chem. Rev.* **2001**, *101*, 4039-4070. (n) Green, M. M.; Jha, S. K. *Chirality* **1997**, *9*, 424-427. (o) Okamoto, Y.; Nakano, T. *Chem. Rev.* **1994**, *94*, 349-372.

6 Natta, G.; Pino, P.; Corradini, P.; Danusso, F.; Mantica, E.; Mazzanti, G.; Moraglio, G. *J. Am. Chem. Soc.* **1955**, *77*, 1708-1710.

7 Pino, P.; Lorenzi, G. P. *J. Am. Chem. Soc.* **1960**, *82*, 4745-4747.

8 Nolte, R. J. M.; Van Beijnen, A. J. M.; Drenth, W. *J. Am. Chem. Soc.* **1974**, *96*, 5932-5933.

and co-workers reported for the fist time the helix sense selective polymerization.[9] This new method, based on the polymerization of an achiral monomer by a chiral catalyst, produced an optically active polymer with a large specific rotation, poly-**4** —derived from the triphenylmethyl metacrylate (TrMA)—, which showed relevant chiral recognition ability for racemic compounds, as well as the ability to keep its helical structure in solution. These features made this polymer a good candidate as chiral stationary phase (CSP) for chiral high performance liquid chromatography (HPLC), one of the most useful applications of materials science nowadays.

Some years after, in 1988, Green discovered a new family of polymers, the poly(isocyanate)s (poly-**5**, Figure 1).[10] These new materials showed a structure composed of right- and left-handed conformations, connected by helical reversals, which could be modified by external stimuli through covalent or non-covalent interactions. This discovery triggered the study of a new family of polymers, the "dynamic helical polymers".

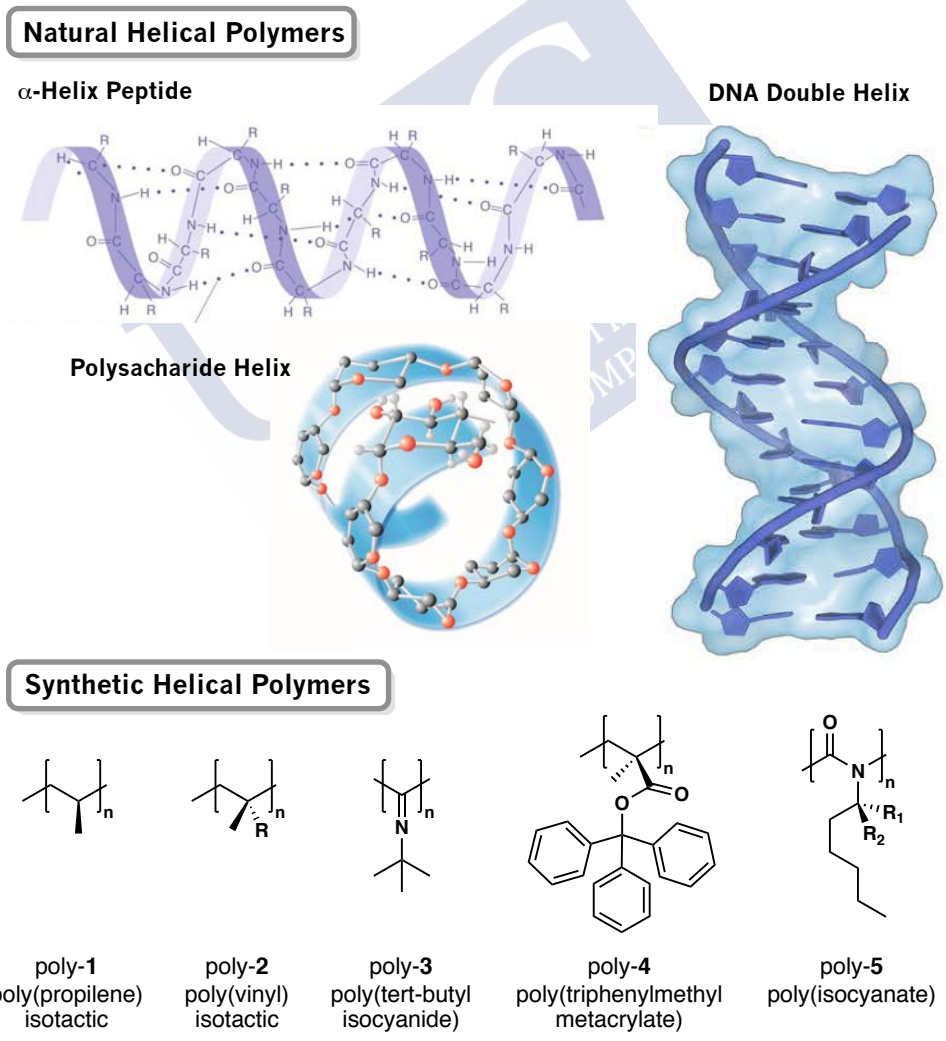

Figure 1. Natural helical polymers and some examples of synthetic helical polymers.

[9] Okamoto, Y.; Suzuki, K.; Ohta, K.; Hatada, K.; Yuki, H. *J. Am. Chem. Soc.* **1979**, *101*, 4763-4765.
[10] Green, M. M.; Andreola, C.; Munoz, B.; Reidy, M. P.; Zero, K. *J. Am. Chem. Soc.* **1988**, *110*, 4063-4065.

1. Classification of the Helical Polymers

The helical polymers can be classified into two main groups, according to the interconversion energy barrier between *P* and *M* helices.

If a polymer presents a high helix inversion barrier, the polymer is formed under kinetic conditions and the incorporation of the monomeric unit is locked once is added to the growing polymer chain.[5d,m] This means that the conformation adopted by the monomer during the polymerization process cannot be modified afterwards. These polymers, usually bearing bulky substituents, are known as the static helical polymers.

On the contrary, the dynamic helical polymers present a low interconversion energy barrier. Hence the helical structure can be tuned from *P* to *M*, or viceversa, by external stimuli.

1.1. Static Helical Polymers

Optically active static helical polymers can be obtained via polymerization of optically bulky monomers or by using a chiral initiator or catalyst to polymerize an achiral or prochiral monomer (helix sense selective polymerization method).[5o] The structural parameters of this family of polymers (helical sense and helical pitch) are determined by the chiral substituents covalently bonded to the polymer backbone or by the chiral initiators or catalysts. The resulting helical conformations cannot be modified and are stable even in solution, due to the steric repulsion between the bulky substituents contained in the polymer chain.

Some examples are: poly(methacrylate)s (poly-**6**), poly(methacrylamide)s (poly-**7**),[11] poly(quinoxaline-2,3-dyl)s (poly-**8**) or poly(guanidine)s (poly-**9**)[5d,l] (Figure 2).

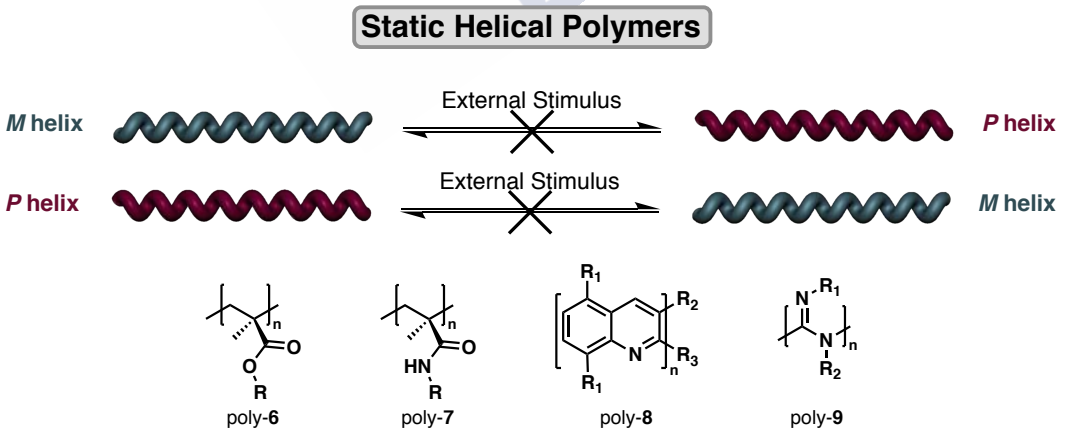

Figure 2. Conceptual representation and some representative scaffolds of the static helical polymers.

[5] (d) Yashima, E.; Maeda, K.; Iida, H.; Furusho, Y.; Nagai, K. *Chem. Rev.* **2009**, *109*, 6102-6211. (l) Nakano, T.; Okamoto, Y. *Chem. Rev.* **2001**, *101*, 4013-4038. (m) Cornelissen, J. J. L. M.; Rowan, A. E.; Nolte, R. J. M.; Sommerdijk, N. A. J. M. *Chem. Rev.* **2001**, *101*, 4039-4070. (o) Okamoto, Y.; Nakano, T. *Chem. Rev.* **1994**, *94*, 349-372.

[11] Hoshikawa, N., Hotta, Y., Okamoto, Y. *J. Am. Chem. Soc.* **2003**, *125*, 12380-12381.

1.2. Dynamic Helical Polymers

Dynamic helical polymers are characterized by a low energy barrier of interconversion. Therefore, the two helical orientations, *P* and *M*, can coexist in equilibrium within the polymer chain but separated by helix reversals. This equilibrium can be easily tuned by the addition of external stimuli, resulting into one-handed helical sense excess.

These polymers can be obtained by polymerizing an optically active monomer[12] or by polymerization of an achiral monomer in presence of a chiral solvent or additive, resulting in a polymer with a predominant helical sense —the equilibrium will be shifted to the conformation that accommodates the best the chiral inducer complexed with the polymer—.

Some examples are: poly(isocyanate)s (poly-**10**),[5d] poly(isocyanide)s (poly-**11**),[5b] poly(silane)s (poly-**12**)[13] or poly(acetylene)s (poly-**13**)[14] (Figure 3).

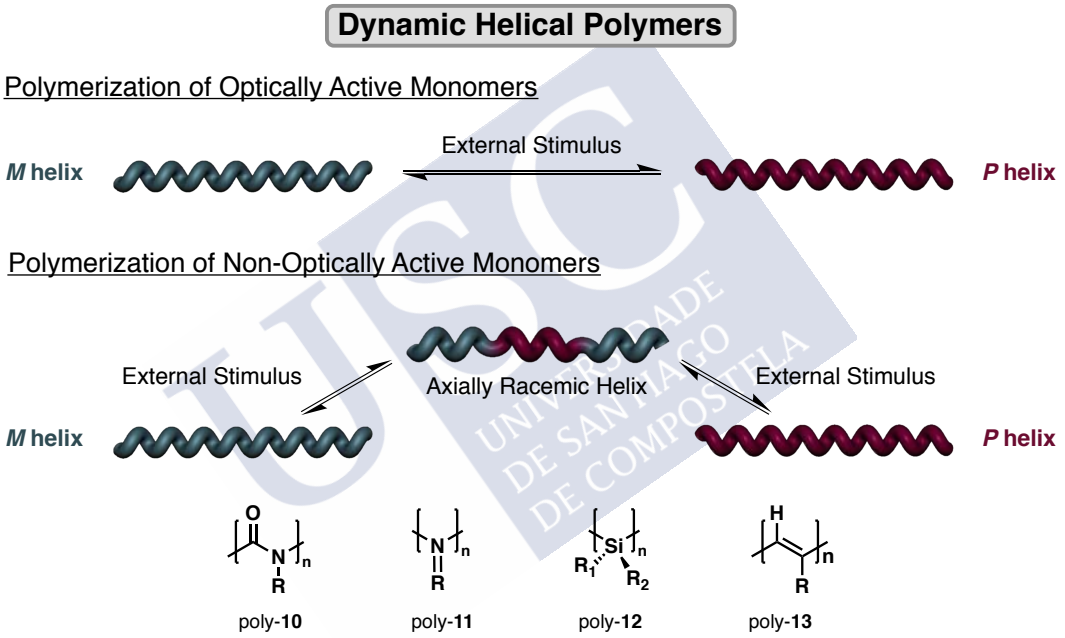

Figure 3. Conceptual representation and some representative scaffolds of the dynamic helical polymers.

1.3. Foldamers

Foldamers are oligomers that in solution fold into a specific conformation. This conformation is stabilized by non-covalent interactions between nonadjacent monomeric units and is always found in equilibrium with the unfolded state (random coil).[15] Attending to the monomeric units that constitute the oligomers, this family can be classified into π-conjugated aromatic foldamers —e.g., oligo(*meta*-phenyleneethynylene)s (poly-**14**) [16] or

[12] Louzao, I.; Seco, J. M.; Quiñoá, E. Riguera, R. *Angew. Chem. Int. Ed.* **2010**, *49*, 1430-1433.
[5] (b) Schwartz, E.; Koepf, M.; Kitto, H. J.; Nolte, R. J. M.; Rowan, E. *Polym. Chem.* **2011**, *2*, 33-47. (d) Yashima, E.; Maeda, K.; Iida, H.; Furusho, Y.; Nagai, K. *Chem. Rev.* **2009**, *109*, 6102-6211.
[13] (a) Fujiki, M. *J. Organomet. Chem.* **2003**, *685*, 15-34. (b) Fujiki, M. *Macromol. Rapid Commun.* **2001**, *22*, 539-563.
[14] Liu, J.; Tang, B. Z. *Acc. Chem. Res.* **2005**, *38*, 745-754.
[15] Hill, D. J.; Mio, M. J.; Prince, R.B.; Hughes, T.S.; Moore, J.S. *Chem. Rev.* **2001**, *101*, 3893-4012.
[16] Appella, D. H.; Christianson, L. A.; Karle, I. L.; Powell, D. R.; Gellman, S. H. *J. Am. Chem. Soc.* **1996**, *118*, 13071-13072.

oligo(pyridinedicarboxyamide)s (poly-**15**)[17]— and into the non-heterocyclic and heterocyclic aromatic oligoamides —oligo(β-aminoacid)s (poly-**16**)— (Figure 4).

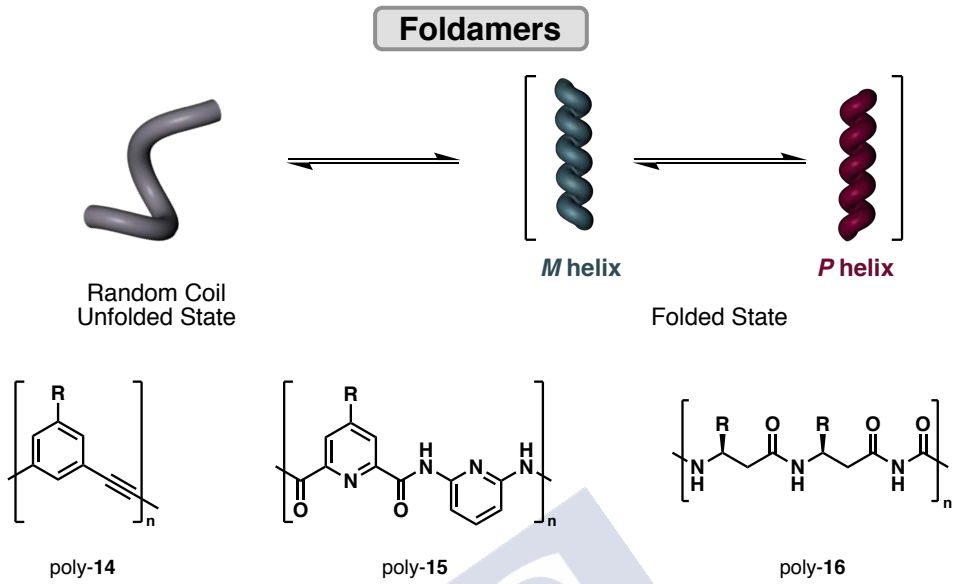

Figure 4. Some examples of foldamers.

2. Poly(acetylene)s and Poly(phenylacetylene)s

The poly(acetylene) (PA) family is one of the most studied in dynamic helical polymers. The interest for these polymers, characterized by a π-conjugated backbone, started in the mid 70's and, on 2000, Heeger, MacDiarmid and Shirakawa won the Nobel Prize in Chemistry for their pioneering work on using these polymers as conductive materials. Moreover these materials present other unique optical and chiroptical properties, which make them suitable for applications such as Chiral Stationary Phases (CSPs) for HPLC, sensors or asymmetric catalysts. PAs are highly stable in solid state, as well as in solution, and can be obtained by the polymerization of optically active phenylacetylenes (m-**17**), propiolic esters (m-**18**), propargyl esters (m-**19**), propargylamides (m-**20**) or aliphatic acetylenes (m-**21**)[5d] (Figure 5a). Among them, poly(phenylacetylene)s (PPAs), derived from m-**17**, are the most studied ones due to their easy synthesis, high stereoregularity and high molecular weight.[5a] During the polymerization process the conjugated double bonds can adopt four possible configurations —*cis*-*cisoid* (*c*-*c*), *cis*-*transoid* (*c*-*t*), *trans*-*cisoid* (*t*-*c*) or *trans*-*transoid* (*t*-*t*)— (Figure 5b), but only the *cis*- configurations will promote the folding into the helical structure; otherwise, if the polymer adopts the *trans*- configuration the helical scaffold cannot be formed. Nowadays, many studies have been carried out for the preparation of PPA-type materials due to their promising high-tech applications as optical polarizing films, asymmetric electrodes, anisotropic molecular devices, chiral sensors...[5e]

[5] (a) Yashima, E.; Ousaka, N.; Taura, D.; Shimomura, K.; Ikai, K.; Maeda, K. *Chem. Rev.* **2016**, *116*, 13752-13990. (d) Yashima, E.; Maeda, K.; Iida, H.; Furusho, Y.; Nagai, K. *Chem. Rev.* **2009**, *109*, 6102-6211.

[17] Zhan, C., Léger, J., Huc, I. *Angew. Chem. Int. Ed.* **2006**, *45*, 4625-4628.

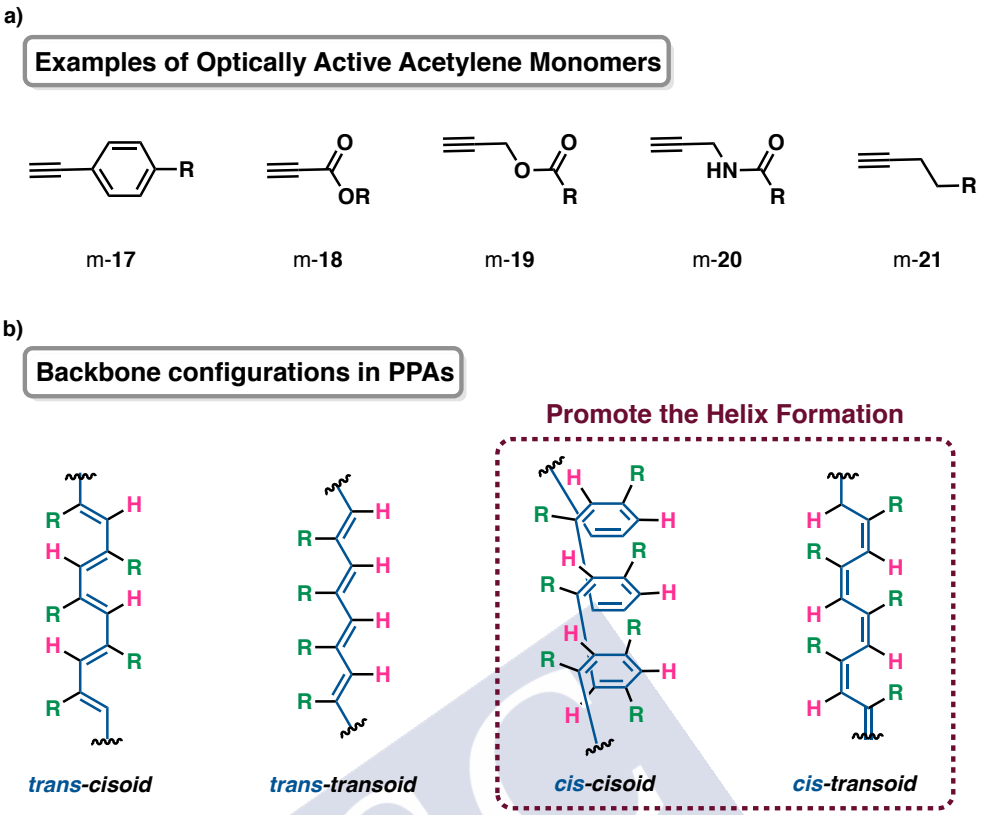

Figure 5. (a) Representative examples of the PA family. (b) Possible configurations that the polyene backbone of the PPAs can adopt.

Noyori and co-workers[18] developed some rhodium based catalysts —$[Rh(nbd)Cl]_2$ (nbd: 2,5-norbornadiene), $[Rh(cod)Cl]_2$ (cod: *cis*,*cis*-1,5-cyclooctadiene) or $[Rh(cod)BF_4]_2$ (BF_4: tetrafluoroborate)— that through a stereospecific living polymerization generate polymers in high yield, with low polydispersity and high *cis*- content of double bonds in the polyene skeleton. The polymerization process consists of a head-to-tail stereospecific and regioselective 2,1-insertion mechanism. This mechanism is produced by the steric repulsion between monomeric units, leading to a highly stereoregular polymer chain (Figure 6). Moreover, all Rh (I) based catalysts are tolerant to polar functional groups and solvents (organic solvents as well as water), what makes them highly versatile catalysts.[19]

[5] (e) Liu, J.; Lam, J. W. Y.; Tang, B. Z. *Chem. Rev.* **2009**, *109*, 5799-5867.

[18] (a) Hirao, K.; Ishii, Y.; Terao, T.; Kishimoto, Y.; Miyatake, T.; Ikariya, T.; Noyori, R. *Macromolecules* **1998**, *31*, 3405-3408. (b) Kishimoto, Y.; Eckerle, P.; Miyatake, T.; Ikariya, T.; Noyori, R. *J. Am. Chem. Soc.* **1994**, *116*, 12131-12132.

[19] (a) Tan, N. S. L.; Lowe, A. B. *Angew. Chem. Int. Ed.* **2020**, *59*, 2-16. (b) Ke, Z.; Abe, S.; Ueno, T.; Morokuma, K. *J. Am. Chem. Soc.* **2011**, *133*, 7926-7941.

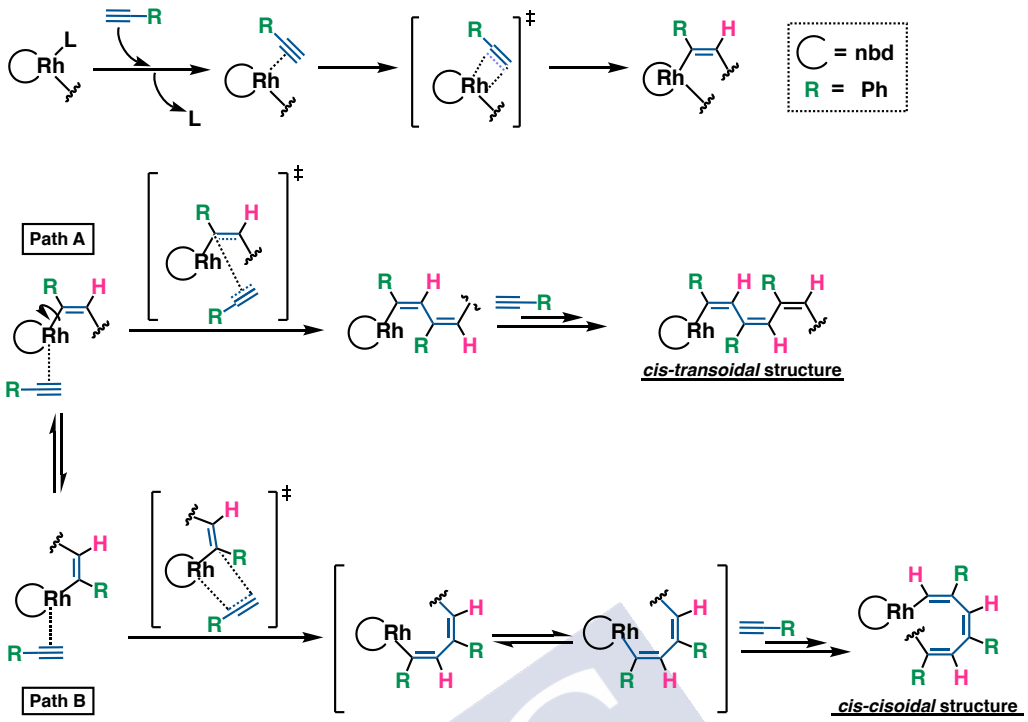

Figure 6. Proposed polymerization mechanism of the PPAs catalysed by Rh (I).

3. Poly(phenylacetylene)s' stability

Some years ago, due to the potential applications of the PPAs in different fields, the necessity of knowing their stability and degradation emerged for *cis*-*cisoidal* and *cis*-*transoidal* scaffolds.[20]

Masuda *et al.* systematically studied some *c*-*t* PPAs, observing that they undergo an autooxidative degradation into oligomers, which was observed to be faster in chloroform and toluene.[21] Percec and co-workers obtained similar results, confirming also the degradation in the solid state by observation of a decrease in both, the *cis*- content of double bonds as well as in the molecular weight.[22] However, this process could be slowed down in vacuum or under inert atmosphere, or speeded up by heating —corroborated by ^{1}H NMR experiments—, which indicates that PPAs are thermosensitive. The degradation mechanism of PPAs consists of an intramolecular electrocyclization followed by a cleavage from the polyenic chain, obtaining a 1,3,5-trisubstituted benzene ring (Figure 7a).

More recently Tabata's group has described another isomerization process through a radical mechanism, as confirmed by electron spin resonance measurements. The

[20] (a) Liu, I.; Namikoshi, T.; Zang, Y.; Aoki, T.; Hadano, S.; Abe, Y.; Wasuzu, I.; Tsutsuba, T.; Teraguchi, M.; Kaneko, T. *J. Am. Chem. Soc.* **2013**, *135*, 602-605. (c) Matsunami, S.; Watanabe, T.; Kamimura, H.; Kakuchi, T.; Ishii, F.; Tsuda, K. *Polymer* **1996**, *37*, 4853-4855.

[21] (a) Deng, J.; Tabei, J.; Shiotsuki, M.; Sandra, F.; Masuda, T. *Polymer* **2004**, *45*, 7395-7400. (b) Abdul Kaim, S. M.; Nomura, R.; Masuda, T. *J. Polym . Sci., Part A: Polym. Chem.* **2001**, *39*, 3130-3136.

[22] (a) Percec, V.; Rudick, J. G. *Macromolecules* **2005**, *38*, 7241-7250. (b) Percec, V.; Rudick, J.; Nomber, P.; Buchowicz, W. J. *Polym. Sci., Part A: Polym. Chem.* **2002**, *40*, 3212-3220. (c) Simonescu, C. I.; Percec, V.; *Polym. Sci., Part A: Polym. Chem.* **1980**, *18*, 147-155.

isomerization from *cis*- to *trans*- can happen during the synthesis or by external factors (application of pressure or electric fields or by heating)[23] (Figure 7b).

The degradation of the PPA scaffold (poly-**22**) can also occur by irradiation with light. Liu *et al.* demonstrated that the photocyclization is possible in the solid state, yielding a 1,3,5-trisubstituted benzene ring derivative (cyclotrimer).[24] Interestingly, it was observed that this reaction only takes place when the polyene backbone displays a *cis-cisoidal* geometry, resulting in a cyclic trimer self-supported membrane (Figure 7c).

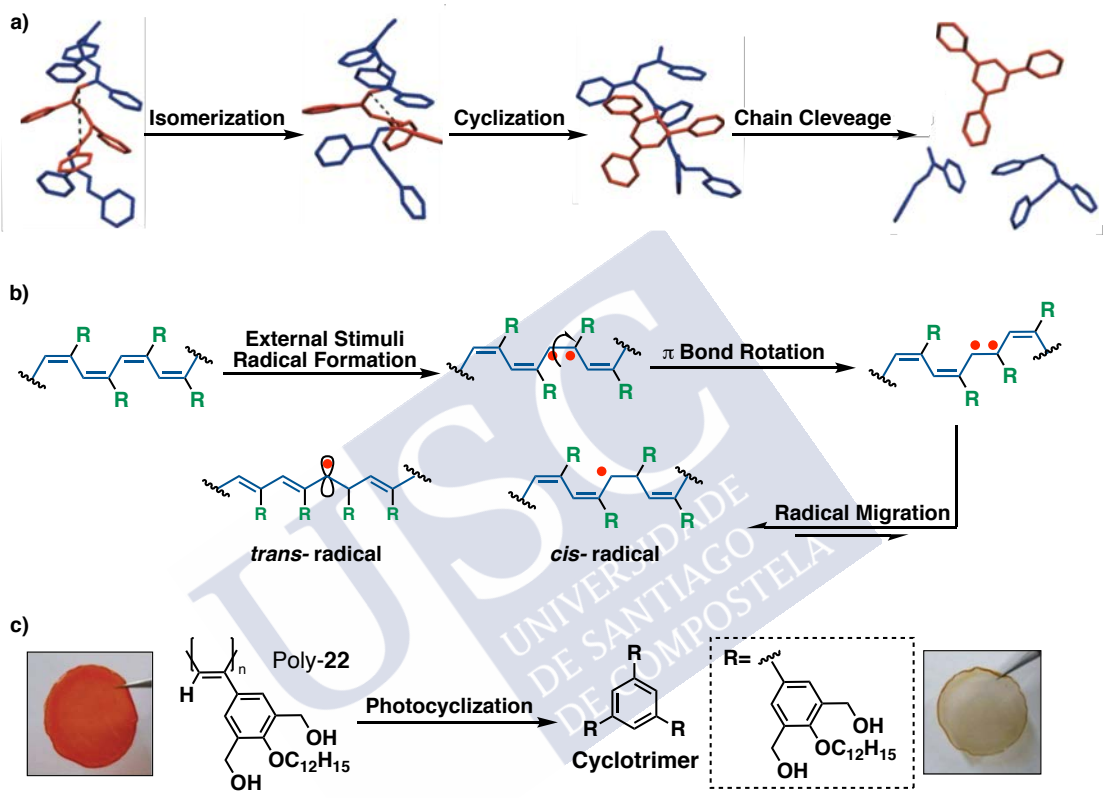

Figure 7. (a) Degradation mechanism by intramolecular electrocyclization. (b) Radical-initiated degradation mechanism. (c) Degradation by photocyclization on the solid state.

4. Structural Elucidation of a Polymeric Helix: the Poly(phenylacetylene) Case

In order to design and develop novel materials the structural knowledge of its secondary structure plays a key role for further applications. A detailed structure determination is essential to understand the helix formation mechanism as well as the helical structure-function relationship. This is a challenging task that can only be overcome by the combination of different techniques.

[23] (a) Huang, K.; Mawatari, Y.; Miyasaka, A.; Sadahiro, Y.; Tabata, M.; Kashiwaya, Y. *Polymer* **2007**, *48*, 6366-6373. (b) Miyasaka, A.; Mawatari, Y.; Sone, T.; Tabata, M. *Polym. Degrad. Stab.* **2007**, *92*, 253-259. (c) Tabata, M.; Tanaka, Y.; Sadahiro, Y.; Sone, T.; Yokota, K.; Miura, I. *Macromolecules* **1997**, *30*, 5200-5204.

[24] (a) Liu, I.; Namikoshi, T.; Zang, Y.; Aoki, T.; Hadano, S.; Abe, Y.; Wasuzu, I.; Tsutsuba, T.; Teraguchi, M.; Kaneko, T. *J. Am. Chem. Soc.* **2013**, *135*, 602. (b) Miyata, M.; Namikoshi, T.; Liu, L.; Zang, Y.; Aoki, T.; Abe, Y.; Yoshiyuki, O.; Tsutsuba, T.; Teraguchi, M.; Kaneko, T. *Polymer* **2013**, *54*, 4431-4435.

4.1. Architecture of the Poly(phenylacetylene)s

It is important to point out that PPAs are composed of two coaxial helices (an internal and an external one) (Figure 8). This structural feature is intrinsic to all PPAs, but is not always discussed.[25,26] Most of the papers found in literature deal with changes on the internal helix, which can be easily followed by ECD, but no information related to the external helix is provided.

The internal helix is the one described by the polymer backbone and is characterized by its flexibility, due to the lack of supramolecular interactions within the polyene skeleton —it is formed by conjugated double bonds—. Hence, the adoption of a preferred helical sense will depend on the conformational composition of the pendant groups and the interactions established among them. This spatial disposition will dictate the dihedral angle between the conjugated double bonds (ω_1) —negative values of ω_1 form an *M* helix, while positive values form a *P* helix— and, consequently, it will determine the presence of a *c*-*c* or *c*-*t* structure. The helical sense and/or elongation of the internal helix can be easily monitored by CD spectroscopy.

The external helix is described by the pendant groups and is generated by the array that they describe around the inner helix. The helical sense of this helix can only be determined by AFM measurements, as well as the structural parameters (helical pitch and packing angle).

It should be noticed that the inner helix and the outer helix can rotate in the same or in opposite helical sense, depending on the scaffold adopted by the polymer.[27] If $\omega_1 < 90°$, the polymer presents a *c*-*c* scaffold with three residues per turn (3/1 helix, compressed structure), where the inner and outer helices rotate in the same direction —i.e., $\omega_1 = -78°$, *M* internal helix (negative CD) and *M* external helix (observed by AFM)—. On the other hand, if $\omega_1 > 90°$, the polymer presents a *c*-*t* scaffold with two residues per turn (2/1 helix, stretched structure), where the inner and outer helices rotate in opposite directions —i.e., $\omega_1 = -140°$, *M* internal helix (negative CD) and *P* external helix (observed by AFM)— (Figure 8).

This clearly demonstrates that the final secondary structure cannot be elucidated only by one technique but by the combination of different ones.

[25] Fernández, B.; Rodríguez, R.; Quiñoá, E.; Riguera, R.; Freire, F. *ACS Omega* **2019**, *4*, 5233-5240.
[26] Fernández, B.; Rodríguez, R.; Rizzo, A.; Quiñoá, E.; Riguera, R.; Freire, F. *Angew. Chem. Int. Ed.* **2018**, *57*, 3666-3670.
[27] Leiras, S.; Freire, F.; Seco, J. M.; Quiñoá, E.; Riguera, R. *Chem. Sci.* **2013**, *4*, 2735-2743.

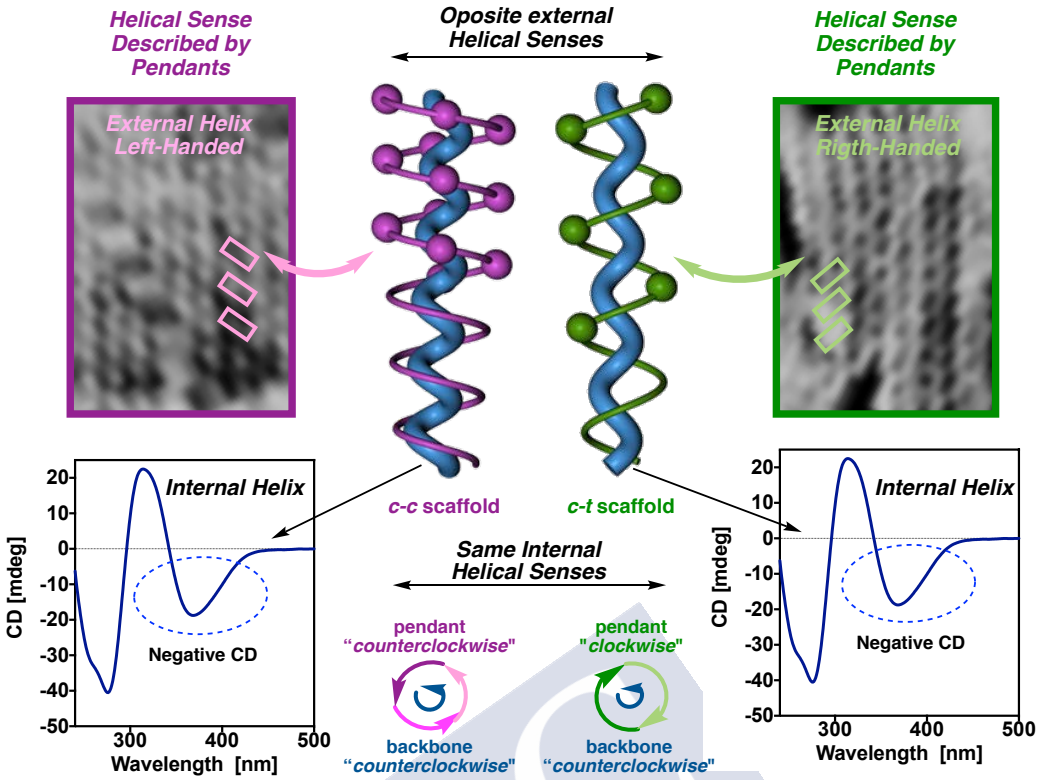

Figure 8. Schematic illustration of two possible scaffolds that a PPA helix can adopt.

4.2. Determination of the Polyene Backbone Configuration

The polyene backbone in PPAs (inner helix) can adopt four possible configurations after polymerization —*cis*-*cisoid*, *cis*-*transoid*, *trans*-*cisoid* or *trans*-*transoid*—. Among these different configurations, only the *cis*- scaffolds will promote the formation of the helix.

Theoretical and experimental ^{1}H NMR studies performed by Percec and co-workers revealed that the vinyl proton resonates differently, depending on the conformation adopted by the polyene backbone. For *trans*- polyenes the chemical shift of the vinyl proton varies between 6.20-7.20 ppm. Moreover, the *trans*-*cisoid* scaffold can be distinguished from the *trans*-*transoid* one by carefully looking at the ^{1}H NMR spectra. For the former the aromatic protons resonate altogether whereas, for the last one, two aromatic protons are shifted upfield. On the other hand, *cis*- polyenes resonate around 5.60-5.80 ppm. As for the *trans*-polyenes, the *cis*- polyenes can be identified by the shift of the aromatic protons. For *cis*-*cisoid* scaffolds one aromatic proton is shifted upfield while, for *cis*-*transoid* scaffolds, two aromatic protons are displaced. Also, for *cis*- scaffolds, the chemical shift of the vinyl proton will depend on the aromatic substitution pattern: 5.80 ppm for the *para*- substituted (*cis*-*cisoid*), 6.85 ppm for the *meta*- substituted (*cis*-*transoid*) and 6.70 ppm for the *ortho*- substituted (*cis*-*transoid*) polymers. Taking this information into account it is possible to quantify the *cis*-content of double bonds in PPAs (Equation 1).

$$\%_{cis} = [A_{cis}/(A_{total} \cdot H_{total})] \cdot 100$$

Equation 1. Mathematical statement to calculate the *cis*- content of double bonds in PPAs.

A_{cis} stands for the peak area of the vinyl proton (5.6-5.8 ppm), A_{total} is the total area of the ^{1}H NMR spectrum and H_{total} is the number of the protons within the pendant.

Another useful technique to elucidate the conformation of the polyene backbone is the Differential Scanning Calorimetry (DSC), which presents characteristic thermograms for *c*-*c* and *c*-*t* backbones. On the one hand, PPAs with a *c*-*c* scaffold show solely an exothermic peak (around 200 °C-240 °C), related to the isomerization from *c*-*c* to *c*-*t* (Figure 9b). On the contrary, *c*-*t* scaffolds display a thermogram with two exothermic peaks, arisen from the isomerization processes, from *c*-*t* to *c*-*c* (ca. 140 °C) and from *c*-*c* to *t*-*t* (ca. 240 °C) (Figure 9c).

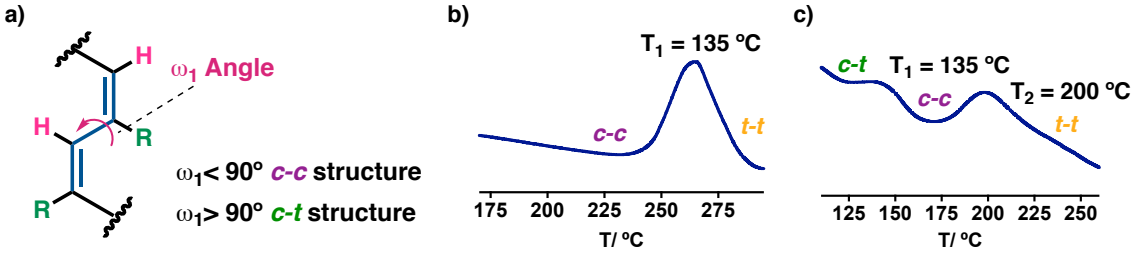

Figure 9. (a) Influence of the ω_1 angle on the final scaffold adopted by the inner helix. Representative DSC thermograms for (b) *c*-*c* and (c) *c*-*t* scaffolds.

Additionally, a different technique used to elucidate the configuration of the double bonds is the Raman spectroscopy. The polyene skeleton is active in Raman spectroscopy, where three different bands are characteristic for this family of compounds. Therefore, in polymers with *cis*- configuration, these bands are C=C_{cis} (ca. 1530 cm^{-1}), C-C_{cis} (ca. 1335 cm^{-1}) and C-H_{cis} (ca. 956 cm^{-1}), while for the *trans*- configuration the characteristic bands are C=C_{trans} (*ca.* 1475 cm^{-1}) and C-C_{trans} (ca. 1200 cm^{-1}).[24,28] Also, by FT-IR is possible to detect the deformation bands for C-H_{cis} (ca. 740 cm^{-1}) and C-H_{trans} (ca. 1015 cm^{-1}).[29]

Among the aforementioned structural techniques, there are other procedures involving the reactivity of the polyene backbone to elucidate the configuration of the double bonds. For instance, the isomerization by light irradiation on the solid state is used to differentiate between *c*-*c* and *c*-*t* scaffolds. As previously explained, the photocyclization is only possible for *c*-*c* scaffolds, obtaining a 1,3,5-trisubstituted benzene ring derivative and leaving the *c*-*t* scaffolds unreacted after irradiation (Figure 7c).[24]

UV-Vis spectroscopy is another useful technique that provides information about the elongation but not of the conformation of the helical scaffold. Comparison between different

[28] (a) Palomo, L; Rodríguez, R.; Medina, S.; Quiñoá, E.; Casado, J.; Freire, F.; Ramírez, F. J. *Angew. Chem. Int. Ed.* **2020**, *59*, 9080-9087. (b) Misayaka, A.; Sone, T.; Mawatari, Y.; Setauesh, S.; Müllen, K.; Tabata, M. *Macromole. Chem. Phys.* **2006**, *207*, 1938-1944.

[29] (a) Ito, T.; Shirakawa, H.; Ikeda, S. *J. Polym. Sci., Part A: Polym. Chem.* **1974**, *12*, 11-20. (b) Shirakawa, H.; Ikeda, S. *Polym. J.* **1971**, *2*, 231-244.

[24] (a) Liu, I.; Namikoshi, T.; Zang, Y.; Aoki, T.; Hadano, S.; Abe, Y.; Wasuzu, I.; Tsutsuba, T.; Teraguchi, M.; Kaneko, T. *J. Am. Chem. Soc.* **2013**, *135*, 602. (b) Miyata, M.; Namikoshi, T.; Liu, L.; Zang, Y.; Aoki, T.; Abe, Y.; Yoshiyuki, O.; Tsutsuba, T.; Teraguchi, M.; Kaneko, T. *Polymer* **2013**, *54*, 4431-4435.

UV spectra gives information about which scaffold is compressed/stretched the most due to hypsochromic/batochromic shifts of the polyene backbone.[30]

4.3. Determination of the Helical Sense of the Polymer

The most common techniques to evidence the formation of a helix with an excess of helical handedness are specific rotation and Circular Dichroism (CD).

4.3.1. Specific Rotation

The optical rotation (α) measures the deviation of a polarized beam when interacting with a chiral solution —difference in velocity between left-handed circularly polarized light (*L*-CD) and right-handed circularly polarized light (*R*-CD)—. This technique is dependent on the solvent used, the temperature, the concentration and the cell length. By applying equation 2, the optical rotation can be transformed into the standardized specific rotation [α]. T indicates the temperature at which the measurement is perform, while λ indicates the wavelength; α_{obs} stands for the observed optical rotation (degrees) that the apparatus provides, c is de concentration (g·mL^{-1}) and l is the cell length (dm).

$$[\alpha]_{\lambda}^{T} = \frac{\alpha_{obs}}{c \cdot l}$$

Equation 2. Equation for the calculation of the specific rotation.

The main drawbacks for this technique are the low sensitivity and the large amount of sample required for the measurement.

In the case of helical polymers, the specific rotation confirms the formation of a helical scaffold with a preferred handedness. The value obtained for the polymer is typically one to ten orders of magnitude bigger than the one for the corresponding monomer.

4.3.2. Circular Dichroism

One of the most useful techniques for determining the presence of a preferred helical sense in macromolecules, as well as a preferential conformation in discrete chiral molecules, is the Circular Dichroism (CD). When a circularly polarized light beam interacts with a chiral molecule bearing one or more chromophores (light-absorbing groups), the light path gets altered. CD spectroscopy records this variation by measuring the difference between the absorption of left-handed circularly polarized light (*L*-CD) and right-handed circularly polarized light (*R*-CD). This technique has been widely used in the analysis of the secondary structure of peptides, as it provides not only information about the chiral content but also about the folding —there are characteristic CD spectra for the most common foldings: α-helix,

[30] (a) Motoshige, A.; Mawatari, Y.; Yoshida, Y.; Matsuyama, C. S.; Tabata, M.J. *Polym. Sci., Part A: Polym. Chem.* **2012**, *50*, 3008-3015. (b) Percec, V.; Peterca, M.; Rudick, J. G.; Aqad, E.; Imam, M. R.; Heiney, P. A. *Chem. Eur. J.* **2007**, *13*, 9572-9581. (c) Percec, V.; Rudick, J. G.; Peterca, M.; Aqad, E.; Imam, M. R.; Heiney, P. A. *J. Polym. Sci., Part A: Polym. Chem.* **2007**, *45*, 4974-4987. (d) Percec, V.; Aqad, E.; Peterca, M.; Rudick, J. G.; Lemon, L.; Ronda, J. C.; De, B. B.; Heiney, P. A.; Meijer, E. W. *J. Am. Chem. Soc.* **2006**, *128*, 16365-16372. (e) V. Percec, J. G. Rudick, M. Peterca, M. Wagner, M. Obata, C. M. Mitchell, W. D. Cho, V. S. K. Balagurusamy and P. A. Heiney, *J. Am. Chem. Soc.* **2005**, *127*, 15257-15264.

β-sheet, β-turn or random coil—. This technique can also be employed to analyse the effect that the environmental conditions have over the studied molecule, as any conformational change will be easily detected. Hence, thermodynamic, kinetic and structural parameters can be obtained.[31,32] The possibility of modifying the experiment conditions as well as the low amount of sample needed, unlike specific rotation, have turned CD into a powerful technique.

For helical polymers (e.g., PPAs) it is possible to determine an excess of a single-handed helix by looking at the CD trace. The presence of a Cotton effect in the vinlylic region, in combination of an increase in the CD intensity when the traces of the monomer and the polymer are compared, is indicative of the formation of the helix. This technique provides information about the helical sense described by the internal helix, the one described by the backbone, and it has been recently reported that a positive Cotton band corresponds to a *P* helix, whereas a negative Cotton effect corresponds to an *M* helix.[25] This correlation was determined by TD-DFT (Time-Dependent Density Function Theory) calculations.

4.3.3. Theoretically Calculated Circular Dichroism

Theoretical calculations have merged in the last years as a useful tool for the elucidation of the helical structure. MMFF94 energy minimization together with ECD simulation, using the time-dependent self-consistent field (SCF) ZernerQs Intermediate Neglect of Differential Overlap (ZINDO/S) method, have been explored as a way to solve the secondary structure of some helical polymers. As an example, Masuda and co-workers confirmed the formation of two different helical scaffolds (different dihedral angle at the single bond along the main chain, ω_1), while studying the substitution effect on a series of polymers derived from propargylamides (m-**20**).[33]

In the case of PPAs only one example has been reported and is focused on the CD bands arose by the pendant and not to those related to the polyene backbone, probably due to the complexity of the helical structure (two coaxial helices).[34] Recently, Rodríguez *et al.* have overcome this challenge, demonstrating that is possible to determine the helical sense of the inner helix just by looking at the CD spectra. To calculate the ECD spectra, the Time-Dependent Density Function Theory (TD-DFT) was employed and as base the 3-21G basis set and the rCAM-B3LYP functional were selected. The good match between the calculated ECD

25 Fernández, B.; Rodríguez, R.; Quiñoá, E.; Riguera, R.; Freire, F. *ACS Omega*, **2019**, *4*, 5233-5240.

31 (a) Hammes, G. G. *Circular Dichroism, Optical Rotatory Dispersion, and Fluorescence Polarization, In Spectroscopy for the Biological Sciences*, John Wiley & Sons, Inc.: Hoboken, New Jersey, 2005, p 63. (b) Berova, N.; Nakanishi, K., Woody, R. W. *Circular Dichroism: Principles and Applications*, 2nd ed., Wiley-VCH: New York, 2000, p 361. (c) Nakanishi, K.; Berova, N. *Circular Dichroism: Principles and Applications*, 2nd ed., Wiley-VCH: New York, 2000, p 912.(d) Harada, N.; Nakanishi, K. *Circular Dichroic Spectroscopy-Exciton Coupling in Organic Stereochemistry*, 2nd ed., University Science Books: Mill Valley, CA, 1983.

32 (a) Suzuki, Y.; Tabei, J.; Shiotsuki, M.; Inai, Y.; Sanda, F.; Masuda, T. *Macromolecules* **2008**, *41*, 1086-1093. (b) Buffeteau, T.; Ducasse, L.; Poniman, L.; Delsuc, N.; Huc, I. *Chem. Commun*. **2006**, 2714-2716. (c) Tang, H. Z.; Novak, B. M.; He, J.; Polavarapu, P. L. *Angew. Chem. Int. Ed*. **2005**, *44*, 7298-7301. (d) Tanatani, A.; Yokoyama, A.; Azumaya, I.; Takakura, Y.; Mitsui, C.; Shiro, M.; Uchiyama, M.; Muranaka, A.; Kobayashi, N.; Yokozawa, T. *J. Am. Chem. Soc*. **2005**, *127*, 8553- 8561.(e) Tabei, J.; Shiotsuki, M.; Sanda, F.; Masuda, T. *Macromolecules* **2005**, *38*, 9448-9454. (f) Kaneko, T.; Umeda, Y.; Yamamoto, T.; Tereguchi, M.; Aoki, T. *Macromolecules* **2005**, *38*, 9420-9426. (g) Takei, F.; Hayashi, H.; Onitsuka, K.; Kobayashi, N.; Takahashi, S. *Angew. Chem. Int. Ed.* **2001**, *40*, 4092-4094.

33 Suzuki, Y.; Tabei, J.; Shiotsuki, M.; Inai, Y.; Sanda, F.; Masuda, T. *Macromolecules* **2008**, *41*, 1086-1093.

34 Kaneko, T.; Umeda, Y.; Yamamoto, T.; Teraguchi, M.; Aoki, T. *Macromolecules* **2005**, *38*, 9420-9426.

spectra for small oligomers and the experimental ECD spectra for some PPAs, with a known helical structure, allowed correlating the experimental CD with the internal helical sense of the PPA. From all the data obtained it was determined that a polymer with a positive Cotton effect in the vinylic region describes a *P* internal helix, whereas if a negative band is observed the polymer will be describing an *M* helix. Moreover, the robustness and reliability of this finding was confirmed by evaluating some PPAs taken from literature and by varying the main dihedral angles of the PPAs that can affect to the ECD spectra.[25,26]

4.3.4. X-ray Diffraction

To get a diffraction pattern of a polymer it is necessary to prepare an oriented film, but this can only be possible if it presents a rigid rod-like structure with tendency to form liquid crystal phases. So, for lyotropic or thermotropic liquid crystals (oriented films with regular helical structure) the films can be prepared by physical shearing or by applying electric or magnetic fields to the sample.[35] Notwithstanding the information that this technique provides about the secondary structure —helical pitch, helix width, helix length and the interpendant distance—, no information about the helical sense is extracted.

4.3.5. Atomic Force Microscopy

Atomic Force Microscopy (AFM) is a powerful structural technique to elucidate the secondary structure of helical polymers, which provides useful information about the packing angle and the helical pitch and, what is more important, about the helical sense of the secondary structure.[36] However, sample preparation is not straightforward; only well-ordered self-assembled monolayers will provide images with resolution enough to extract all the desired data. The substrate used as a support for the monolayer will also be a key factor, as it can affect the intramolecular interactions between chains as well as to the helical conformation. The different approaches developed during the last years to prepare polymer monolayers —drop casting, spin coating and Langmuir-Blodget— are discussed next.

Drop Casting

In a pioneering work, Yashima and co-workers analysed by AFM the helical sense of a PPA copolymer, bearing an achiral bulky C_{60} and an optically active amine (poly-**23**). They drop casted a diluted polymer solution on two different substrates, mica and highly oriented pyrolitic graphite (HOPG), observing different results.[37] The AFM images on mica showed isolated particles due to the repulsive interactions between the hydrophobic C_{60} and the hydrophilic mica substrate, forcing the polymer to aggregate. On the contrary, the AFM images on HOPG revealed some extended and individual copolymer chains with isolated

[25] Fernández, B.; Rodríguez, R.; Rizzo, A.; Quiñoá, E.; Riguera, R.; Freire, F. *Angew. Chem. Int. Ed.* **2018**, *57*, 3666-3670.
[26] Fernández, B.; Rodríguez, R.; Quiñoá, E.; Riguera, R.; Freire, F. *ACS Omega* **2019**, *4*, 5233-5240.
[35] Yashima, E. *Polym. J.* **2010**, *42*, 3-16.
[36] (a) Freire, F.; Quiñoá, E.; Riguera, R. *Chem. Commun.* **2017**, *53*, 481-492. (b) Kumaki, J.; Sakurai, S. I.; Yashima, E. *Chem. Soc. Rev.* **2009**, *38*, 737.
[37] Nishimura, T.; Takatani, K.; Sakurai, S.; Maeda, K.;.Yashima, E. *Angew. Chem. Int. Ed.* **2002**, *41*, 3602-3604.

particles (Figure 10a). These studies revealed the importance that the substrate employed has over the scaffold adopted. This, combined with the selection of the pendant groups of the polymer, can be used for the formation of certain supramolecular structures.[38]

Similar studies carried out for poly(4-carboxyphenylacetylene) (poly-**24**) complexed with (*R*)-naphtylethylamine and also for its corresponding amide (poly-**25**) showing, in both cases, isolated helical chains (Figure 10b and 10c respectively). The resolution of the AFM images on mica was not good enough, therefore only the helical sense could be determined.[39]

The visualization of right-handed and left-handed helices by AFM on mica was feasible using a bulky chiral ruthenium complex (poly-**26**, Figure 10d). Although in this case the helical sense could be determined, other structural parameters such as the helical pitch and packing angle could not be obtained due to the poor quality of the images.[40]

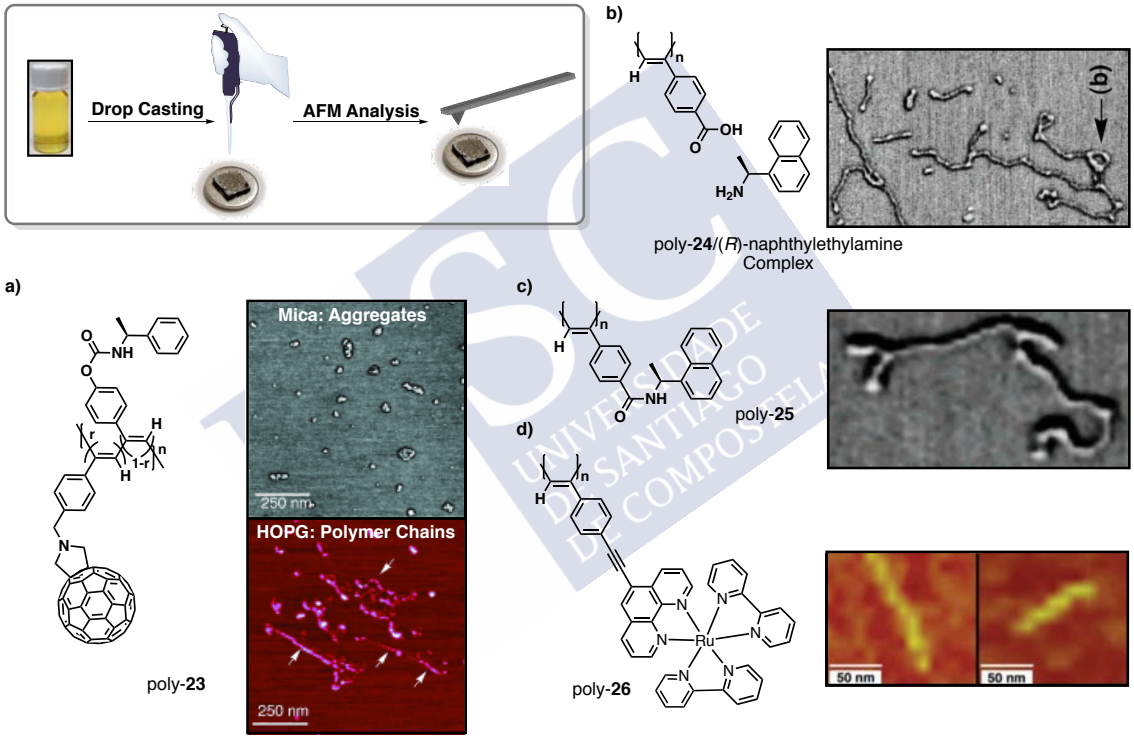

Figure 10. (a) Structure and AFM images for poly-**23** drop casted onto different substrates. (b) Structure and AFM image for poly-**24**/(*R*)-naphtylethylamine. (c) Structure and AFM image for poly-**25**. (d) Structure and AFM images for poly-**26**.

Spin Coating

Taking this information into account, Yashima *et al.* developed a new strategy. They decided to introduce a long alkyl chain in the pendant moiety of the PPA to promote the self-assembly and favour the monolayer formation via chain interdigitation.[41] To facilitate this, a dilute solution of the sample was spin coated onto HOPG and kept under solvent vapours

[38] Nishimura, T.; Maeda, K.; Ohsawa, S.; Yashima, E *Chem. Eur. J.* **2005**, *11*, 1181-1190.
[39] Sakurai, S. I.; Kuroyanagi, K.; Morino, K.; Kunitake, M.; Yashima, E. *Macromolecules* **2003**, *36*, 9670-9674.
[40] Sakurai, S. I.; Ohira, A.; Suzuki, Y.; Fujito, R.; Nishimura, T.; Kunitake, M.; Yashima, E. J. *Polym. Sci. Part A: Polym. Chem.* **2004**, *42*, 4621-4640.
[41] Okoshi, K.; Sakurai, S. I.; Ohsawa J. K.; Yashima, E. *Angew. Chem. Int. Ed.* **2006**, *45*, 1245-1248.

overnight, allowing the nucleation and growth of 2D crystals. Following this approach, they obtained the corresponding monolayers for poly-(*L*)-**27** and poly-(*D*)-**27** (derived from *L*-alanine and *D*-alanine respectively). The formation of these crystals under the described conditions forced a strong and epitaxial adsorption of the pendants on the graphite substrate.

AFM images of poly-(*L*)-**27** revealed the presence of *M* helices described by the pendant groups. Direct observation of AFM images allows the visualization of the external helix of the polymer. This helix has a helical pitch of 2.34 nm and a packing angle of 40º, which corresponds to a *cis-transoidal* 11/5 helix (two residues per turn) (Figure 11a). In such a case, the internal and external helices should rotate in opposite directions, as confirmed by CD that showed the presence of a right-handed helix. Moreover, they observed that the dynamic behaviour of poly-(*L*)-**27** could also be analysed not only in solution but also on the solid state. Polarity changes of the solvent used to generate the overnight vapours provided 2D crystals with opposite helical sense for poly-(*D*)-**27**.[42]

The same group also studied by AFM the helical structure of an achiral PPA, bearing α-aminoisobutiric acid (Aib) *n*-decyl esters as pendants (poly-**28**).[43] They observed that right- and left-handed helices were contained within the same 2D crystal, but displaying two different patterns: homochiral helices (red bars only) —helices paralleled packed; same helical sense— and heterochiral helices (red and blue bars) —packed in a parallel fashion but with an alteration; helix reversals (dashed white line)— (Figure 11b). Again, the high resolution of the images allowed the extraction of the structural parameters for the *P* helix (helical pitch: 2.01 nm and packing angle: +43º) and *M* helix (helical pitch: 2.05 nm and packing angle: -45º). The information extracted from the AFM measurements together with other experimental data (NMR, X-ray diffraction and Raman), allowed the elucidation of the secondary structure for poly-**28**.

In an analogous way, Percec and co-workers developed a similar protocol to obtain 2D crystals.[44] The sample deposition (onto mica or HOPG) is the same as the described in Prof. Yashima's procedure, but instead of exposing the sample to solvent vapours to promote the self-assembly, the sample is submitted to a thermal annealing. These studies were performed for dendronized PPAs bearing long alkyl chains, essential for the pendants interdigitation (poly-**29**). In this case, the substrate employed as support plays a key role on the final shape of the polymer chains —oblate cylindrical in HOPG and cylindrical in mica—. Although good 2D crystals were obtained by this procedure, the resolution of the images was not good

[42] Sakurai, S. I.; Okoshi, K.; Kumaki, J.; Yashima, E. *J. Am. Chem. Soc.* **2006**, *128*, 5650-5651.

[43] (a) Ohsawa, S.; Sakurai, S. I.; Nagai, K.; Maeda, K.; Kumaki, J.; Yashima, E. *Polym. J.* **2012**, *44*, 42-50. (b) Ohsawa, S.; Sakurai, S. I.; Nagai, K.; Banno, M.; Maeda, K.; Kumaki, J.; Yashima, E. *J. Am. Chem. Soc.* **2011**, *133*, 108-114. (c) Sakurai, S. I.; Ohsawa, K.; Nagai, K.; Okoshi, K.; Kumaki, J.; Yashima, E. *Angew. Chem., Int. Ed.* **2007**, *46*, 7605-7608.

[44] (a) Percec, V.; Rudick, J. G.; Wagner, M.; Obata, M.; Mitchell, C. M.; Cho W.-D.; Magonov, S. N. *Macromolecules* **2006**, *39*, 7342-7351. (b) Percec, V.; Rudick, J. G; Peterca, M.; Staley, S. R.; Wagner, M.; Obata, M.; Mitchell, C. M.; Cho, W.-D.; Balagurusamy, V. S. K.; Lowe, J. N.; Glodde, M.; Weichold, O.; Chung, K. J.; Ghionni, N.; Magonov S. N.; Heiney, P. A. *Chem. Eur. J.* **2006**, *12*, 5731-5746. (c) V. Percec, M. Obata, J. G. Rudick, B. B. De, M. Glodde, T. K. Bera, S. N. Magonov, V. S. K. Balagurusamy, P. A. Heiney, *J. Polym. Sci. Part A: Polym. Chem.* **2002**, *40*, 3509-3533.

enough to extract all the helical parameters —helical sense, helical pitch and packing angle— (Figure 11c).

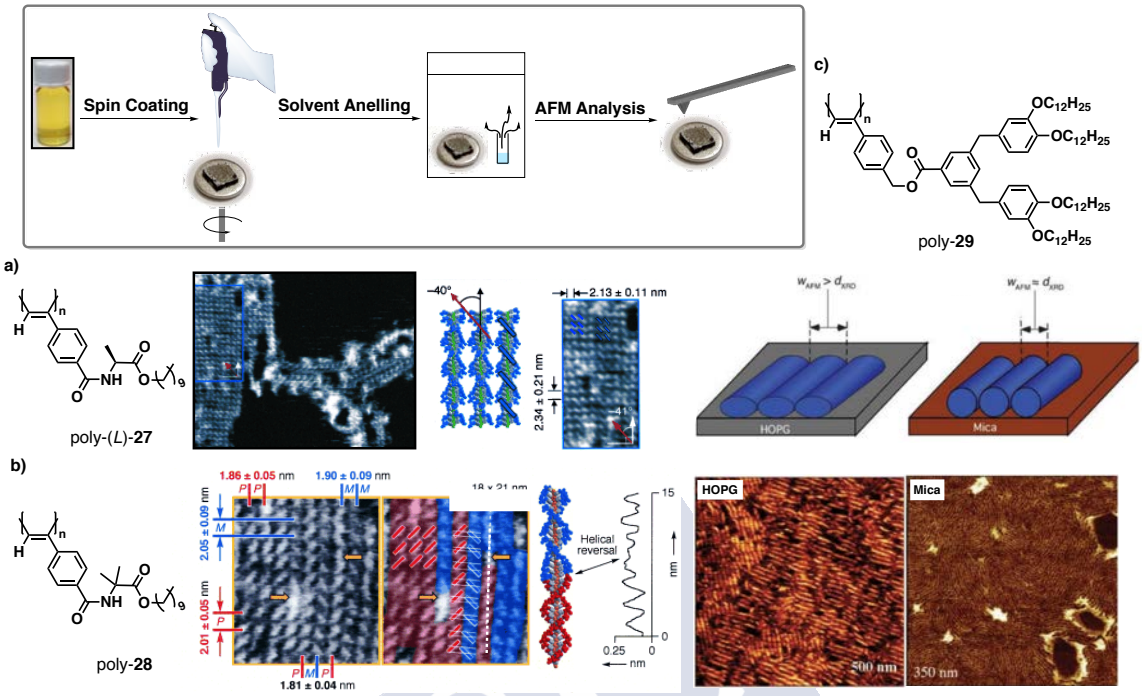

Figure 11 (a) Structure and AFM image for poly-(*L*)-**27**. (b) Structure and AFM image for poly-**28** showing the *M* and *P* domains. (c) Structure and AFM images for poly-**29** spin coated into HOPG and mica.

Following Yashima's approach we succeed in the preparation of 2D crystals for several PPAs bearing short pendants, demonstrating that the presence of long alkyl chains is not strictly necessary for obtaining a well-ordered monolayer.[45] During our studies, we found a difficulty in the generation of 2D crystals for poly-**30** that bears the anilide of the α-methoxy-α-phenylacetic acid (MPA). A dilute solution of poly-**30** was deposited onto a freshly cleaved HOPG substrate and subjected to solvent vapours overnight, but no ordered 2D crystals were observed by AFM —probably due to the highly dynamic behaviour of this polymer (two conformations, the antiperiplanar (*ap*) and the synperiplanar (*sp*), into a 1:1 equilibrium)—. However, we know that this dynamism of poly-**30** can be manipulated upon addition of metal ions[46] (*ap* conformation for M^+ and *sp* conformation for M^{2+}) (Figure 12a). Hence, spin coating of a diluted polymer-metal complex solution, followed by THF vapours exposure, produced well ordered right-handed or left-handed monolayers. AFM measurements revealed the helical pitch (ca. 3.2 nm), the packing angle (ca. 60°) and the helical sense —*M* helix— for the poly-**30**/M^+ complex (Figure 12b) as well as for the poly-**30**/M^{2+} complex —*P* helix— (Figure 12c). Additionally we have also demonstrated in solution, as well as on the solid state, that the left-handed helix (poly-**30**/M^+ complex) (Figure 12d) can be selectively inverted into a right-

45 Freire, F.; Seco, J. M.; Quiñoá, E.; Riguera, R. *Angew. Chem. Int. Ed.* **2011**, *50*, 11692-11696.

46 (a) Arias, S.; Freire, F; Quiñoá, E.; Riguera, R. *Angew. Chem. Int. Ed.* **2014**, *53*, 13720-13724. (b) Freire, F.; Seco, J. M.; Quiñoá, E.; Riguera, R. *J. Am. Chem. Soc.* **2012**, *134*, 19374-19383.

handed one by cleavage of the cation-π interaction, by the addition of a small amount of a cosolvent (Figure 12e).[47]

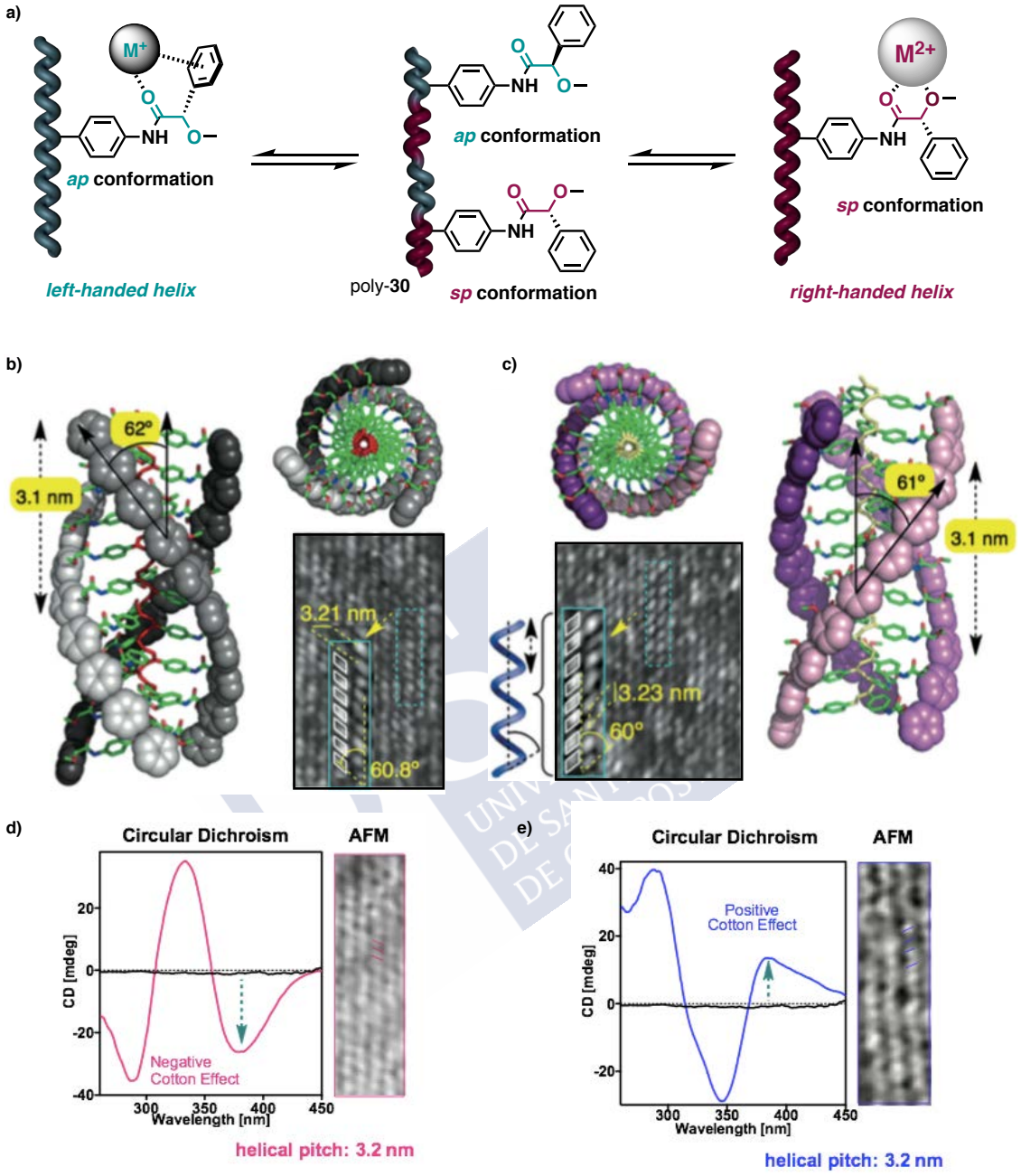

Figure 12. (a) Representation of the conformational equilibrium for poly-**30** and the selective metal mediated right-/left-handed amplification. (b) 3D model and 2D crystal for poly-**30**/M^+ complex. (c) 3D model and 2D crystal for poly-**30**/M^{2+} complex. (d) CD and AFM spectra for poly-**30**/Na^+, cation-π interaction. (e) CD and AFM spectra for poly-**30**/Na^+ complex after the addition of a cosolvent, inversion of the helical sense and cation-π deactivation.

Langmuir-Blodgett

In the previously described methods, the preparation of a well-ordered PPA monolayer occurs at the air/solid interphase by solvent evaporation of a polymer solution drop on the solid support. Thus, the interactions of the polymer with the support as well as the

[47] Arias, S.; Freire, F.; Quiñoá E.; Riguera, R. *Polym. Chem.* **2015**, *6*, 4725-4733.

evaporation rate of the solvent will be the critical factors. An alternative to this monolayer preparation is the Langmuir-Blodgett (LB) method, in which the monolayers are formed at the air/water interphase when the solid support is introduced in a water pool. Here the hydrophobic/hydrophilic character of the polymer and the solid support will be determinant.[48]

To perform these studies, a dilute solution of the polymer in $CHCl_3$ (0.1 mg mL^{-1}, 200 μL) is spread drop by drop via Hamilton syringe on the water surface. After the $CHCl_3$ evaporation took place (around 5-10 minutes), the barriers are gradually closed observing an increase on the surface pressure. Once the monolayer is formed the substrate is removed from the pool taking the monolayer attached to it (Figure 13a).

Tang and co-workers studied different PPAs bearing hydrophobic backbones and hydrophilic pendants by this technique, using mica as the solid support. Although AFM revealed the formation of ordered 2D crystals, the quality was not good enough to obtain the structural parameters (helical sense, packing angle or helical pitch) (Figure 13b, c).[49]

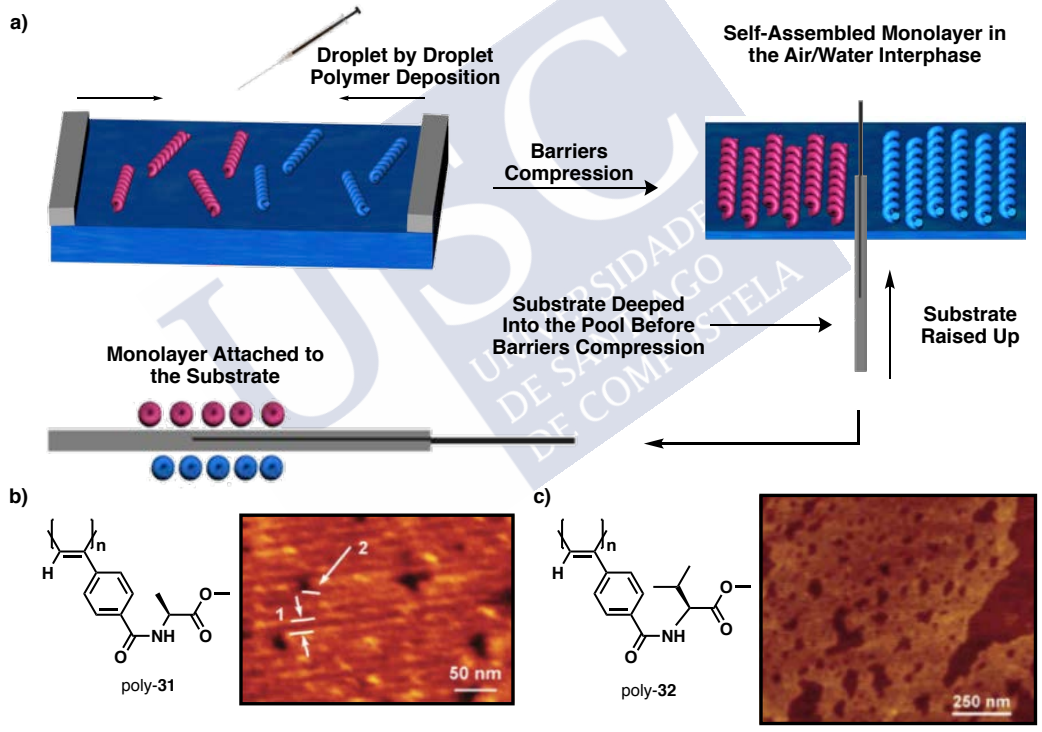

Figure 13. (a) Schematic illustration of the LB technique. Structure and AFM image obtained by LB for (b) poly-**31** and (c) poly-**32**.

Langmuir-Schaefer

As shown before, LB can be the technique of choice for polymers with amphiphilic character, where the hydrophilic part attaches to the mica (hydrophilic support). However, in PPAs the best images are obtained when HOPG is used as solid support but the hydrophobic character of this substrate makes it inadequate to be used in the LB approximation.

[48] (a) Kawauchi, T.; Kumaki, J.; Kitaura,A.; Okoshi,K.; Kusanagi, H.; Kobayashi, K.; Sugai, T.; Shinohara,H.; Yashima, E. *Angew. Chem. Int. Ed.* **2008**, *47*, 515-519. (b) Roberts, G. G. *Langmuir-Blodgett Films*, 1st ed.; Plenum: New York, 1990.

[49] (a) Li, B. S.; Lam, J. W. Y.; Yu Z.-Q.; Tang, B. Z. *Langmuir* **2012**, *28*, 5770-5774. (b) Li, B. S.; Kang, S. Z.; Cheuk, K. K. L.; Wan, L.; Ling, L.; Bai, C.; Tang, B. Z. *Langmuir* **2004**, *20*, 7598-7603;

Thus we reasoned that the Langmuir-Schaefer (LS) method,[50] which directly exfoliates the HOPG from the air/water interphase, could be the solution. We tested our theory by preparing some 2D crystals for poly-**30** getting successful results.[51] The formation of well-ordered monolayers for this highly dynamic polymer, provide information about the different helical parameters necessary to solve the secondary structure of poly-**30**, which was not feasible by other techniques. It was found that the polymer folds into enantiomeric 2D crystals made by helices with the same scaffold but different helical sense (Figure 14b). The values obtained were consistent with the ones previously observed for the polymer complexated with monovalent or divalent metal ions —axially racemic poly-**30** did not produce 2D crystals by spin coating (Figure 12)—.[45] This technique also allowed us to obtain monolayers for polymers with different substitution pattern on the aryl ring of the PPA.[52]

The procedure for LS is the same as the above described for the LB method. The only difference is that the HOPG is approached to the water surface instead of immersed and, therefore, the monolayer is transferred into the substrate due to the attractive interactions established (Figure 14a).

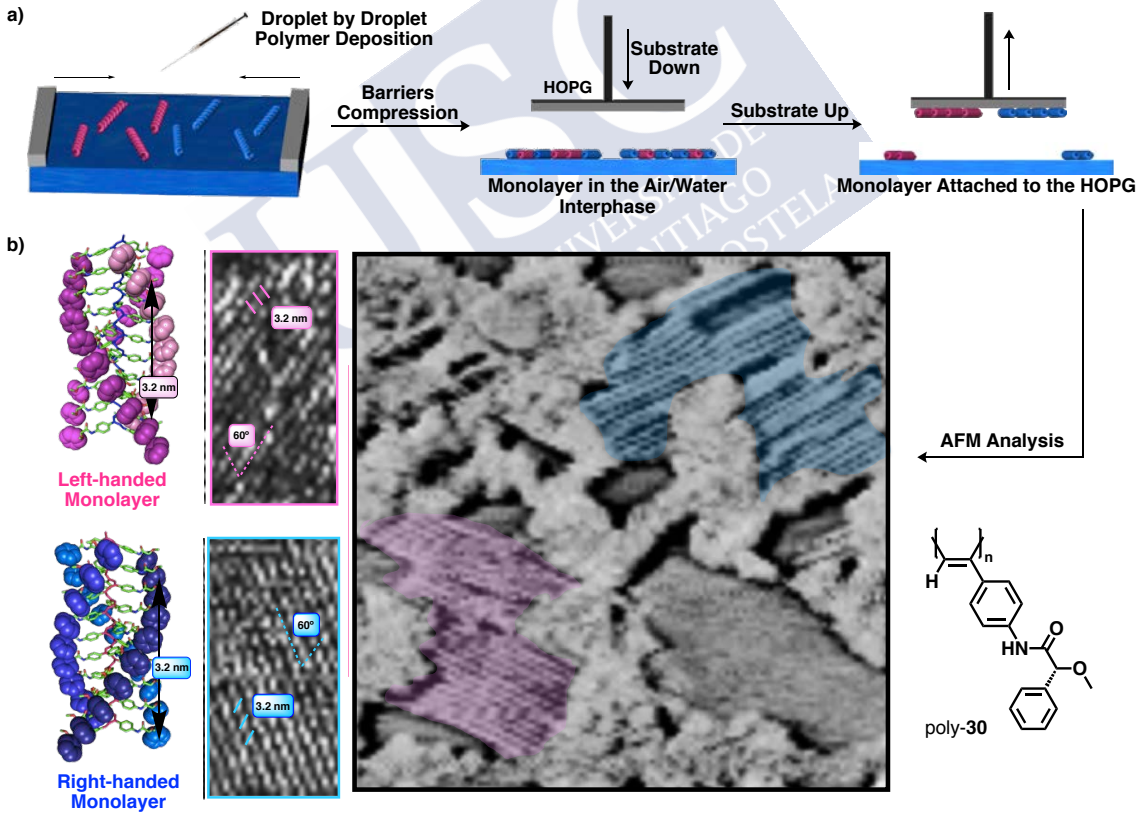

Figure 14. (a) Schematic illustration for the LB technique. (b) Structure, 3D model and AFM image showing the *P* and *M* helix domains for poly-**30**.

50 Ulman, A. *An Introduction to Ultrathin, Organic Films-From Langmuir-Blodgett to Self-Assembly*, 1st ed.; Academic Press: New York, 1991.
51 Rodríguez, R.; Ignés-Mullol, J.; Sagués, F.; Quiñoá, E.; Riguera, R.; Freire, F. *Nanoscale* **2016**, *8*, 3362-3367.
45 Freire, F.; Seco, J. M.; Quiñoá, E.; Riguera, R. *Angew. Chem. Int. Ed.* **2011**, *50*, 11692-11696.
52 Rodríguez, R.; Quiñoá, E.; Riguera, R.; Freire, F. *J. Am. Chem. Soc.* **2016**, *138*, 9620-9628.

5. Properties of Dynamic Helical Polymers

Since the discovery of the dynamic helical polymers, the total control of the helix —sense and elongation— has been one of the most ambitious goals. The need to control the polymer helical structure lies on the potential application of these new materials as chiral sensors, molecular machines, conductive materials...

The main properties present in the dynamic helical polymers are discussed next.

5.1 Helix Induction

As previously mentioned, a dynamic helical polymer can be prepared starting from an achiral monomer resulting in a racemic helical polymer —equal population of left-handed and right-handed helices—. Further addition of chiral solvents or chiral additives will promote the adoption of a single helical sense through a specific non-covalent bonding. It is important to point out that the helix formed (the most stable one) will have a diastereomeric nature due to the chiral component added and complexed to the achiral polymer.[5d,h]

Yashima *et al.* reported the first example of helix induction (Figure 15a). They synthesized a polymer derived from the 4-ethynylbenzoic acid obtaining an axially racemic polymer (poly-**33**) —null CD—, with an equal population of left-handed and right-handed helices.[53] The addition of chiral amines in DMSO to poly-**33** will bias this equilibrium, observing the appearance of an active CD trace. The final helical sense adopted by the polymer scaffold will be determined by the absolute configuration of the amine added, that will establish an acid-base interaction with the pendant. This process is reversible and the addition of a stronger acid (e.g., trifluoroacetic acid) results into a disappearance of the induced helix. This process was not only observed in solution but also on the solid state, on the gel state and on liquid crystalline phase.[54]

5.2 Memory of Macromolecular Helicity

As previously mentioned, the helix induction is a dynamic process and the obtained CD disappears if the chiral additive is removed. However, Yashima and co-workers observed that the helical sense induced in poly-**33** could be retained by replacing the chiral amine in the polymer/chiral amine complex (preferred helical sense) with an achiral amine, resulting in a CD trace virtually unaltered.[55] The formation of a salt bridge, between the achiral amine and the complex, stabilizes the initial helical sense due to electrostatic repulsions between pendant groups. This process is known as the memory of macromolecular helicity (Figure 15b).

---

[5] (d) Yashima, E.; Maeda, K.; Iida, H.; Furusho, Y.; Nagai, K. *Chem. Rev.* **2009**, *109*, 6102-6211. (h) Yashima, E.; Maeda, K. *Macromolecules* **2008**, *41*, 3-12.

[53] (a) Yashima, E.; Maeda, K.; Okamoto, Y. *Nature* **1999**, *399*, 449-451. (b) Yashima, E.; Matsushima, T.; Okamoto, Y. *J. Am. Chem. Soc.* **1995**, *117*, 11596-11597..

[54] Goto, H.; Zhang, H. Q.; Yashima, E. *J. Am. Chem. Soc.* **2003**, *125*, 2516-2523.

[55] (a) Hase, Y.; Nagai, K.; Iida, H.; Maeda, K.; Ochi, N.; Sawabe, K.; Sakajiri, K.; Okoshi, K.; Yashima, E. *J. Am. Chem. Soc.* **2009**, *131*, 10719-10732. (b) Hasegawa, T.; Maeda, K.; Ishiguro, H.; Yashima, E. *Polymer J.* **2006**, *38*, 912-919.

Before this finding, helical polymers with optical activity due to macromolecular helicity were prepared either by the polymerization of optically active monomers or by the asymmetric polymerization of achiral or prochiral monomers with chiral catalysts or initiators.[56]

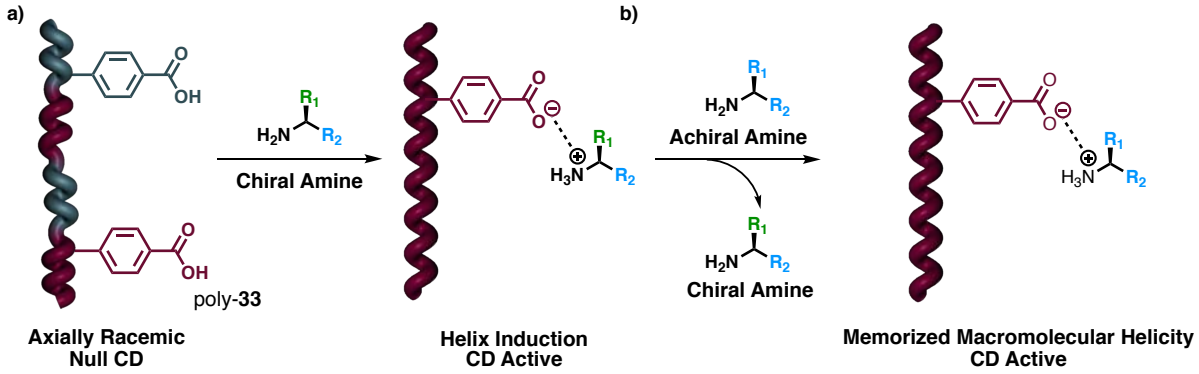

Figure 15. Conceptual representation of the (a) helix induction and (b) memory of macromolecular helicity.

5.3 Chiral Amplification

The addition of a small amount of a chiral or achiral additive to an initially axially racemic state can result into an improvement of the final chiral content, through covalent or non-covalent interactions. This process is called chiral amplification.

Working in this direction, our research group has developed an axially racemic PPA —null CD signal— derived from the (*R*)-α-methoxy-α-phenylacetic acid (MPA) (poly-**30**).[57] This polymer presents two conformers in a 1:1 equilibrium, the *sp* conformer (synperiplanar orientation of the carbonyl and methoxy groups, dihedral angle [C=O-C-OMe] ca. 0º) and the *ap* conformer (antiperiplanar orientation of the carbonyl and methoxy groups, dihedral angle [C=O-C-OMe] ca. 180º) (Figure 16a). However, this conformational equilibrium can be biased. More precisely, monovalent metal ions (M^+: Li^+, Ag^+ or Na^+) will coordinate to the pendant group through the carbonyl group and also through the phenyl group (via a cation-π interaction), fixing the *ap* conformation (*M* helix). On the other hand, if divalent metal ions (M^{2+}: Ba^{2+}) are added, the *sp* conformation will be promoted due to the coordination of the metal to carbonyl and methoxy groups (*P* helix). Hence, depending on the valence of the metal added (only a small amount is required, < 10%), the polymer will adopt an *M* or *P* helix. The reversibility of this process was demonstrated by the addition of a metal resin scavenger to the metal-polymer complex. By employing this resin, the metal ion is removed and the original null CD trace is recovered. Arias *et al.* reported that the cation-π interaction that stabilizes the *ap* conformation in poly-**30** can be selectively switched off by removing the metal ion complexed to the pendant group.[47] Moreover, the addition of a cosolvent disrupts this cation-π interaction and modifies the pendant conformation from *ap* to *sp*, inducing a

[56] Yashima, E.; Maeda, K.; Nishimura, T *Chem. Eur. J.* **2004**, *10*, 42-51.
[57] Freire, F.; Seco, J. M.; Quiñoá, E.; Riguera, R. *Angew. Chem. Int. Ed.* **2011**, *50*, 11692-11696.
[47] Arias, S.; Freire, F.; Quiñoá E.; Riguera, R. *Polym. Chem.* **2015**, *6*, 4725-4733.

helix inversion in the polymer. Therefore, it is possible to induce whether a left-handed or right-handed helical sense in poly-**30** by the addition of a monovalent metal ion and further modification of the coordination mode by the addition of a cosolvent. Moreover, removal of the metal ion recovers the axially racemic starting material (Figure 16b).

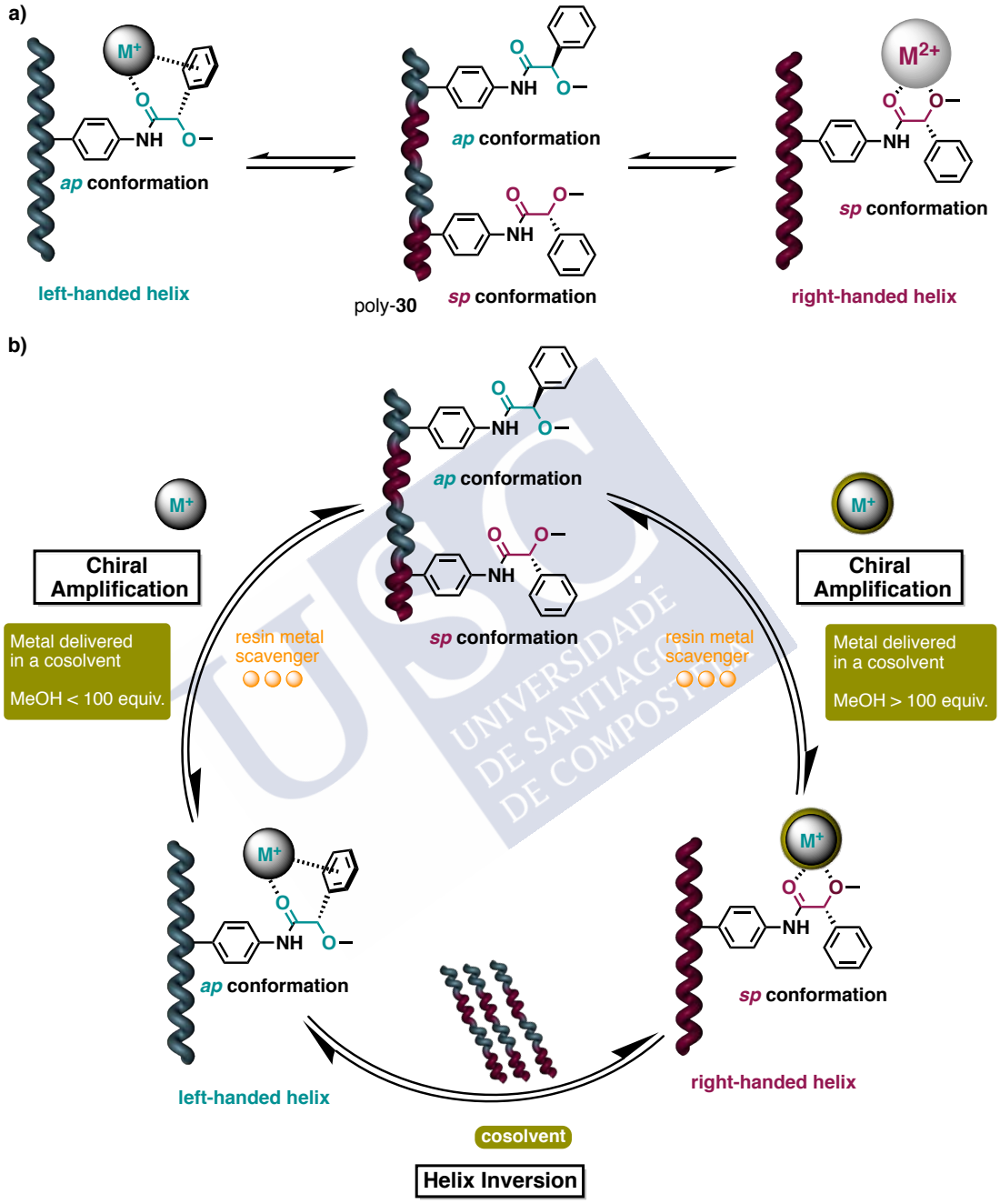

Figure 16. (a) Representation of the conformational equilibrium for poly-**30** and the selective metal-mediated right-/left-handed amplification. (b) Selection of the right-/left-handed helical sense by the activation/deactivation of the cation-π interaction.

Green *et al.* extensively studied the chiral amplification phenomena in helical poly(isocyanate)s (poly-**10**, Figure 3) formed by left-handed and right-handed helices and connected through helix reversals. Over the past three decades the processes described by

this group have been widely studied for a wide variety of covalent and non-covalent polymeric systems. These chiral amplification processes are described next.

5.3.1 Sergeants and Soldiers Effect

This chiral amplification, first described by Prof. Green in 1988, consists in the introduction of a small amount of a chiral unit (less than 1%) in a polymer chain made up by achiral units (left-handed and right-handed helices). Through a cooperative communication mechanism, the chiral unit (Sergeant) is able to command the achiral ones (Soldiers) to fold the copolymer into a preferred helical sense (Figure 17).[58] Since this seminal discovery, observed in poly(isocyanate)s (poly-**10**, Figure 3), this effect was proven in other dynamic and static helical polymers —e.g., poly(silane)s (poly-**12**, Figure 3), poly(acetylene)s (poly-**13**, Figure 3) or poly(methacrylate)s (poly-**6**, Figure 2)— obtaining similar results.

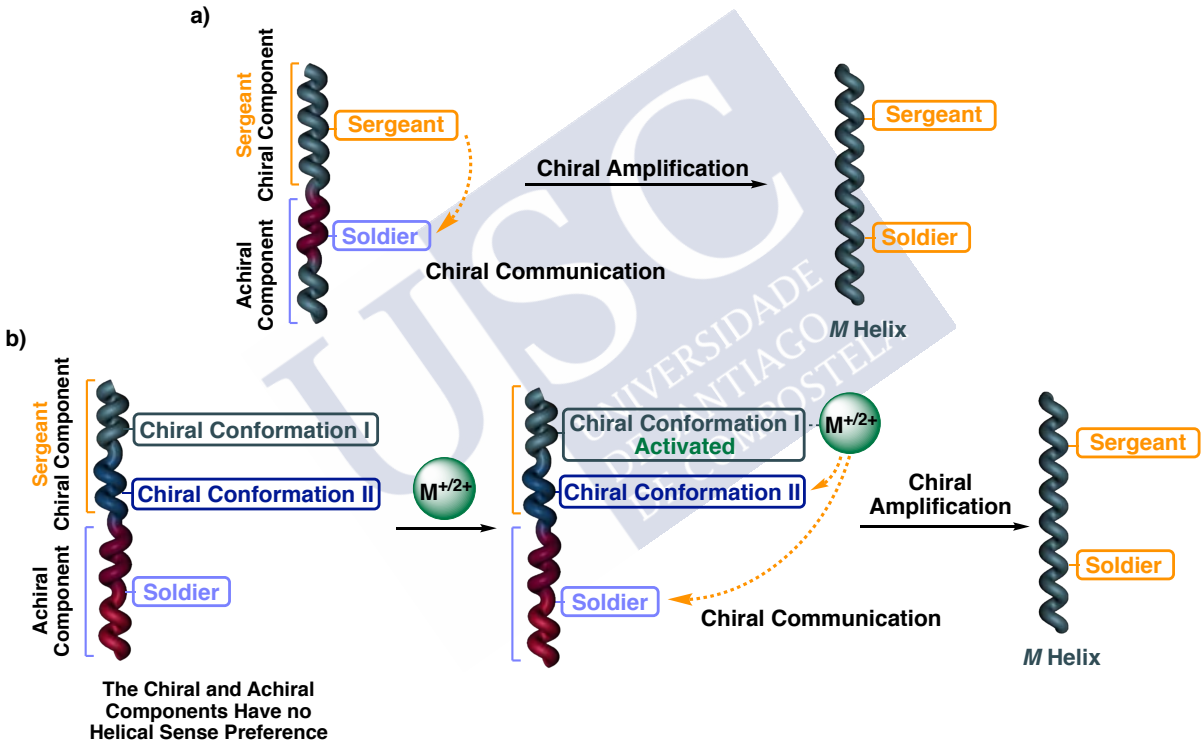

Figure 17. Conceptual representation of the Sergeants and Soldiers effect resulting into a chiral amplification via a (a) classical approach and a (b) metal-driven coordination approach.

Despite the advantages, the main drawback of the Sergeants and Soldiers effect is that the final helical sense is determined by the chirality of the Sergeant and cannot be modified. In our research group we surpass this limitation by combining the selective chiral amplification of poly-**30** (MPA, Figure 12a) and the Sergeants and Soldiers effect.[59] Unlike Green's report, in this case the Sergeant derived from MPA, although chiral, produces an

[58] (a) Green, M. M.; Park, J. W.; Sato, T.; Teramoto, A.; Lifson, S.; Selinger, R. L. B.; Selinger, J. V. *Angew. Chem. Int. Ed.* **1999**, *38*, 3138-3154. (b) Green, M. M.; Peterson, N. C.; Sato, T.; Teramoto, A.; Cook, R.; Lifson, S. *Science* **1995**, *268*, 1860-1886. (c) Green, M. M.; Garetz, B. A.; Munoz, B.; Chang, H. P.; Hoke, S.; Cooks, R. G. *J. Am. Chem. Soc.* **1995**, *117*, 4181-4182. (d) Green, M. M.; Reidy, M. P.; Johnson, R.D.; Darling, G.; O'Leary, D. J.; Willson, G. *J. Am Chem. Soc.* **1989**, *111*, 6452-6454.

[59] Bergueiro, J.; Freire, F.; Wendler, E. P.; Seco, J. M.; Quiñoá, E.; Riguera, R. *Chem. Sci.* **2014**, *5*, 2170-2176.

axially racemic helix due to the presence of two major conformations (*ap* and *sp*) in equilibrium at the pendant moiety. Hence, the Sergeant and the Soldier will induce the formation of an axially racemic helix —mixtures of *P* and *M* helices in equal ratio—. Ulterior addition of a metal ion (M^+ or M^{2+}) to this copolymer will shift the conformational composition of the MPA moiety into a single conformer depending on the valence of the metal ion —i.e., *ap*/monovalent metal ion or *sp*/divalent metal ion—. In turn, this single conformation fixed at the pendant will command the achiral soldier to adopt a preferred conformer, which further induces a fully folded copolymer, where the helical sense is determined by the conformation fixed at the MPA moiety. Moreover, Arias *et al.*[60] have demonstrated that the opposite helical sense can be obtained in case of using monovalent metal ions as external stimuli, by switching on/off the cation·π interaction. Thus, if Na^+ is added in the presence of low amounts of a cosolvent, the MPA moiety will adopt the *ap* conformation due to the cation·π interaction, whereas if the metal (Na^+) is added in the presence of high amount of cosolvent, the cation·π interaction is disrupted leading to an *sp* conformation (Figure 18).

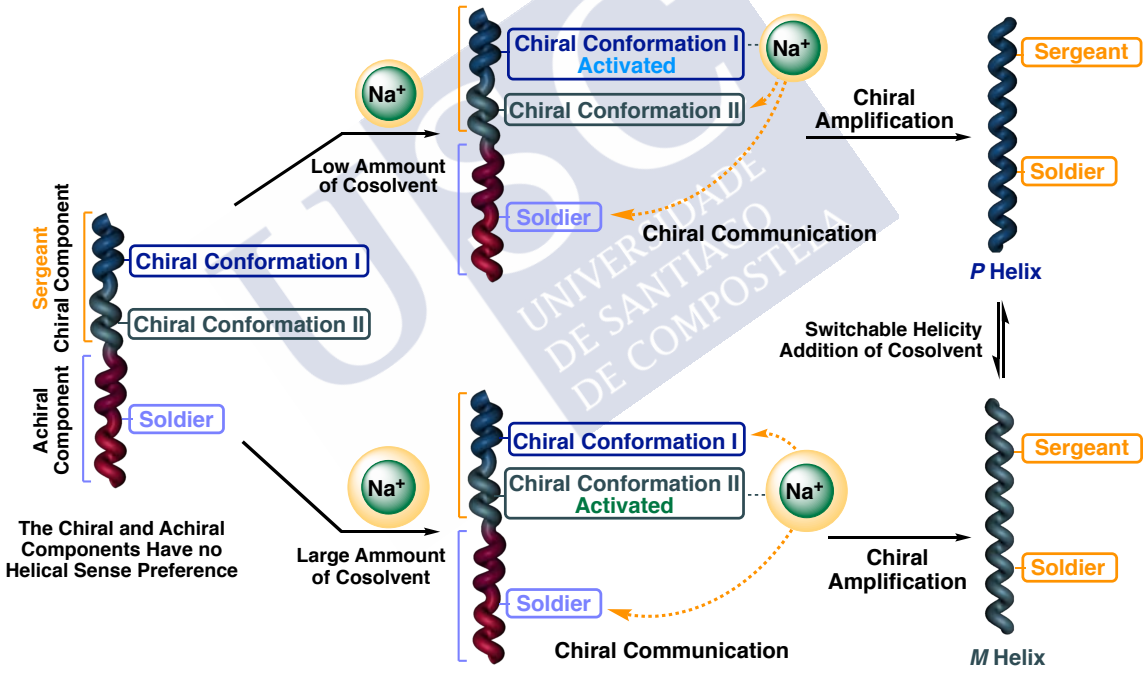

Figure 18. Conceptual representation of the total control of the helical sense of a PPA copolymer through the Sergeants and Soldiers effect and a selective tuning of the cation·π interaction mediated by the amount of cosolvent [Sergeant = (*R*)-MPA].

5.3.2 Chiral Coalition

Recently our research group introduced a new chiral enhancement effect, the Chiral Coalition.[61] In a more complex situation than the abovementioned for the Sergeants and

[60] Arias, S.; Bergueiro, J.; Freire, F.; Quiñoá, E.; Riguera, R. *Small* **2016**, *12*, 238-244.

[61] (a) Arias, S.; Rodríguez, R.; Quiñoá, E.; Riguera, R.; Freire, F. *J. Am. Chem. Soc.* **2018**, *140*, 667-674. (b) Cobos, K.; Quiñoá, E.; Riguera, R.; Freire, F. *J. Am. Chem. Soc.* **2018**, *140*, 12239-12246.

Soldiers effect (chiral soldier and achiral sergeant), the copolymer in the Chiral Coalition will be composed of a Sergeant and a Soldier both chiral and with different structure.

The chiral Sergeant and the chiral Soldier were chosen according to the conformational composition of the corresponding monomers, as well as the dynamic helical behaviour of their corresponding homopolymers. It was observed that, in all the copolymers evaluated, the Soldier is the one that commands the helical sense of the copolymer. The Sergeant (minor component) acts as a chiral dopant, inducing the Soldier (major component) to adopt a specific conformation (identical in all cases), which is independent of the absolute configuration of the Sergeant (*R*/*S*). For instance, if the (*R*)-Soldier (major component) commands a left-handed (*M* helix), both *R* and *S* enantiomers of the Sergeant (minor component) will adopt the same *M* helix, even though their intrinsic chiralities are the opposite —*M* helix$_1$, [(*R*)-Sgt$_{minor}$-co-(*R*)-Sold$_{major}$]; *M* helix$_2$, [(*S*)-Sgt$_{minor}$-co-(*R*)-Sold$_{major}$]—. The same effect was observed when the *S* enantiomer of the Soldier was used to induce a single-handed helix (*P* helix) —*P* helix$_1$, [(*R*)-Sgt$_{minor}$-co-(*S*)-Sold$_{major}$]; *P* helix$_2$, [(*S*)-Sgt$_{minor}$-co-(*S*)-Sold$_{major}$]—. Hence, the helical sense of the copolymer (inner helix, *P* or *M*) is determined by the absolute configuration of the Sergeant (minor component; fixed conformation), while the intrinsic chirality of the Soldier (major component; two possible conformations) defines the chirality at the periphery of the helix (Figure 19).

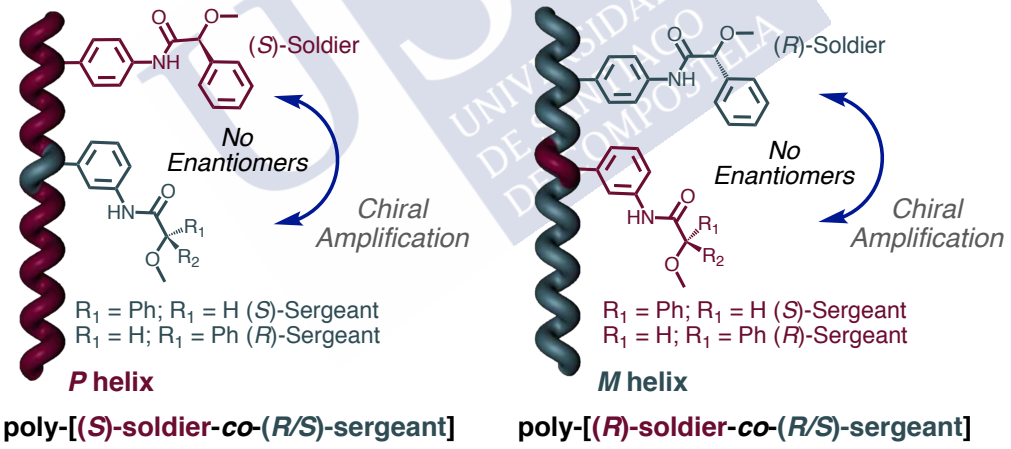

Figure 19. Conceptual representation of the Chiral Coalition.

From these studies we extracted that, in order to obtain an effective chiral-to-chiral communication along the copolymer chain and, in consequence, a single-handed copolymer, the two chiral monomers forming the copolymer have to present the following characteristics: (1) both chiral monomers (Sergeant and Soldier) must promote similar helical scaffolds in their corresponding homopolymers; (2) the chiral Soldier must display a conformational equilibrium between, at least, two conformers in the corresponding homopolymer (null CD at the vinylic region); (3) the chiral Sergeant must show a preferred conformation in the corresponding homopolymer to avoid the bond rotation and therefore, the communication of

orders with opposite information (e.g., one conformer induces a *P* helix and a second conformer induces a *M* helix).

5.3.3 Chiral Conflict

Opposite to the Chiral Coalition effect is the Chiral Conflict. This phenomena was also described by Green and co-workers for copolymers of poly(isocyanate)s (poly-**10**, Figure 3), composed by two chiral monomeric units with different structure and configuration. To produce a chiral conflict effect two monomers will induce opposite helical senses within the polymer chain resulting into a non-ordered structure.[62] The nature and the ratio of comonomers present in the polymer chain will play a key role in the initial helical sense as well as in the inversion temperature (Figure 20a). At a certain monomer ratio the copolymer will show, at a given temperature (T_c, conflict temperature), a null optical activity (CD = 0), which can be transformed into an optically active material by varying the temperature.

Our group has reported, to our knowledge, the only practical application of this chiral conflict effect in dynamic helical copolymers.[63] It was demonstrated that PPA copolymers showing chiral conflict adopt an excess of a helical sense by the addition of an appropriate external stimulus, which will act on the conformational composition of one of the constituting comonomers. In this way, it is possible to tune the excess of the helical content by playing with different stimuli (e.g., valence of the metal ion) without affecting the copolymer composition. Surprisingly, if the external stimuli acts on both of the comonomers at the same time, an axially mirror image is generated, where the global helical sense is cancelled by the two opposite helicities induced by the constituent monomers (Figure 20b).

[62] (a) V. Jain, K.-S. Cheon, K. Tang, S. Jha, M. M. Green *Isr. J. Chem.* **2011**, *51*, 1067–1074. (b) Tang, K.; Green, M. M.; Cheon, K. S.; Selinger, J. V.; Garetz, B. A. *J. Am. Chem. Soc.* **2003**, *125* ,7313-7323.

[63] Alzubi, M.; Arias, S.; Rodríguez, R.; Quiñoá, E.; Riguera, R.; Freire, F. *Angew. Chem. Int. Ed.* **2019**, *58*, 13365-13369.

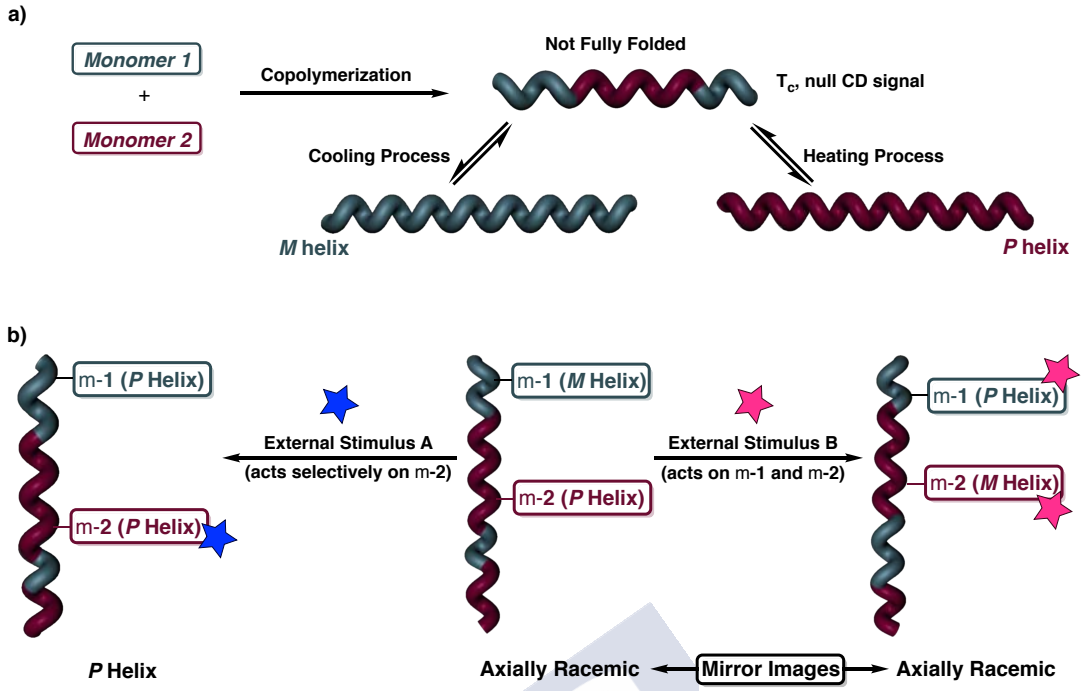

Figure 20. (a) Conceptual representation of the Chiral Conflict described by Prof. Green. (b) Conceptual representation of the Chiral Conflict effect tuned by external stimuli.

5.3.4 Majority Rules

This chiral amplification phenomena was also described by Green and co-workers for poly(isocyanate)s (poly-**10**, Figure 3). If two enantiomers of a molecule are mixed together in the presence of a small imbalance of one of them —a 0.12% of enantiomeric excess is enough—, the mixture will adopt a preferred helical sense. Due to a cooperative effect, the minor component will adopt the conformation commanded by the major component in order to avoid the presence of helix reversals (Figure 21a).[58c,62a]

This effect was also observed in dynamic helical polymers involving non-covalent interactions. Prof. Yashima's group designed a PPA bearing as pendant group a bulky aza-18-crown ether (CD=0), a receptor typically involved in recognition processes.[64] If a chiral aminoacid is added to the achiral PPA a supramolecular complex is formed, as confirmed by CD, obtaining a polymer with a preferred helical sense, which will be determined by the absolute configuration of the aminoacid (Figure 21b). poly-**34** is one of the most sensitive and useful receptor for detecting the aminoacids chirality —the presence of 0.005% of enantiomeric excess is enough to command the helix—.

58 (c) Green, M. M.; Garetz, B. A.; Munoz, B.; Chang, H. P.; Hoke, S.; Cooks, R. G. *J. Am. Chem. Soc.* **1995**, *117*, 4181-4182.
62 (a) V. Jain, K.-S. Cheon, K. Tang, S. Jha, M. M. Green *Isr. J. Chem.* **2011**, *51*, 1067–1074.
64 Nonokawa, R.; Yashima, E. *J. Am. Chem. Soc.* **2003**, *125*, 1278-1283.

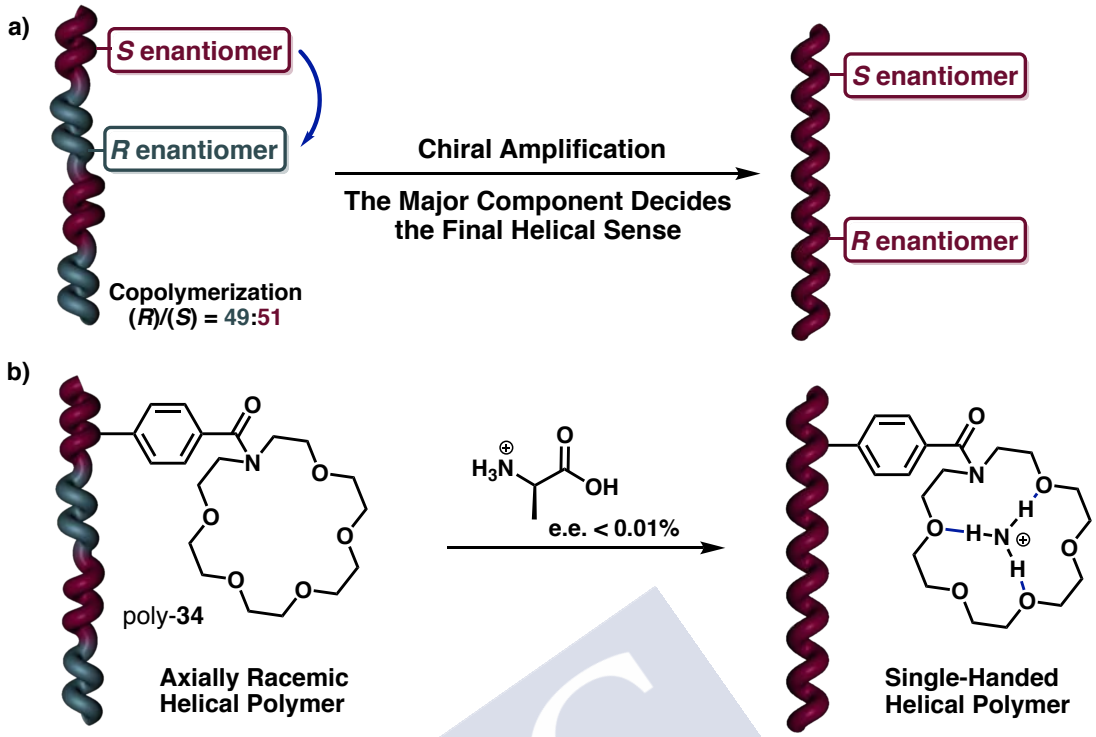

Figure 21. (a) Conceptual representation of the Majority Rule. (b) Majority Rule in PPA commanded by a supramolecular interaction.

5.3.5 Domino Effect

This chiral amplification phenomenon consists in the introduction of a chiral residue in the terminal position of an achiral oligomer, obtaining a preferred helical sense. The introduction of the chiral residue can be accomplished via covalent [65] or non-covalent interactions[66] and it was also described for polymers and oligomers (Figure 22a).

Inai and co-workers reported the most representative example of the Domino Effect.[67] They synthesized some optically inactive peptides (CD null), composed of fragments of α-aminoisobutiric acid (Aib) and (Z)-α,β-didehydrophenylalanine (Δ^zPhe) (poly-**35**) or Aib and (Z)-β-(4,4'-biphenyl)- α,β-didehydropalanine (Δ^zBip) (poly-**36**), with the N-terminal position unprotected. The chiral information of the added aminoacid that covalently attaches to the N-terminus is transferred to the whole peptide chain, resulting into a fully folded helical structure (CD active) (Figure 22b).

[65] (a) Obata, K.; Kira, M. *Macromolecules* **1998**, *31*, 4666-4668. (b) Maeda, K.; Matsuda, M.; Nakano, T.; Okamoto, Y. *Polym. J.* **1995**, *27*, 141-146. (c) Obata, K.; Kabuto, C.; Kira, M. *J. Am. Chem. Soc.* **1997**, *119*, 11345-11346.

[66] (a) Sanji, T.; Takase, K.; Sukaria, H. *J. Am. Chem. Soc.* **2001**, *123*, 12690-12691. (b) Inai, Y.; Tagawa, K.; Takasu, A.; Hirabayashi, T.; Oshikawa, T.; Yamashita, M. *J. Am. Chem. Soc.* **2000**, *122*, 11731-11732

[67] (a) Ousaka, N.; Inai, Y. *J. Org. Chem.* **2009**, *74*, 1429-1439. (b) Inai, Y.; Ousaka, N.; Okabe, T. *J. Am. Chem. Soc.* **2003**, *125*, 8151-8162.

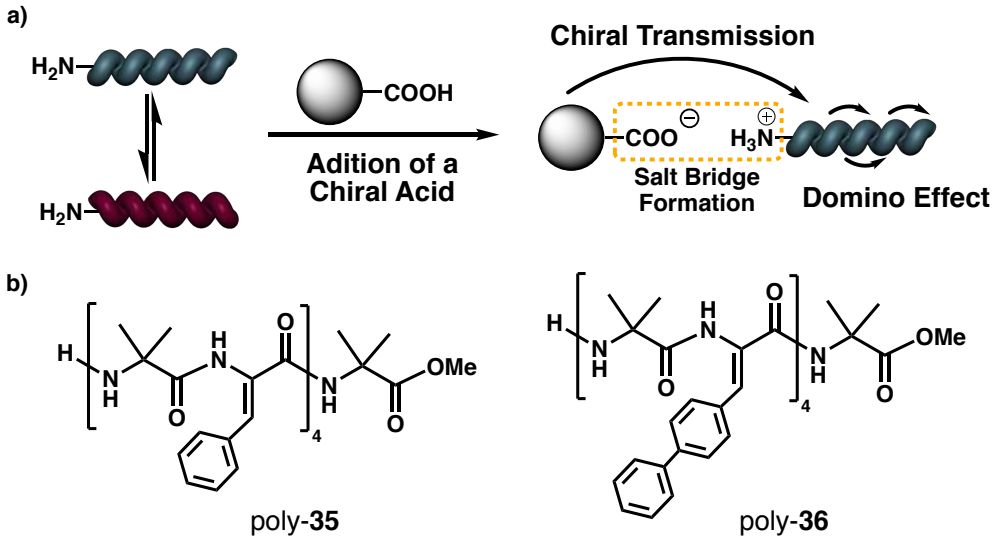

Figure 22. (a) Conceptual representation of the Domino Effect. (b) Some of the most representative examples of peptides that show Domino Effect.

5.4 Helix Inversion

The inversion of the helical sense is an interesting and unique feature of the dynamic helical polymers. Due to the high sensitivity of the aforementioned polymers to subtle changes in the environment, the helix inversion can be easily triggered by different external stimuli such as solvent polarity, temperature, addition of metal ions, light irradiation...

In our research group we have developed a dynamic helical PPA derived from the (*S*)-phenylglycine methyl ester (poly-**37**, Figure 23a).[12] In low polar solvents (e.g., $CHCl_3$) this polymer shows a negative Cotton effect, related to the less polar *anti* conformation adopted by the pendants —dihedral angle between carbonyl groups 180°—. However, if a metal ion (e.g., Ba^{2+}) is added a helical inversion is observed —*syn* conformation, dihedral angle between carbonyl groups 0°—, due to the coordination in a bidentate fashion of the pendant group to the metal. This conformational change arranges the phenyl ring in opposite orientations, triggering the helix inversion process (Figure 23a).

More recently, Feringa and co-workers have reported a PPA bearing a chiral amine (poly-**38**) that interacts with a chiral acid molecular motor, observing a chiral amplification. The conformation of the chiral acid can be modified by light irradiation, inducing a helix inversion process due to the rearrangement in the polymer structure to optimize the supramolecular interaction between the acid and the pendant group (Figure 23b).[68]

[12] Louzao, I.; Seco, J. M.; Quiñoá, E. Riguera, R. *Angew. Chem. Int. Ed.* **2010**, *49*, 1430-1433.
[68] Van Leeuwen, T.; Heideman, G. H.; Zhao, D.; Wezenberg, S. J.; Feringa, B. L. *Chem. Commun.* **2017**, *53*, 6393-6396.

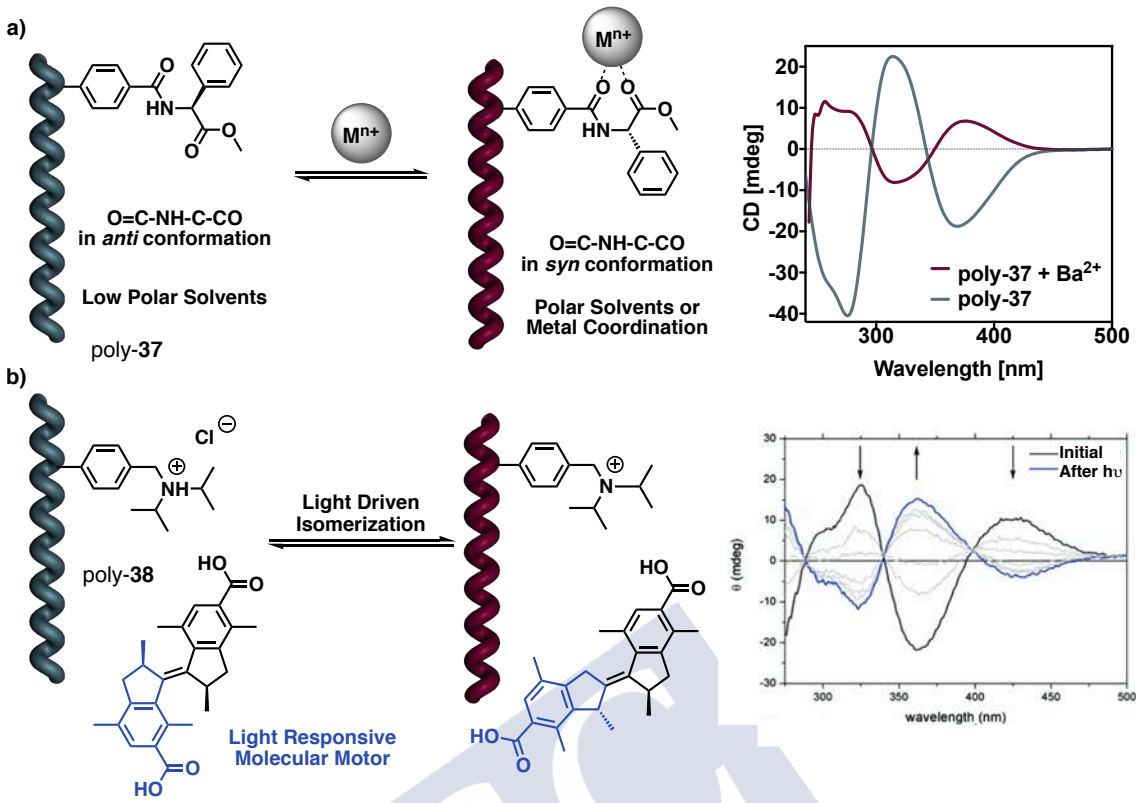

Figure 23. (a) Helix inversion in a PPA due to a change in the conformation of the pendant aroused by external stimuli. (b) Structure of poly-**38** and CD spectra showing the helix inversion in a PPA at the supramolecular level mediated by light irradiation.

5.5 Control Over the Elongation of the Polymer Chain in PPAs

As previously mentioned, the control over the optical and chiroptical properties of a polymer is key for the potential applications of these materials. Two structural factors determine these properties, the helical sense (*P* or *M* helix) and the elongation (compression/stretching) of the polymer backbone.

The elongation of the helical scaffold depends on the nature of the pendants and the possible interactions that these may form with the external stimuli. This change can be easily recorded by UV-Vis spectroscopy and, sometimes, it can even be observed by the naked eye. A helix stretching is related to a red-shift in the UV-Vis spectra (bathochromic shift), due to an increase in the conjugation of the polymer backbone (longer wavelengths), while a helix compression corresponds to a hypsochromic shift.[30a]

Having this information in mind, Maeda and co-workers developed different PPAs bearing several cyclodextrins (CyD) (α, β and γ-CyD) as pendant groups (linked to the backbone by ester, ether or amide connections) (poly-**39**).[69] It was observed that the elongation and the helical sense could be tuned by external stimuli and they applied these features in the

[30] (a) Motoshige, A.; Mawatari, Y.; Yoshida, Y.; Matsuyama, C. S.; Tabata, M.J. *Polym. Sci., Part A: Polym. Chem.* **2012**, *50*, 3008-3015.

[69] (a) Maeda, K.; Mochizuki, H.; Watanabe, M.; Yashima, E. *J. Am. Chem. Soc.* **2006**, *128*, 7639-765. (b) Yashima, E.; Maeda, K.: Sato, O. *J. Am. Chem. Soc.* **2001**, *123*, 8159-8160.

development of a new direct colorimetric detection system for neutral chemical molecules, including enantiomers (Figure 24a).

More recently, Tabata et al. reported a polymer presenting fragments of stretched and compressed scaffolds coexisting in the same backbone.[70] Changing the temperature can modify the population of these fragments, obtaining a higher proportion of contracted helix upon increasing heating. They named this phenomenon as accordion-like oscillation helix effect, HELIOS-effect (Figure 24b). Variations in the elongation of the polymer chain can also be done if a rotaxane is employed as pendant group (poly-**40**).[71] Moreover the addition of Et_3N or heating the compressed poly-**40** will recover the original stretched scaffold (Figure 24c).

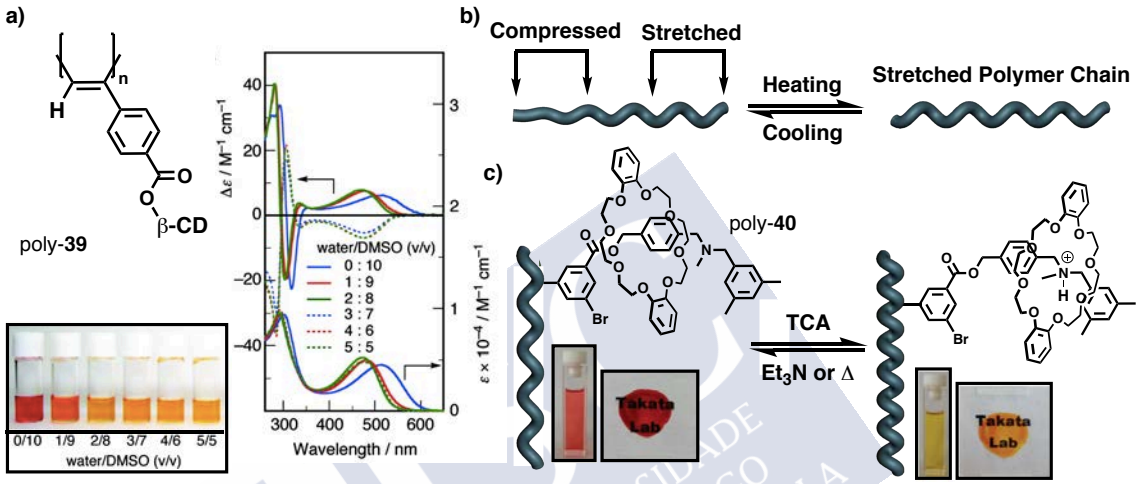

Figure 24. (a) β-cyclodextrine employed for colorimetric detection. (b) Conceptual representation of the HELIOS effect. (c) Elongation control in poly-**40** mediated by the addition of acid.

In our research group we have developed a polymer derived from the (*R*)-α-methoxy- α-trifluoromethylphenylacetic acid ((*R*)-MTPA, poly-**41**), in which the helical sense and the elongation can be selectively modulated.[27] This polymer presents two different tuneable bonds within the pendant group. On the one hand, the amide bond that can be switched from *cis*- (donor solvents) to *trans*- (non-donor solvents) depending on the donor/acceptor properties of the solvent and is responsible for the elongation of the polymer scaffold (easily tracked by UV-Vis). On the other hand, the O=C-C-OMe bond presents two major conformers that can be selectively chosen by the polarity of the media: the less polar one, the *sp* conformer —carbonyl and methoxy groups are in synperiplanar conformation (O=C-C-OMe dihedral angle, 0°)— and the more polar one, the *ap* conformer —carbonyl and methoxy groups are in antiperiplanar conformation (O=C-C-OMe dihedral angle, 180°)—. Hence, this special feature results in a polymer that can adopt four different structures (Figure 25).

[27] Leiras, S.; Freire, F.; Seco, J. M.; Quiñoá, E.; Riguera, R. *Chem. Sci.* **2013**, *4*, 2735-2743.
[70] Yoshida, Y.; Mawatari, Y.; Motoshige, A.; Motoshige, R.; Hiraoki, T.; Wagner, M.; Mullen , K.; Tabata, M. *J. Am. Chem. Soc.* **2013**, *135*, 4110-4116.
[71] (a) Ishiwari, F.; Nakazono, K.; Koyama, Y.; Takata, T. *Angew. Chem. Int. Ed.* **2017**, *56*, 14858-14862. (b) Zhu, N.; Nakazono, K.; Takata, T. *Chem. Commun.* **2016**, *52*, 3647-3649. (c) Ishiwari, F.; Nakazono, K. ;Koyama, Y.; Takata, T. *Chem. Commun.* **2011**, *47*, 11739-11741.

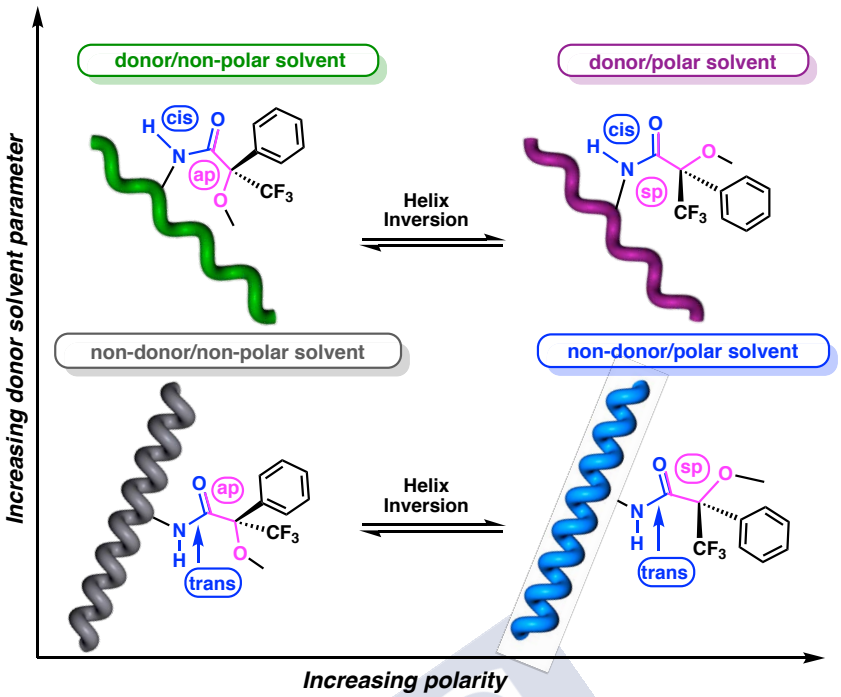

Figure 25. Conformational changes observed for poly-**41** when by modifying the solvent polarity and/or the donor/acceptor properties of the solvent.

More recently, Rodríguez *et al.*[52] described the remarkable effect that the substitution pattern on the aryl ring has over the helical scaffold. The *para*-, *meta*- and *ortho*- substituted polymers derived from MPA were synthesized. Within this polymer series (*para*-, *meta*- and *ortho*-) differences in the elongation and dynamic behaviour were encountered due to the difficulties of the pendant groups to accommodate within the helical scaffold when approaching to the backbone. The *para*-MPA (poly-**30**) presents a highly dynamic stretched helix, whereas the *ortho*-MPA (*o*-poly-**30**) is completely static and has an almost planar structure with a high tendency to the aggregation. Interestingly, the behaviour of the *meta*-(*m*-poly-**30**) counterpart lies in between, is less dynamic, showing a weak response to external stimuli, and it exists as an equilibrium of two helices, one compressed and the one stretched (Figure 26).

[52] Rodríguez, R.; Quiñoá, E.; Riguera, R.; Freire, F. *J. Am. Chem. Soc.* **2016**, *138*, 9620-9628.

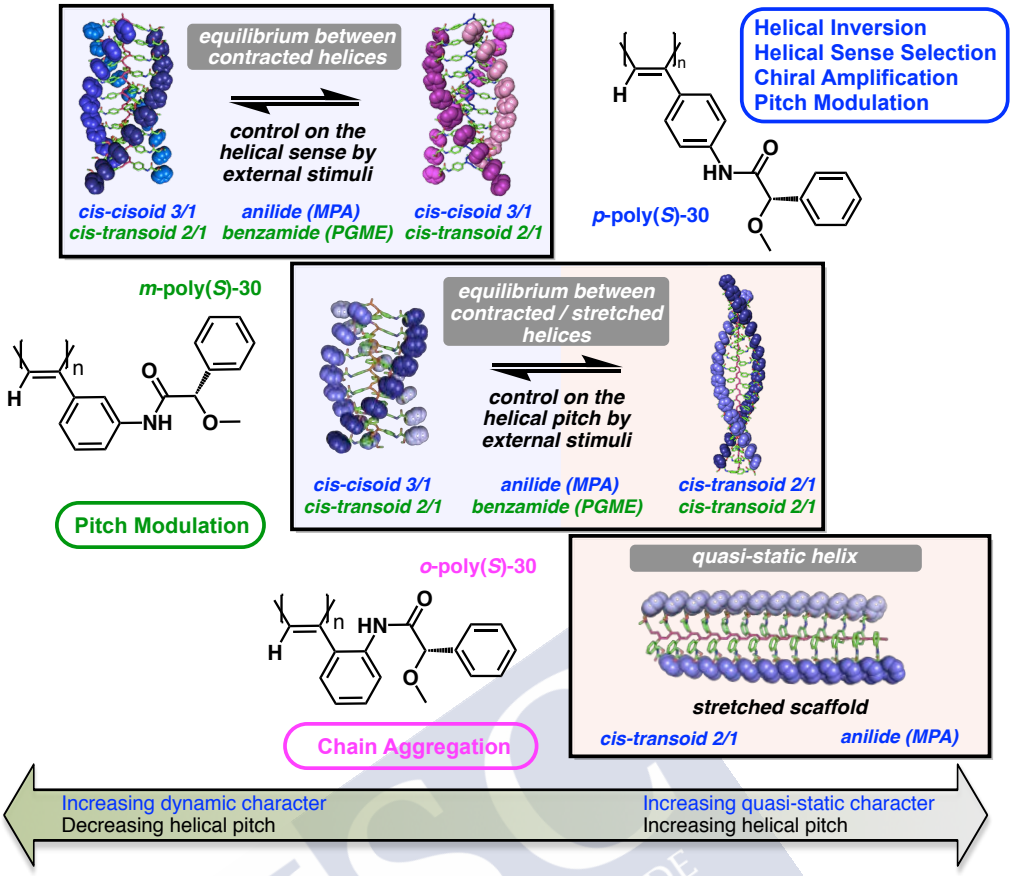

Figure 26. Schematic illustration of the effect that the different substitution pattern on the aryl ring has over the helical scaffold and the responsiveness towards external stimuli.

6. Supramolecular Assemblies of Helical Polymers

The evolution of Chemistry in the last 60 years can be illustrated by the introduction of three new concepts: macromolecules[72] —1953 Nobel Prize recognized the Prof. Staudinger's studies—, molecular recognition and supramolecular assembly[73] —these last two fields gave, in 1987, the Nobel Prize to Profs. Cram, Lehn and Pedersen—.

In biological systems, self-assembled helical scaffolds, rather than monomeric helices, are of extreme importance due to their sophisticated functions. Depending on the type of non-covalent bonding —hydrogen bonding, π-π aromatic stacking, ionic interactions, charged electrostatic interactions or their combinations— and how the molecular components are spatially arranged, different supramolecular helical architectures can be observed (films, layers, membranes, spheres and so on). Moreover, if the molecular components are chiral, the absolute configuration will be transferred to the assembly, inducing a supramolecular chirality. These features constitute the supramolecular assemblies as a very appealing topic.

[72] (a) Percec, V. Hierarchical Macromolecular Structures: 60 Years after the Staudinger Nobel Prize I. *Advances in Polymer Science*, *261*, Springer, New York, 2013. (b) Percec, V. Hierarchical Macromolecular Structures: 60 Years after the Staudinger Nobel Prize II. *Advances in Polymer Science*, 262, Springer, New York, 2013.

[73] (a) Steed, J. W.; Atwood, J. L. *Supramolecular Chemistry.* John Wiley & Sons Ltd: West Sussex, United Kingdom, 2009. (b) Cragg, P. J. *A Practical Guide to Supramolecular Chemistry*. John Wiley & Sons Ltd: West Sussex, United Kingdom, 2005. (c) Lenh, J. M. *Supramolecular Chemistry. Concepts and Perspectives.* Wiley-VCH: Weinheim, Germany, 1995.

6.1. Fibers and Superhelices

Helical PPAs can self-assemble into fiber-like structures by supramolecular interactions between the pendants of different chains. This aggregation requires the presence of adequate functional groups as well as a certain complementarity between the interacting chains. An example of this are the stereocomplexes (SCs), supramolecular assemblies formed by the interaction of stereochemically complementary stereoregular polymers. In general the SCs show better thermal and mechanical resistance and a slower degradation process than the constituting homopolymers. The forces that usually stabilize the SC are Van der Waals and electrostatic interactions.[74]

The first SC was reported in 1958, a supramolecular assembly formed by the combination of a isotactic poly(methylmethacrylate) (*it*-PMMA, *it*-poly-**42**) and an syndiotactic poly(methylmethacrylate) (*st*-PMMA, *st*-poly-**42**).[75] Nevertheless, its molecular structure, as well as the mechanism of formation, remains unsolved. Nowadays, only few examples have been reported to form SCs and are limited to the poly(methylmethacrylate) (PMMA) (poly-**42**),[76] the poly(lactic) (PLA) (poly-**43**)[77] and some polypeptides (Figure 27a).[78]

Recently, our research group described for the first time the formation of a PPA SC.[79] When the PPA, derived from MTPA (poly-**41**), is dissolved in a donor solvent (i.e., THF), the amide bond will adopt the *cis*- conformation and, as a consequence, the helical scaffold is stretched. In such a case, the external crests of the helix will be decorated with functional groups exposed and ready to form cooperative supramolecular hydrogen bonding with the complementary helix. The SC formation process starts with the dimer aggregation, evolving into a fiber-like structure that will transform into a soft gel (Figure 27b). Moreover, the formation of the SC can be reverted by modifying the conformation of the amide bond —changing the donor/acceptor properties of the media or by thermal effects—.

[74] (a) Bertin, A. *Macromol. Chem. Phys.* **2012**, *213*, 2329-2352. (b) Slager, J.; Domb, A. *J. Adv. Drug Delivery Rev.* **2003**, *55*, 549-583.

[75] Fox, T. G.; Garrett, B. S.; Goode, W. E.; Gratch, S.; Kincaid, J. F.; Spell, A.; Stroupe, J. D. J. *Am. Chem. Soc.* **1958**, *80*, 1768-1769.

[76] (a) Hatada, K.; Kitayama, T. *Polym. Int.* **2000**, *49*, 11-47. (b) Brinkhuis, R. H. G.; Schouten, A. J. *Macromolecules* **1992**, *25*, 6173-6178. (c) Spevácek, J.; Scheinder, B. *Adv. Colloid Interface Sci.* **1987**, *27*, 81-150.

[77] (a) Akagi, T.; Fujiwara, T.; Akashi, M. *Angew. Chem. Int. Ed.* **2012**, *51*, 5493-5496. (b) Furuhashi, Y.; Kimura, Y.; Yoshie, N. *Polym. J.* **2006**, *38*, 1061-1067. (c) Tsuji, H. *Macrom. Biosci.* **2005**, *5*, 569-597.

[78] (a) Nakayama, H. Manaka, T.; Iwamoto, M.; Kimura, S. *Soft. Matter* **2012**, *8*, 3387-3392. (b) Pauling, L.; Corey, R. B. *Proc. Natl, Acad. Sci. U.S.A.* **1953**, *39*, 253-256.

[79] Leiras, S.; Freire, F.; Quiñoá, E.; Riguera, R. *Chem. Sci.* **2015**, *6*, 246-253.

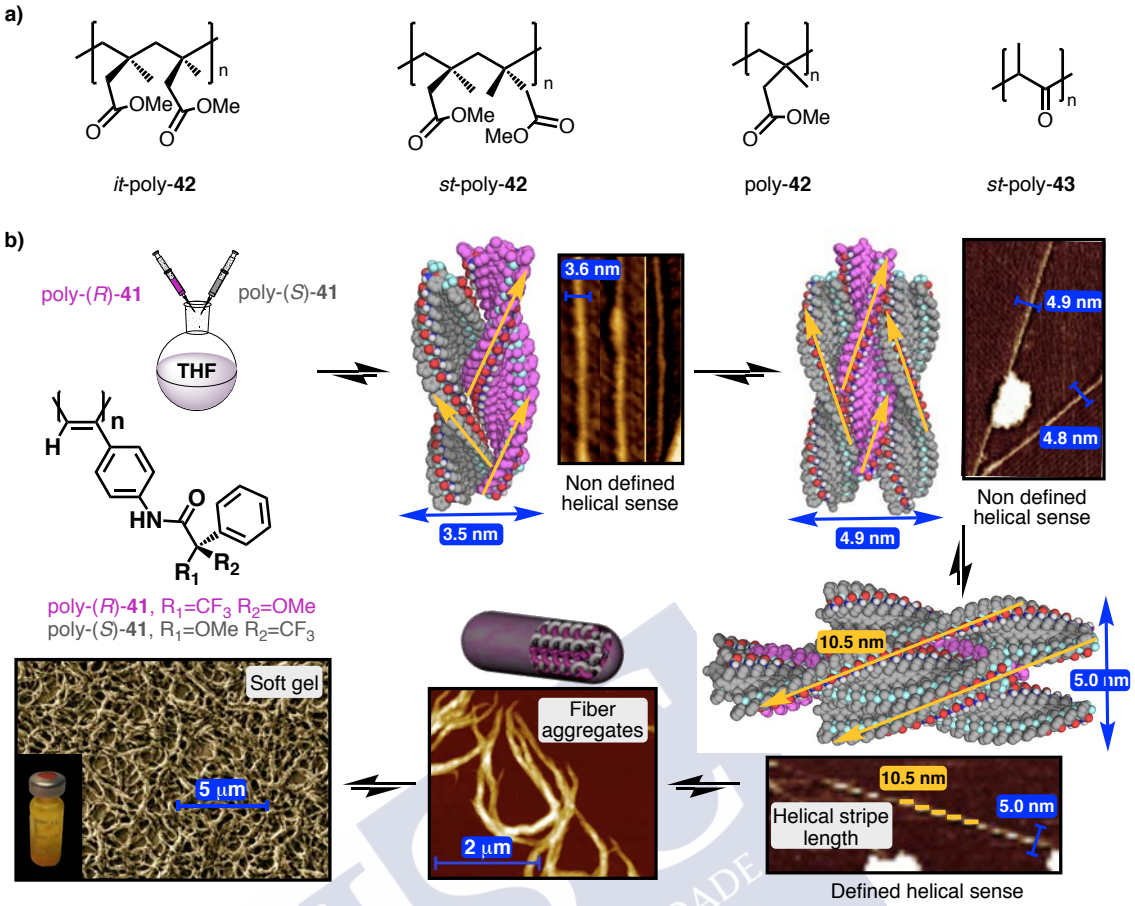

Figure 27. (a) Some examples of polymers that produce SCs. (b) Structure and conceptual representation of the sterocomplexation process for poly-**41**.

Shinohara and co-workers demonstrated the formation of double helices, by STM (Scanning Tunneling Microscopy), of an optically active PPA bearing methoxycarbonylamino groups (poly-**44**). Interestingly, during these experiments they discovered that the helix could be moved due to the interaction with the STM probe, producing the loose of the helical sense. These results pointed out the need to develop new methods to fix the molecules to the substrate.[80]

In a similar way, Tang et al. studied the supramolecular interactions established between PPAs containing different aminoacid residues (i.e., alanine (poly-**45**)).[49,81] In all cases the aminoacids were linked to the backbone by an amide linkage and the *C*-terminus could form the aggregates either protected as methyl ester (-COOMe) or free as acid (-COOH). NMR studies confirmed the intramolecular hydrogen bonding in non-polar solvents and AFM images demonstrated the formation of fibers of different diameter and length (Figure 28a and c). Interestingly, when these PPAs are dissolved in polar solvents (e.g., MeOH), different

[49] (a) Li, B. S.; Lam, J. W. Y.; Yu Z.-Q.; Tang, B. Z. *Langmuir* **2012**, *28*, 5770-5774. (b) Li, B. S.; Kang, S. Z.; Cheuk, K. K. L.; Wan, L.; Ling, L.; Bai, C.; Tang, B. Z. *Langmuir* **2004**, *20*, 7598-7603;

[80] Shinohara, K.; Yasuda, S.; Kato, G.; Fujita, M.; Shigekawa, H. *J. Am. Chem. Soc.* **2001**, *123*, 3619-3620.

[81] (a) Cheuk, K. K. L.; Li, B. S.; Lam, J. W. Y.; Xie, Y.; Tang, B. Z. *Macromolecules* **2008**, *41*, 5997-6005. (b) Li, B.S.; Cheuk, K. K. L.; Ling, L.; Chen, J. Xiao, X.; Bai, C.; Tang, B. Z. *Macromolecules* **2003**, *36*, 77-85. (c) Li, B. S.; Chreuk, K. K. L.; Yang, D.; Lam, J. W. Y.; Wan, L. J.; Bai, C.; Tang, B. Z. *Macromolecules* **2003**, *36*, 5447-5450. (d) Cheuk, K. K. L.; Lam, J. W. Y.; Chen, J.; Lai, L. M.; Tang, B. Z. *Macromolecules* **2003**, *36*, 5947-5959. (e) Li, B. S:; Cheuk, K. K. L.; Salhi, F.; Lam, J. W. Y.; Cha, J. A. K.; Xiao, X.; Bai, C, Tang, B. Z. *Nano Lett.* **2001**, *1*, 323-328.

aggregation structures, such as micelles, are obtained —PPA backbone in the core and aminoacids exposed to the solvent; the PPA presents an amphiphilic character— (Figure 28d). These micelles can form intermolecular hydrogen bonds, resulting into larger micelles that will eventually collapse into fiber-like structures (Figure 28b).

Akagi and co-workers reported the formation of PA superhelical structures in liquid crystals (poly-**46**) doped with chiral dopants. The initial single polymer chains grow to form polymer bundles that will finally self-assemble into nest-like spiral structures (Figure 28e, f).[82]

Additionally, Yashima's group demonstrated that the introduction of repulsive forces among the pendants, either by steric hindrance (poly-**39**)[83] or by repulsive electrostatic forces (poly-**47**)[84], produced supramolecular aggregates —formed due to the planarity induced in the helix by the pendants— (Figure 28g and h respectively).

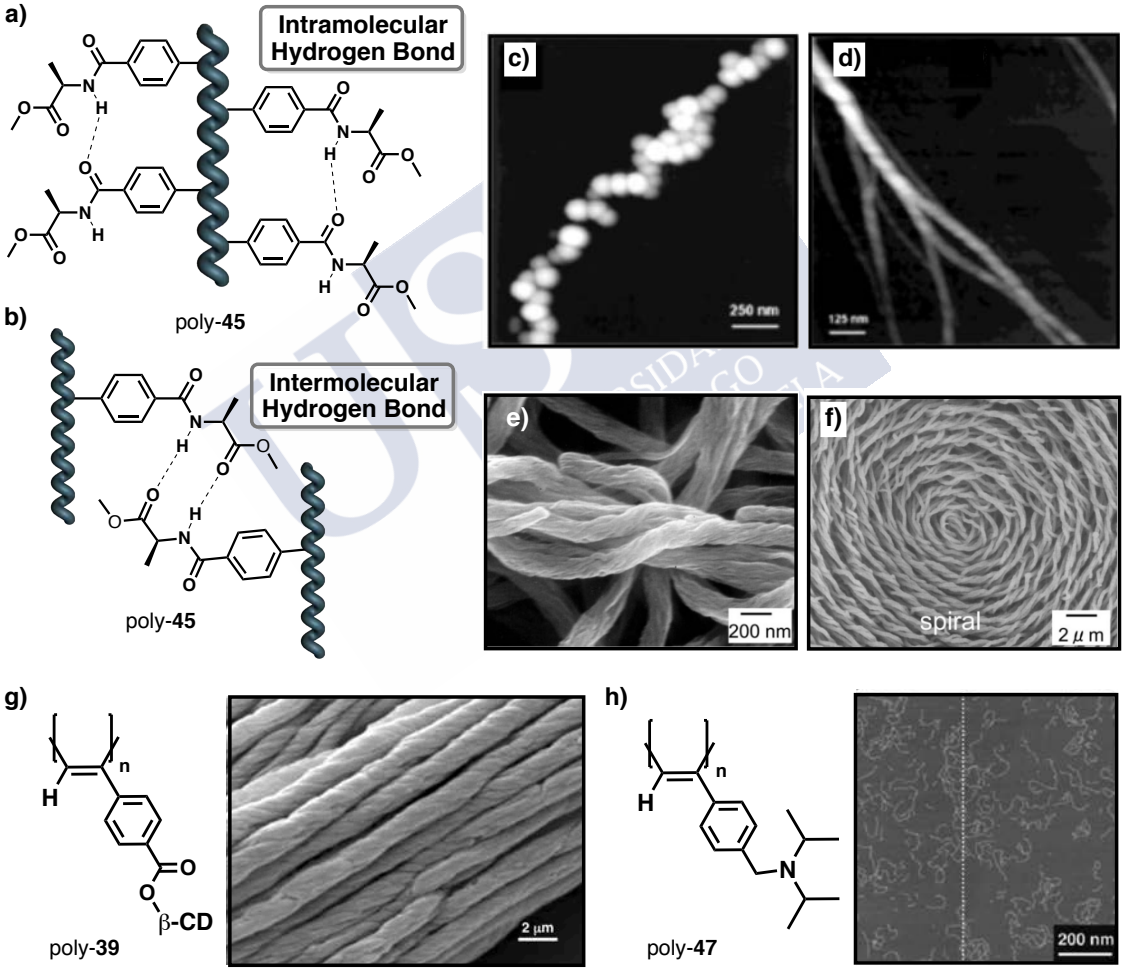

Figure 28. Schematic illustration of the formation of the supramolecular structure for poly-**45** via (a) intramolecular or (b) intermolecular interactions. AFM images for the (c) pearl-like and (d) superhelical structures of poly-**45** (e), (f) SEM (Scanning Electron Microscopy) images of the superhelical structures generated by poly-**46**. (g) SEM image of the self-assemble structure obtained for poly-**39**. (h) AFM image of the individual fibres obtained for poly-**47** due to the repulsive forces formed after the addition of a chiral acid.

[82] Akagi, K. *Chem. Rev.* **2009**, *109*, 5354-5401.
[83] Maeda, K.; Mochizuki, H.; Osato, K.; Yashima, E. *Macromolecules* **2011**, *44*, 3217-3226.
[84] Nagai, K.; Maeda, K.; Takeyama, Y.; Sato, T.; Yashima, E. *Chem. Asian J.* **2007**, *2*, 1314-1321.

6.2. Nanoparticles Based on PPAs

Polymer nanoparticles can be defined as nanospheres or nanocapsules made of any type of polymer and with a range size between 10 nm and 1000 nm. Nanospheres are spherical and solid and, frequently, are used to adsorb molecules on their surface. Nanocapsules are colloidal particles consisting of a hollow core surrounded by the polymeric cover. Due to their empty nature, these vesicles are usually employed for encapsulation.[85]

The possibility to selectively choose the size and morphology, as well as the introduction of chirality into these nanostructures, has attracted great interest into the scientific community during the last decade.

The main protocols for preparing polymer nanoparticles are discussed next.

Emulsification Method

In this method the mixture of the corresponding polymer solution together with a surfactant produces the polymer particles as an emulsion (Figure 29). Deng *et al.* used this procedure for the formation of nanoparticles derived from PPAs, concluding that the nanoparticles size depends on the emulsifier concentration: the higher the concentration (more micelles in the medium), the smaller is the particle size.[86]

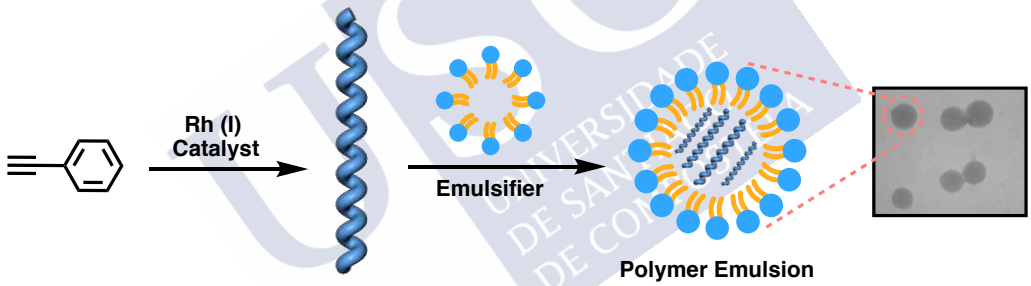

Figure 29. Schematic illustration of the emulsification method for the formation of nanonparticles.

Emulsion Polymerization

Unlike the emulsification method, in this process the polymerization takes place *in situ*, in a heterogeneous system generally formed by an aqueous phase and a non-aqueous phase (Figure 30). Hence, it requires a monomer with low solubility in water, a water-soluble initiator and a surfactant.

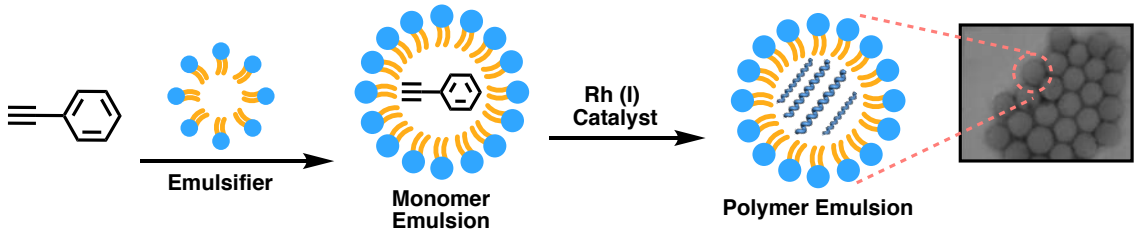

Figure 30. Schematic illustration of the emulsification polymerization process for the formation of nanonparticles.

[85] Freire, F.; Quiñoá, E.; Riguera, R. *Chem. Rev.* **2016**, *116*, 1242-1271.
[86] Zhang, Y. Y.; Luo, X. F.; Deng, J. P.; Yang, W. T. *Macromol. Chem. Phys.* **2011**, *212*, 353-360.

Also Deng's group explored this method. Starting from several PAs they were able to produce optically active nanoparticles. In addition they also described the formation of small-sized (90 nm) macroscopically racemic PPAs particles.[87]

Metal-Driven Nanostructuration

Nanoparticles based on PPAs can also be obtained by using non-covalent cross-linking agents. Our research group reported, for the first time, the formation of polymer nanoparticles by using metal cations as supramolecular cross-linking agents. For poly-**30** it was observed that the addition of a metal ion produced not only a chiral amplification, but also a nanosphere.[46b] Moreover, the size and chiral content of this nanostructure can be controlled by the polymer/metal ratio and the solvents used to dissolve the polymer[46a] as well as by the metal ion valence.[60,88] Hence, when a cosolvent of high boiling point is added, nanotubes are produced, while toroids are obtained if the cosolvent added reduces the solubility of the polymer and, by changing the valence of the metal ion, the chirality of the surface is modified. The encapsulation ability of these nanostructures was further demonstrated by the encapsulation of iron oxide magnetic particles, quantum dots or organic molecules such as fluorescent dyes (Figure 31).[46b]

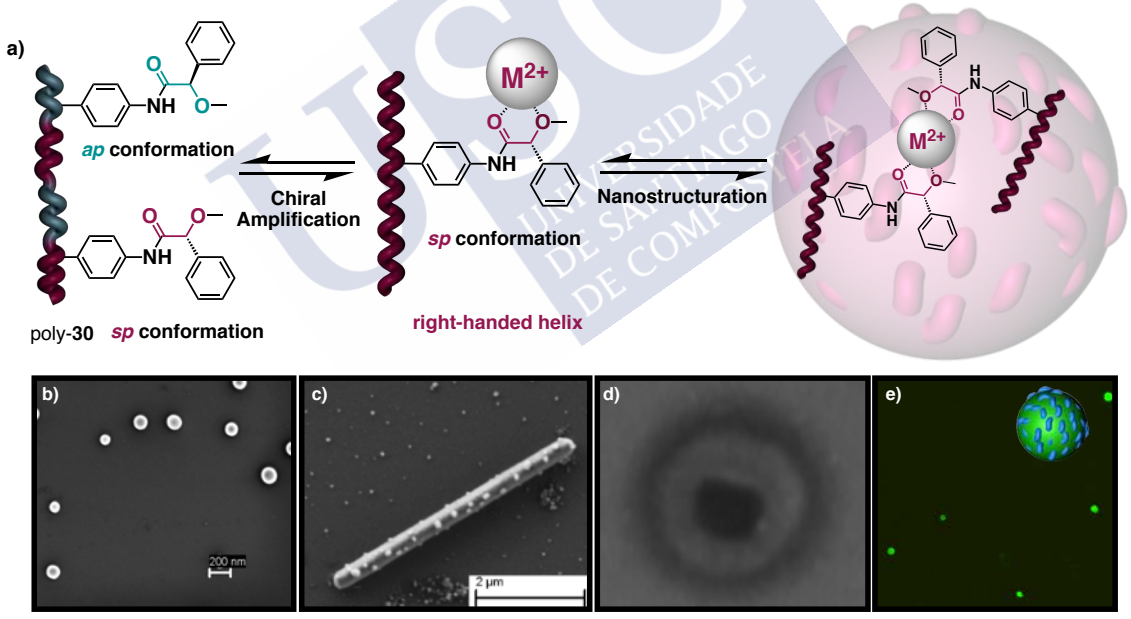

Figure 31. (a) Schematic illustration of the formation of nanospheres by using metal cations as cross-linking agents to obtain a helical polymer-metal complex (HPMC). (b) SEM images of nanospheres based on HPMCs. (c) SEM images of nanotubes based on HPMCs. (d) SEM images of nanotorus based on HPMCs. (e) Confocal image of HPMCs containing fluorescein.

87 (a) Chen, B.; Liu, X.; Xu, C.; Song, C.; Luo, X.; Yang, W.; Deng, J. *Macromol. Chem. Phys.* **2012**, *213*, 603-609. (b) Luo, X. F.; Kai, N. W.; Li, L.; Deng, J. P.; Yang, W. T. J. *Polym. Sci., Part A: Polym. Chem.* **2010**, *48*, 1661-1668. (c) Chen, B.; Deng, J.; Tong, L.; Yang, W. Macromolecules **2010**, 43, 9613–9619. (d) Deng, J. P.; Chen, B.; Luo, X. F.; Yang, W. T. *Macromolecules* **2009**, *42*, 933-938.

46 (a) Arias, S.; Freire, F; Quiñoá, E.; Riguera, R. *Angew. Chem. Int. Ed.* **2014**, *53*, 13720-13724. (b) Freire, F.; Seco, J. M.; Quiñoá, E.; Riguera, R. *J. Am. Chem. Soc.* **2012**, *134*, 19374-19383.

88 (a) Arias, S.; Núñez-Martínez, M.; Quiñoá, E.; Riguera, R.; Freire, F. *Small* **2017**, *13*, 1602398. (b) Arias, S.; Núñez-Martínez, M.; Quiñoá, E.; Riguera, R.; Freire, F. *Polym. Chem.* **2017**, *8*, 3740-3745.

60 Arias, S.; Bergueiro, J.; Freire, F.; Quiñoá, E.; Riguera, R. *Small* **2016**, *12*, 238-244.

7. Applications of the PPAs

7.1. Chiral Recognition

Chiral HPLC is one of the most powerful techniques for the separation of enantiomers nowadays. The development of new materials for Chiral Stationary Phases (CSPs) showing good chiral recognition ability towards the different racemates is essential for their practical use (in analytical and preparative purposes). The different chiral selectors used as CSPs for HPLC can be based either on small molecules (polysaccharides or proteins) or polymers. Although several CSPs are commercially available, not all existing racemates can be resolved yet.[89]

In 1979, Okamoto and co-workers reported a CSP based on an optically active poly(metacrylate) (poly-**6**, Figure 2) that showed, for the first time, a high chiral recognition ability.[90] The chirality of poly-**48** to discriminate between enantiomers, attributed to its rigid helical structure, was evaluated for two different types of CSPs —one of them was prepared by grounding the polymer into small particles while the other by coating macroporus silica with poly-**48**—. These CSPs showed different chiral recognition abilities for several racemates, such as **49**. This is due to the different orientation of the polymer in the bulk and on the surface of the silica gel (Figure 32).[91] Moreover, this milestone discovery allowed the efficient resolution of racemates with any functional group, which were difficult to resolve on other CSPs.

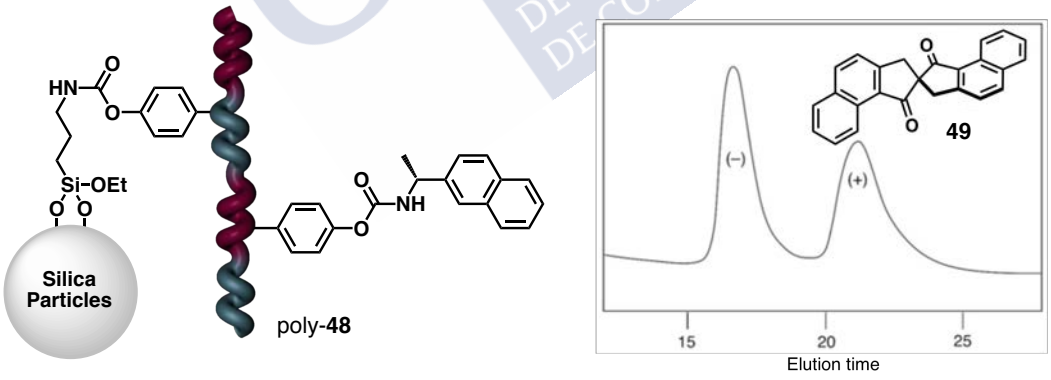

Figure 32. (a) Structure of poly-**48** and chromatogram showing the different retention times for the enantiomers of **49**.

PPAs have also been applied as CSPs into chiral HPLC. As an example, Maeda *et al.* developed an elution order switchable CSP by switching the helical sense of the polymer employed for chiral recognition. This polymer, derived from 2-2'-byphenol (axially racemic)

89 Okamoto, Y.; Ikai, T. *Chem. Soc. Rev.* **2008**, *37*, 2593-2608.
90 Okamoto,Y.; Suzuki, K.; Ohta, K.; Hatada, K.; Yuki, H. *J. Am. Chem. Soc.* **1979**, *101*, 4763-4765.
91 (a) Okamoto, Y.; Mohri, H.; Hatada, K. *Polym. J.* **1989**, *21*, 439-445. (b) Yuki, H.; Okamoto, Y.; Okamoto, I. *J. Am. Chem. Soc.* **1980**, *102*, 6356-6358.

(poly-**50**), shows a preferred helical sense upon addition of (*R*) or (*S*)-phenylethanol ((*R*)-**51** and (*S*)-**51**) and, after the removal of the chiral alcohol, the adopted helical sense is retained. Now, the initially axially racemic (poly-**50**), is capable of separating the racemates (i.e., *trans*-stilbene (**52**)) (Figure 33).[92] More recently, Maeda's group, in collaboration with our research group, has developed a novel three-state switchable CSP based on poly-**30**.[93]

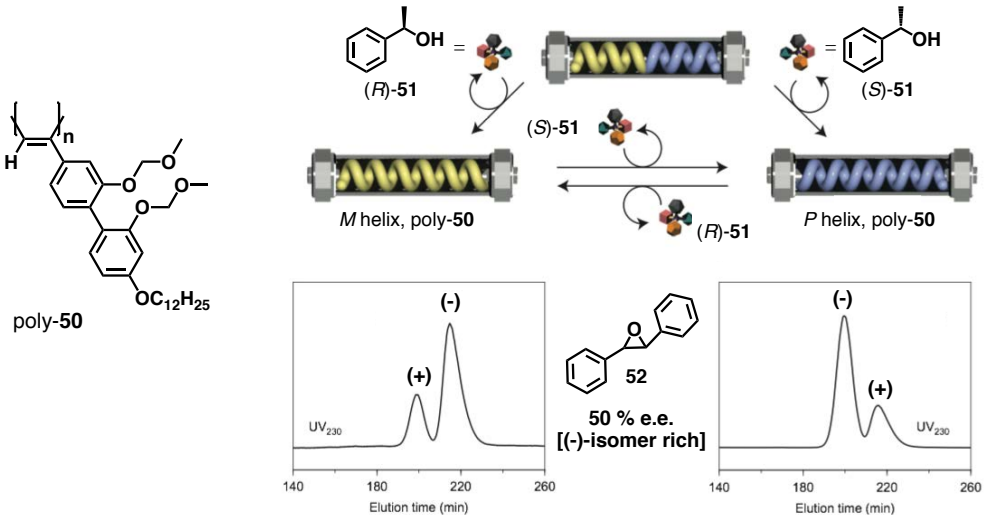

Figure 33. Structure of poly-**50** and conceptual representation of the effect that the chiral amplification and the memory of macromolecular helicity have over the final enantioseparation (e.g., *trans*-stilbene, **52**).

7.2. Sensors

The possibility of tuning the helical polymers by the addition of external stimuli makes these materials suitable for their use as sensors. Different PPAs have been designed for the detection of metals,[94] anions or even as thermal sensors.[95]

In our research group several sensors have been developed. As previously mentioned, poly-**30**[45] can differentiate between monovalent or divalent metal ions, producing enantiomeric CD traces, while poly-**37**[12] or poly-**53**[96] —which is derived from a dipeptide of glycine and (*R*)-α-methoxy-α-phenylacetic acid— can classify the solvents according to their polarity. Moreover, in a more complex example, poly-**41** will modify not only its helical sense but also its elongation, attending to the polarity and the donor/non-donor properties of the solvent.[27]

The aforementioned poly-**39**, described by Yashima *et al.*, can act as a colorimetric sensor. Upon complexation with chiral guests molecules a helical inversion accompanied by a

12 Louzao, I.; Seco, J. M.; Quiñoá, E. Riguera, R. *Angew. Chem. Int. Ed.* **2010**, *49*, 1430-1433.
27 Leiras, S.; Freire, F.; Seco, J. M.; Quiñoá, E.; Riguera, R. *Chem. Sci.* **2013**, *4*, 2735-2743.
45 Freire, F.; Seco, J. M.; Quiñoá, E.; Riguera, R. *Angew. Chem. Int. Ed.* **2011**, *50*, 11692-11696.
92 Shimomura, K.; Ikai, T.; Kanoh, S.; Yashima, E.; Maeda, K. *Nat. Chem.* **2014**, *6*, 429-434.
93 Hirose, D.; Isobe, A.; Quiñoá, E.; Freire, F.; Maeda, K. *J. Am. Chem. Soc.* **2019**, *141*, 8592-8598.
94 Alzubi, M.; Arias, S.; Louzao, I.; Quiñoá, E.; Riguera, R.; Freire, F. *Chem. Commun.* **2017**, *53*, 8573-8576.
95 Zhou, Y.; Zhang, C.; Qiu, Y.; Liu, L.; Yang, T.; Dong, H.; Satoh, T.; Okamoto, Y. *Molecules* **2016**, *21*, 1583.
96 Rodríguez, R.; Quiñoá, E.; Riguera, R.; Freire, F. *Small* **2019**, *15*, 1805413.

colour change is observed, as it happens when changing the solvent composition or the temperature (Figure 34a). Additionally, poly-**39** can selectively distinguish the 1-phenylethylamine enantiomers and, depending on the CyD attached to the backbone, molecules with similar size and functional groups (Figure 34b).[69,83]

In a similar way, Kakuchi and co-workers developed some colorimetric sensors for the detection of anions in organic solvents (poly-**54**), as well as in aqueous media.[97] The anions interact with the pendants of the polymer producing a deprotonation. Due to the proximity of the pendants within the helical scaffold this deprotonation generates electrostatic repulsions between charges, forcing the helical scaffold to adopt a stretched structure. This stretching can be easily observed not only microscopically but also macroscopically; therefore the initial yellow solution will become red after deprotonation (Figure 34c).

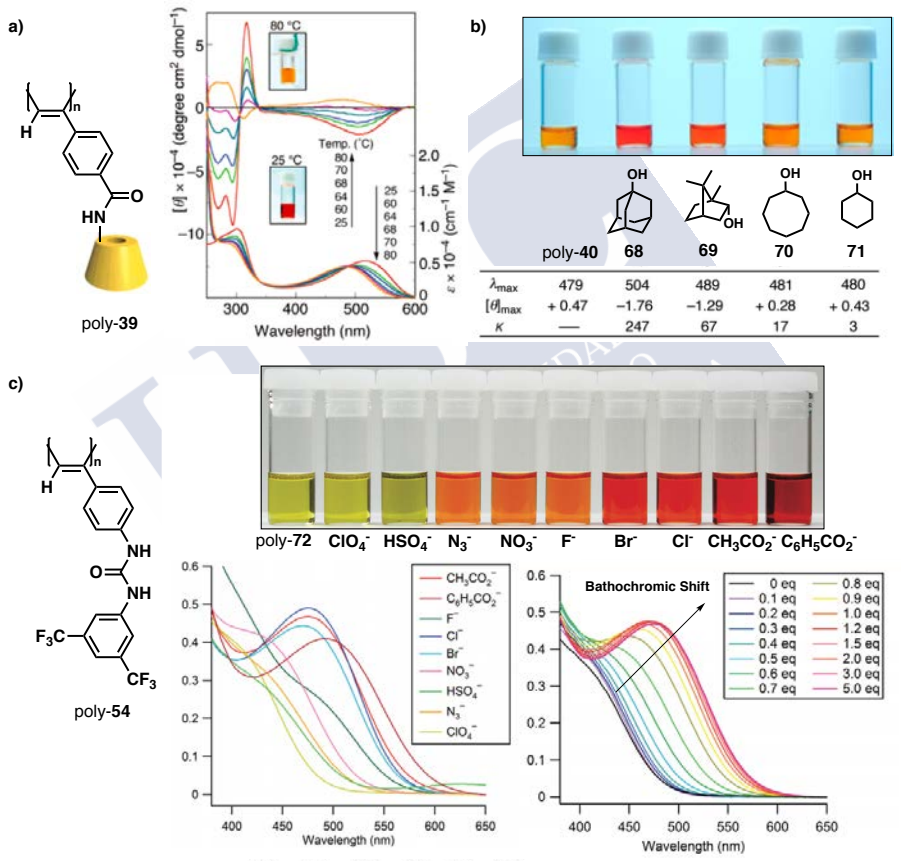

Figure 34. (a) Structure of poly-**39** and temperature dependent CD showing the stretching upon increasing the temperature. (b) Colorimetric detection by poly-**39** of different alcohols. (c) Structure of poly-**54**. The panel on the left shows the detection ability of poly-**54** towards different anions. On the right, a titration with increasing amounts of acetate anion is depicted, showing the bathochromic shift in the polyenic band.

69 (a) Maeda, K.; Mochizuki, H.; Watanabe, M.; Yashima, E. *J. Am. Chem. Soc.* **2006**, *128*, 7639-765. (b) Yashima, E.; Maeda, K.: Sato, O. *J. Am. Chem. Soc*. **2001**, *123*, 8159-8160.

83 Maeda, K.; Mochizuki, H.; Osato, K.; Yashima, E. *Macromolecules* **2011**, *44*, 3217-3226.

97 (a) Sakai, R.; Barasa, E. B.; Sakai, N.; Sato, S.-I; Satoh, T.; Kakuchi, T. *Macomolecules* **2012**, *45*, 8221-8227. (b) Sakai, R.; Sakai, N.; Satoh, T.; Li, W; Zhang, A.; Kakuchi, T. *Macromoleules* **2011**, *44*, 4249-4257.(c) Sakai, R.; Okade, S.; Barasa, E. B. Kakuchi, R. Ziabka, M.; Umeda, S.; Tsuda, K.; Satoh, T.; Kakuchi, T. *Macromolecules* **2010**, *43*, 7406-7411. (d) Qu, Y.; Hua, J.; Jiang,, Y.; Tian, H. J. *Polym. Sci. Part A: Polym. Chem.* **2009**, *47*, 1544-1552. (e) Kakuchi, R.; Nagata, S.; Tago, Y.; Sakai, R.; Otsuke, I.; Satoh, T.; Kakuchi, T. *Macromolecule*s **2009**, *42*, 1476-1481. (f) Kakuchi, R.; Kodama, T.; Shimada, R.; Tago, Y.; Sakai, R.; Satoh, T.; Kakuchi, T. *Macromolecules* **2009**, *42*, 3892-3987. (g) Kakuchi, R.; Nagata, S.; Saki, R.; Otsuka, I.; Nakada, H.; Satoh, T.; Kakuchi, T. *Chem. Eur. J.* **2008**, *14*, 10259-10266.

7.3. Asymmetric Catalysis

Much interest has been focused on the development of polymers based on chiral ligands for catalytic asymmetric synthesis due to their easy recovery and recyclability. The pioneering work of Regellin and coworkers reported the formation of a complex between a poly(metacrylate) —containing a bis(2-pyridyl)phenylmethyl— and palladium (poly-**55**), resulting into a catalytic system that promoted an asymmetric allylic alkylation. Although the novelty of this approximation, the e.e. was still moderate (60%) and a high amount of catalyst was needed (25% mol) (Figure 35a).[98]

Since this grounbreaking discovery, many different examples based on poly(quinoxilane)s, poly(isocyanide)s or PPAs have been described. As an example, Yashima *et al.* published several PPAs bearing cinchona as chiral inductor (poly-**56**). They observed that by modifying the connection to the backbone (i.e., ester, amide, sulphonamide...) these PPAs could be used for different asymmetric catalysis reactions, such as: the Henry reaction, enantioselective desymmetrization of prochiral cyclic anhydrides or aza-Michael additions among others (Figure 35b).[99]

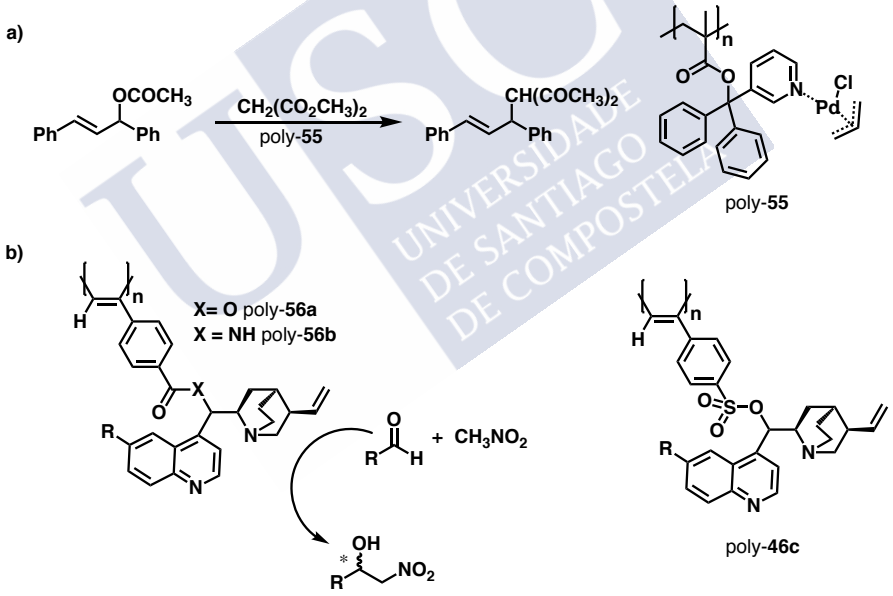

Figure 35. Some examples on asymmetric catalysis employing helical polymers.

[98] (a) Reggelin, M.; Doerr, S.; Klussmann, M.; Schultz, M.; Holbach, M. *Proc. Natl. Acad. Sci. U.S.A.* **2004**, *101*, 5461-5466. (b) Reggelin, M.; Schultz, M.; Holbach, M. *Angew. Chem. Int. Ed.* **2002**, *41*, 1614-1617. (c) Yashima, E.; Maeda, Y.; Okamoto, Y. *Polym. J.* **1999**, *31*, 1033-1036.

[99] (a) Takata, L. M. S.; Iida, H.; Shimomura, K.; Hayashi, K.; DosSantos, A. A.; Yashima, E. *Macromol. Rapid Commun.* **2015**, *36*, 2047-2054. (b) Tang, Z.; Iida, H.; Hu, H. Y.; Yashima, E. *ACS Macro Lett.* **2012**, *1*, 261-265. (d) Miyake, G. M.;Iida, H.; Hu, H. Y.; Tang, Z.; Chen, E. Y. X.; Yashima, E. *J. Polym. Sci. Part A: Polym. Chem.* **2011**, *49*, 5192.

8. Supramolecular Helical Polymers

Helical polymers can be obtained by covalent or non-covalent interactions. The covalent polymerization mostly occurs under kinetic control and becomes irreversible due to the high potential barrier for depolymerisation, which is larger than the forward reaction. As a result, dilution or heating of the macromolecule will not result in a decrease of the molecular weight, due to the covalent forces established among pendants.

In an opposite scenario, helical polymers obtained by supramolecular interactions are characterised by a high reversibility. This is arisen by the moderately strong non-covalent forces —e.g., hydrogen bonding, π·π stacking and Van der Waal's forces— that bring the monomers together. Hence, the stability of these high molecular weight linear polymers will be dependent on the concentration, temperature and pressure.

8.1. Thermodynamic Parameters

Considering the mechanistic viewpoint for supramolecular polymers, the polymerization process is considered to occur through a set of chemical equilibriums, each one described by its equilibrium constant (K_{nuc} and K_{elo}). Attending to the mechanism through which each monomer is added, supramolecular polymers can be formed by an isodesmic or a cooperative polymerization process.[100]

During the isodesmic polymerization process, the non-covalent interactions established among pendants remain unaffected by increasing the length chain. As each addition is equivalent (same equilibrium constant; $K_{nuc} = K_{elo}$), the polymer growth will be favoured by increasing the concentration of monomers in solution or by decreasing the temperature of the sample (Figure 36b).

The cooperative polymerization process typically occurs under thermodynamic control and involves two phases, a less favoured nucleation stage (K_{nuc}) followed by a favoured polymerization phase (K_{elo}). The formation of long polymer chains will depend on the monomer concentration as well as on the temperature or the solvent composition, resulting into a sharp transition from a regime dominated by free monomers as small aggregates to a regime composed, mostly, by large polymers (Figure 36b).

The mechanism of self-assembly in organic solvents has been widely studied through temperature dependent UV-Vis and CD spectroscopy, allowing the identification of these two self-assembly processes. Plotting the variation of an intrinsic property (typically the normalized spectroscopic signal at a certain wavelength) as a function of the temperature provides the cooling curve. If the resulting curve is sigmoidal the polymerization will follow an isodesmic process, whether if a hyperbole along a slope with no angle is obtained the polymerization will follow a cooperative process (Figure 36a). In all cases the cooling curves

[100] Dorca, Y.; Greciano, E. E.; Valera, J. S.; Gómez, R.: Sánchez, L. *Chem. Eur. J.* **2019**, *25*, 5848-5864.

need to be recorded at slow rates to avoid the possible hysteresis and ensure that the system remains in thermodynamic control.

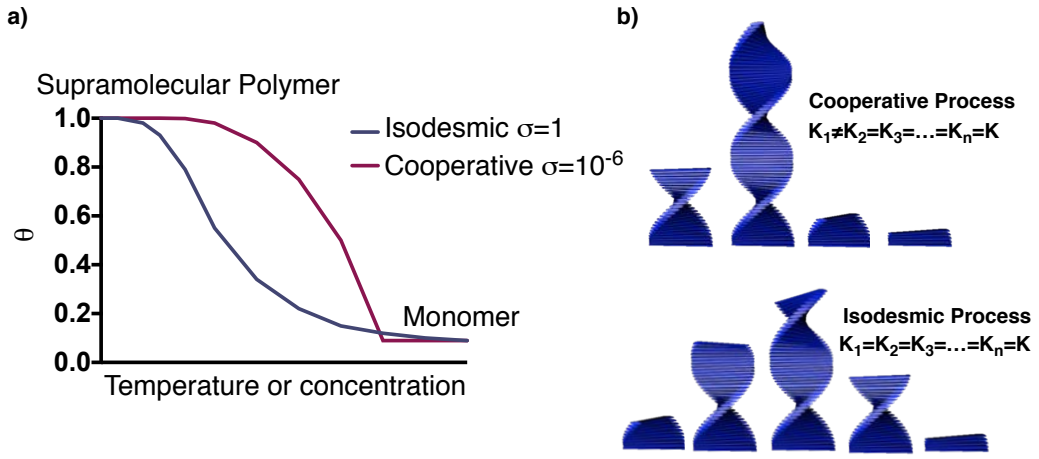

Figure 36. (a) Typical cooling curves for the isodesmic and cooperative processes. (b) Conceptual representation of the influence of the polymerization mechanism over the final outcome.

The obtained cooling curves are typically fitted with the Mass-Balance (MB) mathematical model. In this case, the fraction of aggregated species at different temperatures is simulated based on Mass-Balance equations for different sets of thermodynamic parameters that describe the equilibrium in the nucleation phase (K_{nuc}, characterized by ΔH_{nuc} and ΔS_{nuc}), as well as in the equilibrium in the elongation phase (K_{elo}, characterized by ΔH_{elo} and ΔS_{elo}), and both phases are separated by the characteristic temperature T_e (elongation temperature). The accuracy of the obtained values is kept by fitting the cooling curve at multiple concentrations. The cooperativity is quantified by the following expression (Equation 3).

$$\sigma = \frac{K_{nuc}}{K_{elo}} = e^{\Delta H_{np}/R \cdot T}$$

Equation 3. Mathematical statement to determine the degree of cooperativity of the polymerization process.

In equation 3 it is assumed that $\Delta S_{elo} = \Delta S_{nuc}$ to facilitate the fitting, therefore a new expression has to be introduced, the nucleation penalty ΔH_{np} —defined as ΔH_{elo}-ΔH_{nuc}—. The more negative ΔH_{np} becomes, the smaller σ is and higher is the cooperativity ($\sigma < 0$). In case $\Delta H_{elo} = \Delta H_{nuc}$, $\sigma = 1$ and the system will follow an isodesmic process.[101]

8.2. Cooperative Polymerization

Usually, during the supramolecular polymerization process the monomer first aggregates into a kinetically preferred structure that depolymerizes and subsequently polymerizes into the thermodynamically stable aggregate. Self-assembled systems, particularly those governed by a cooperative mechanism, often exist as more than one single structure, suggesting that not only the parameter time but also the kinetic contributions will play a key role in the final outcome.

[101] Kulkarni, C.; Meijer, E. W.; Palmans, A. R. A. *Acc. Chem. Res.* **2017**, *50*, 1928-1936.

8.2.1. Thermodinamically Controlled Polymerization

One of the most known examples of supramolecular polymers is the 1,3,5-benzenetricarboxamides (BTAs) (poly-**57**), described by Meijer *et al.*[102] The three amide groups present in the monomer core form a triple array of hydrogen bonds, placing the adjacent molecules one on top of the other with a rotation angle of 60°, which allows the effective π stacking of aromatic units. The VT-UV-Vis and VT-CD experiments, recorded in *n*-heptane at dilute concentrations for a BTA bearing chiral alkyl chains, revealed a non-sigmoidal behaviour. Fitting the data to the MB model yields the cooperativity factor, $\sigma = 5.7 \cdot 10^{-7}$, confirming the cooperative nature of the polymerization process. DFT calculations based on computations of BTA oligomers indicated that the hydrogen bonds between monomers are the main forces involved in the stabilization of the assembly and that the most likely size of the nucleus is a dimer or trimer. Further monomer additions exert no effect on the stabilization of the aggregate (Figure 37a).[103]

The cooperative self-assembly was also observed in BTAs bearing linear and branched alkyl chains as substituents (poly-**58**)[103,104] as well as in BTAs with inverted amide linkage (poly-**59**)[105] or even bearing thioamides (poly-**60**) (Figure 37b, c and d respectively).[106]

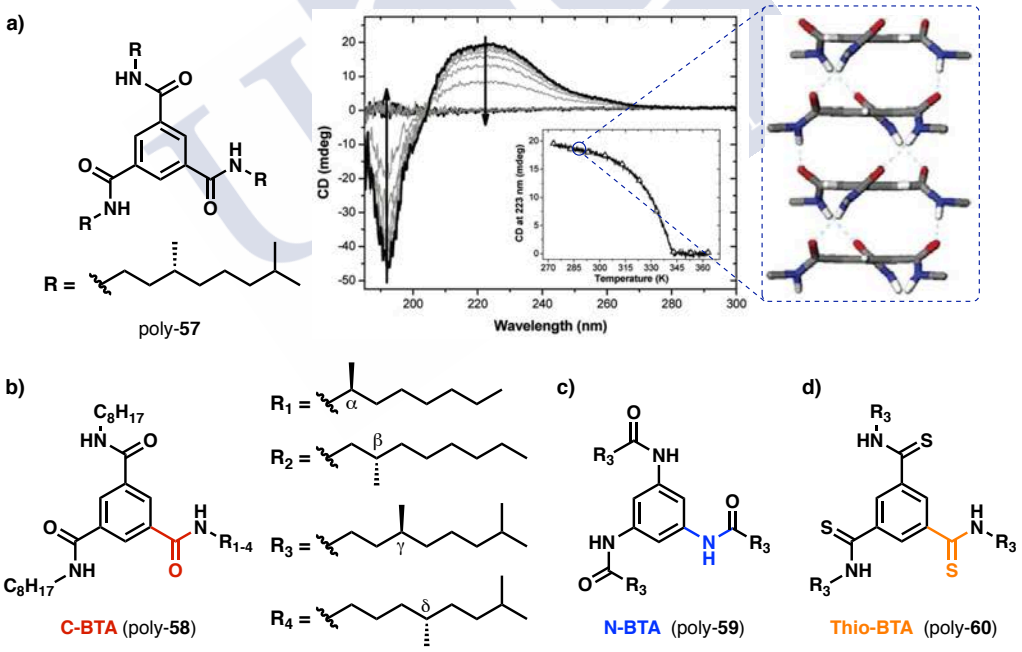

Figure 37. (a) Structure and CD spectra of poly-**57** in heptane ($1.4 \cdot 10^{-5}$ M). The inset shows the decrease of ellipticity at 223 nm when increasing the temperature. Model of the right-handed helix proposed for poly-**57** based. (b) C centred BTA (poly-**58**). (c) N centred BTA (poly-**59**). (d) Thio-based BTA (poly-**60**).

[102] (a) Smulders, M. M. J.; Filot, I. A. W.; Leenders, J. M. A.; van der Schoot, P.; Palmans, A. R. A.; Schenning, A. P. H. J.; Meijer, E. W. *J. Am. Chem. Soc.* **2010**, *132*, 611-619. (b) Smulders, M. M. J.; Stals, P. J. M.; Mes, T.; Paffen, T. F. E.; Schenning, A. P. H. J.; Palmans, A. R. A.; Meijer, E. W. *J. Am. Chem. Soc.* **2010**, *132*, 620-626.

[103] Smulders, M. M. J.; Schenning, A. P. H. J.; Meijer, E. W. *J. Am. Chem. Soc.* **2008**, *130*, 606-611.

[104] Stals, P. J. M.; Smulders, M. M. J.; Martín-Rapún, R.; Palmans, A. R. A.; Meijer, E. W. *Chem. Eur. J.* **2009**, *15*, 2071-2080.

[105] Stals, P. J. M.; Everts, J. C.; de Brujin, R.; Filot, I. A. W.; Smulders, M. M. J.; Martín-Rapún, R.; Pidko, E. A.; de Greef, T. F.A.; Palmans, A. R. A., Meijer, E. W. *Chem. Eur. J.* **2010**, *16*, 810-821.

[106] Mes, T.; Cantekin, S.; Balkenende, D. W. R.; Frissen, M. M. M.; Gillisen, M. A. J.; De Waal, B. F. M.; Voets, I. K.; Meijer, E. W.; Palmans, A. R. A. *Chem. Eur. J.* **2013**, *19*, 8642-8649.

Inspired by these studies Sánchez *et al.* have also investigated the supramolecular aggregation in π extended C_3-symmetric platforms bearing chiral and achiral oligo(phenyleneethynylene) (OPE) tricarboxiamides as substituents (poly-**61**).[107] Experimental and theoretical studies for different monomers revealed that the self-assembly occurs in most of the cases via a cooperative process (Figure 38). These aggregates are stabilized by a triple array of hydrogen bonds and π-π stacking of the aromatic rings. The cooperativity factor value for poly-**61** was also comparable to those obtained for the BTAs.

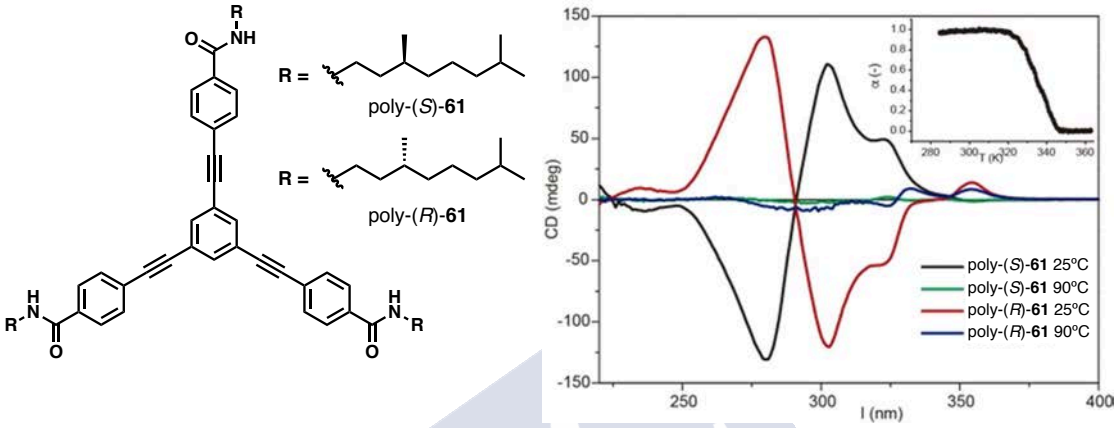

Figure 38. Structure and CD spectra for poly-(*S*)-/poly-(*R*)-**61** (MCH, $1 \cdot 10^{-6}$ M) at 25 °C and 90 °C. Inset of the cooling curve obtained for poly-(*S*)-**61** showing the decrease of ellipticity when increasing the temperature.

Interestingly, Fernández *et al.* described for the fist time in 2013 the supramolecular assembly of small molecules by metal-metal interaction.[108] They have demonstrated that the cooperative self-assembly of an OPE-based Pd (II) pyridyl complex (poly-**62**) is mainly ruled by metallophilic interactions (Figure 39a). Cooling down a molecularly dissolved solution of poly-**62** —from 50 °C (non-aggregated state) to room temperature (aggregated state)— revealed the appearance of a red-shifted band at r.t. in the UV-Vis spectra (Figure 39b). This band is ascribed to cooperative metallophilic interactions between the Pd (II) centers and the π-π interactions between OPEs. This assumption was supported by comparing this system with a metal free counterpart as well as by DFT calculations. AFM images demonstrated the formation of fibrillar aggregates (Figure 39d). More recently, they have demonstrated that by modifying the experimental conditions,[109] as well as by changing the metal[110] that binds the OPE units, different helical scaffolds can be obtained.

[107] (a) García, F.; Korevaar, P. A.; Verlee, A, Meijer, E. W.; Palmans, A. R. A.; Sánchez, L. *Chem. Commun*, **2013**, *49*, 8674-8676. (b) García, F.; Viruela, P. M.; Matesanz, E.; Ortí, E.; Sánchez, L. *Chem. Eur. J.* **2011**, *17*, 7755-7759.

[108] Mayoral, M. J.; Rest, C.; Stepanenko, V.; Schellheimer, J.; Albuquerque, R. Q.; Fernández, G. *J. Am. Chem. Soc.* **2013**, *135*, 2148-2151.

[109] Langenstroer, A.; Kartha, K. K.; Dorca, Y.; Droste, J.; Stepanenko, V.; Albuquerque, R. Q.; Hansen, M. R.; Sánchez, L.; Fernández, G. *J. Am. Chem. Soc.* **2019**, *141*, 5192-5200.

[110] Coelho, J. P.; Matern, J.; Albuquerque, R. Q.; Fernández, G. *Chem. Eur. J.* **2019**, *25*, 8960-8964.

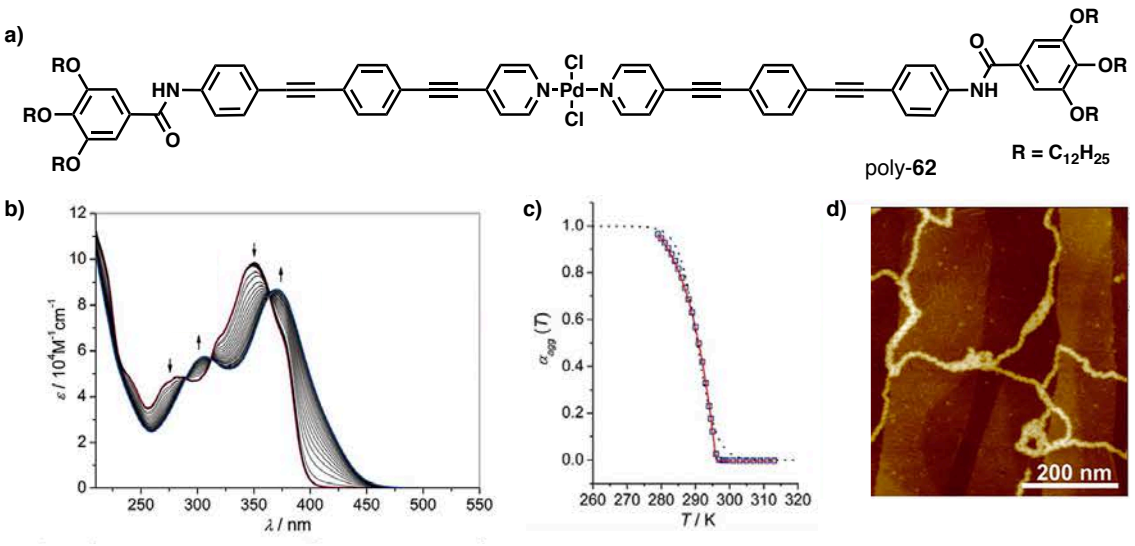

Figure 39. (a) Structure of poly-**62**. (b) Temperature-dependent UV-Vis experiments for poly-**62** (MCH, $1.6 \cdot 10^{-4}$ M); arrows indicate the spectral changes upon decreasing the temperature. (c) Fitting of the cooling curve indicates that the polymerization follows a cooperative process. (d) AFM image for poly-**62** obtained by spin coating.

8.2.2. Kinetically Controlled Polymerization

The molecules discussed in the previous section self-assemble via a cooperative mechanism leading only to one type of helical aggregate. However, this is not the case if the polymerization is influenced by the kinetics. Experimental studies on kinetically controlled processes are more challenging than the ones performed for thermodynamically controlled processes. In the case of kinetic assemblies the obtained structure will be dependent on several variables such as the preparation method, the ranging from temperature modulation...[111]

Meijer *et al.* reported a linear π-conjugated oligomer (OPV, poly-**63**) that self assembles into dimers via π-π stacking, leading to the formation of a left-handed (*M*-type) helical aggregate. However, they demonstrated that this OPV (oligo(phenylenevinylene)) could also form opposite helical aggregates by quenching a solution of monomeric units in an ice bath. It was observed that the resulting right-handed helical aggregates (*P*-type) evolved over time into thermodynamically stable *M*-type helices (Figure 40a).[112] This represented the first example of pathway complexity —competition between kinetics and thermodynamics during the supramolecular polymerization—, involving an off-pathway *P*-type kinetic metastable aggregate that is converted into the on-pathway *M*-type thermostable aggregate upon time. Working in this direction, Würthner and co-workers developed a system (poly-**64**, Figure 40b) showing three different states with an off-pathway intermediate (H1) (Figure 40c). The initial self-assembly of bis(merocyanine) (poly-**64**) dyes dimer leads to a random-coiled

[111] Wehner, M.; Würthner, F. *Nature Reviews Chemistry* **2020**, *4*, 38-53.

[112] (a) Korevaar, P. A.; George, S. J.; Markvoort, A. J.; Smulders, M. M. J.; Hilbers, P. A. J.; Schenning, A. P. H. J.; De Greef, T. F. A.; Meijer, E. W. *Nature* **2012**, *481*, 492-497. (b) Jonkheijm, P.; van der Schoot, P.;. Schenning, A. P. H. J;. Meijer, E. W. *Science* **2006**, *313*, 80-83. (c) Schenning, A. P. H. J.; Jonkheijm, P.; Peeters, E.; Meijer, E. W. *J. Am. Chem. Soc.* **2001**, *123*, 409-416.

supramolecular polymer (D state), that evolves after fourteen minutes into helical extended nanorods (H1) and, eventually, into a denser nanorod with opposite helical sense (H2) after disassembly of the H1 nanorods (Figure 40d).[113]

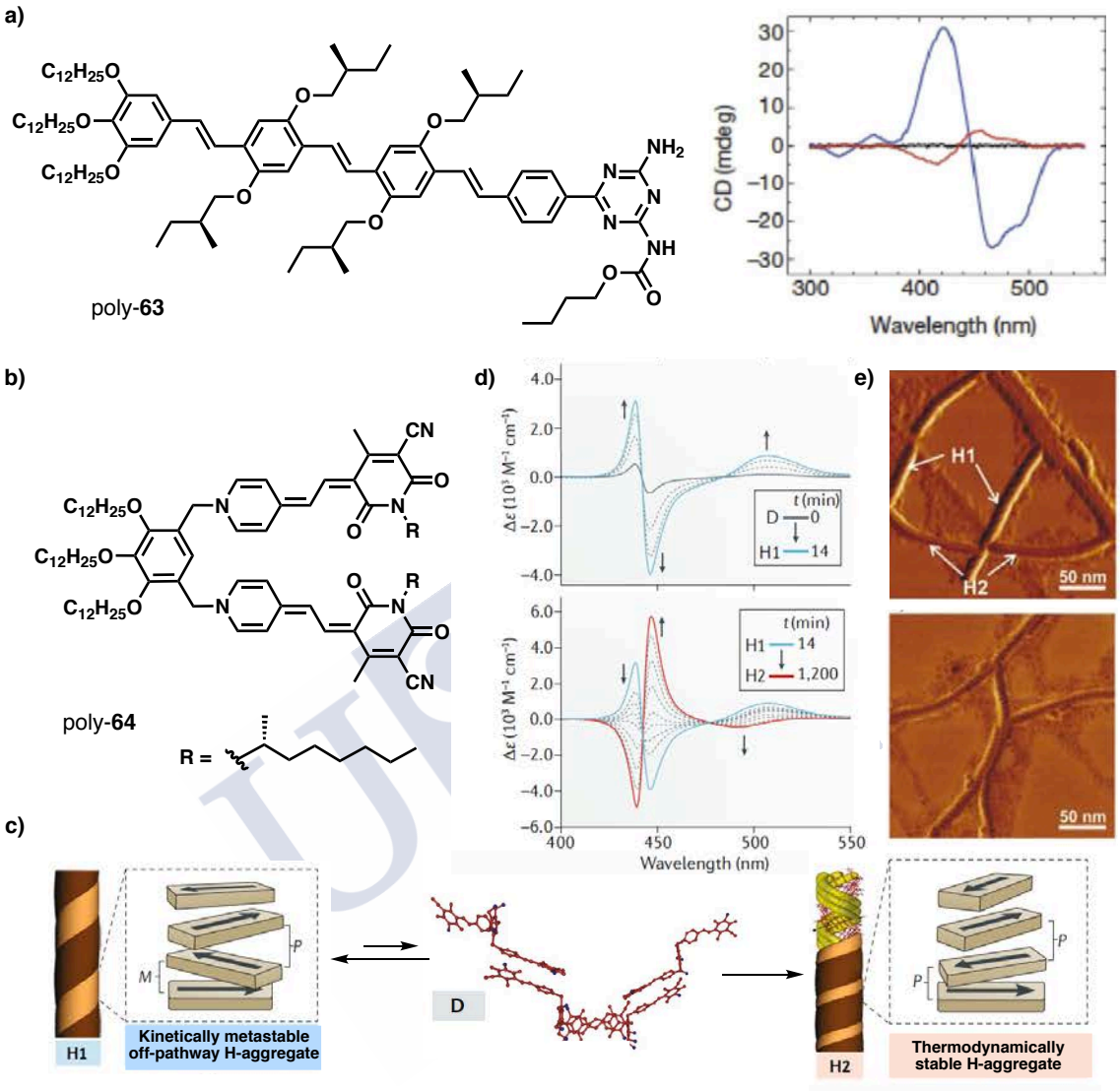

Figure 40. (a) Structure for poly-**63** and CD spectra in disassembled state (70 °C, black line), thermodynamically stable *M*-type species (0 °C, blue line) and a mixture of thermodynamically and metastable species (0 °C, red line). (b) Structure of poly-**64**. (c) Schematic representation of the three different supramolecular polymers that are involved in the supramolecular stereomutation of poly-**64**. (d) Time-dependent CD spectra of the kinetically controlled supramolecular polymerization showing the evolution from an initially kinetically metastable aggregate towards a thermodynamically stable one. (e) AFM images of poly-**64** prepared by spin coating at different times after the initiation of the self-assembly (top, showing the presence of the two kind of aggregates: 11 hours; bottom: 22 hours).

Furthermore, the kinetic control over supramolecular polymerization can also be achieved via living supramolecular polymerization (LSP). The addition of seeds larger than the critical nucleus size in the presence of a sufficiently high nucleation barrier can prevent undesired spontaneous nucleation, forcing the supramolecular system to directly evolve into

[113] (a) Lohr, A.; Würthner, F. *Isr. J. Chem.* **2011**, *51*, 1052-1066. (b) Lohr, A.; Lysetska, M.; Würthner, F. *Angew. Chem. Int. Ed.* **2005**, *44*, 5071-5074.

the elongation phase, obtaining a less polydisperse aggregate. A prerequisite for LSP is the retardation of spontaneous self-assembly of the thermodynamically favoured species.[111] On 2014 Takeuchi *et al.* reported the first example of LSP when investigating a Zn porphyrin (ZnP) (poly-**65**) that self-assembles through two cooperative pathways. They observed that the initial J-type aggregates formed by the ZnP (poly-**65**) evolved into H-type aggregates after certain time and, interestingly, this process can be accelerated by the addition of the H-type thermodynamic aggregates to a solution of J-type kinetics aggregates (Figure 41).[114] Sánchez *et al.* have also demonstrated that the addition of seeds of the on-pathway J aggregate to a solution of an off-pathway H aggregate speeds up the conversion of the later one in Carbonyl-Bridged Triarylamines (CBTs) (poly-**66**).[115]

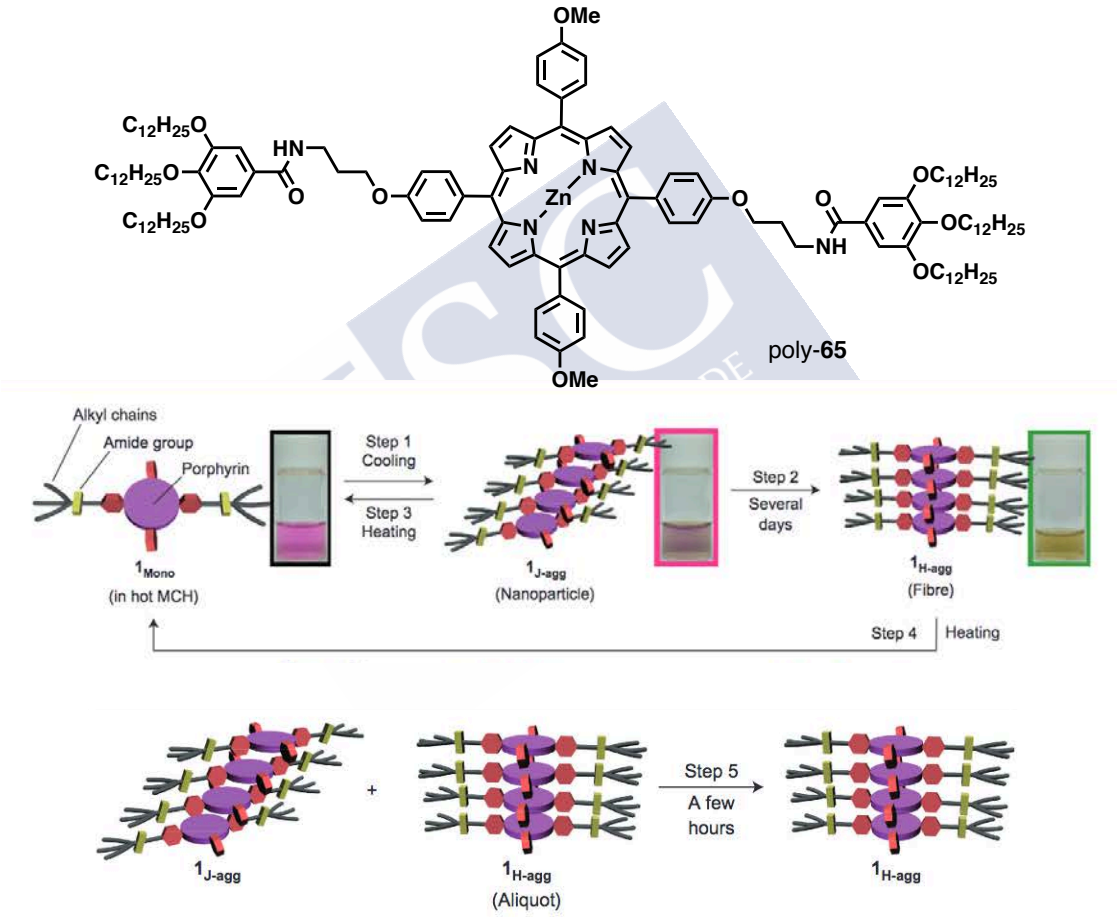

Figure 41. Structure of poly-**65** and schematic representation of the self-assembly of poly-**65** in MCH. The monomer self-assembles upon cooling to form nanoparticles composed of J-aggregates (step 1) that, after a certain time, evolve into fibres composed of H-aggregates (step 2). Both steps are reversible upon heating recovering the initially disassembled monomer (steps 3 and 4 respectively) that can self-assemble again if cooled. The transformation from the J-aggregate to the H-aggregate can be shortened in the presence of an aliquot of H-aggregate (step 5).

[111] Wehner, M.; Würthner, F. *Nature Reviews Chemistry* **2020**, *4*, 38-53.
[114] Ogi, S.; Sugiyasu, K.; Manna, S.; Samitsu, S.; Takeuchi, M. *Nat. Chem.* **2014**, *6*, 188-195.
[115] Valera, J. S.; Gómez, R.; Sánchez, L. *Small* **2018**, *14*, 1702437.

8.3. Supramolecular Helicity form Axial Chirality

Helical supramolecular polymers can be formed, as previously mentioned, by the transmission of chiral information from the side chains to the aromatic core, which will determine the chirality of the final structure (point chirality). However, these chiral aggregates can also be obtained when elements of asymmetry, such as chiral planes, chiral axes or helical molecular chirality are present in the monomer. In this case, the final handedness of the supramolecular aggregate will be defined by these elements of asymmetry over the point chirality.

It is known that bay-substituted perylenebisimides (PBIs) can rapidly interconvert into *P* and *M* atropo-isomers. Nevertheless, this rapid racemization can be cancelled if an oligoether is used to bridge the 1- and 7- positions (bay-substituents) to block one the two π faces of the PBI (poly-*M*-**67** and poly-*P*-**67**). As a result, two atropo-enantiomers with self-discrimination (social self-sorting) over self-recognition (narcissistic self-sorting) are obtained (Figure 42a). This characteristic will dictate the final morphology of the self-assembly; the racemic form will result into irregular sized particles (Figure 42b), whereas the non-racemic form will aggregate into helical fibers due to the complementary hydrogen bonding between the imide units and the π-stacking of the non-shielded π-face of the PBI (Figure 42c, d).[116]

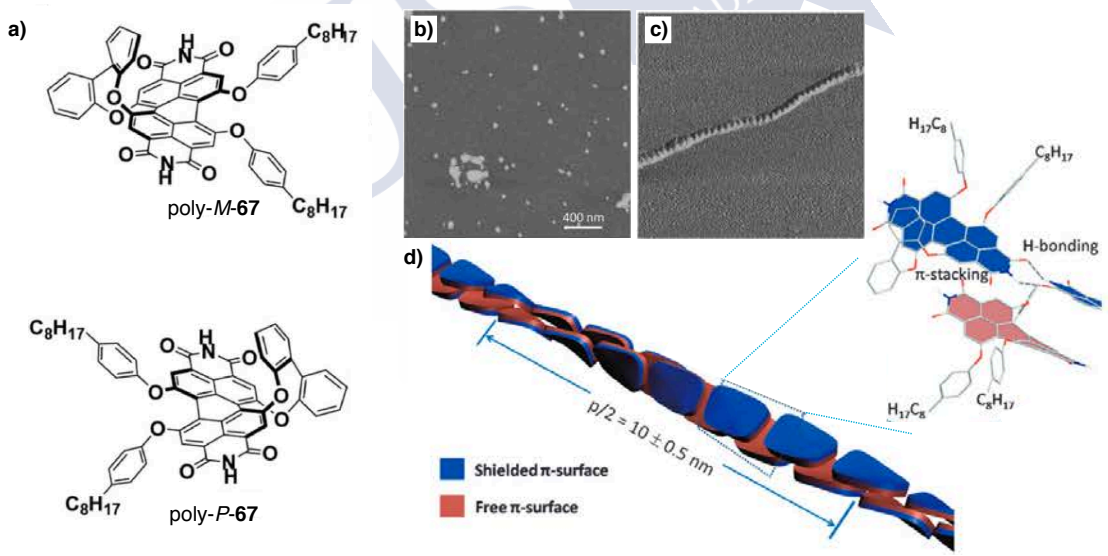

Figure 42. (a) Structures of the two atropoisomers. AFM images of spin coated solutions for (b) poly-*M*-**67** and (c) poly-rac-**67** showing the different morphologies obtained. (d) Schematic representation of the aggregate on enantiopure poly-*M*-**67** favoured by hydrogen bonding and the selective π stacking of the aromatic moieties of the PBI core.

[n]helicenes (n ≥ 4) can also lead to the formation of two enantiomers in supramolecular polymers, this is due to its inherently twisted geometry of the π-conjugated system. Yamaguchi *et al.* have widely demonstrated how the interconnection of oligomeric units leads

[116] (a) Safont-Sempere, M. M.; Osswald, P.; Radacki, K. Würthner, F. *Chem. Eur. J.* **2010**, *16*, 7380-7384. (b) Osswald, P.; Würthner, F. *J. Am. Chem. Soc.* **2007**, *129*, 14319-14326.

to the formation of double-helical strands. Lately, they have reported an unprecedented inverse thermoresponsiveness of two strands of oligomeric [4]helicenes with polar oligoether termini (poly-**68**). [117] Heating up a solution of the oligomer dissolved in a mixture water/acetone/triethylamine results into a dimerization, instead of the expected separation of the strands, due to the loss of non-covalent interactions of the polar side chains with the polar solvent molecules. Decreasing the temperature will revert this process, as the non-covalent interactions will be formed again (Figure 43).

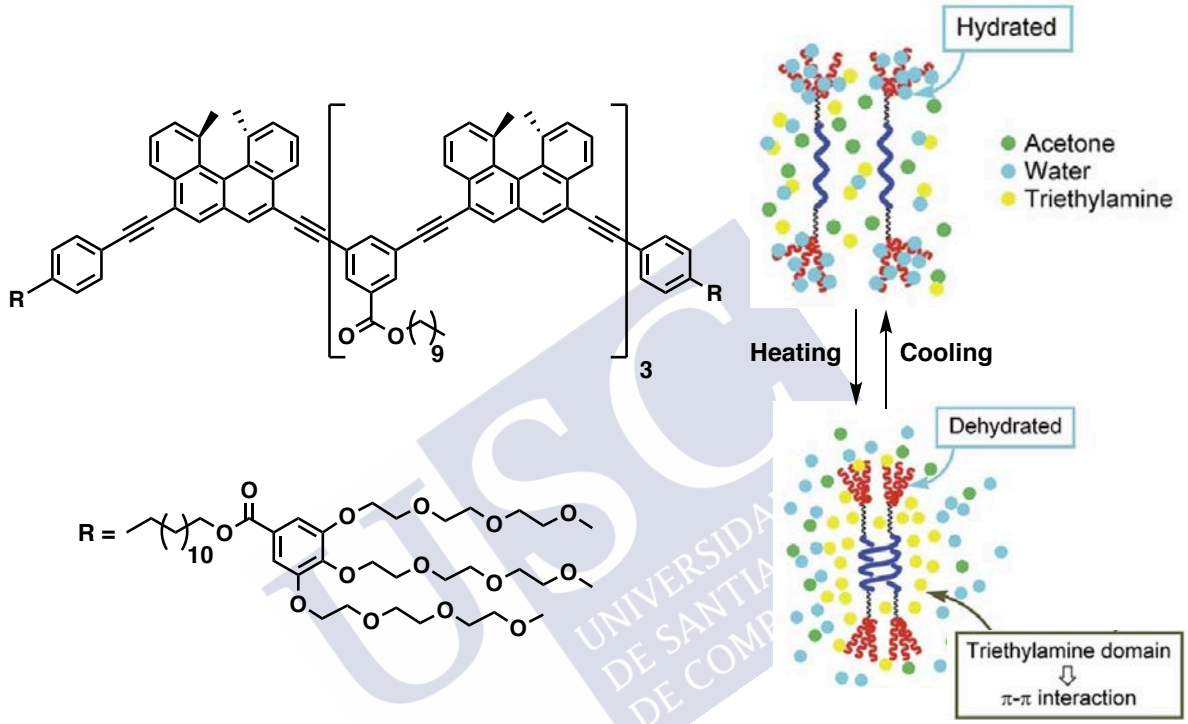

Figure 43. Structure of poly-**68** and schematic representation of the inverse thermoresponse in a mixture of acetone/water/triethylamine (1:2:1).

8.4. Properties of Supramolecular Polymers

Tailoring the supramolecular scaffold is a challenging task due to the inherent lability of the non-covalent bonds. The main properties that these polymers present are described next.

8.4.1. Chiral Amplification

In supramolecular polymers mainly two mechanisms, the Sergeants and Soldiers effect and the Majority Rules can produce a chiral amplification phenomenon.

In the late 90's, Meijer and co-workers reported this effect in supramolecular polymers for the first time.[118] They described the copolymerization of a disc-shaped molecule with C_3-symmetry, derived from pyridine (BiPy-BTA) bearing chiral alkyl chains (Soldier, **68**), with the analogous achiral BiPy-BTA (Sergeant, **69**) (Figure 44a). It was observed that the addition of a

[117] Saito, N.; Kobayashia, H.; Yamaguchi, M. *Chem. Sci.* **2016**, *7*, 3574-3580.
[118] Palmans, A. R. A.; Vekemans, J.; Havinga, E. E.; Meijer, E. W. *Angew. Chem. Int. Ed.* **1997**, *36*, 2648-2651.

2.5% of chiral units is able to organize the achiral counterparts into a one-handed supramolecular polymer. Remarkably, Sánchez *et al.* have also demonstrated how an initially microcrystalline lamellae —achiral N,N'-1,2-ethanediylbisbenzamide, Soldier— (**71**, Figure 44c) can be transformed into twisted ribbons after the addition of 5% of the Sergeant —chiral N,N'-1,2-ethanediylbisbenzamide— (**70**, Figure 44d). This effect was also reported for other supramolecular systems with different cores.[119]

Also Meijer's group reported, for the first time, the Majority Rules amplification phenomena at the supramolecular level. By combining the two enantiomers of **68** they demonstrated that a small imbalance of one of them is sufficient to promote the formation of a one-handed helix.[120]

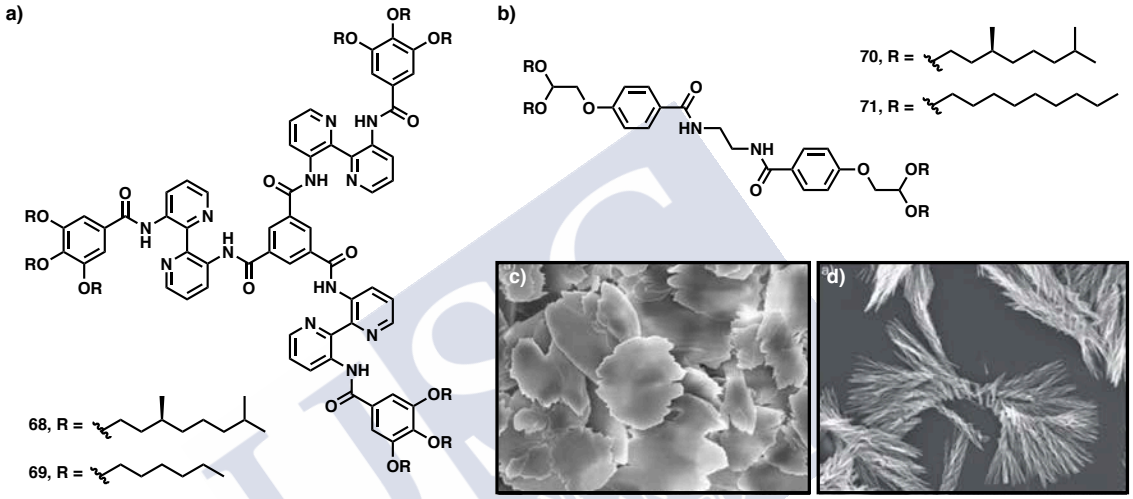

Figure 44. (a) Structure for **68** and **69**. (b) Structure for **70** and **71**. SEM images for (c) the microcrystalline lamellae obtained for **71** and the (d) twisted nanoribons formed after the addition of the Sergeant (**70**).

8.4.2. Helix Inversion

The control over the helical sense in supramolecular systems can be achieved by using stimuli-responsive building blocks. In these polymers the helical preference is modulated by external stimuli such as pH,[121] temperature[122] or light irradiation[123].

In this regard, Meijer *et al.* have reported a solvent-driven helicity inversion of a chiral water-soluble poly(ureidophtalimide) (poly-**72**) decorated with hydrophobic side chains in THF/water mixtures (Figure 46a).[124] This effect is due to the differences in the hydrogen-

[119] (a) García, F.; Viruela, P. M.; Matesanz, E.; Ortí, E.; Sánchez, L. *Chem. Eur. J.* **2011**, *17*, 7755-7759. (b) Helmich, F.; Lee, C. C.; Schenning, A. P. H. J.; Meijer, E. W. *J. Am. Chem. Soc.* **2010**, *132*, 16753-16755. (c) Masuda, M.; Jonkheijm, P.; Sijbesma, R. P.; Meijer, E. W. *J. Am. Chem. Soc.* **2003**, *125*, 15935-15940. (d) van Gorp, J. J.; Vekemans, J. A. J. M.; Meijer, E. W. *J. Am. Chem. Soc.* **2002**, *124*, 14759-14769.

[120] Smulders, M. M. J.; Stals, P. J. M.; Mes, T.; Paffen, T. F. E.; Schenning, A. P. H. J.; Palmans, A. R. A.; Meijer, E. W. *J. Am. Chem. Soc.* **2010**, *132*, 620-626. (b) van Gestel, J.; Palmans, A. R. A.; Titulaer, B.; Vakemans, J. A. J. M.; Meijer, E. W. *J. Am. Chem. Soc.* **2005**, *127*, 5490-5494.

[121] Janssen, P. G. A.; Ruiz-Carretero, A.; González-Rodríguez, D. Meijer, E. W. Schenning, A. P. H. J. *Angew. Chem., Int. Edit.* **2009**, *48*, 8103-8106.

[122] (a) Go, M.; Choi, H.; Kim, K. Y.; Moon, C. J.; Choi, Y.; Miyake, H.; Lee, S. S.; Jung, S. H.; Choi, M. Y.; Jung, J. H. *Org. Chem. Front.* **2019**, *6*, 1100-1108. (b) Huang, Z.; Kang, S. K.; Banno, M.; Yamaguchi, T.; Lee, D.; Seok, C.; Yashima, E. Lee, M. *Science* **2012**, *337*, 1521-1526.

[123] Gopal, A.; Hifsudheen, M.; Furumi, S.; Takeuchi, M.; Ajayaghosh, A. *Angew. Chem. Int. Ed.* **2012**, *51*, 10505-10509.

[124] Sinkeldam, R. W.; van Houtem, M.; Pieterse, K.; Vekemans, J.; Meijer, E. W. *Chem. Eur. J.* **2006**, *12*, 6129-6137.

bonding interactions with the two solvents and the different conformation that the chiral side chain can adopt —a gauche conformation along the C-C axis and a *trans* conformation along the C-O axis are favoured for the oligo(ethylene oxide) tails in water—.

More recently it was demonstrated the inversion of the helical sense in a liquid crystal by light irradiation (**73**, Figure 47b). The initial cholesteric phase turns into a nematic phase with opposite helical sense (Figure 47c, d, e) and, after further irradiation, the fingerprint texture reappears, indicative of the recovery of the initial cholesteric phase and of the original helical sense (Figure 47f, g, h).[125]

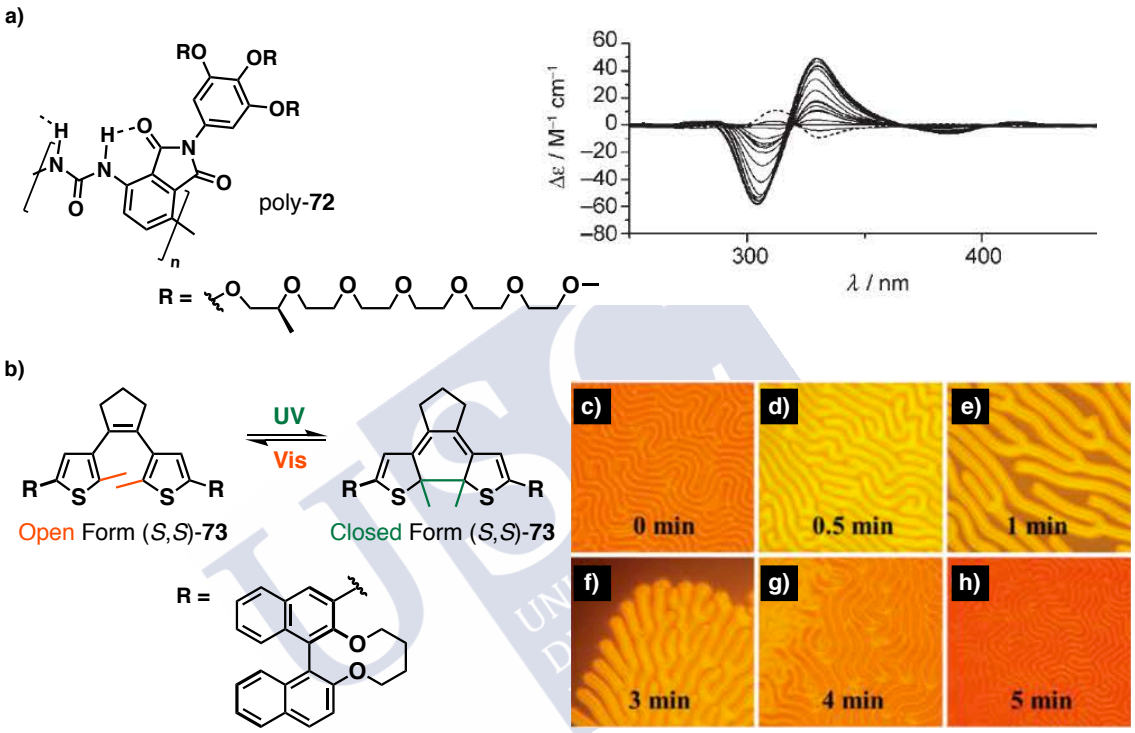

Figure 46. (a) Structure for poly-**72** and CD trace showing the helical inversion from THF (dashed line) to water (solid line). (b) Open and closed structure for 73 and POM (Polarized Light Microscopy) images showing the helix inversion by changes in the organization of the liquid crystal —from (c) to (e) cholesteric to nematic and from (f) to (h) nematic to cholesteric—.

[125] Wang, L.; Dong, H; Li, Y.; Liu, R.; Wang Y.F.; Bisoyi, H. K.; Sun, L.-D.; Yan, C.-H.; Li, Q. *Adv. Mater.* **2015**, *27*, 2065-2069.

Objectives

USC
UNIVERSIDADE
DE SANTIAGO
DE COMPOSTELA

Objectives

Covalent and supramolecular helical polymers, although being constituted by different linking forces —non-reversible and reversible bonds—, share common properties. In both cases, the study of the secondary structure is key for further manipulation of the helix, as well as for the rational design for their possible applications.

This Doctoral Thesis is focused on the study of the properties that covalent and supramolecular polymers may present, to finally encompass them into a single helical polymer creating a novel material, the matryoshka-like helical polymers.

Chapter I. Chiral Information Harvesting in Helical Poly(acetylene) Derivatives Using Oligo(*p*-phenyleneethynylene)s as Spacers

Since their discovery, dynamic helical polymers have attracted the attention of the scientific community and mastering their helical sense has emerged as an attractive task. Different mechanisms for the transmission of chiral information have been described for polymers bearing flexible spacers, although the study of this communication process employing rigid spacers remains quite unexplored.

The main goal of this project is to demonstrate another remote chiral induction mechanism for polymers bearing long and rigid spacers, the chiral information harvesting process. In this communication process the chiral information is transmitted from the chiral moiety to the spacer array within the helical scaffold, which is finally harvested by the polyene backbone resulting in an effective helix induction.

Publication associated with this objective: Fernández, Z.; Fernández, B.; Quiñoá, E.; Riguera, R.; Freire, F. *Chem. Sci.* **2020**, *11*, 7182-7187.

Chapter II. Aromatic Substitution Pattern Effects in Poly[[oligo(phenylene ethynylene)]phenylacetylene]s: Modulation of the Helical Periphery Without Affecting the Folding of the Main Chain

In dynamic helical polymers, such as poly(phenylacetyelene)s (PPAs), the aromatic substitution pattern has a significant role in the final structure adopted by the polymer chain —*cis*-*cisoidal* or *cis*-*transoidal*—, as well as on the flexibility that they may present —stretched or compressed—. This is due to the proximity between the pendant and the backbone when the former is moved from the *para*- to the *ortho*- position, which results into an increasing steric hindrance.

Herein, searching for novel scaffolds to overpass this problem we will describe a novel family of helical polymers, the poly[oligo(phenyleneethynylene)phenylacetylene]s —POPEPAs—, in which the chiral information will be transmitted by the aforementioned chiral harvesting mechanism. In this polymers a rigid oligo(phenyleneethynylene)$_n$ (OPE, n = 1, 2)

spacer will be introduced between the pendant and the backbone, aiming to reduce the congestion observed for the *meta*- and *ortho*- PPAs derivatives.

Chapter III. Complex Supramolecular Polymerization Pathway of an Asymmetrical and Rigid OPE Derivative: The Role of the Supramolecular Polymerization Degree in the Aggregate Morphology

Supramolecular helical polymers are obtained from the non-covalent interaction of building blocks. The presence of these reversible and weak interactions provide to these polymers a dynamic character, non-observed in their covalent counterparts.

With this information in mind and taking advantage of the information extracted from the study of the communication process from POPEPAs (Chapters I and II), we decided to evaluate the self-assembly properties of an asymmetrical and rigid OPE. The OPE monomers will be composed by a short chiral moiety and a π conjugated core, ensuring the stabilization of the obtained aggregates by π-π and hydrogen bonding interactions mainly. Furthermore, the study of these OPE based supramolecular polymers will be interesting due to their potential applications in optoelectronics.

Chapter IV. Supramolecular Triangular Tessellation Produced by the Self-Assembly of Chiral Helical Oligomers Obtained from OPE Derivatives

From literature it is known that the formation of supramolecular polymers is favoured by the introduction of long alkyl chains, which improve their solubility in low-polar solvents and also promote the chain-to-chain interdigitation. Moreover, in most of the reported examples, the building blocks are usually symmetric and only few examples are found to be chiral.

Prompted by this studies, we decided to evaluate the self-assembly of an asymmetric rigid OPE bearing at one of the edges a dodecyl alkyl chain. This will allow us to explore the effect that this long substituent will have over the final morphology and study the supramolecular polymerization mechanism that yields the chiral aggregate.

Chapter V. Matryoshka-like Helical Polymers: When Supramolecular and Covalent Helical Polymers are Mixed Up

Modelling and experimental studies for POPEPAs revealed that, as in the case of PPAs, *cis-cisoidal* polyene scaffolds produce the classical scaffold made-up by two coaxial helices; an internal one described by the conjugated polyene backbone and an external one outlined by the pendants. As a consequence, the OPE units will describe a large tilting degree between them. This chiral arrangement between OPE spacers, observed when analysing the communication process for POPEPAs (Chapters I and II), persuade us to study the self-assembly properties of the asymmetric OPE units (Chapters III and IV).

On the other hand, computational studies also suggested that if the POPEPA adopts a stretched *cis-transoidal* scaffold, two additional helices —described by the OPE arrangement;

small tilting degree— will be found in addition to the two classical ones —described by the polyene backbone and the pendants—. Therefore, the objective of this project will be the synthesis of a *cis-transoidal* POPEPA, in which a non-covalent helix will be incorporated within a covalent one, producing the matryoshka-like helical polymers. To this end the monomer employed for the supramolecular studies in Chapter IV will be used, as it is known that benzamide connectors promote the formation of *cis-transoidal* structures.

USC
UNIVERSIDADE
DE SANTIAGO
DE COMPOSTELA

Chapter I

Chiral Information Harvesting in Helical Poly(acetylene) Derivatives Using Oligo(*p*-phenyleneethynylene)s as Spacers

USC
UNIVERSIDADE
DE SANTIAGO
DE COMPOSTELA

Chapter I. Chiral Information Harvesting in Helical Poly(acetylene) Derivatives Using Oligo(*p*-phenyleneethynylene)s as Spacers

Adapted from:

Fernández, Z.; Fernández, B.; Quiñoá, E.; Riguera, R.; Freire, F.*

Chem. Sci. **2020**, *11*, 7182-7187

Abstract: *A chiral harvesting transmission mechanism is described in poly(acetylene)s bearing oligo(p-phenyleneethynylene)s (OPEs) used as rigid achiral spacers and derivatized with chiral pendant groups. The chiral moieties induce a positive or negative tilting degree in the stacking of OPE units along the polymer structure, which is further harvested by the polyene backbone adopting either a P or M helix.*

USC
UNIVERSIDADE
DE SANTIAGO
DE COMPOSTELA

During the last years, dynamic helical polymers have attracted the attention of the scientific community due to the possibility of tuning the helical sense and/or the elongation of the helical structure by using external stimuli. [1-14]

In the case of a chiral dynamic helical polymer, modifications in its structure —helical sense enhancement or helix inversion— arise from conformational changes induced at its chiral pendants —usually, with just one stereocenter—, by stimuli such as variations in solvent polarity or temperature, the addition of certain ions and so (Figure 1a).[15] On the other hand, if a helical polymer is achiral (i.e., bearing achiral pendants), the chiral amplification phenomena can emerge from interactions between the polymer and external chiral molecules.[16] In both the above cases, the changes produced in the helical structures are related to the spatial dispositions adopted by the substituents or associated species at the pendant groups.[17-19]

A step forward in the helical sense control of poly(phenylacetylene)s (PPA)s is to study different mechanisms of transmission of chiral information from the pendant to the polyene backbone by introducing achiral spacers. The goal is to demonstrate how far it is possible to place the chiral center and still have an effective chiral induction on the polyene backbone. Therefore, transmission of the chiral information from a remote position can occur through space, thus overpassing the distance generated by the spacer —tele-induction— (Figure 1b), [20-28] or through the achiral spacer itself, producing in it a preferred structure, such as a helical

1 Yashima, E.; Ousaka, N.; Taura, D.; Shimomura, K.; Ikai, T.; Maeda, K. *Chem. Rev.* **2016**, *116*, 13752-13990.
2 Yashima, E.; Maeda, K.; Furusho, Y. *Acc. Chem. Res.* **2008**, *41*, 1166-1180.
3 Yashima, Y.; Maeda, K; Iida, H.; Furusho, Y.; Nagai, K. *Chem. Rev.* **2009**, *109*, 6102-6211.
4 Liu, J.; Lam, L. W. Y.; Tang, B. Z. *Chem. Rev.* **2009**, *109*, 5799-5867.
5 Rosen, B. M.; Wilson, C. J.; Wilson, D. A.; Peterca, M.; Imam, M. R.; Percec, V. *Chem. Rev.* **2009**, *109*, 6275-6540.
6 Schwartz, E.; Koepf, M.; Kito, H. J.; Nolte, R. J. M.; Rowan, A. E. *Polym. Chem.* **2011**, *2*, 33-47.
7 Anger, E.; Iida, H.; Yamaguchi, T.; Hayashi, K.; Kumano, D.; Crassous, J.; Vanthuyne, N.; Roussel, C.; Yashima, E. *Polym. Chem.* **2014**, *5*, 4909-4914.
8 Iida, H.; Miki, M.; Iwahana, S.; Yashima, E. *Chem. Eur. J.* **2014**, *20*, 4257-4262.
9 Sakurai, S.; Okoshi, K.; Kumaki, J.; Yashima, E. *J. Am. Chem. Soc.* **2006**, *128*, 5650-5651.
10 Okoshi, K.; Sakurai, S.; Ohsawa, S.; Kumaki, J.; Yashima, E. *Angew. Chem. Int. Ed.* **2006**, *45*, 8173-8176.
11 Pijper, D.; Jongejan, M. G. M.; Meetsma, A.; Feringa, B. L. *J. Am. Chem. Soc.* **2008**, *130*, 4541-4552.
12 Feringa, B. L. *Acc. Chem. Res.* **2001**, *34*, 504-513.
13 Suárez-Picado, E.; Quiñoá, E.; Riguera, R.; Freire, F. *Chem. Mater.* **2018**, *30*, 6908-6914.
14 Suárez-Picado, E.; Quiñoá, E.; Riguera, R.; Freire, F. *Angew. Chem. Int. Ed.* **2020**, *59*, 5437-4543.
15 Leiras, S.; Freire, F.; Seco, J. M.; Quiñoá, E.; Riguera, R. *Chem. Sci.* **2013**, *4*, 2735-2743.
16 Hase, Y.; Nagai, K.; Iida, H.; Maeda, K.; Ochi, N.; Sawabe, K.; Sakajiri, K.; Okoshi, K.; Yashima, E. *J. Am. Chem. Soc.* **2009**, *131*, 10719-10732.
17 Cornelissen, J. J. L. M.; Rowan, A. E.; Nolte, R. J. M.; Sommerdijk, N. A. J. M. *Chem. Rev.* **2001**, *101*, 4039-4070.
18 Cornelissen, J. J. L. M.; Donners, J. J. J. M.; de Gelder, R.; Graswinckel, W. S.; Metselaar, G. A.; Rowan, A. E.; Sommerdijk, N. A. J. M.; Nolte, R. J. M. *Science* **2001**, *293*, 676-680.
19 Kamikawa, Y.; Kato, T.; Onouchi, H.; Kashiwagi, D.; Maeda, K.; Yashima, E. *Polym. Sci. A Polym. Chem.* **2004**, *42*, 4580-4586.
20 Ramos, E.; Bosch, J.; Serrano, J. L.; Sierra, T.; Veciana, J. *J. Am. Chem. Soc.* **1996**, *118*, 4703-4704.
21 Amabilino, D. B.; Ramos, E.; Serrano, J. L.; Sierra, T.; Veciana, J. *J. Am. Chem. Soc.* **1998**, *120*, 9126-9134.
22 Amabilino, D. B.; Ramos, E.; Serrano, J. L.; Sierra, T.; Veciana, J. *Polymer* **2005**, *46*, 1507-1521.
23 Gomar-Nadal, E.; Veciana, J.; Rovira, C.; Amabilino, D. B. *Adv. Mater.* **2005**, *17*, 2095-2098.
24 Percec, V.; Aqad, E.; Peterca, M.; Rudick, J. G.; Lemon, L.; Ronda, J. C.; De, B. B.; Heiney, P. A.; Meijer, E. W. *J. Am. Chem. Soc.* **2006**, *128*, 16365-16372.
25 Percec, V.; Peterca, M.; Rudick, J. G.; Aqad, E.; Imam, M. R.; Heiney, P. A. *Chem. Eur. J.* **2007**, *13*, 9572-9581.
26 Abe, Y.; Aoki, T.; Jia, H.; Hadano, S.; Namikoshi, T.; Kakihana, Y.; Liu, L.; Zang, Y.; Teraguchi, M.; Kaneko, T. *Chem. Lett.* **2012**, *41*, 244-246.
27 Rodríguez, R.; Quiñoá, E.; Riguera, R.; Freire, F. *Chem. Mater.* **2018**, *30*, 2493-2497.
28 Rodríguez, R.; Quiñoá, E.; Riguera, R.; Freire, F. Small **2019**, 15, 1805413.

structure and where the orientation of the achiral helix is further transmitted to the polyene backbone —conformational switch— (Figure 1c).[29-31]

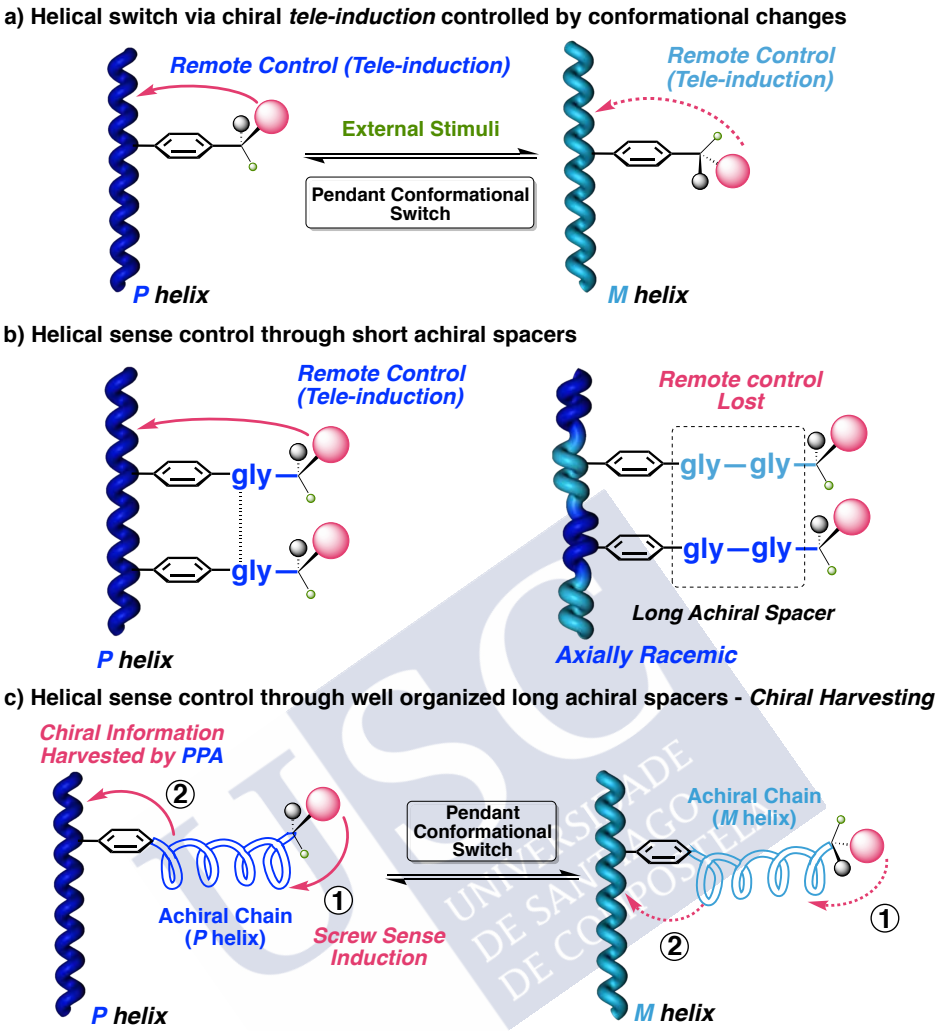

Figure 1. Several scenarios depicting conceptual representations of the transmission of chiral information. (a) Helical switch via chiral tele-induction. (b) Effect of distance on chiral tele-induction from multichiral pendants. (c) Helicity controlled by the conformational composition of achiral spacers.

For the first mechanism —chiral tele-induction—, both flexible and rigid spacers have been designed.[20-28] In all cases, supramolecular interactions, such as H bonding or π-π stacking, generate organized structures. As a result, the chiral center is located into a specific

29 Inai, Y.; Ousaka, N.; Okabe, T. *J. Am. Chem. Soc.* **2003**, *125*, 8151-8162.
30 Ousaka, N.; Inai, Y. *J. Org. Chem.* **2009**, *74*, 1429-1439.
31 Fukuda, M.; Rodríguez, R.; Fernández, Z.; Nishimura, T.; Hirose, D.; Watanabe, G.; Quiñoá, E.; Freire, F.; Maeda, K. *Chem. Commun.* **2019**, *55*, 7906-7909.
20 Ramos, E.; Bosch, J.; Serrano, J. L.; Sierra, T.; Veciana, J. *J. Am. Chem. Soc.* **1996**, *118*, 4703-4704.
21 Amabilino, D. B.; Ramos, E.; Serrano, J. L.; Sierra, T.; Veciana, J. *J. Am. Chem. Soc.* **1998**, *120*, 9126-9134.
22 Amabilino, D. B.; Ramos, E.; Serrano, J. L.; Sierra, T.; Veciana, J. *Polymer* **2005**, *46*, 1507-1521.
23 Gomar-Nadal, E.; Veciana, J.; Rovira, C.; Amabilino, D. B. *Adv. Mater.* **2005**, *17*, 2095-2098.
24 Percec, V.; Aqad, E.; Peterca, M.; Rudick, J. G.; Lemon, L.; Ronda, J. C.; De, B. B.; Heiney, P. A.; Meijer, E. W. *J. Am. Chem. Soc.* **2006**, *128*, 16365-16372.
25 Percec, V.; Peterca, M.; Rudick, J. G.; Aqad, E.; Imam, M. R.; Heiney, P. A. *Chem. Eur. J.* **2007**, *13*, 9572-9581.
26 Abe, Y.; Aoki, T.; Jia, H.; Hadano, S.; Namikoshi, T.; Kakihana, Y.; Liu, L.; Zang, Y.; Teraguchi, M.; Kaneko, T. *Chem. Lett.* **2012**, *41*, 244-246.
27 Rodríguez, R.; Quiñoá, E.; Riguera, R.; Freire, F. *Chem. Mater.* **2018**, *30*, 2493-2497.
28 Rodríguez, R.; Quiñoá, E.; Riguera, R.; Freire, F. Small **2019**, 15, 1805413.

orientation, producing an effective helical induction. Additionally, those studies allow evaluating how distances and sizes have an effect on this phenomenon.

In the second strategy, the helix induction is transmitted through conformational changes along an achiral spacer that is harvested by the polyene. For instance, an achiral peptide or an achiral polymeric helix derivatized at one end with a chiral residue and linked to the polymer main chain at the other end. In such cases, changes on the absolute configuration or even just a conformational change at the chiral center can induce an opposite helical structure into the achiral spacer, which in turn will be harvested by the polymer main chain (Figure 1c).[29-31]

Herein we will demonstrate another remote chiral induction mechanism based on a different chiral harvesting process. In this case, the chiral center does not produce a conformational change at the achiral spacer, but affects to its array within the helical scaffold. To perform these studies we decided to introduce the use of oligo(*p*-phenyleneethynylene)s (m = 1, 2, 3) (OPEs) as rigid spacers to separate the distant chiral center from the polyene backbone. These OPE units have been used in the formation of benzene-1,3,5-tricarboxamide (BTA) based supramolecular helical polymers, demonstrating their ability to stack with a certain tilting degree commanded by the chiral center.[32-34]

Hence, in our design, the chiral moiety will determine the supramolecular chiral orientation of the OPE groups used as spacers, which is further harvested by the polyene backbone. The overall process yields a helix with a preferred screw sense (Figure 2).

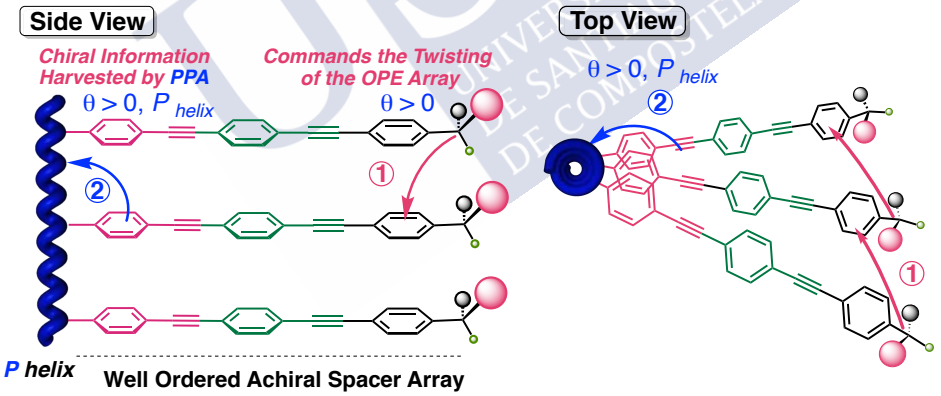

Figure 2. Conceptual side view and top view of the chiral information transmission mechanism from stereocenters at the far end of oligo(*p*-phenyleneethynylene) spacers to the polyene backbone via chiral harvesting.

To perform these studies, we used as model compounds two PPAs —poly-(*R*)-**1** and poly-(S)-**1**—derived from the 4-ethynylanilide of (*S*)- and (*R*)-α-methoxy-α-phenylacetic acid (MPA, m-(*S*/*R*)-**1**), whose helical structures and dynamic behaviors have been deeply studied by our

29 Inai, Y.; Ousaka, N.; Okabe, T. *J. Am. Chem. Soc.* **2003**, *125*, 8151-8162.
30 Ousaka, N.; Inai, Y. *J. Org. Chem.* **2009**, *74*, 1429-1439.
31 Fukuda, M.; Rodríguez, R.; Fernández, Z.; Nishimura, T.; Hirose, D.; Watanabe, G.; Quiñoá, E.; Freire, F.; Maeda, K. *Chem. Commun.* **2019**, *55*, 7906-7909.
32 Aparicio, F.; García, F.; Fernández, G.; Matesanz, E.; Sánchez, L. *Chem. Eur. J.* **2011**, *17*, 2769-2776.
33 García, F.; Sánchez, L. *J. Am. Chem. Soc.* **2012**, *134*, 734-742.
34 Greciano, E. E.; Calbo, J.; Buendía, J.; Cerdá, J.; Aragó, J.; Ortí, E.; Sánchez, L. *J. Am. Chem. Soc.* **2019**, *141*, 7463-7472.

group —poly-(*R*)-**1** and poly-(*S*)-**1**— (Figure 3).[35-46] By using these polymers as reference materials, four novel PPAs were designed introducing two OPE spacers —4-[(*p*-phenyleneethynylene)$_n$]ethynylanilide (n = 1, 2)— between the phenyl acetylene group and the (*S*)- or (*R*)-α-methoxy-α-phenylacetic acid (MPA) chiral group. Thus, monomers m-(*S*)- and m-(*R*)-**2** and m-(*S*)- and m-(*R*)-**3** (Figure 3a) were prepared and submitted to polymerization by using a Rh (I) catalyst. Poly-(*S*)- and poly-(*R*)-**2** and poly-(*S*)- and poly-(*R*)-**3** (Figure 3b) were obtained in high yield and showed Raman spectra characteristic of *cis* polyene backbones (see Experimental Section Chapter I, Figures S11 and S12).

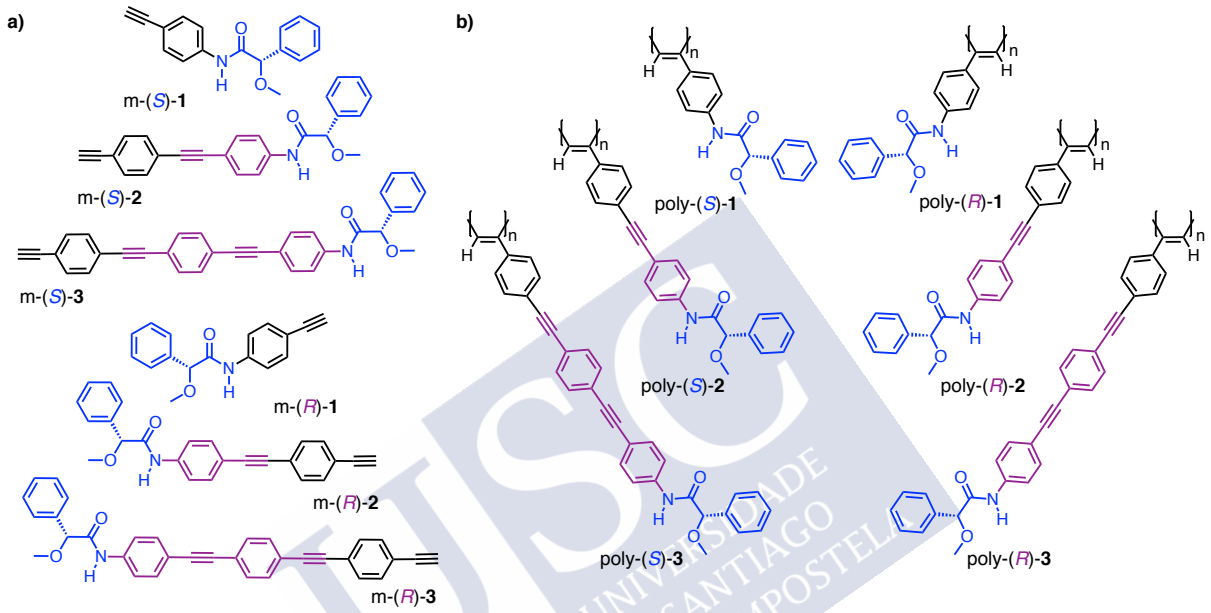

Figure 3. (a) Monomers and (b) polymers synthetized in this study.

X-ray structures of the monomers show a preferred *antiperiplanar* (*ap*) orientation between the carbonyl and methoxy groups (O=C-C-OMe) for m-(*R*)-**2** and m-(*S*)-**3**, whereas in the case of m-(*S*)-**1** a *synperiplanar* (*sp*) geometry is favoured (Figure 4a).[35] In complementary studies, CD spectra of monomers m-(*S*)-[**1**-**3**] in $CHCl_3$ show negative Cotton effects, indicative of major *ap* conformations in solution (Figure 4b),[35] further corroborated by theoretical calculations (see Experimental Section, Figure S10). Interestingly, the maximums of the Cotton effects in CD undergo a bathochromic shift —from 266 nm in m-**1** to 327 nm in m-**3**— due to a larger conjugation of the π electrons (from the anilide to the alkyne group) when the length of the spacer increases (Figure 4b).

35 Freire, F.; Seco, J. M.; Quiñoá, E.; Riguera, R. *Angew. Chem. Int. Ed.* **2011**, *50*, 11692-11696.
36 Freire, F.; Seco, J. M.; Quiñoá, E.; Riguera, R. *J. Am. Chem. Soc.* **2012**, *134*, 19374-19383.
37 Bergueiro, J.; Freire, F.; Wendler, E. P.; Seco, J. M.; Quiñoá, E.; Riguera, R. *Chem. Sci.* **2014**, *5*, 2170-2176.
38 Arias, S.; Freire, F.; Quiñoá, E.; Riguera, R. *Angew. Chem. Int. Ed.* **2014**, *53*, 13720-13724.
39 Arias, S.; Freire, F.; Quiñoá, E.; Riguera, R. *Polym. Chem.* **2015**, *6*, 4725-4733.
40 Arias, S.; Berguerio, J.; Freire, F.; Quiñoá, E.; Riguera, R. *Small* **2016**, *12*, 238-244.
41 Rodríguez, R.; Ignés-Mullol, J.; Sagués, F.; Quiñoá, E.; Riguera, R.; Freire, F. *Nanoscale* **2016**, *8*, 3362-3367.
42 Rodríguez, R.; Quiñoá, E.; Riguera, R.; Freire, F. *J. Am. Chem. Soc.* **2016**, *138*, 9620-9628.
43 Arias, S.; Núñez-Martínez, M.; Quiñoá, E.; Riguera, R.; Freire, F. *Polym. Chem.* **2017**, *8*, 3740-3745.
44 Arias, S.; Quiñoá, E.; Riguera, R.; Freire, F. *J. Am. Chem. Soc.* **2018**, *140*, 667-674.
45 Cobos, K.; Quiñoá, E.; Riguera, R.; Freire, F. *J. Am. Chem. Soc.* **2018**, *140*, 12239-12246.
46 Alzubi, M.; Arias, S.; Rodríguez, R.; Quiñoá, E.; Riguera, R.; Freire, F. *Angew. Chem. Int. Ed.* **2019**, *58*, 13365-13369.

CD studies of the polymer series bearing OPE spacers —poly-(*R*)- and poly-(*S*)-[**2-3**]— in different solvents show the formation of a PPA helical structure with a preferred helical sense, while the parent polymer, poly-**1**, devoid of the OPE unit, has a poor CD. This is a very interesting phenomena that indicates that the OPE spacers work as transmitters of the chiral information from remote chiral centers to the polyene backbone —placed at 1.7 nm for poly-**2** and at 2.4 nm for poly-**3**— (Figure 4a). These large distances between the chiral center and the polymer main chain indicate that other mechanisms of chiral induction, such as chiral tele-induction effect, should be almost null in these cases.

In these two polymers (poly-**2** and poly-**3**), the chiral information transmission mechanism must occur in different sequential steps. First, the chiral centers possessing a major (*ap*) conformation induce a certain tilting degree (Θ) in the achiral spacer array. This step resembles the helical induction mechanism found in supramolecular helical polymers bearing OPE units.[32-34] Next, the chiral array induced in the OPE units is harvested by the polyene backbone, resulting in an effective *P* or *M* helix induction (Figure 2).[34,47]

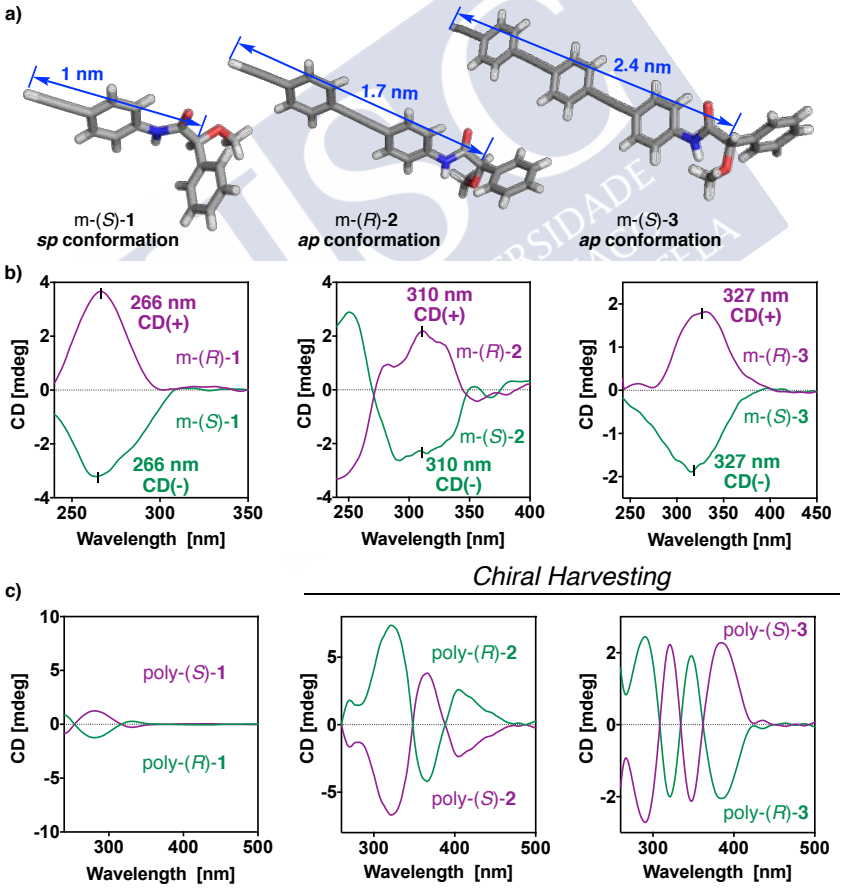

Figure 4. (a) X-ray structures of m-(*S*)-**1**, m-(*R*)-**2** and m-(*S*)-**3**. (b) CD traces of m-(*S*)- and m-(*R*)-**1**; m-(*S*)- and m-(*R*)-**2**; m-(*S*)- and m-(*R*)-**3** in $CHCl_3$ (0.1 mg·mL^{-1}). (c) CD spectra for poly-(*S*)- and poly-(*R*)-**1** in $CHCl_3$ (0.1 mg·mL^{-1}); poly-(*S*)- and poly-(*R*)-**2** in DMSO (0.1 mg·mL^{-1}); poly-(*S*)- and poly-(*R*)-**3** in DMSO (0.1 mg·mL^{-1}).

32 Aparicio, F.; García, F.; Fernández, G.; Matesanz, E.; Sánchez, L. *Chem. Eur. J.* **2011**, *17*, 2769-2776.
33 García, F.; Sánchez, L. *J. Am. Chem. Soc.* **2012**, *134*, 734-742.
34 Greciano, E. E.; Calbo, J.; Buendía, J.; Cerdá, J.; Aragó, J.; Ortí, E.; Sánchez, L. *J. Am. Chem. Soc.* **2019**, *141*, 7463-7472.
47 Kartha, K.; Wendler, F.; Rudolph, T.; Biehl, P.; Fernández, G.; Schacher, F. H. *Chem. Eur. J.* **2019**, *25*, 10464-10471.

Additional structural studies were carried out in poly-(*S*)-**2** and poly-(*S*)-**3** to obtain an approximated secondary structure of these polymers and determine their dynamic behaviour.

From literature it is known that the conformational equilibrium of poly-**1** can be altered in solution by the presence of metal ions. The addition of monovalent ions (e.g., Li^+) stabilizes the *ap* conformer at the pendant group by cation-π interactions, while divalent ions (e.g., Ca^{2+}) stabilize the *sp* conformations by chelation with the methoxy and carbonyl groups.[36,38,39,43] As a result, both the *P* or *M* helical senses can be selectively induced in poly-**1** by the action of metal ions.

Therefore, we decided to add different perchlorates of monovalent and divalent metal ions to solutions of poly-(*S*)-**2** and poly-(*S*)-**3** with the aim of determining the conformational composition at the pendant groups. Thus, when monovalent metal ions (Li^+, Ag^+ and Na^+) are added to a chloroform solution of poly-(*S*)-**2**, a chiral enhancement is observed (Figure 5d for Li^+ and see Experimental Section Chapter I, Figure S16 for Na^+ and Ag^+). IR and ^{7}Li-NMR studies show that those ions stabilize the *ap* conformer at the pendant group in a similar fashion to poly-**1**, this is by coordination to the carbonyl group of the MPA (Figure 5g) and the presence of a cation-π interaction with the aryl ring of the chiral ($|\Delta\delta|$ ^{7}Li ca., 3.75 ppm) (Figure 5f and see Experimental Section Chapter I). Therefore, addition of Li^+ produces a larger number of pendant groups with *ap* conformation among poly-**2,** which triggers a chiral enhancement effect through a cooperative process.

On the contrary, the addition of perchlorates of divalent metal ions, such as $Ca^{2+}$and Zn^{2+}, produced an inversion of the third Cotton band —310 nm— associated to the MPA moiety and the disappearance of both first and second Cotton effects (Figure 5e for Ca^{2+} and see Experimental Section Chapter I, Figure S17 for Zn^{2+}). This is a very interesting outcome because, although the conformational equilibrium at the MPA group changes from *ap* to *sp* after the addition of Ca^{2+}, the number of pendant groups with *sp* conformation do not reach the number needed to trigger the helix inversion process and in fact, a mixture of *P* and *M* helices at the polyene backbone is obtained.

The helical structures adopted by both polymer systems, PPAs (poly-**1**) and poly[oligo(*p*-phenyleneethynylene)phenylacetylene]s (POPEPAs) (poly-**2** and poly-**3**), are defined by two coaxial helices, one formed by the polyene backbone (internal helix, CD active) and the other constituted by the pendants (external helix, observed by AFM).

36 Freire, F.; Seco, J. M.; Quiñoá, E.; Riguera, R. *J. Am. Chem. Soc*. **2012**, *134*, 19374-19383.
38 Arias, S.; Freire, F.; Quiñoá, E.; Riguera, R. *Angew. Chem. Int. Ed*. **2014**, *53*, 13720-13724.
39 Arias, S.; Freire, F.; Quiñoá, E.; Riguera, R. *Polym. Chem*. **2015**, *6*, 4725-4733.
43 Arias, S.; Núñez-Martínez, M.; Quiñoá, E.; Riguera, R.; Freire, F. *Polym. Chem*. **2017**, *8*, 3740-3745.

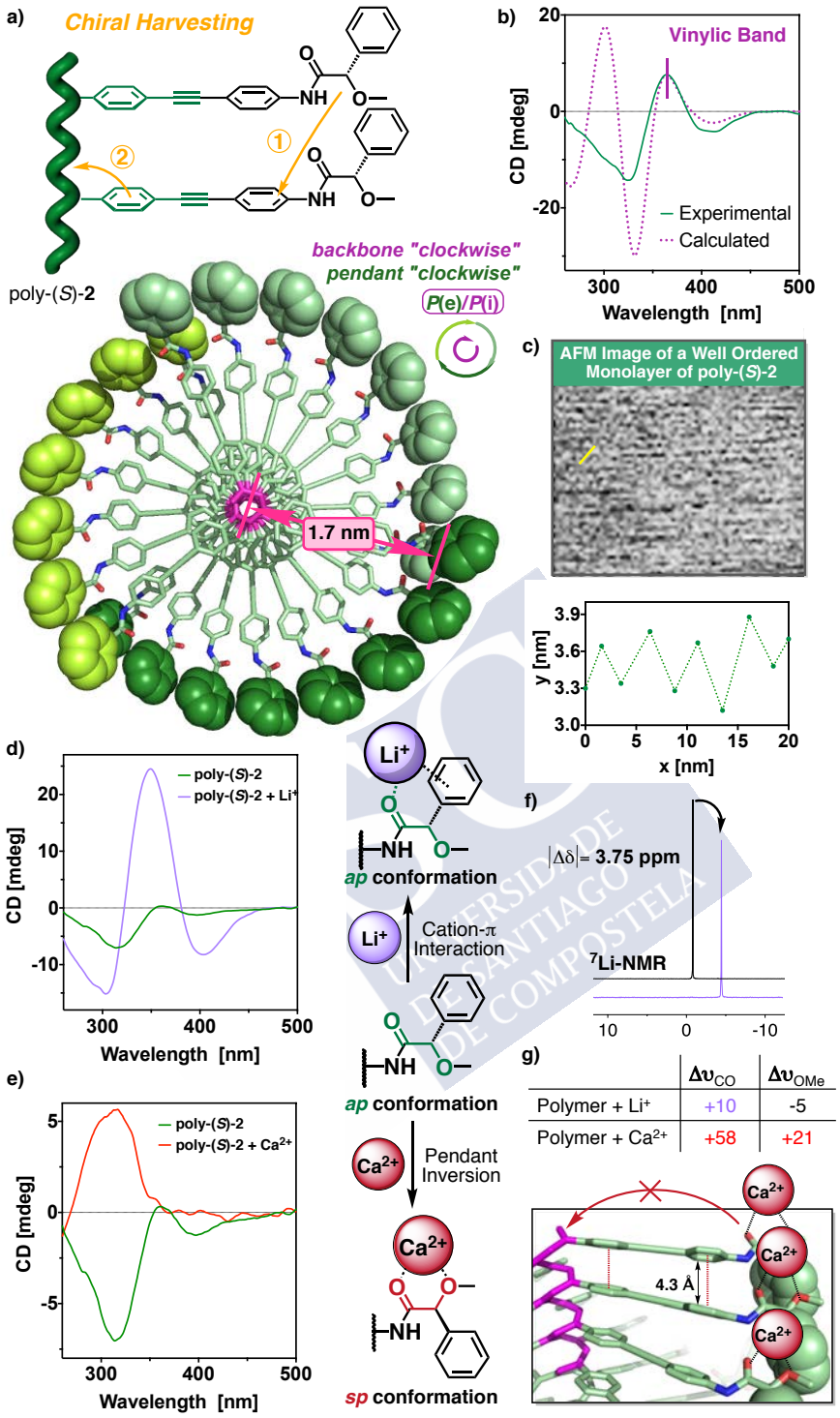

Figure 5. (a) Conceptual representation of the chiral information harvesting and top view of the 3D model for poly-(*S*)-**2**. (b) CD spectra of poly-(*S*)-**2** (0.2 mg·mL^{-1}) in DMSO vs calculated ECD spectra. Full Width at Half-Maximum (FWHM) equals 20 nm. (c) Low-resolution AFM image from a poly-(*S*)-**2** monolayer and profile depicting the chain separation of the yellow highlighted area in the AFM image. (d) CD spectra showing the chiral enhancement after the addition of Li^+ (50 mg·mL^{-1}, THF) to a poly-(*S*)-**2** solution (0.1 mg·mL^{-1}, $CHCl_3$). (e) CD trace of poly-(*S*)-**2** (0.1 mg·mL^{-1}, $CHCl_3$) before and after the addition of a Ca^{2+} solution (50 mg·mL^{-1}, THF). (f) ^{7}Li-NMR spectra substantiating the cation-π interaction. (g) IR shifts observed for carbonyl and methoxy groups after the addition of $LiClO_4$ and $Ca(ClO_4)_2$ (50 mg·mL^{-1}, THF) to a poly-(*S*)-**2** solution (3 mg·mL^{-1}, $CHCl_3$). The coordination modes of the MPA moiety with Li^+ and Ca^{2+} are shown vertically in the middle of the Figure.

These two helices can rotate in either the same or the opposite sense, depending on the dihedral angle between conjugated double bonds. Thus, internal and external helices rotate in the same direction in *cis-cisoidal* polymers, while they rotate in opposite directions in *cis-transoidal* ones.[14,42,48,49]

In order to find out an approximated helical structure for poly-(*S*)-**2**, DSC studies were performed. The thermogram shows a compressed *cis-cisoidal* polyene skeleton (see Experimental Section Chapter I, Figure S13a) similar to the one obtained for poly-**1**.[42] Moreover, although AFM studies on a 2D crystal of poly-(*S*)-**2** did not produce high-resolution AFM images, some parameters such as helical pitch (ca., 2.8 nm) and packing distance between helices of (ca., 6 nm) could be extracted from the well-ordered monolayer analyzed (Figure 5c).

Previous structural studies in PPAs found that it is possible to correlate the internal helical sense with the Cotton band associated to the polyene backbone —CD (+), P_{int}; CD (-), M_{int}—.[50,51] Herein, the positive Cotton effect observed for the polyene backbone [$CD_{365\ nm}$ = (+)] in poly-(*S*)-**2** is indicative of a *P* orientation of the internal helix, which correlates with a *P* orientation of the external helix in a *cis-cisoidal* polyene scaffold. To summarize, DSC, AFM and CD studies agree that poly-(*S*)-**2** is made up of a *cis-cisoidal* framework with P_{int} and P_{ext} helicities (Figure 5a).

Computational studies [TD-DFT(CAM-B3LYP)/3-21G] were carried out on a *P* helix of an n = 9 oligomer of poly-(*S*)-**2**, possessing a *cis-cisoidal* polyene skeleton (ω_1 = +50°, ω_3 = -40°) and an *antiperiplanar* orientation of the carbonyl and methoxy groups at the pendants. The theoretical ECD spectrum obtained from these studies (Figure 5b and see Experimental Section Chapter I) is in good agreement with the experimental one, indicating that our model structure is a good approximation of the helical structure adopted by poly-(*S*)-**2**.

Next, a similar set of DSC and AFM studies were carried out for poly-(*S*)-**3**, that bears an OPE spacer with n = 2. The data showed that this polymer presents a compressed *cis-cisoidal* polyene skeleton, similar to those obtained for poly-**1** and poly-**2** (see Experimental Section Chapter I, Figure S13b), with a helical pitch of 3.8 nm and a P_{ext} helical sense (Figures 6a, c).

UV studies indicate that, in poly-(*S*)-**3**, the polyene backbone absorbs at ca. 380 nm, coincident with the first Cotton effect, that is positive (see Experimental Section Chapter I, Figure S15b). Therefore, it reveals that poly-(*S*)-**3** adopts a P_{int} helicity (Figure 6b). Thus, as expected for *cis-cisoidal* scaffolds, the orientations of the two coaxial helices are coincident.

Computational studies [TD-DFT(CAM-B3LYP)/3-21G] were carried out on a *P* helix of an n = 9 oligomer of poly-(*S*)-**3**, possessing a *cis-cisoidal* polyene skeleton (ω_1 = +63°, ω_3 = -40°) and

14 Suárez-Picado, E.; Quiñoá, E.; Riguera, R.; Freire, F. *Angew. Chem. Int. Ed.* **2020**, *59*, 5437-4543.
42 Rodríguez, R.; Quiñoá, E.; Riguera, R.; Freire, F. *J. Am. Chem. Soc.* **2016**, *138*, 9620-9628.
48 Palomo, L.; Rodríguez, R.; Medina, S.; Quiñoá, E.; Casado, J.; Freire, F.; Ramírez, F. J. *Angew. Chem. Int. Ed.* **2020**, *59*, 9080-9087.
49 Freire, F.; Quiñoá, E.; Riguera, R. *Chem. Commun.* **2017**, *53*, 481-492.
50 Fernández, B.; Rodríguez, R.; Rizzo, A.; Quiñoá, E.; Riguera, R.; Freire, F. *Angew. Chem. Int. Ed.* **2018**, *57*, 3666-3670.
51 Fernández, B.; Rodríguez, R.; Quiñoá, E.; Riguera, R.; Freire, F. *ACS Omega* **2019**, *4*, 5233-5240.

an *antiperiplanar* orientation of the carbonyl and methoxy groups at the pendants. The theoretical results (Figure 6b and see Experimental Section Chapter I) match with the experimental data, indicating that our model structure is a good approximation to the helical structure adopted by poly-(*S*)-**3**.

Finally, the stimuli response properties of poly-(*S*)-**3** were explored by CD. These experiments revealed that the addition of monovalent or divalent metal ions to a chloroform solution of poly-(*S*)-**3** does not produce any significant effect in the structural equilibrium of this polymer (see Experimental Section Chapter I, Figure S18). This fact, in addition to the previous results obtained from the interaction of poly-(*S*)-**2** with divalent metal ions, corroborates the decrease of the dynamic character of helical PPAs when large OPEs are used as spacers.

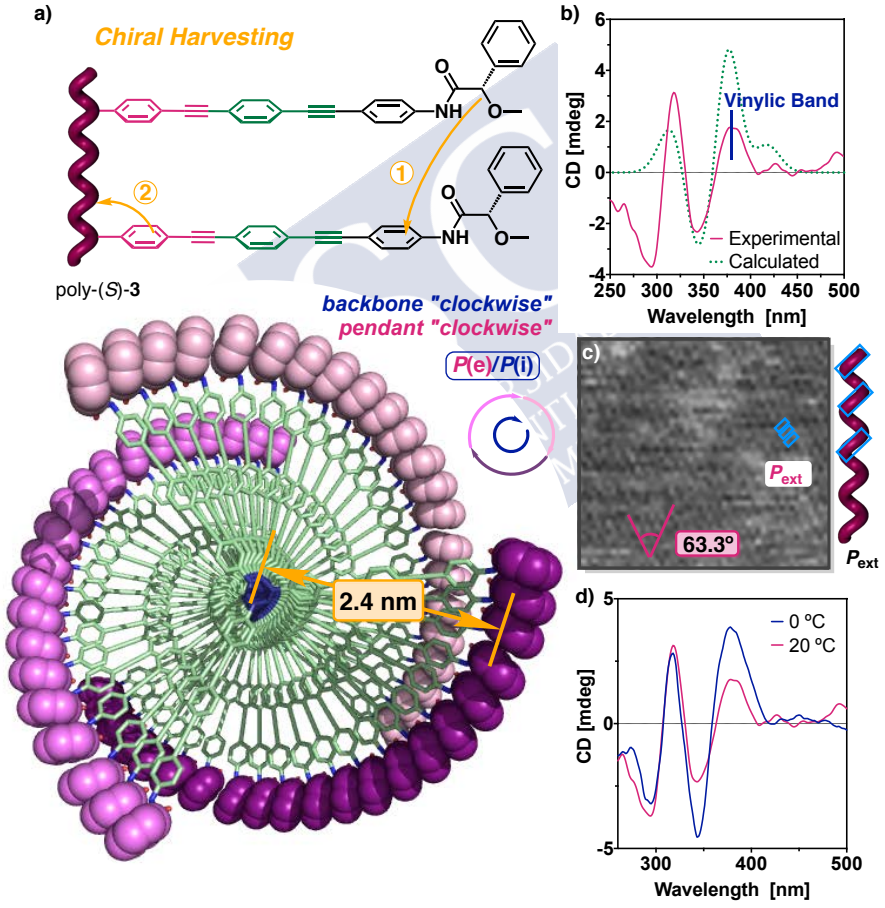

Figure 6. (a) Conceptual representation of the chiral information harvesting and top view of the 3D model for poly-(*S*)-**3**. (b) CD spectrum of poly-(*S*)-**3** in THF (0.2 mg·mL^{-1}) and comparison to the calculated ECD spectra. Full Width at Half-Maximum (FWHM) equals 20 nm. (c) AFM image obtained from a poly-(*S*)-**3** monolayer. (d) CD traces for poly-(*S*)-**3** in THF (0.2·mg mL^{-1}) polymerized at different temperatures.

The poor dynamic behaviour was further demonstrated by polymerizing m-(*S*)-**3** at a lower temperature (0 °C) (Figure 6d). In this case, the region around 240-350 nm remains unaffected, indicating that the pendant is ordered in a similar manner in both batches of polymers, regardless of the temperature at which they were synthesized (20 °C and 0 °C).

Interestingly, the magnitude of the first Cotton band is duplicated when the polymer is obtained at low temperature due to a stronger helical sense induction at the polyene backbone. This result indicates that a preorganization process may occur during polymerization, affecting the screw sense excess of the PPA.

Chapter II

Aromatic Substitution Pattern Effects in Poly[[oligo(phenyleneethynylene)]phenylacetylene]s: Modulation of the Helical Periphery Without Affecting the Folding of the Main Chain

USC
UNIVERSIDADE
DE SANTIAGO
DE COMPOSTELA

Chapter II. Aromatic Substitution Pattern Effects in Poly[[oligo(phenylene ethynylene)]phenylacetylene]s: Modulation of the Helical Periphery Without Affecting the Folding of the Main Chain

Abstract: *The different ortho-, meta- and para- aromatic substitution pattern in poly(phenylacetylene)s (PPAs) has a large effect over the helical structure of the polymer, due to the steric repulsions between the pendant and the polyene backbone, as well as in the flexibility of the polyene backbone. Hence, the helical periphery and the helical scaffold of PPAs are largely affected by mutations in the aryl ring. This problem is surpassed by the introduction of a rigid spacer such as an oligo(p-phenyleneethynylene)$_n$ (OPE, n = 1, 2) between these two structural motifs —pendant and backbone—, resulting in a release of the congestion suffered in the meta- and ortho- derivatives. Additionally, this novel family of helical polymers presents, among the different aromatic substituted polymers, the same helix induction due to the presence of a chiral harvesting mechanism; generating a helical structure with a resembling scaffold —similar stretching degree and identical P or M helical sense— but with different decoration at the periphery, where the pendant groups are located in different positions at the outer helix.*

USC
UNIVERSIDADE
DE SANTIAGO
DE COMPOSTELA

Biomolecules such as DNA, polysaccharides or proteins adopt helical structures that are directly related to their biological functions. Non-natural macromolecules such as helical polymers offer the possibility of creating new structures with novel functionalities with applications in different fields such as sensing,[10-10] chiral recognition,[11-13] chiral stationary phases,[14,15] asymmetric catalysts,[16-23] chiral templates,[24-26] building blocks in supramolecular chemistry,[117-31] optical switches[32,33] or emitting devices,[34] among others. As their applicability relies on the helical structure adopted by the polymer, the elucidation of the secondary structure is an important topic that still remains challenging nowadays. The main difficultness found in the structural elucidation of these materials is the presence of a monomer repeating unit (m.r.u.) along the polymer chain, which makes classical and powerful structural techniques like Nuclear Magnetic Resonance (NMR) or X-ray useless.

In general, to obtain the secondary structure of a helical polymer such as a poly(phenylacetylene) (PPA) it is necessary to combine information from different structural techniques —NMR, X-ray, Atomic Force Microscopy (AFM), Circular Dichroism (CD), UV-Vis, Time-Dependent Density Functional Theory (TD-DFT) computational studies, Vibrational Circular Dichroism (VCD), Raman Optical Activity (ROA) and so—. However, in many cases the data obtained from these studies does not fit well to solve the puzzle of the polymer helical structure. Despite this difficulty encountered when solving the secondary structure of a helical

10 Maeda, K.; Hirose, H.; Okoshi, N.; Shimomura, K.; Wada, Y.; Ikai, T.; Kanoh, S.; Yashima, E. *J. Am. Chem. Soc*. **2018**, *140*, 3270-3276.
2 Maeda, K.; Yashima, E. *Top. Curr. Chem.* **2017**, *375*, 72.
3 Pauly, A. C.; Theato, P. *Macromol. Rapid Commun*. **2013**, *34*, 516-521.
4 Yashima, E.; Maeda, K. Macromolecules **2008**, 41, 3-12.
5 Maeda, K.; Morioka, K.; Yashima, E. *Macromolecules* **2007**, *40*, 1349-1352.
6 Maeda, K.; Mochizuki, H.; Watanabe, M.; Yashima, E. *J. Am. Chem. Soc*. **2006**, *128*, 7639-7650.
7 Maeda, K.; Yashima, E. *Top. Curr. Chem.* **2006**, *265*, 47.
8 Maeda, K.; Kamiya, N.; Yashima, E. *Chem. Eur. J.* **2004**, *10*, 4000-4010.
9 Onouchi, H.; Maeda, K.; Yashima, E. *J. Am. Chem. Soc.* **2002**, *123*, 7441-7442.
10 Yashima, E.; Maeda, Y.; Matsushima, T.; Okamoto, Y. *Chirality* **1997**, *9*, 593-600.
11 Anger, E.; Iida, H.; Yamaguchi, T.; Hayashi, K.; Kumano, D.; Crassous, D.; Vanthuyne, N.; Rousselc, C.; Yashima, E. *Polym. Chem.* **2014**, *5*, 4909-4914.
12 Iida, H.; Miki, M.; Iwahana, S.; Yashima, E. *Chem. Eur. J.* **2014**, *20*, 4257-4262.
13 Yashima, E.; Maeda, K.; Sato, O. *J. Am. Chem. Soc*. **2001**, *123*, 8159-8160.
14 Hirose, D.; Isobe, A.; Quiñoá, E.; Freire, F.; Maeda, K. *J. Am. Chem. Soc.* **2019**, *141*, 8592-8598.
15 Shimomura, K.; Ikai, T.; Kanoh, S.; Yashima, E.; Maeda, K. *Nat. Chem*. **2014**, *6*, 429-434.
16 Yamamoto, T.; Murakami, R.; Komatsu, S.; Suginome, M. *J. Am. Chem. Soc.* **2018**, *140*, 3867-3870.
17 Yamamoto, T.; Murakami, R.; Suginome, M. *J. Am. Chem. Soc.* **2017**, *139*, 2557-2560.
18 Taura, D.; Hioki, S.; Tanabe, J.; Ousaka, N.; Yashima, E. *ACS Catal.* **2016**, 6, 4685-4689.
19 Yuan-Zhen, K.; Nagata, Y.; Yamada, T.; Suginome, M. *Angew. Chem. Int. Ed.* **2015**, *54*, 9333-9337.
20 Liu, L.; Long, Q.; Aoki, T.; Zhang, G.; Kaneko, T.; Teraguchi, M.; Zhang, Ch.; Wang, Y. *Chirality* **2015**, *27*, 454-458.
21 Iida, H.; Tang, Z.; Yashima, E. *J. Polym. Sci., Part A: Polym. Chem.* **2013**, *51*, 2869-2879.
22 Tang, Z.; Iida, H.; Hu, H.-Y.; Yashima, E. *ACS Macro Lett.* **2012**, *1*, 261-265.
23 Megens, R. P.; Roelfes, G. *Chem. Eur. J.* **2011**, *17*, 8514-8523.
24 Nieto-Ortega, B.; Rodríguez, R.; Medina, S.; Quiñoá, E.; Riguera, R.; Casado, J.; Freire, F.; Ramírez, J. *J. Phys. Chem. Lett*. **2018**, *9*, 2266-2270.
25 Miyagawa, T.; Yamamoto, M.; Muraki, R.; Onuchi, H.; Yashima, E. *J. Am. Chem. Soc.* **2007**, *129*, 3676-3682.
26 Onuchi, H.; Miyagawa, T.; Morino, K.; Yashima, E. *Angew. Chem Int. Ed*. **2006**, *45*, 2381-2384.
27 Freire, F.; Quiñoá, E.; Riguera, R. *Chem. Rev*. **2016**, *116*, 1242-1271.
28 Arias, S.; Núñez-Martínez, M.; Quiñoá, E.; Riguera, R.; Freire, F. *Small* **2016**, *13*, 1602398.
29 Arias, S.; Freire, F.; Quiñoá, E.; Riguera, R. *Angew. Chem., Int. Ed.* **2014**, *53*, 13720-13724.
30 Freire, F.; Seco, J. M.; Quiñoá, E.; Riguera, R. *Adv. Polym. Sci*. 2013, *262*, 123-140.
31 Freire, F.; Seco, J. M.; Quiñoá, E.; Riguera, R. *J. Am. Chem. Soc.* 2012, *134*, 19374-19383.
32 Rodríguez, R.; Quiñoá, E.; Riguera, R.; Freire, F. *Small* **2019**, *15*, 1805413.
33 Rodríguez, R.; Quiñoá, E.; Riguera, R.; Freire, F. *Chem. Matter.* **2018**, *30*, 2493-2497.
34 Lam, J. W. Y.; Tang, B. Z. *J. Polym. Sci., Part A: Polym. Chem.* **2003**, *41*, 2607-2629.

polymer, in literature there are reported some approximated 3D structures of several helical polymers such as PPAs.[24,125-53] By combination of all the structural information extracted from these PPAs, our group could establish a relationship between the helical scaffold adopted by the polymer and some structural features of the monomer. This fact suggests that is possible to predict an approximated secondary structure of a helical PPA by monomer design. To this end, two important parameters have to be taken into account: 1.- the functional group used as connector between the pendant and the phenylacetylene backbone and 2.- the aromatic substitution pattern of the aryl ring of the PPA.[54]

Recently, our group has reported a novel family of helical polymers derived from PPAs that use oligo(phenyleneethynylene)s —OPEs— as spacers, the poly[oligo(phenyleneethynylene)phenylacetylene]s —POPEPAs—.[55] In these materials the mechanism of helix induction depends on the size of the oligomer used as spacer between the chiral moiety and the polyene main chain. Thus, while in a classical PPA the helix induction is produced mainly by chiral tele-induction —spatial location of the substituents at the chiral moiety— (Scheme 1a), in PPAs bearing OPEs (POPEPAs), the helix induction is produced by a combination of a chiral tele-induction together with a chiral harvesting process —the chiral information of the asymmetric center is transmitted to the achiral spacer resulting into a stacking of the OPEs, which is further harvested by the polyene backbone— (Scheme 1b). The strength of this mechanism is directly related to the OPE length; in a short OPE (n = 1) both mechanisms take place, while in larger OPEs ($n \geq 2$) the chiral harvesting process masters the chiral induction.

24 Nieto-Ortega, B.; Rodríguez, R.; Medina, S.; Quiñoá, E.; Riguera, R.; Casado, J.; Freire, F.; Ramírez, J. *J. Phys. Chem. Lett.* **2018**, *9*, 2266-2270.
125 Freire, F.; Quiñoá, E.; Riguera, R. *Chem. Commun.* **2016**, *53*, 481-492.
36 Ohsawa, S.; Sakurai, S.-I.; Nagai, K.; Banno, M.; Maeda, K.; Kumaki, J.; Yashima, E. *J. Am. Chem. Soc.* **2011**, *133*, 108-114.
37 Yashima, E. *Polym. J.* **2010**, *42*, 3-16.
38 Kumaki, J.; Sakurai, S.-I.; Yashima, E. *Chem. Soc. Rev.* **2009**, *38*, 737-746.
39 Sakurai, S.-I.; Ohsawa, K.; Nagai, K.; Okoshi, K.; Kumaki, J.; Yashima, E. *Angew. Chem., Int. Ed.* **2007**, *46*, 7605-7608.
40 Okoshi, K.; Sakurai, S.; Ohsawa, J. K.; Yashima, E. *Angew. Chem., Int. Ed.* **2006**, *45*, 1245-1248.
41 Sakurai, S.-I.; Okoshi, K.; Kumaki, J.; Yashima, E. *J. Am. Chem. Soc.* **2006**, *128*, 5650-5651.
42 Nishimura, T.; Takatani, K.; Sakurai, S.; Maeda, K.; Yashima, E. *Angew. Chem., Int. Ed.* **2002**, *41*, 3602-3604.
43 Kumaki, J. *Polym. J.* **2016**, *48*, 3-14.
44 Percec, V.; Rudick, J. G.; Wagner, M.; Obata, M.; Mitchell, C. M.; Cho, W.-D.; Magonov, S. N. *Macromolecules* **2006**, *39*, 7342-7351.
45 Percec, V.; Rudick, J. G.; Peterca, M.;Staley S. R.; Wagner, M.; Obata, M.; Mitchell, C. M.; Cho, W.-D.; Balagurusamy, V. S. K.; Lowe, J. N.; Glodde, M.; Weichold, O.; Chung, K. J.; Ghionni, N.; Magonov, S. N.; Heney, P. A. *Chem. Eur. J.* **2006**, *12*, 5731-5746.
46 Fernández, B.; Rodríguez, R.; Quiñoá, E.; Riguera, R.; Freire, F. *ACS Omega* **2019**, *4*, 5233-5240.
47 Fernández, B.; Rodríguez, R.; Rizzo, A.; Quiñoá, E.; Riguera, R.; Freire, F. *Angew. Chem. Int. Ed.* **2018**, *57*, 3666-3670.
48 Hase, Y.; Nagai, K.; Iida, H.; Maeda, K.; Ochi, N.; Sawabe, K.; Sakajiri, K.; Okoshi, K.; Yashima, E. *J. Am. Chem. Soc.* **2009**, *131*, 10719-10732.
49 Fukuda, M.; Rodríguez, R.; Fernández, Z.; Nishimura, T.; Hirose, D.; Watanabe, G.; Quiñoá, E.; Freire, F.; Maeda, K. *Chem. Commun*. **2019**, *55*, 7906-7909.
50 Li, G.; Kessler, J.; Cheramy, J.; Wu, T.; Poopari, M. R.; Bour, P.; Xu, Y. *Angew. Chem. Int. Ed.* **2019**, *58*, 16495-16498.
51 Lizio, M. G.; Andrushchenko, V.; Pike, S. J.; Peters, D. A.; Whitehead, G. F. S.; Vitórica-Yrezábal, I. J.; Mutter, S. T.; Clayden, J.; Bour, P.; Xu, Y. *Chem. Eur. J.* **2018**, *24*, 9399-9408.
52 Rodríguez, R.; Ignés-Mullol, J.; Sagués, F.; Quiñoá, E.; Riguera, R.; Freire, F. *Nanoscale* **2016**, *8*, 3362-3367.
53 Palomo, L.; Rodríguez, R.; Medina, S.; Quiñoá, E.; Casado, J.; Freire, F.; Ramírez, F. J. *Angew. Chem. Int. Ed.* **2020**, *59*, 9080-9087.
54 Rodríguez, R.; Quiñoá, E.; Riguera, R.; Freire F. *J. Am. Chem. Soc.* **2016**, *138*, 9620-9628.
55 Fernández, Z.; Fernández, B.; Quiñoá, E.; Riguera, R.; Freire, F. *Chem. Sci.* **2020**, *11*, 7182-7187.

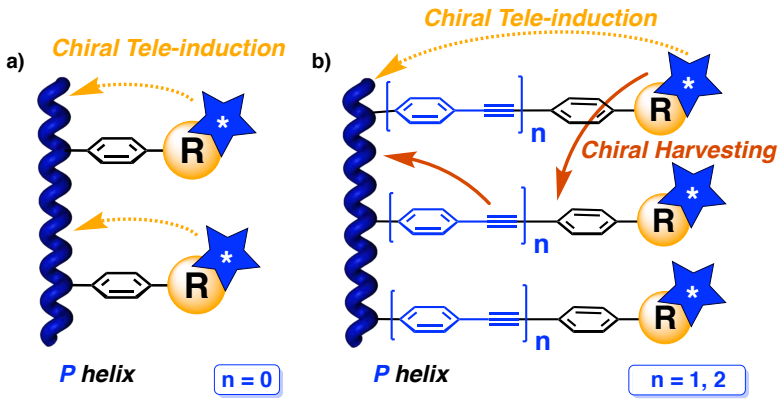

Scheme 1. Schematic representation of the helix induction mechanism found in (a) PPAs —chiral tele-induction— and (b) POPEPAs —chiral tele-induction and chiral harvesting—.

The introduction of an achiral spacer between the chiral pendant and the polyene backbone reduces the steric hindrance between these two structural moieties. As a result, compressed helices will be obtained when compared with the corresponding PPA equivalents. This fact drove us to explore how the different aromatic substitution pattern in the external aryl group of the POPEPAs affects to the helical scaffold and dynamic behaviour comparing to their PPAs counterparts (Scheme 2).

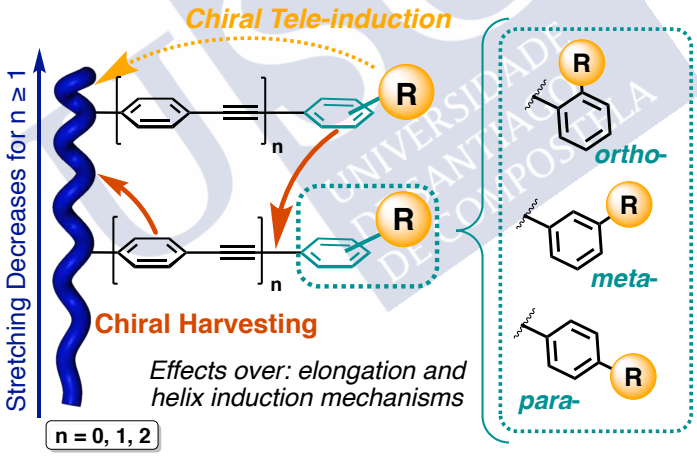

Scheme 2. Conceptual representation of the aromatic substitution effects in POPEPAs.

To carry out these studies, six oligo(*p*-phenyleneethynylene)$_n$phenylacetylene (OPE) monomers (n = 1, 2) containing the *ortho*-, *meta*- and *para*- ethynilanilide of (*S*)-α-methoxy-α-phenylacetic acid (MPA) were synthetized —*o*-, *m*- and *p*-M-(*S*)-**2**; *o*-, *m*- and *p*-M-(*S*)-**3**— and further polymerized by using a Rh (I) catalyst (Figure 1 and see Experimental Section Chapter II).

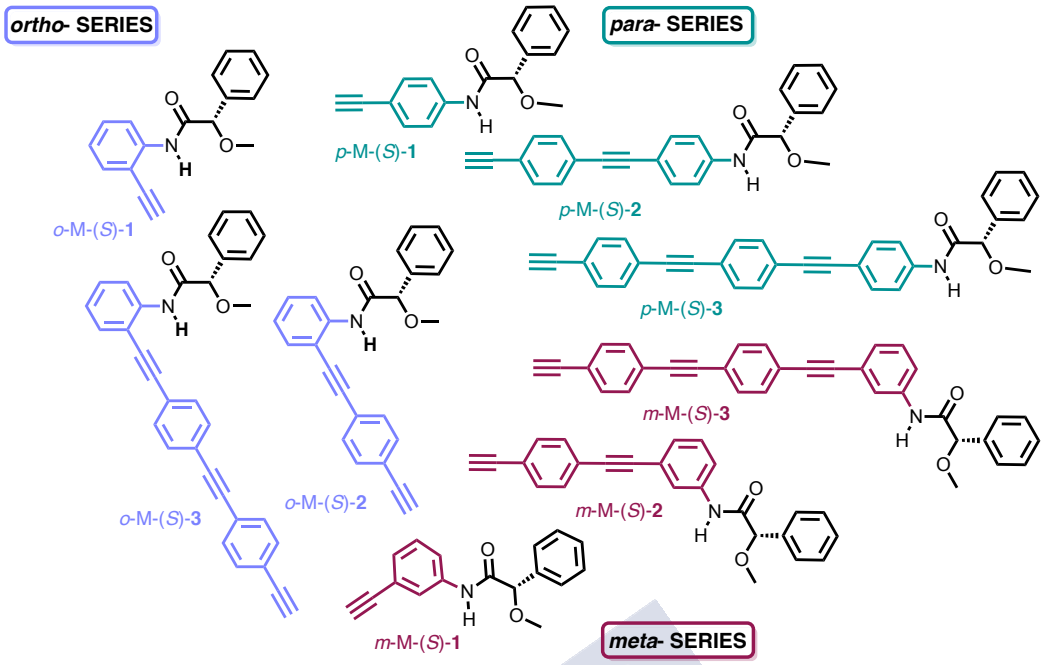

Figure 1. Structures of monomers *o*, *m*, *p*-M-(*S*)-[**1**-**3**].

Next, structural and dynamic behaviour studies of these polymers were carried out and compared to their corresponding PPAs counterparts, the poly-**1** series (Figure 1).[54]

Structural studies for *p*-poly-**2** revealed the presence of a *cis-cisoidal* polyene skeleton,[55] while DSC studies for *m*-poly-**2** and *o*-poly-**2** indicate the presence of a more stretched *cis-transoidal* polyene backbone, necessary to accommodate the pendant groups in a closer position regarding to the polyene backbone (see Experimental Section Chapter II, Figure S16a-b). This helical stretching is confirmed by comparing the UV-Vis traces for the three different aromatic substituted poly-**2** series (Figure 2b), which shows a bathochromic shift when the pendant is placed towards the backbone, from the *para*- to the *ortho*- position (Figure 2b).

It should be noted the role played by the OPE spacer in the elongation of the polyene backbone. For the poly-**1** series, devoid of the OPE spacer, a large bathochromic shift is observed when the pendant is approached to the backbone (ca., 90 nm; Figure 2a), whereas in the case of the poly-**2** series this bathochromic shift is reduced (ca., 40 nm; Figure 2b). This fact indicates that in an *ortho*- substituted PPA, such as *o*-poly-**1**, the congestion present in the helical scaffold induced by the proximity of the pendant to the backbone is released by a large stretching of the polyene backbone. On the other hand, in the poly-**2** series —i.e., *o*-poly-**2**—, the insertion of a phenyleneethynylene group as spacer results in a better accommodation of the pendant group at the *ortho*- position and only a small elongation of the polyene backbone is produced.

[54] Rodríguez, R.; Quiñoá, E.; Riguera, R.; Freire F. *J. Am. Chem. Soc.* **2016**, *138*, 9620-9628.
[55] Fernández, Z.; Fernández, B.; Quiñoá, E.; Riguera, R.; Freire, F. *Chem. Sci.* **2020**, *11*, 7182-7187.

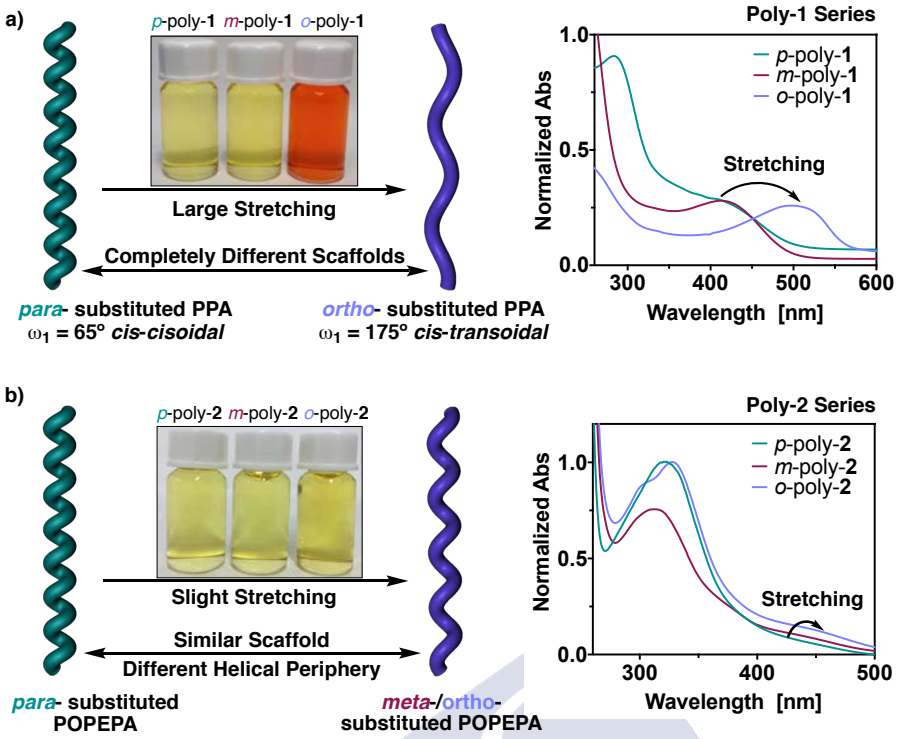

Figure 2. Overlay of the normalized UV-vis spectra for (a) *p*-poly-**1**, *m*-poly-**1** and *o*-poly-**1** (0.1 mg·mL^{-1}, $CHCl_3$) and (b) for *p*-poly-**2**, *m*-poly-**2** and *o*-poly-**2** (0.2 mg·mL^{-1}, DCM).

In the case of the polymer series bearing an OPE spacer with n = 1 —poly-**2** series; *p*-, *m*- and *o*-poly-**2**—, it was found that the three polymers adopt a preferred *P* helix that cannot be inverted by changing the polarity of the media (Figure 3 and see Experimental Section Chapter II, Figure S18a-c). The helical sense induction in the poly-**2** series is produced due to a combination of two different chiral information transmission mechanisms, chiral tele-induction and chiral harvesting (Figure 3). The medium size of the achiral spacer —OPE n = 1—, which separates the chiral group and the polyene backbone, is still short enough [1.7 nm in *p*-poly-**2**, 1.4 nm in *m*-poly-**2**, and 1.0 nm in *o*-poly-**2**] to have an operative chiral tele-induction mechanism (Figure 3). This tele-induction effect is accompanied by a chiral harvesting process, which is produced due to a chiral organization of the achiral spacers along the polymer and further harvested by the polyene backbone (Figure 3).

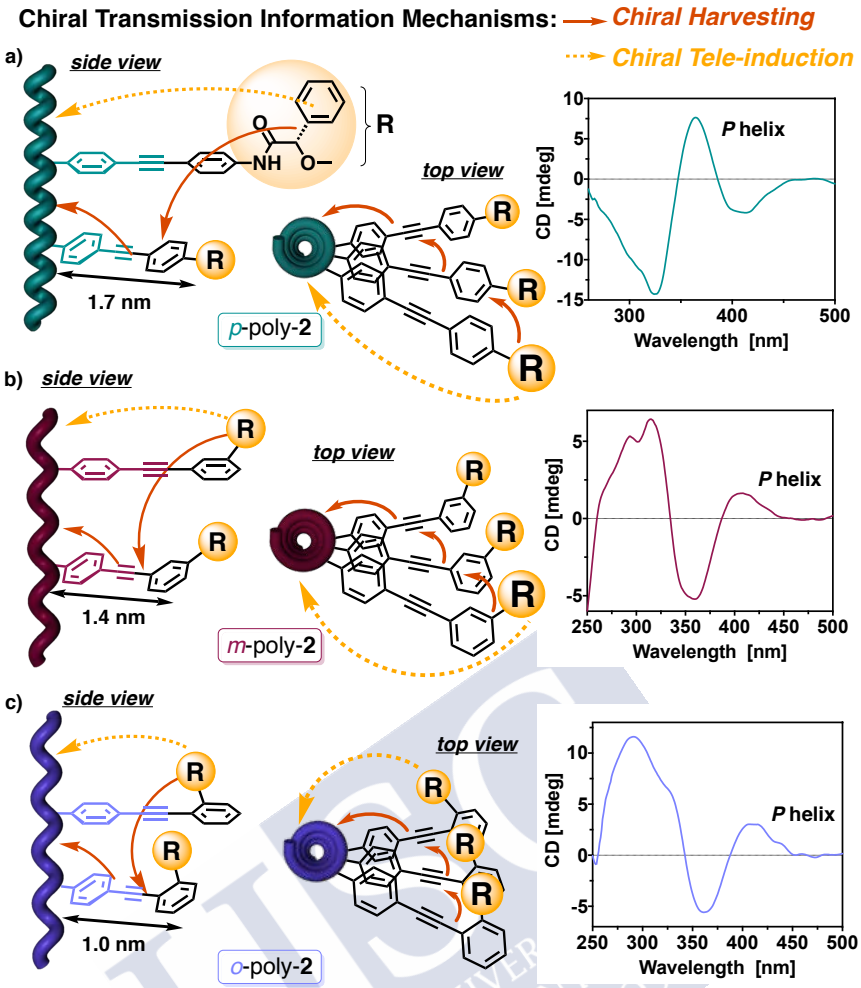

Figure 3. CD traces for (a) *p*-poly-**2** (0.2 mg·mL^{-1}, DMF), (b) *m*-poly-**2** (0.2 mg·mL^{-1}, DCM), (c) *o*-poly-**2** (0.2 mg·mL^{-1}, DMF).

Finally, the helical scaffold and dynamic behaviour of the poly-**3** series —*p*-, *m*- and *o*-poly-**3**— bearing an OPE with n = 2 as achiral spacer was analysed (Figure 4).

CD studies within this polymer series indicate that while *p*- and *o*-poly-**3** show the presence of a biased *P* helical sense, due to an effective chiral transmission harvesting process —from the remote chiral center to the polyene backbone; 2.4 nm in *p*-poly-**3** (Figure 4a) and 1.7 nm in *o*-poly-**3** (Figure 4c)—, *m*-poly-**3** appears as an axially racemic helix (Figure 4b). The absence of helical induction in *m*-poly-**3** occurs as a consequence of the two possible *meta*-orientations that the pendant group in *m*-poly-**3** can adopt.[56,57] This fact, in combination with the remote location of the chiral center regarding to the polyene backbone, results in an equal population of the *P* and *M* helical structures.

Structural studies such as DSC experiments, revealed that the three polymers adopt a compressed *cis-cisoidal* scaffold with a single exothermic peak —287°C for *p*-poly-**3**;[55] 261°C for *m*-poly-**3**; and 196°C for *o*-poly-**3** (see Experimental Section Chapter II, Figure S16c-d)—.

[56] Goto, H.; Morino, K.; Morishita, T.; Maeda, K.; Yashima, E. *Kobunshi Ronbunshu* **2006**, *63*, 325-330.
[57] Maeda, K.; Okada, S.; Yashima, E.; Okamoto, Y. *J. Polym. Sci. A Polym. Chem.* **2001**, *39*, 3180-3189.
[55] Fernández, Z.; Fernández, B.; Quiñoá, E.; Riguera, R.; Freire, F. *Chem. Sci.* **2020**, *11*, 7182-7187.

UV-vis experiments confirmed the presence of a similar scaffold for the three different *ortho*-, *meta*- and *para*- substituted polymers of the poly-**3** series, where no bathochromic or hypsochromic shifts for the polyene backbone are observed (Figure 4d). Therefore, these results indicate that in POPEPAs bearing an OPE spacer with n = 2, the steric hindrance caused by the pendant group is vanished, as no variations are observed by UV-Vis.

The location of the pendant group in a remote position regarding to the polyene backbone (> 1.7nm) within this polymer series —*o*-, *m*-, *p*-poly-**3**—, in combination with the small size of the pendant group, indicates that the mechanism of helix induction in the poly-**3** series is ruled by the chiral information harvesting process (Figure 4).

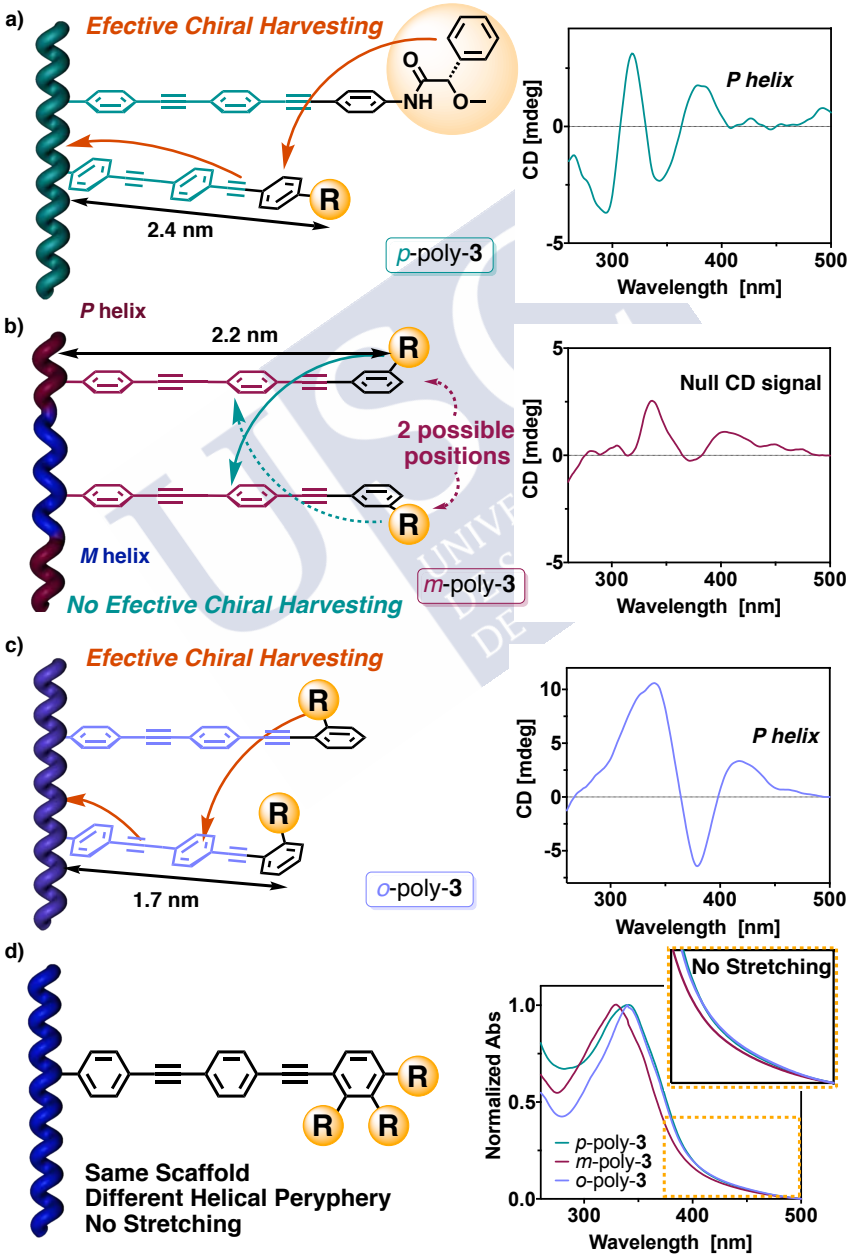

Figure 4. CD traces for (a) *p*-poly-**3** (0.2 mg·mL^{-1}, THF), (b) *m*-poly-**3** (0.2 mg·mL^{-1}, THF), (c) *o*-poly-**3** (0.1 mg·mL^{-1}, THF). (d) Overlay of the normalized UV-vis spectra for *p*-poly-**3**, *m*-poly-**3** (0.2 mg·mL^{-1}, THF) and *o*-poly-**3** (0.1 mg·mL^{-1}, THF).

USC
UNIVERSIDADE
DE SANTIAGO
DE COMPOSTELA

Chapter III

Complex Supramolecular Polymerization Pathway of an Asymmetrical and Rigid OPE Derivative: The Role of the Supramolecular Polymerization Degree in the Aggregate Morphology

USC
UNIVERSIDADE
DE SANTIAGO
DE COMPOSTELA

Chapter III. Complex Supramolecular Polymerization Pathway of an Asymmetrical and Rigid OPE Derivative: The Role of the Supramolecular Polymerization Degree in the Aggregate Morphology

Abstract: *The polymerization of a short and rigid oligo(phenyleneethynylene) (OPE,* **1***) produces a complex supramolecular polymerization pathway in a MCH:DCM (99:1) solvent mixture, where a kinetic —***Agg**$_{\mathbf{I}}$*— and a thermodynamic —***Agg**$_{\mathbf{II}}$*— aggregate are formed via an isodesmic process. Both aggregates show opposite axial chirality and different polymer length, which are responsible for the different aggregate morphology. Thus, while the formation of short P-twisted oligomers (off-pathway,* **Agg**$_{\mathbf{I}}$*) produces in-plane aggregation to generate brick-like nanostructures; the formation of large supramolecular helical polymers (on-pathway,* **Agg**$_{\mathbf{II}}$*) yields M type columnar helical aggregates, which can be visualized by AFM. Interestingly,* **Agg**$_{\mathbf{I}}$ *(off-pathway) can be kinetically trapped by changing the solvent conditions to MCH:Tol:DCM (97:2:1), remaining stable for days.*

USC
UNIVERSIDADE
DE SANTIAGO
DE COMPOSTELA

Supramolecular polymers (SP) arise from the self-assembly of small organic molecules via non-covalent interactions. The dynamic and reversible character of these weak forces provides unique properties to these materials, revealing promising applications in fields such as pharmaceuticals,[1] nanoelectronics[2] or catalysis,[3] among others.

The inherent properties that these polymers may present are determined by the growth mechanism that binds the monomeric units together. Related to this, Meijer *et al.* have extensively studied several supramolecular polymers build-up by different self-assembling systems. From these studies they inferred that, according to the mechanism for aggregate formation, the polymerization process could be mainly classified either as isodesmic or as cooperative.[4] Whether the polymer formation follows a mechanistic pathway or another depends on the non-covalent interactions present throughout the supramolecular structure; primarily hydrogen-bonding and **π-π** stacking, in combination with other non-directional forces.[5] Therefore, the design of the monomeric units that build up the supramolecular scaffold is key for an effective organization.

In addition to the above classification of the supramolecular polymerization mechanism, more complex SPs, in which the self-assembly process is governed by kinetics and not only by thermodynamics, have recently been described. These out-of-equilibrium states can be classified as non-dissipative non-equilibrium states —i.e., metastable and kinetically trapped states— or as dissipative non-equilibrium states —i.e., fueled aggregation and competitive or consecutive supramolecular polymerization— yielding, from the same building block, different self-assembled structures just by adjusting the experimental conditions.[6]

From literature it is known that within all supramolecular polymers, those formed by building blocks containing π-conjugated cores —perylenebisimides [PBIs];[7] benzene-1,3,5-tricarboxiamides [BTAs];[8] oligo(phenyleneethynylene)s [OPEs];[9] *peri*-hexabenzenecoronenes

---

1 (a) Goor, O. J. G. M.; Hendrikse, S. I. S.; Dankers, P. Y. W.; Meijer, E. W. *Chem. Soc. Rev.* **2017**, *46*, 6621-6637. (b) Bakker, M. H.; Lee, C. C.; Meijer, E. W.; Dankers, P. Y. W.; Albertazzi, L. *ACS Nano* **2016**, *10*, 1845-1852. (c) Aida, T.; Meijer, E. W.; Stupp, S. I. *Science* **2012**, *335*, 813-817. (d) Biswas, S.; Kinbara, K.; Oya, N.; Ishii, N.; Taguchi, H.; Aida, T. A. *J. Am. Chem. Soc.* **2009**, *131*, 7556-7557.

2 (a) Dumele, O.; Chen, J.; Passarelli, J. V.; Stupp, S. I. *Adv. Mater.* **2020**, 1907247. (b) Zhang, J.; Dong, S.; Zhang,K.; Liang, A.; Yang, X.; Huang, F.; Cao, Y. *Chem. Commun.* **2014**, *50*, 8227-8230. (c) Tovar, J. D. *Acc. Chem. Res.* **2013**, *46*, 1527-1537. (d) Yamamoto, Y.; Fukushima, T.; Suna, Y.; Ishii, N.; Saeki, A.; Seki, S.; Tagawa, S.; Taniguchi, M.; Kawai, T.; Aida, T. *Science* **2006**, *314*, 1761-1764. (e) Yamaguchi, Y.; Ochi, Y.; Miyamura, S.; Tanaka, T.; Kobayashi, S.; Wakamiya, T.; Matsubara, Y.; Yoshida, Z. *J. Am. Chem. Soc.* **2006**, *128*, 4504-4505. (f) Schenning, A. P. H. J.; Meijer E. W. *Chem. Commun.* **2005**, 3245-3258.

3 (a) Li, Y.; Hammoud, A.; Bouteiller, L.; Raynal, M. *J. Am. Chem. Soc.* **2020**, *142*, 5676-5688. (b) Saint-Denis, T. G.; Zhu, R.-Y.; Chen, G.; Wu, Q.-F.; Yu, J.-Q. *Science* **2018**, *359*, 6377. (c) Desmarchelier, A.; Caumes, X.; Raynal, M.; Vidal-Ferran, A.; van Leeuwen, P. W. N. M.; Bouteiller, L. *J. Am. Chem. Soc.* **2016**, *138*, 4908-4916. (d) Huerta, E.; van Genabeek, B.; Lamers, B. A. G.; Koenigs, M. M. E.; Meijer, E. W.; Palmans, A. R. A. *Chem. Eur. J.* **2015**, *21*, 3682-3290. (e) Raynal, M.; Portier, F.; van Leeuwen, P. W. N. M.; Bouteiller, L. *J. Am. Chem. Soc.* **2013**, *135*, 17687-17690.

4 (a) Kulkarni, C.; Meijer, E. W.; Palmans, A. R. A. *Acc Chem. Res.* **2017**, *50*, 1928-1936. (b) de Greef, T. F. A.; Smulders, M. M. J.; Wolffs, M.; Schenning, A. P. H. J.; Sijbesma, R. P.; Meijer E. W. *Chem. Rev.* **2009**, *109*, 5687-5754.

5 (a) Dorca, Y.; Matern, J.; Fernández, G.; Sánchez, L. *Isr. J. Chem.* **2019**, *59*, 869-880. (b) Lübtow, M.; Helmers, I.; Stepanenko, V.; Albuquerque, R. Q.; Marder, T. B.; Fernández, G. *Chem. Eur. J.* **2017**, *23*, 6198-6205.

6 (a) Sorrenti. A.; Leira-Iglesias, J.; Markvoort, A. J.; de Greef, T. F. A.; Hermans, T. M. *Chem. Soc. Rev.* **2017**, *46*, 5476-5490. (b) Greciano, E. E.; Calbo, J.; Ortí, E.; Sánchez, L. *Angew. Chem. Int. Ed.* **2020**, *132*, 17670-17677.

7 (a) Wehner, M.; Röhr, M. I. S.; Bühler, M.; Stepanenko, V.; Wagner, W.; Würthner, F. *J. Am. Chem. Soc.* **2019**, *141*, 6092-6107. (b) Würthner, F.; Möller, C. R. S.; Fimmel, B.; Ogi, S.; Leowanawat, P.; Schmidt, D. *Chem. Rev.* **2016**, *116*, 962-1052. (c) Ogi, S.; Stepanenko, V.; Sugiyasu, K.; Takeuchi, M.; Würthner, F. *J. Am. Chem. Soc.* **2015**, *137*, 3300-3307.

8 (a) Weyandt, E.; ter Huurne, G. M.; Vantomme, G.; Markvoort, A. J.; Palmans, A. R. A.; Meijer, E. W. *J. Am. Chem. Soc.* **2020**, *142*, 6295-6303. (b) Smulders, M. M. J.; Stals, P. J. M.; Mes, T.; Paffen, T. F. E.; Schenning, A. P. H. J.; Palmans, A. R. A.; Meijer, E. W. *J. Am. Chem. Soc.* **2010**, *132*, 620-626. (c) Smulders, M. M. J.; Filot, I. A. W.; Leenders, J. M. A.; van der Schoot, P.; Palmans, A. R. A.; Schenning, A. P. H. J.; Meijer, E. W. *J. Am. Chem. Soc.* **2010**, *132*, 611-619.

[HBCs][10] and so on[11]— constitute a very interesting family. As previously mentioned, the supramolecular polymerization of these building blocks is triggered by π-π interactions in addition to other non-covalent forces. Moreover, the self-assembly of these molecules is favoured by the introduction of long alkyl chains, which play a twofold role: 1.- ensure a good solubility of the monomeric unit in non-polar solvents, such as heptane or cyclohexane, and 2.- trigger the formation of a preferential helicity in the supramolecular aggregates. In this regard, linear OPEs have attracted much attention, not only for their good supramolecular properties, but also due to the possibility of being used in molecular electronic devices.[12] Several examples have been reported using linear achiral OPEs as building blocks for generating supramolecular scaffolds. Most representatives bear long alkyl chains at both edges of the OPE building blocks, or even in all the aromatic rings of the OPE unit[13] however, scarce examples are found to be chiral.[14]

Herein we describe the complex aggregation pathway of a novel asymmetrical OPE endowed with a short chiral moiety at one end and a terminal alkyne group at the opposite terminus. The supramolecular forces involved in the supramolecular polymerization process —mainly hydrogen bonding and π-π interactions— of the OPE monomers lead to a complex aggregation pathway, where a thermodynamic or a kinetically trapped aggregate, showing opposite supramolecular chirality, can selectively be obtained. Moreover, microscopy studies revealed the different morphology of the chiral aggregates.

To this end, a building block based on an OPE trimer was prepared bearing at one edge the anilide of the (*S*)-α-methoxy-α-phenylacetic acid (MPA), while at the opposite edge the alkyne remains unaltered (**1**, Figure 1a). Next, aggregation studies were carried out for **1**. This monomer is not soluble in pristine methylcyclohexane (MCH), thus a small amount of other solvents —such as dichloromethane (DCM) or chloroform ($CHCl_3$)— is necessary to solubilize the monomer.

ECD and UV-Vis studies in different MCH:DCM solvent mixtures confirmed the formation of a chiral supramolecular aggregate at low DCM ratios —up to 4%—, achieving the best conditions for obtaining the chiral aggregate (**Agg_I**) at a 99% MCH:1% DCM solvent mixture.

---

9 (a) Hifsudheen, M.; Mishra, R. K.; Vedhanarayanan, B.; Praveen, V. K.; Ajayaghosh, A. *Angew. Chem. Int. Ed.* **2017**, *56*, 12634-12638. (b) Buendía, J.; García, F.; Yélamos, B.; Sánchez, L. *Chem. Commun.* **2016**, *52*, 8830-8833. (c) Buendía, J.; Calbo, J.; García, F.; Aragó, J.; Viruela, P. M.; Ortí, E.; Sánchez, L. *Chem.Commun.* **2016**, *52*, 6907-6910. (d) García, F.; Korevaar, P. A.; Verlee, A.; Meijer, E. W.; Palmans, A. R. A.; Sánchez, L. *Chem.Commun.* **2013**, *49*, 8674-8676. (e) Aparicio, F.; García, F.; Fernández, G.; Matesanz, E.; Sánchez, L. *Chem. Eur. J.* **2011**, *17*, 2769-2776. (f) Fernández, G.; García, F.; Aparicio, F.; Matesanz, E.; Sánchez, L. *Chem. Commun.* **2009**, 7155-7157. (g) García, F.; Fernández, G.; Sánchez, L. *Chem. Eur. J.* **2009**, *15*, 6740-6747.

10 (a) Zhang, W.; Jin, W.; Fukushima, T.; Ishii, N.; Aida, T. *J. Am. Chem. Soc.* **2013**, *135*, 114-117. (b) Zhang, W.; Jin, W.; Fukushima, T.; Ishii, N.; Aida, T. *Angew. Chem. Int. Ed.* **2009**, *48*, 4747-4750. (c) Jin, W.; Fukushima, T.; Niki, M.; Kosaka, A.; Ishii, N.; Aida, T. *Proc. Natl. Acad. Sci., U.S.A.* **2005**, *102*, 10801-10806.

11 Dorca, Y.; Greciano, E. E.; Valera, J. S.; Gómez, R.; Sánchez, L. *Chem. Eur. J.* **2019**, *25*, 5848-5864.

12 (a) Jagtap, S. P.; Mukhopadhyay, S.; Coropceanu, V.; Brizius, G. L.; Brédas, J.-L.; Collard, D. M. *J. Am. Chem. Soc.* **2012**, *134*, 7176-7185. (b) Xiao, X.; Nagahara, L. A.; Rawlett, A. M.; Tao, N. *J. Am. Chem. Soc*. **2005**, *127*, 9235-9240.

13 (a) Philips, D. S.; Kartha, K. K.; Politi, A. T.; Krügger, T.; Albuquerque, R. Q.; Fernández, G. *Angew. Chem. Int. Ed.* **2019**, *58*, 4732-4736. (b) Albert, S. K.; Golla, M.; Thelu, H. V. P.; Krishnan, N.; Varghese, R. *Chem. Eur. J.* **2017**, *23*, 8348-8352. (c) Rudolph, T.; Allampally, N. K.; Fernández, G.; Schacher, F. H. *Chem. Eur. J.* **2014**, *20*, 13871-13875. (d) Mayoral, M. J.; Rest, C.; Schellheimer, J.; Stepanenko, V.; Fernández, G. *Chem. Eur. J.* **2012**, *18*, 15607-15611.

14 (a) Langenstroer, A.; Kartha, K. K.; Dorca, Y.; Dröste, J.; Stepanenko, V.; Albuquerque, R. Q.; Hansen, M. R.; Sanchez, L.: Fernández, G. *J. Am. Chem. Soc.* **2019**, *141*, 5192-5200. (b) Hifsudheen, M.; Mishra, R. K.; Vedhanarayanan, B.; Praveen, V. K.; Ajayaghosh, A. *Angew. Chem. Int. Ed.* **2017**, *56*, 12634-12638.

Increasing the amount of DCM results in a null ECD spectrum, whereas a magnification is observed in the UV-Vis trace, associated to the molecularly dissolved monomer state (Figure 1b, c).

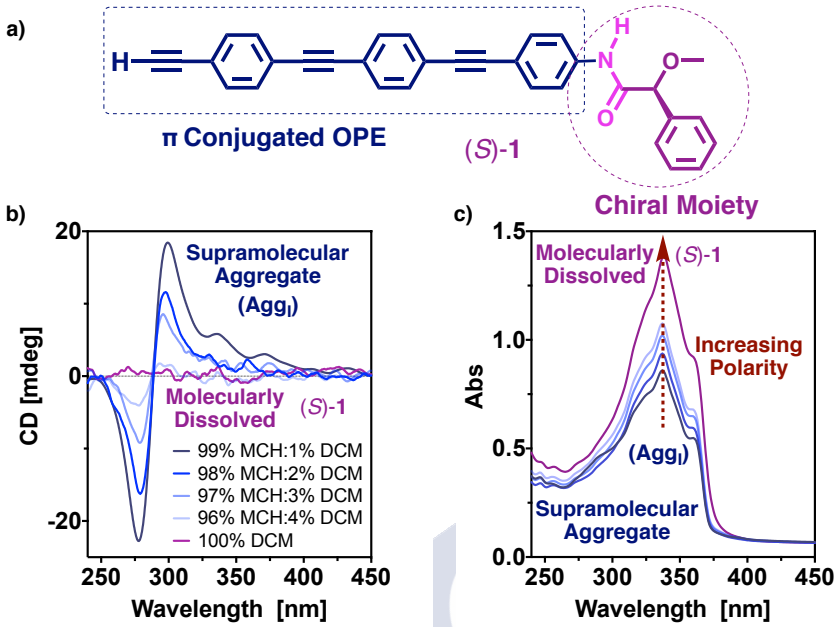

Figure 1. (a) Chemical structure of compound **1**. ECD spectra and UV-Vis traces of the disassembly process for **Agg$_I$** upon increasing the polarity (b, c) of the solvent mixture —99% MCH:1% DCM to 96% MCH:4% DCM and 100% DCM—. ECD and UV measurements were performed in a 1mm quartz cuvette for [**1**] = 100 μM.

Similar results are obtained when a MCH:DCM (99:1) solution of **1**, is heated up to 353 K (Figure 2a, b). Increasing the temperature of the polymer solution produces the disassembly of the aggregate due to the breaking of all the supramolecular interactions —mainly hydrogen bonds and π·π interactions—, resulting into a null CD. This CD vanishing is concomitant with a magnification in the UV-Vis spectra, related to the molecularly dissolved state (Figure 2a, b).

Time dependent CD studies for **Agg$_I$** —[**1**] = 100 μM in 99% MCH:1% DCM— showed the formation of a metastable aggregate (Figure 2c, d). The CD trace obtained for a freshly prepared sample of **Agg$_I$** becomes null with time, indicating the formation of a kinetic aggregate that evolves towards another species, as also observed by UV-Vis spectroscopy.

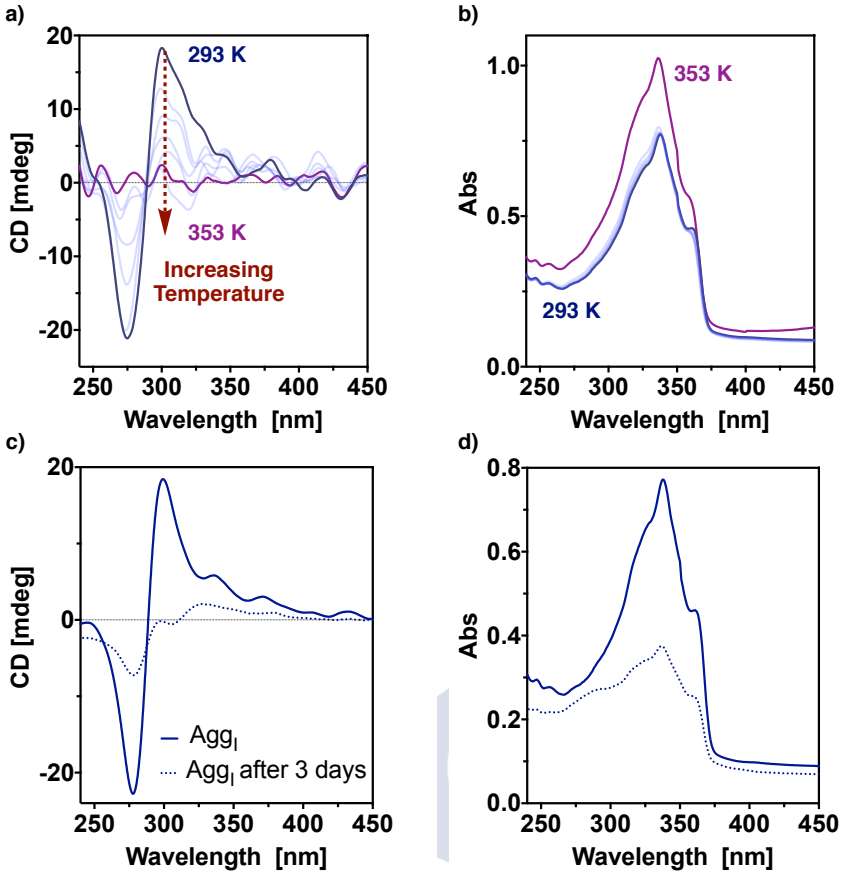

Figure 2. (a, b) ECD spectra and UV-Vis traces of the disassembly process for **Agg$_I$** by increasing the temperature. Time dependent (c) ECD and (d) UV-Vis for **Agg$_I$**. ECD and UV measurements were performed in a 1mm quartz cuvette for [**1**] = 100 μM.

In order to study the aggregation mechanism, a freshly prepared solution of **Agg$_I$** —[**1**] = 100 μM in 99% MCH:1% DCM— was heated up to 353 K and slowly cooled down to 273 K at 1 K·min^{-1}. At 353 K **Agg$_I$** is disassembled (molecularly dissolved) and cooling to 293 K produces no changes in the CD and UV-Vis spectra but, once reached 273 K, a novel aggregate is formed (Figure 3a, b). Interestingly, this aggregate, **Agg$_{II}$**, shows opposite chirality when compared to **Agg$_I$** and it was found to be stable over time at room temperature —thermodynamic aggregate— (see Experimental Section Chapter III, Figure S1). The same thermal study was performed for other MCH:DCM (99:1) solutions of **1** (**Agg$_I$**) at different concentrations —[**1**] = 80 μM and 60 μM—. By plotting the degree of aggregation (α_{agg}) at λ = 274 nm versus the temperature, an isodesmic supramolecular polymerization mechanism is observed (Figure 3c).[15] The difference between the disassembly (heating curves) and the assembly (cooling curves) processes (thermal hysteresis) is indicative of a complex supramolecular polymerization mechanism, due to the presence of a kinetic (**Agg$_I$**) and a thermodynamic (**Agg$_{II}$**) aggregate.

[15] Smulders, M. M. J.; Nieuwenhuizen, M. M. L.; de Greef, T. F. A.; van der Schoot, P.; Schenning, A. P. H. J.; Meijer, E. W. *Chem. Eur. J.* **2010**, *16*, 362-367.

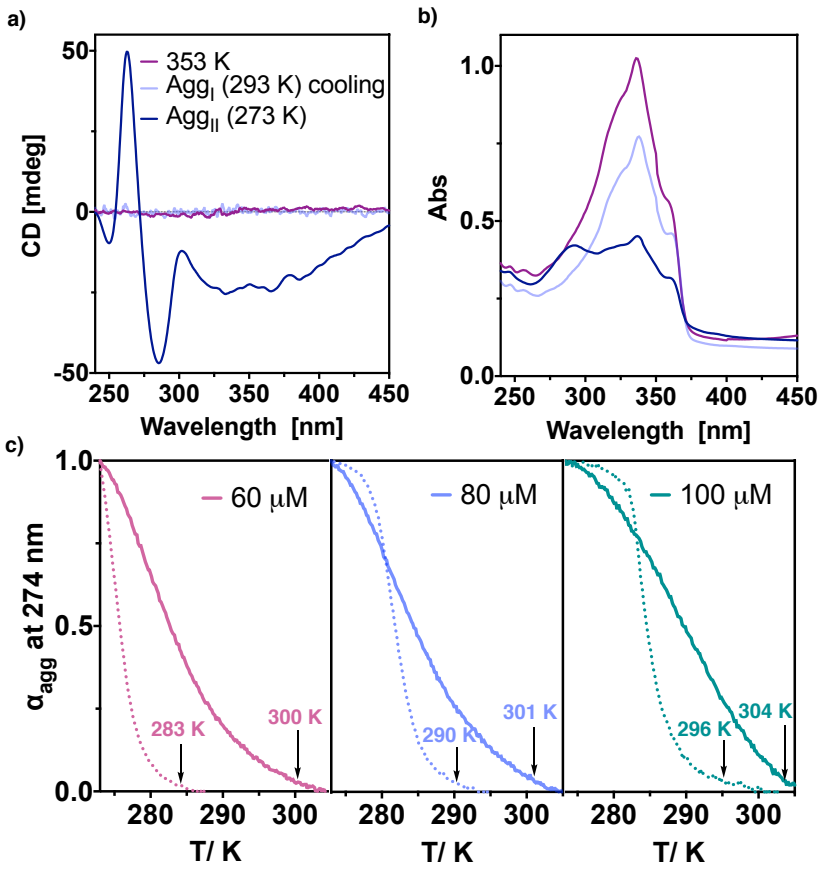

Figure 3. (a) ECD and (b) UV-Vis cooling from 353 K to 273 K. [**1**] = 100 μM in MCH:DCM (99:1). (c) Thermal analysis of the aggregation behaviour for [**1**] = 60, 80 and 100 mM in MCH:DCM (99:1) —solid line: heating cycle; dashed line: cooling cycle—. ECD and UV measurements were performed in a 1mm quartz cuvette.

Next, the morphology of the different aggregates (**Agg$_I$** and **Agg$_{II}$**) was analyzed by AFM. Thus, a solution of **1** ([**1**] = 100 μM, 99% MCH:1% DCM) was spin coated onto HOPG before (**Agg$_I$**) and after (**Agg$_{II}$**) the thermal treatment. AFM studies revealed the different morphology of the two aggregates, which is also indicative of their different stability. The AFM images obtained for the kinetic aggregate —**Agg$_I$**— show the presence of large sheet-like nanomaterials. The arrangement of these structures can be explained by the formation of short oligomers of **1** —**Agg$_I$**—, where the absence of a macromolecular helix, in combination with a large hydrophobic surface, produced the transformation from the in-plane aggregation towards extended and slightly twisted sheet-like nanostructures (Figure 4a). Moreover, these aggregates can evolve generating more complex brick-like nanostructures.

Theoretical ECD studies —TD-DFT(CAM-B3LYP)/3-21G—[16] were carried out on a short supramolecular oligomer of **1** (octamer) to explain the chirality of these twisted sheets (see Experimental Section Chapter III for detailed information). This oligomer was built using a rotation angle within the adjacent monomeric units (Θ) of ca. 11°, a distance ($d_{\pi-\pi}$) between OPE units of 3.1 Å and a N-H···O=C distance (d_H) of 2.0 Å, which produces a columnar

[16] (a) Runge, E.; Gross, E. K. U. *Phys. Rev. Lett.* **1984**, *52*, 997-1000. (b) Yanai, Y.; Tew, D. P.; Handy, N. C. *Chem. Phys. Lett.* **2005**, *393*, 51-57. (c) Binkley, J. S.; Pople, J. A.; Hehre, W. J. *J. Am. Chem. Soc.* **1980**, 102, 939-947.

aggregate for **Agg$_I$**. This supramolecular aggregate describes an axial *P* twist with a large hydrophobic surface, favoring its self-assembly into planar nanostructures (Figure 4a and see Experimental Section Chapter III, Figure S3). The theoretical ECD spectrum obtained for this oligomer shows a bisignate (+/-) that matches the experimental one, corroborating that during the formation of the metastable aggregate **Agg$_I$** a *P* twist is produced (Figure 4a).

Additionally, high-resolution AFM images of the thermodynamic aggregate —**Agg$_{II}$**— show the presence of supramolecular helical polymer chains, which appear as isolated chains or forming self-assembled monolayers (2D-crystal). From these images it is possible to extract important helical parameters such as the helix width —ca., 2.3 nm—, the packing angle —ca., 50°— and the helical sense —*M* helix—. These data allow us to build up an approximated columnar supramolecular helix for **Agg$_{II}$** by using a rotation angle within the adjacent monomeric units (Θ) of ca. -11°, a distance ($d_{\pi\text{-}\pi}$) between OPE units of 3.1 Å and a N-H···O=C distance (d_H) of 2.0 Å (Figure 4b), This 3D-model of the **Agg$_{II}$** supramolecular helix comprises all the experimental data obtained from the AFM measurements (Figure 4b and see Experimental Section Chapter III, Figure S4).

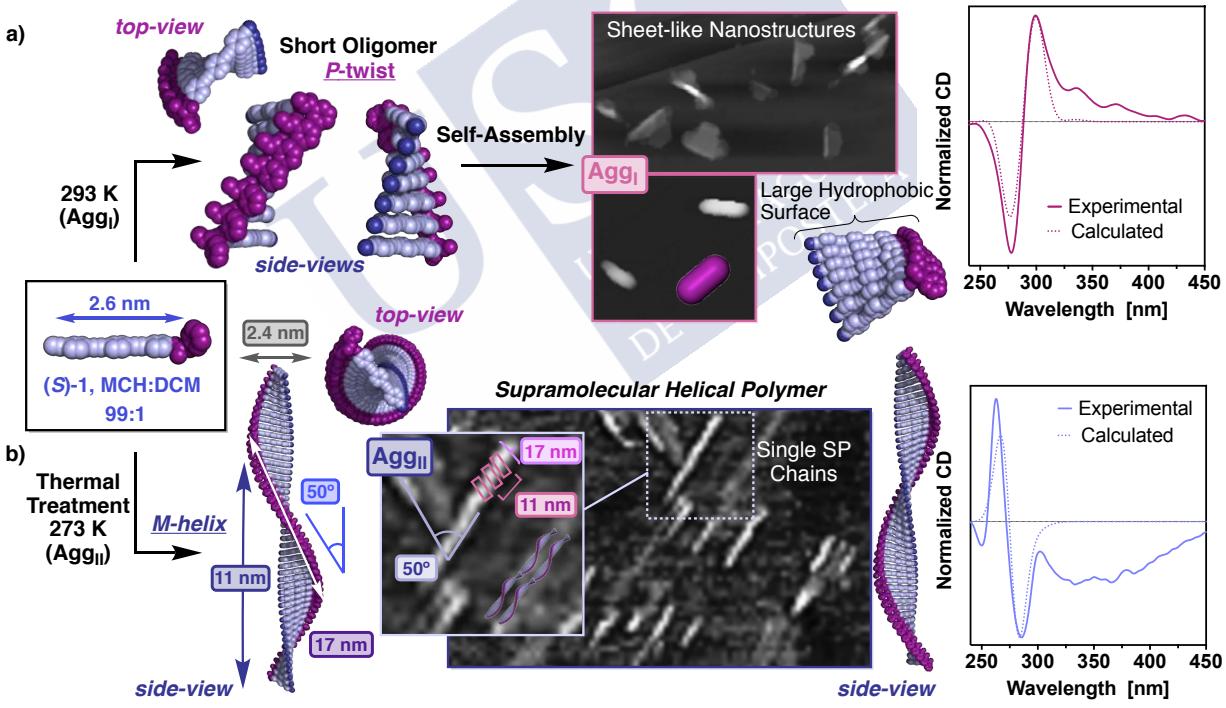

Figure 4. Supramolecular polymerization of (*S*)-**1** into (a) *P*-twisted oligomers —**Agg$_I$**—, yielding sheet-like nanostructures, and (b) a *M* supramolecular helical polymer —**Agg$_{II}$**—, as determined by AFM and TD-DFT(CAM-B3LYP)/3-21G studies.

Theoretical ECD studies —TD-DFT(CAM-B3LYP)/3-21G—on a dodecamer of **Agg$_{II}$** provide a CD spectrum showing a bisignate (-/+) that matches the one obtained experimentally, corroborating the formation of a *M* helix. Moreover, the presence of a complete turn in the supramolecular oligomer produces an ECD Cotton band at 350 nm, whose sign (-) indicates

the presence of a *M* helix for the OPE supramolecular array (Figure 4b and see Experimental Section Chapter III for detailed information).

Finally, diverse studies were done in order to trap the kinetic aggregate —**Agg$_I$**—. Several approximations, such as the addition of seeds or the use of different solvent mixtures, were used to generate a stable **Agg$_I$** aggregate.[17] From all the tested conditions, it was observed that a freshly prepared solution of **1** (100 μM), in a MCH:Tol:DCM solvent mixture (97:2:1 ratio), produces the desired aggregate. The ECD spectrum recorded in these conditions matches that previously obtained for the metastable **Agg$_I$** aggregate (Figure 5a, b), which indicates the formation of short supramolecular oligomers, due to the lack of a Cotton band at ca. 350 nm. In these conditions the aggregate proved to be stable over time up to one day (Figure 5a, b). Cooling this solution from a molecularly dissolved state —from 353 K to 273 K, 1 K·min^{-1}— results in a CD trace coincident with the one initially obtained (Figure 5c, d). This suggests that the small amount of toluene (Tol) added is not only responsible for the stabilization of the aggregate, but also avoids the formation of long *M* helical chains.

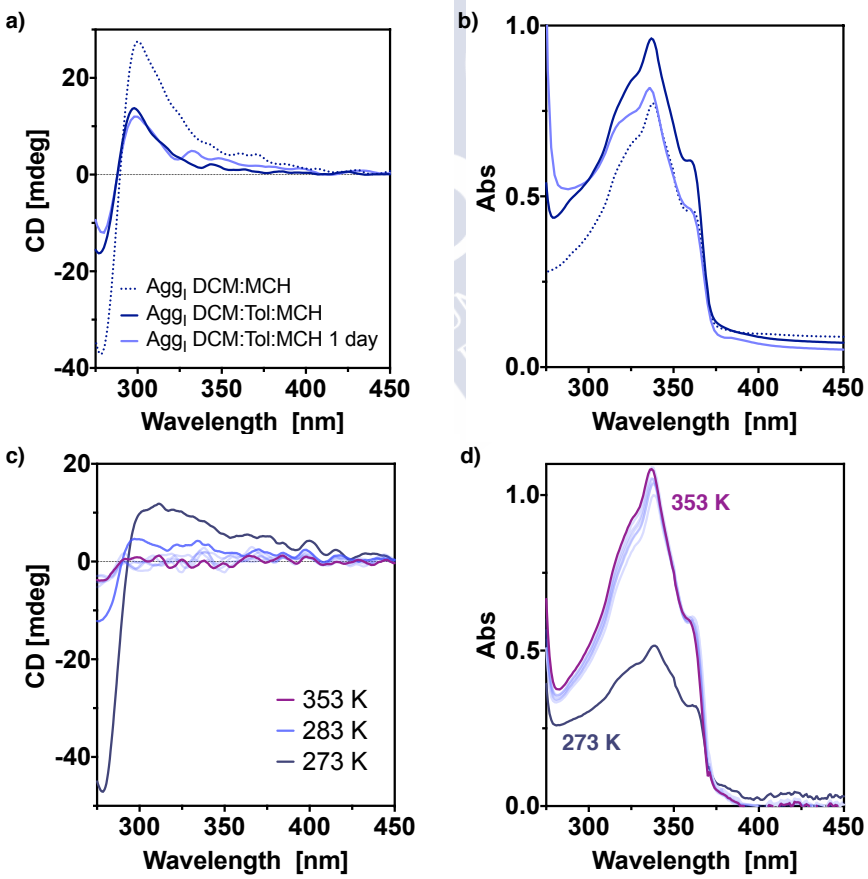

Figure 5. (a) ECD and (b) UV spectra of **Agg$_I$** prepared as the metastable (MCH:DCM) or the kinetically trapped aggregate (MCH:Tol:DCM). ECD and UV-Vis traces recorded after a day show the stability of the kinetically trapped **Agg$_I$** over time. (c) ECD and (b) UV-vis spectra depicting the stability of the kinetically trapped aggregate after thermal treatment. ECD and UV measurements were performed in a 1mm quartz cuvette for [**1**] = 100 μM.

[17] Matern, J.; Dorca, Y.; Sánchez, L.; Fernández, G. *Angew. Chem. Int. Ed.* **2019**, *58*, 16730-16740.

The polymerization and depolymerization processes were monitored as a function of temperature (1 $K \cdot min^{-1}$) obtaining sigmoidal curves for both processes. The large difference between the disassembly (T_e) and assembly (T_e') temperatures indicates, once again, hysteresis (see Experimental Section Chapter III, Figure S2), revealing the complexity of the polymerization process.

Chapter IV

Supramolecular Triangular Tessellation Produced by the Self-Assembly of Chiral Helical Oligomers Obtained from OPE Derivatives

USC
UNIVERSIDADE
DE SANTIAGO
DE COMPOSTELA

Chapter IV. Supramolecular Triangular Tessellation Produced by the Self-Assembly of Chiral Helical Oligomers Obtained from OPE Derivatives

Abstract: *Supramolecular polymerization of an asymmetric OPE derivative, bearing a long alkyl chain at one end and a terminal alkyne at the other termini, results in a cooperative polymerization process presenting thermodynamic parameters similar to those found in BTAs. The self-assembly produces the thermodynamic product, although the hysteresis observed between the heating/cooling cycles indicates the presence of other short oligomers in solution. AFM studies revealed the presence of the expected individual supramolecular helix accompanied by a novel 2D-extended nanostructure, consisting of a triangular lattice that produces a regular tessellation on the HOPG surface. This novel nanomaterial is produced due to a second order supramolecular self-assembly of the OPE oligomers during the drop casting and solvent evaporation of the sample.*

USC
UNIVERSIDADE
DE SANTIAGO
DE COMPOSTELA

Supramolecular interactions are found in nature in hierarchically structured helical materials, such as DNA, collagen, chitin or cellulose, whose supramolecular helical structures are directly related to the function developed by the biomaterial.[1] These findings have inspired the scientific community to pursuit novel helical structures, made up by the non-covalent bonding of monomeric species, to explore the generation of innovative materials with new functionalities.[2-10] Notwithstanding, creating sophisticated scaffolds inspired in biomolecules remains as a challenging task, since the phenomena observed at the molecular level has to be conveyed to larger scales (2D structures). In case of supramolecular helical polymers, the chiral information of the monomeric unit has to be transferred into the supramolecular assemblies and finally into the macroscopic superstructures by a self-assembly process.[11,12] However, this ideal aggregation process can be altered by the presence of kinetic effects, which may lead to the formation of complex aggregation pathways.[13] In this line, our group reported the complex aggregation pathway of an asymmetrical OPE [oligo(phenyleneethynylene)] bearing a short chiral moiety on one of the rims (Figure 1).[14] It was found that by controlling the experimental conditions of the supramolecular polymerization process, it is possible to selectively obtain either a kinetic or a thermodynamic aggregate, with opposite axial chirality and different polymer length. Thus, by activation of the kinetic process (off-pathway, $\mathbf{Agg_I}$) *P* twisted oligomers are produced —which converge into sheet-like nanostructures—, whereas activation of the thermodynamic conditions (on-pathway, $\mathbf{Agg_{II}}$) results in the formation of *M* type long helical aggregates. These studies revealed that $\mathbf{Agg_I}$ is a metastable state that disaggregates over time; nevertheless, we succeed in the preparation of the kinetically trapped aggregate (off pathway) by modifying the polarity of the solvent (i.e., addition of a small amount of toluene). In this work, besides studying the supramolecular polymerization mechanism of the OPE derivative, we also analyzed in great detail the 3D-structure of the supramolecular aggregates.

1 Chung, W.-J.; Oh, J.-W.; Kwak, K.; Lee, B. Y.; Meyer, J.; Wang, E.; Hexemer, A.; Lee, S.-W. *Nature* **2011**, *478*, 364-368.
2 Morgese, G.; de Waal, B.F.M.; Varela-Aramburu, S.; Palmans, A. R. A.; Albertazzi, L.; Meijer, E. W. *Angew. Chem. Int. Ed.* **2020**, *21*, 17229-17233.
3 Salikolimi, K.; Praveen, V. K.; Sudhakar, A. A.; Yamada, K.; Horimoto, N. N.; Ishida, Y. *Nat. Commun.* **2020**, *11*, 2311.
4 Dumele, O.; Chen, J.; Passarelli, J. V.; Stupp, S. I. *Adv. Mater.* **2020**, 1907247.
5 Goor, O. J. G. M.; Hendrikse, S. I. S.; Dankers, P. Y. W.; Meijer, E. W. *Chem. Soc. Rev.* **2017**, *46*, 6621-6637.
6 Yashima, E.; Ousaka, N.; Taura, D.; Shimomura, K.; Ikai, T.; Maeda, K. *Chem Rev.* **2016**, *116*, 13752-13990.
7 Leiras, S.; Freire, F.; Quiñoá, E; Riguera, R. *Chem. Sci.* **2015**, 6, 246-253.
8 Korevaar, P. A.; de Greef, T. F. A.; Meijer, E. W. *Chem. Mater.* **2014**, *26*, 576-586.
9 Aida, T.; Meijer, E. W.; Stupp, S. I. *Science* **2012**, *335*, 813-817.
10 Whitesides, G. M.; Grzybowski, B. *Science* **2002**, *295*, 2418-2421.
11 Greciano, E. E.; Rodríguez, R.; Maeda, K.; Sánchez, L. *Chem. Commun.* **2020**, *56*, 2244-2247.
12 Dorca, Y.; Greciano, E. E.; Valera, J. S.; Gómez, R. Sánchez, L. *Chem. Eur. J.* **2019**, *25*, 5848-5864.
13 (a) Wehner, M.; Würthner, F. *Nat. Rev. Chem.* **2020**, *4*, 38-53. (b) Matern, J.; Dorca, Y.; Sánchez, L.; Fernández, G. *Angew. Chem. Int. Ed.* **2019**, *58*, 16730-16740.
14 See Chapter III.

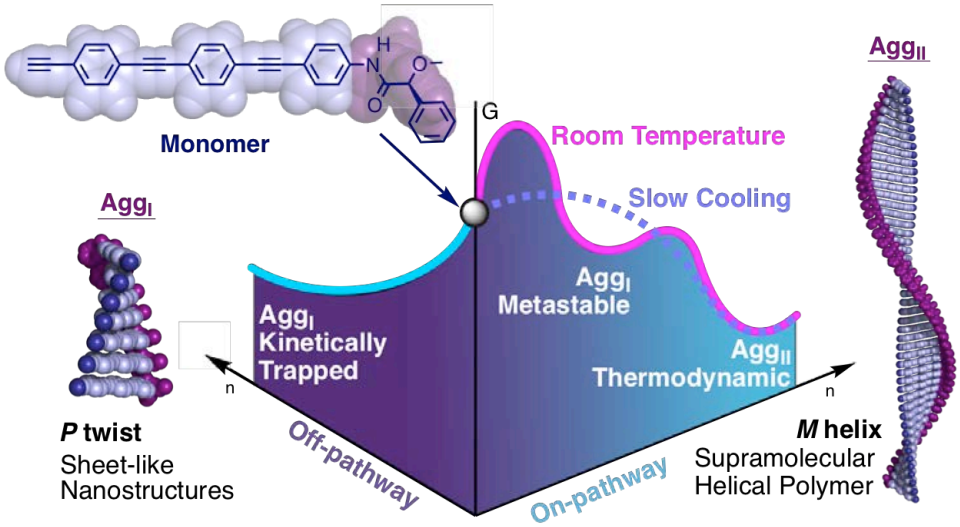

Figure 1. Conceptual representation of the pathway complexity in asymmetrical OPEs.

In literature it is found that supramolecular polymers can lead to the formation of large hierarchical structures, which produce materials with different morphologies.[15] An example of this is the formation of non-covalent 2D structures displaying regular patterns, such as Archimedean or Kagomé tiling scaffolds.[16] Usually these intriguing structures are produced by the aggregation of highly symmetrical molecules bearing long alkyl chains or from the self-assembly of metallosupramolecular structures.[17] For instance, Sugiyasu *et al.*[18] have recently reported a porphyrinato zinc derivative that forms a 1D supramolecular polymer (SP) that, depending on the concentration employed and the interactions established between monomers, can evolve into a 2D nanosheet or produce more complex Archimedean spirals.

Encouraged by these results, we decide to explore the effect of the introduction of a long alkyl chain in an asymmetrical OPE, analyzing not only the changes in the morphology of the aggregate but also variations in the supramolecular polymerization mechanism. To this end, a π-conjugated chiral OPE trimer was designed, introducing at one of the OPE edges a chiral moiety derived from the decyl-(*L*)-alaninate, and keeping the alkyne unaltered at the other end [(*L*)-**1**] (Figure 2a). This design ensures the stabilization of the aggregate by means of π-π interactions and hydrogen bonding, whereas the dodecyl alkyl chain promotes the solubility in low-polar solvents, as well as the chain-to-chain interdigitation.

Monomer (*L*)-**1** was synthesized according to common organic synthetic procedures (see Experimental Section Chapter IV) and aggregation studies were carried out in

[15] (a) Zeng, X.; Khan, S. B.; Mahmooda, A.; Lee, S.-L. *Nanoscale* **2020**, *12*, 15072-15080. (b) Danila, I.; Pop, F.; Escudero, C.; Feldborg, L. N.; Puigmartí-Luis, J.; Riobé, F.; Avarvari, N.; Amabilino, D. B. *Chem. Commun.* **2012**, *48*, 4552-4554.

[16] (a) Furukawa, S.; Uji-i, H.; Tahara, K.; Ichikawa, T.; Sonoda, M.; De Schryver, F. C.; Tobe, Y.; De Feyter, S. *J. Am. Chem. Soc.* **2006**, *128*, 3502-3503. (b) Stepanenko, V.; Kandanelli, R.; Uemura, S.; Würthner, F.; Fernández, G. *Chem. Sci.* **2015**, *6*, 5853-5858. (c) Chen, T.; Chen, Q.; Zhang, X.; Wang, D.; Wan, L.-J. *J. Am. Chem. Soc.* **2010**, *132*, 5598-5599. (d) Mo, Y.-P.; Liu, X.-H.; Wang, D. *ACS Nano* **2017**, *11*, 11694-11700. (e) Fujita, D.; Ueda, Y.; Sato, S.; Mizuno, N.; Kumasaka, T.; Fujita, M. Self-assembly of Tetravalent Goldberg Polyhedral From 144 Small Components. *Nature* **2016**, *540*, 563-566.

[17] Zhang, Z.; Li, Y.; Son, B.; Zhang, Y.; Jiang, X.; Wang, M.; Trumbleson, R.; Liu, C.; Wang, P.; Hao, X.-Q.; Rojas, T.; Ngo, A. T.; Sessler, J. L.; Newkome, G. R.; Hla, S. W.; Li, X. *Nat. Chem.* **2020**, *12*, 468-474.

[18] C Sasaki, N.; Mabesoone, M. F. J.; Kikkawa, J.; Fukui, T.; Shioya, N.; Shimoaka, T.; Hasegawa, T.; Takagi, H.; Haruki, R.; Shimizu, N.; Adachi, S.-I.; Meijer, E. W.; Takeuchi, M.; Sugiyasu, K. *Nat Commun.* **2020**, *11*, 3578.

methylclyclohexane (MCH) —[(*L*)-**1**] = 147 μM—. First, variable temperature CD (VT-CD) measurements were performed by slowly cooling (10 K·min^{-1}) the (*L*)-**1** solution from a molecularly dissolved state —353 K to 293 K—, revealing the formation of a chiral aggregate when the solution temperature reaches 293 K (negative exciton band centered at 286 nm, $CD_{286} < 0$; Figure 2b). Additionally, variable temperature UV-Vis (VT-UV-Vis) studies registered the formation of a novel band at ca. 286 nm (Figure 2b) for 293 K, coincident with the UV band observed for other long helical OPE aggregates.[14]

In order to gain insight into the supramolecular polymerization mechanism that rules the formation of the helical structure, VT-CD experiments —T = 353 K to 293 K, at 1 K·min^{-1}— were carried out for (*L*)-**1** in MCH at different concentrations —[(*L*)-**1**] = 147 μM, 166 μM and 184 μM—. Registering the variation of the degree of aggregation (α_{agg}) at λ = 280 nm versus the temperature, reveals that the self-assembly of (*L*)-**1** follows a cooperative mechanism (Figure 2c). It should be pointed out that the elongation temperatures obtained for the heating (T_e) and cooling (T_e') processes differ. This thermal hysteresis between the heating and cooling cycles during temperature dependent measurements indicates the presence of kinetically trapped states in the cooling cycle, since the structural changes required in the molecules for an effective supramolecular polymerization are too slow.[13a,14,19]

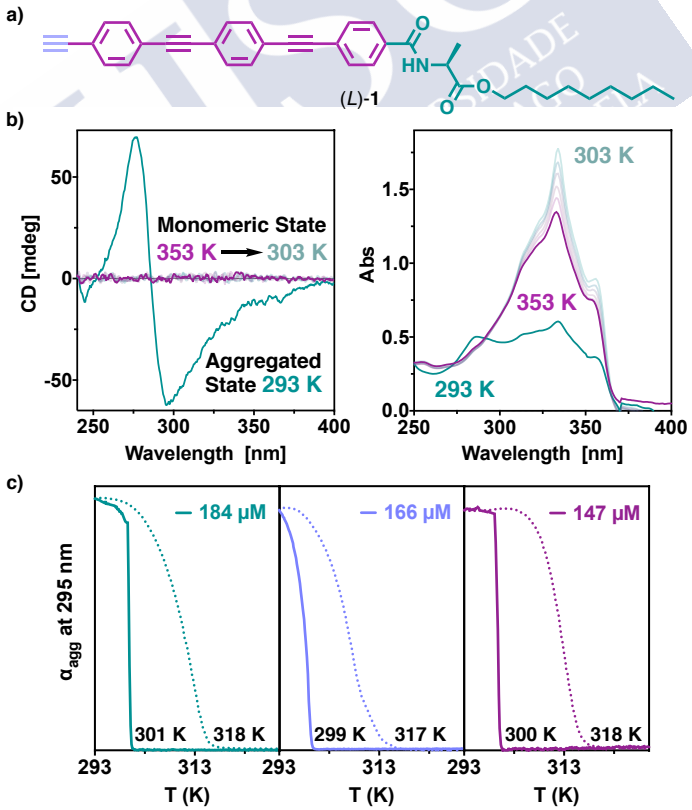

13 (a) Wehner, M.; Würthner, F. *Nat. Rev. Chem.* **2020**, *4*, 38-53.
14 See Chapter III.
19 Greciano, E. E.; Sánchez, L. *Chem. Eur. J.* **2016**, *22*, 13724-13730.

Figure 2. (a) Chemical structure for (*L*)-**1**. (b) VT-CD and VT-UV-Vis cooling 10 K·min^{-1} from 353 K to 293 K —[(*L*)-**1**] = 147 μM —. (c) Heating and cooling curves (dashed and solid lines, respectively) —1 K·min^{-1}; 293 K to 393 K and reverse— recorded for different concentrations of **1**. Experiments performed in a 1 mm quartz cuvette.

Fitting the obtained cooling curves to the mass balance (MB) model[20] allows the calculation of the different thermodynamic parameters. The enthalpy of elongation (ΔH_e = -149.9 kJ·mol^{-1}), the entropy of elongation (ΔS_e = -424.4 J·mol^{-1} K^{-1}) and the nucleation penalty (ΔH_{np} = -29.3 kJ·mol^{-1}) extracted from this fitting are used to determine the nucleation factor ($\sigma = 6.0 \cdot 10^{-6}$; calculated at 293 K), which quantifies the cooperativity of the supramolecular polymerization process —the smaller the σ-value becomes, the higher is the cooperativity in the system; this indicates that if σ = 1 the self-assembly follows an isodesmic mechanism—. The value obtained for the nucleation factor of (*L*)-**1** in MCH approximates the ones obtained for other well-known family of building blocks, such as the symmetrically substituted BTAs (benzene-1,3,5-tricarboxiamides).[21]

Next, the helical structure of the supramolecular polymer and the morphology of the aggregate were analyzed by theoretical ECD studies and AFM measurements. In a previous work it was found that theoretical ECD calculations —TD-DFT(CAM-B3LYP)/3-21G— on a supramolecular oligomer of an unsubstituted OPE (dodecamer) leads to a bisignate (-/+), which corresponds to a *M* orientation of the SP.[14] Herein, the same bisignated (-/+) ECD trace is obtained for (*L*)-**1** in MCH at 293K —[(L)-**1** = 147 μM], indicating that the obtained SP adopts a *M* rotation sense.

To confirm the *M* orientation of the supramolecular polymer, AFM measurements were carried out. A solution of the (*L*)-**1** in MCH (368 μM) was drop casted into a HOPG substrate and submitted to AFM studies, generating high-resolution AFM images. By analyzing the different AFM images obtained it is possible to observe the formation of isolated helical polymer chains and extract different helical parameters from them, such as the helix width —ca., 2.6 nm—, the packing angle —ca., 33°—, the helical pitch —ca., 15 nm— and the *M* orientation of the supramolecular helix (Figure 3a), coincident with the one suggested by ECD calculations.[14] By using these experimental data an approximated columnar *M* oriented SP was built, possessing a rotation angle within the adjacent monomeric units (Θ) of ca. 8°, a distance between OPE units ($d_{\pi\text{-}\pi}$) of 3.3 Å and a N-H···O=C distance (d_H) of 1.7 Å. The resulting 3D-model comprises the π-π interactions and the hydrogen bonds necessary to form the SP (Figure 3a).

Remarkably, during the AFM studies a triangular shaped lattice, which appears in several regions of the AFM substrate, is also observed (Figure 3f). Some areas of the HOPG substrate show a complete triangular shaped lattice, while in other regions of the substrate this triangular lattice is partially generated (see Experimental Section Chapter IV, Figure S10b).

[14] See Chapter III.
[20] ten Eikelder, H. M. M.; Markvoort, A. J.; de Greef, T. F. A.; Hilbers, P. J. A. *J. Phys. Chem. B* **2012**, *116*, 5291-5301.
[21] Kulkarni, C.; Meijer, E. W.; Palmans, A. R. A. *Acc. Chem. Res.* **2017**, *50*, 1928-1936.

These results may indicate a crystallization process during the drop casting and solvent evaporation of the sample, where short oligomers of (*L*)-**1** self-assemble creating this triangular lattice. The triangles observed in the different AFM images show a regular structure with a side length of ca. 65 nm and a height of around 1 nm (Figure 3f).

This thickness of the triangular tessellation (1 nm) indicates that each polygon should be composed by short oligomers constructed from the self-assembly of only four monomers. A closer look to these regular structures reveals a honeycomb-like aggregate made up by regular hexagons (Figure 3e). These hexagonal gaps found within the triangles present an internal diameter of ca. 15.4 nm and a side length of ca. 7.8 nm (Figure 3d). This side length of the hexagon is coincident with two (*L*)-**1** oligomers (monomer length ca. 3.7 nm) non-covalently connected and interacting by interdigitation of the alkyl chains.

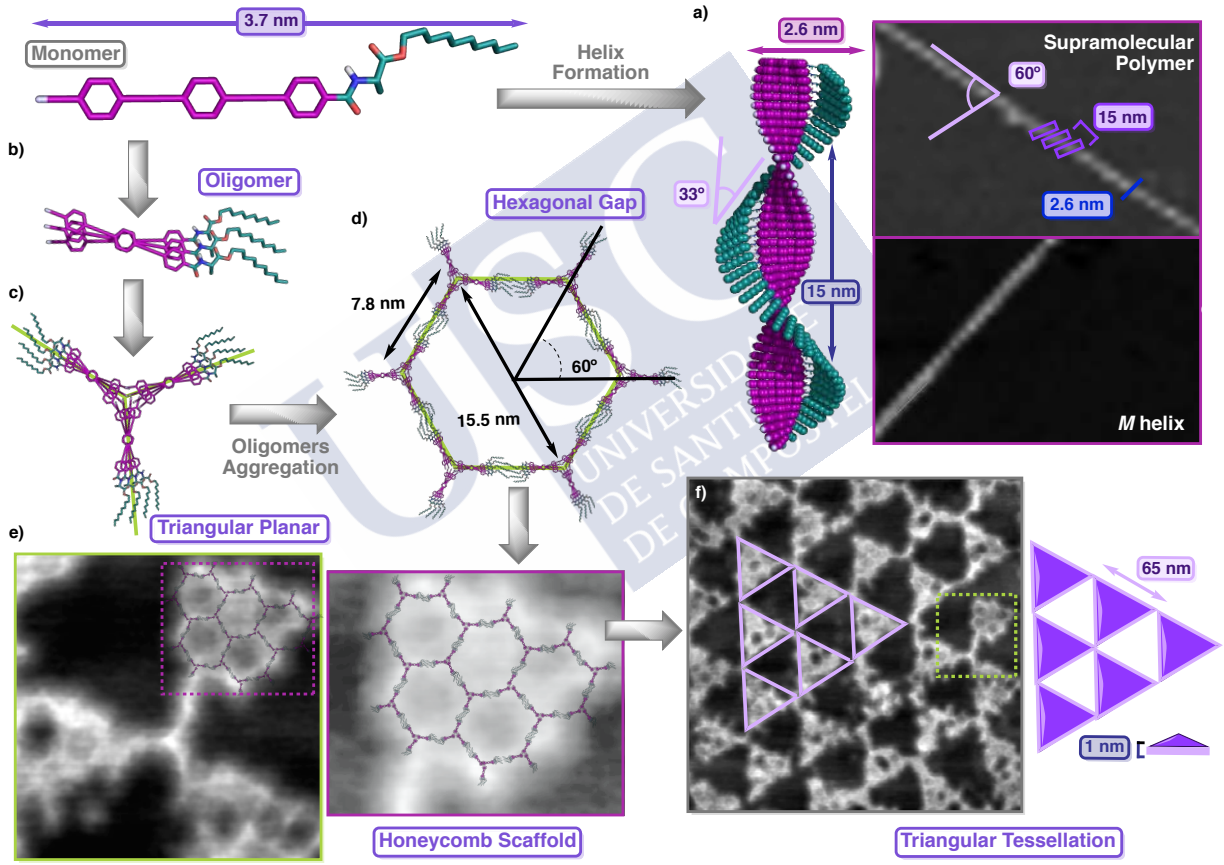

Figure 3. (a) 3D model and AFM image depicting the single-stranded helix obtained from the self-assembly of **1**. (b)-(f) Proposed hierarchical process for the crystallization of the short oligomers (b) to yield the triangular tessellation (f). The AFM images show the intermediate honeycomb-like scaffold (e) as well as the final geometric pattern (f).

To explain this large hierarchical structure, the asymmetric structure of (*L*)-**1** has to be taken into account, as within this molecule there are two different structural motifs —one rigid (OPE) and one flexible (long alkyl chain)— (Figure 3). Oligomerization of (*L*)-**1** orients all the OPE units at one side of the aggregate, while the alkyl chains stabilize the aggregate due to weak London forces at the other end (Figure 3b). During the drop-casting and solvent evaporation, short oligomers interact through the interdigitation of alkyl chains, which

generates one side of the hexagonal structure. These dimers interact head to head —OPE moieties— through electron poor terminal alkyne·π interactions[22] generating an unexpected geometric pattern, in this case a triangular planar structure (Figure 3c) which, by expansion of this structure, produces a regular hexagon (Figure 3d). This triangular planar structure can continuously grow until reach a honeycomb regular structure made by five fused rings (Figure 3e), or interact with another planar triangular structure, producing a linear tetramer of short oligomers with a side length of 15.4 nm. This structure is extended along the HOPG substrate to form the final triangle lattice (Figure 3f). The defects found in some areas of the HOPG substrate where this triangle lattice is observed are due to the fast solvent evaporation, avoiding the tessellation of the AFM substrate.

[22] Li, Q.; Han, C.; Horton, S. R.; Fuentes-Cabrera,M.; Sumpter, B. G.; Lu, W.; Bernholc, J.; Maksymovych, P.; Pan, M. *ACS Nano* **2012**, *6*, 566-572.

Chapter V

Matryoshka-like Helical Polymers: When Supramolecular and Covalent Helical Polymers are Mixed Up

USC
UNIVERSIDADE
DE SANTIAGO
DE COMPOSTELA

Chapter V. Matryoshka-like Helical Polymers: When Supramolecular and Covalent Helical Polymers are Mixed Up

Abstract: *Supramolecular and covalent helical polymers share multiple structural features such as chiral amplification, helix inversion, Sergeants and Soldiers or Majority Rules among others. These properties are determined by the axial helical structure presented in both materials. Herein, a novel material obtained through the combination of information from both fields, covalent [poly(acetylene) (PA)] and supramolecular [oligo(phenyleneethynylene) (OPE)] helical polymers, is presented. To achieve this goal, the polyacetylene has to adopt a dihedral angle between conjugated double bonds (ω_1) larger than 165°. In such cases, the tilting degree (Θ) between OPE units is 11°, similar to the one observed in supramolecular helical arrays of these molecules. Polymerization of oligo[(p-phenyleneethynylene)$_n$]phenylacetylene monomers (n = 1, 2) bearing the (L)-decyl alaninate as pendant group yielded the desired scaffolds. The corresponding polymers adopt a stretched almost planar polyene helix, where the OPE units are arranged describing a helical structure. As a result, a novel multi-helical material was prepared —the matryoshka helix—, where the ECD spectra is dominated by the OPE axial array.*

USC
UNIVERSIDADE
DE SANTIAGO
DE COMPOSTELA

The helix is an abundant structural motif present in nature in many macromolecules such as peptides, proteins, DNA or polysaccharides and is directly related to the biological functions carried out by these biomolecules. This structure/function relationship aimed the scientific community to look for novel materials that adopt helical structures, such as covalent and supramolecular helical polymers.[1-16] Nowadays it is possible to understand how these polymers are folded and which are the structural features of the building blocks that induce them to adopt a helical structure. Moreover, these studies led to the development of the dynamic helical polymers —covalent and supramolecular— whose helical sense (*P* or *M*),[17-22] elongation (compressed/stretched)[23-27] or aggregate shape (J-aggregate, H-aggregate and so on)[28-32] can be altered by the presence of different external stimuli (e.g., solvent polarity, pH, temperature, metal ions, chiral additives or light). This dynamicity revealed different communication mechanisms between components in both, covalent and supramolecular copolymers. Therefore, different chiral amplification or chiral enhancement effects such as Sergeants and Soldiers, Majority Rules, Chiral Coalition, Chiral Accord or Chiral Conflict have been observed.[33-46] Interestingly, although the two families of helical polymers —covalent and

1 Yashima, E.; Ousaka, N.; Taura, D.; Shimomura, K.; Ikai, T.; Maeda, K. *Chem. Rev.* **2016**, *116*, 13752-13990.
2 Yashima, E.; Maeda, K.; Furusho, Y. *Acc. Chem. Res.* **2008**, *41*, 1166-1180.
3 Yashima, E.; Maeda, K.; Iida, H.; Furusho, Y.; Nagai, K. *Chem. Rev.* **2009**, *109*, 6102-6211.
4 Yu, Z.; Hecht, S. Remote control over folding by light. Chem. Commun. **2016**, *52*, 6639-6653.
5 Schwartz, E.; Koepf, M.; Kito, H. J.; Nolte, R. J. M.; Rowan, A. E. *Polym. Chem.* **2011**, *2*, 33-47.
6 Rodríguez, R.; Suárez-Picado, S.; Quiñoá, E.; Riguera, R.; Freire, F. *Angew. Chem. Int. Ed.* **2020**, *59*, 8616-8622.
7 Feringa, B. L. *Acc. Chem. Res.* **2001**, *34*, 504-513.
8 Van Leeuwen, T.; Heideman, G. H.; Zhao, D.; Wezenberg, S. J.; Feringa, B. L. *Chem. Commun.* **2017**, *53*, 639-6396.
9 Suárez-Picado, E.; Quiñoá, E.; Riguera, R.; Freire, F. *Chem. Mater.* **2018**, *30*, 6908-6914.
10 Fukuda, M.; Rodríguez, R.; Fernández, Z.; Nishimura, T.; Hirose, D.; Watanabe, G.; Quiñoá, E.; Freire F.; Maeda, K. *Chem. Commun.* **2019**, *55*, 7906-7909.
11 Liu, J.; Lam, J. W. Y.; Tang, B. Z. *Chem. Rev.* **2009**, *109*, 5799-5867.
12 Liu,M.; Zhang, L.; Wang, T. *Chem. Rev.* **2015**, *115*, 7304-7397.
13 Ghosh, G.; Dey, P.; Ghosh, S. *Chem. Commun.* **2020**, *56*, 6757-6769.
14 Dorca, Y.; Greciano, E. E.; Valera, J. S.; Gómez, R.; Sánchez, L. *Chem. Eur. J.* **2019**, *25*, 5848-5864.
15 Aida, T.; Meijer, E. W.; Stupp, S. I. *Science* **2012**, *335*, 813-817.
16 Aida, T.; Meijer, E. W. *Isr. J. Chem.* **2020**, *60*, 33-47.
17 Bergueiro, J.; Núñez-Martínez, M.; Arias, S.; Quiñoá, E.; Riguera, R.; Freire, F. *Nanoscale Horiz.* **2020**, *5*, 495-500.
18 Arias, S.; Núñez-Martínez, M.; Quiñoá, E.; Riguera, R.; Freire, F. *Small* **2017**, *13*, 1602398.
19 Yamamoto, T.; Murakami, R.; Komatsu, S.; Suginome, M. *J. Am. Chem. Soc.* **2018**, *140*, 3867-3870.
20 Freire, F.; Seco, J. M.; Quiñoá, E.; Riguera, R. *Angew. Chem. Int. Ed.* **2011**, *50*,11692-11696.
21 Maeda, K.; Mochizuki, H.; Watanabe, M.; Yashima, E. *J. Am. Chem. Soc.* **2006**, *128,* 7639-7650.
22 Greciano, E. E.; Rodríguez, R.; Maeda, K.; Sánchez, L. *Chem. Commun.* **2020**, *56*, 2244-2247.
23 Cobos, K.; Rodríguez, R.; Domarco, O.; Fernández, B.; Quiñoá, E.; Riguera, R.; Freire, F. *Macromolecules* **2020**, *53*, 3182-3193.
24 Rodríguez, R.; Quiñoá, E.; Riguera, R.; Freire, F. *Small* **2019**, *15*, 1805413.
25 Rodríguez, R.; Quiñoá, E.; Riguera, R.; Freire F. *J. Am. Chem. Soc.* **2016**, *138*, 9620-9628.
26 Leiras, S.; Freire, F.; Seco, J. M.; Quiñoá, E.; Riguera, R. *Chem. Sci.* **2013**, *4*, 2735-2734.
27 Maeda, K.; Kamiya, N.; Yashima, E. *Chem. Eur. J.* **2004**, *10*, 4000-4010.
28 Matern, J.; Kartha, K. K.; Sánchez, L.; Fernández, G. *Chem. Sci.* **2020**, *11*, 6780–6788.
29 Sasaki, N.; Mabesoone, M. F. J.; Kikkawa, J.; Fukui, T.; Shioya, N.; Shimoaka, T.; Hasegawa, T.; Takagi, H.; Haruki, R.; Shimizu, N.; Adachi, S.; Meijer, E. W.; Takeuchi, M.; Sugiyasu, K. *Nat. Comm.* **2020**, *11*, 3578.
30 Bäumer, N.; Kartha, K. K.; Palakkal, J. P.; Fernández, G. *Soft Matter* **2020**, *16*, 6834-6840.
31 Valera, S.; Gómez, R.; Sánchez, L. *Small* **2018**, *14*, 1702437.
32 Sorrenti, A.; Leira-Iglesias, J.; Markvoort, A. J.; de Greef, T. F. A: Hermans, T. M. *Chem. Soc. Rev.* **2017**, *46*, 5476-5490.
33 Alzubi, M.; Arias, S.; Rodríguez, R.; Quiñoá, E.; Riguera, R.; Freire, F. *Angew. Chem. Int. Ed.* **2019**, *58*, 13365-13369.
34 Cobos, K.; Quiñoá, E.; Riguera, R.; Freire, F. *J. Am. Chem. Soc.* **2018**, *140*, 12239-12246.
35 Arias, S.; Rodríguez, R.; Quiñoá, E.; Riguera, R.; Freire, F. *J. Am. Chem. Soc.* **2018**, *140*, 667-674.
36 Arias, S.; Bergueiro, J.; Freire, F.; Quiñoá, E.; Riguera, R. *Small* **2016**, *12*, 238-244.
37 Nagata, Y.; Nishikawa, T.; Suginome, M. *ACS Macro Lett.* **2016**, *5*, 519-522.
38 Ke, Y.-Z.; Nagata, Y.; Yamada, T.; Suginome, M. *Angew. Chem. Int. Ed.* **2015**, *54*, 9333-9337.
39 Tang, K.; Green, M. M.; Cheon, K. S.; Selinger, J. V.; Garetz, B. A. Chiral Conflict. *J. Am. Chem. Soc.* **2003**, *125*, 7313-7323.
40 Vantomme, G.; ter Huurne, G. M.; Kulkarni, C.; ten Eikelder, H. M. M.; Markvoort, A. M.; Palmans, A. R. A.; Meijer, E. W. *J. Am. Chem. Soc.* **2019**, *141*, 18278-18285.

supramolecular— share many common properties no studies have been done combining the two structural motifs.

Recently, our group has reported a novel family of helical polymers, the POPEPAs (poly[oligo(*p*-phenyleneethynylene)acetylene]s).[4 7-48] In these polymers, although being the chiral center located in a remote position from the backbone, a helix induction is produced due to the chiral arrangement of the achiral spacers, which is finally harvested by the polyene backbone. Hence, in a first step, the stereogenic centers of the monomer repeating units command the achiral rigid OPE (oligo(*p*-phenyleneethynylene)) spacers to be arrayed with a specific tilting degree (Θ), whose value depends on the absolute configuration of the chiral moiety. This chiral arrangement of the OPE units, stabilized through π·π interactions, is further harvested by the polyene backbone, through the adoption of a specific *P* or *M* helical sense (Figure 1a).

The chiral arrangement of the OPE units in POPEPAs drove us to study the supramolecular self-assembly of the monomer units. It was observed that these monomers arrange into a supramolecular helical polymer, stabilized by hydrogen bond interactions between the amide groups of the chiral moieties and π·π interactions among OPE units (Figure 1b).[49,50]

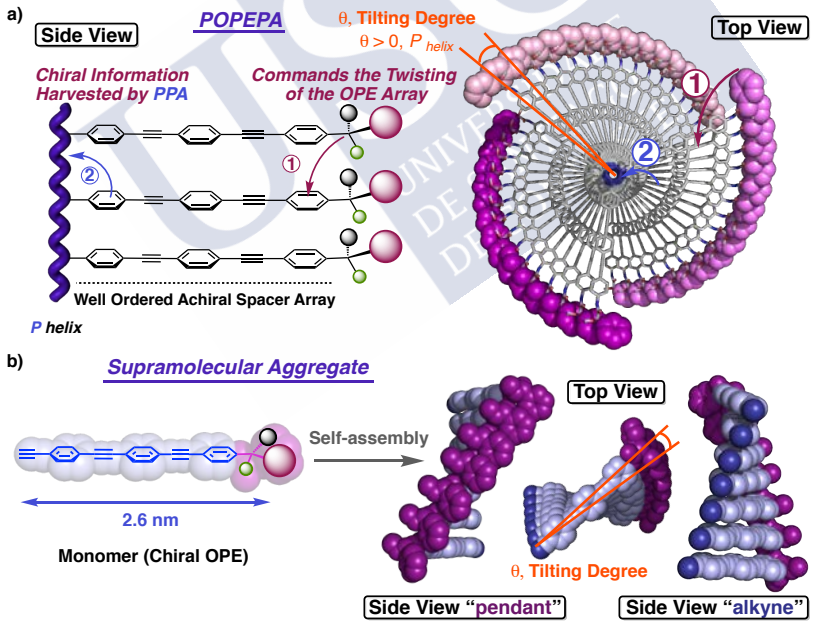

Figure 1. Chiral OPE arrays in (a) covalent and (b) supramolecular helical polymers.

41 Adelizzi, B.; Van Zee, N. J.; de Windt, L. N. J.; Palmans, A. R. A.; Meijer, E. W. *J. Am. Chem. Soc.* **2019**, *141*, 15, 6110-6121.
42 García, F.; Sánchez, L. *J. Am. Chem. Soc.* **2012**, *134*, 734-742.
43 Smulders, M. M. J.; Stals, P. J. M.; Mes, T.; Paffen, T. F. E. Schenning, A. P. H. J.; Palmans, A. R. A.; Meijer, E. W. *J. Am. Chem. Soc.* **2010**, *132*, 620-626.
44 Smulders, M. M. J.; Filot, I. A. W.; Leenders, J. M. A.; van der Schoot, P.; Palmans, A. R. A; Schenning, A. P. H. J.; Meijer, E. W. *J. Am. Chem. Soc.* **2010**, *132*, 611-619.
45 van Gestel, J.; Palmans, A. R. A.; Titulaer, B.; Vekemans, J. A. J. M.; Meijer, E. W. *J. Am. Chem. Soc.* **2005**, *127*, 5490-5494.
46 Wilson, A. J.; Masuda, M.; Sijbesma, R. P.; Meijer, E. W. *Angew. Chem. Int. Ed.* **2005**, *44*, 2275-2279.
47 Fernández, Z.; Fernández, B.; Quiñoá, E.; Riguera, R.; Freire, F. *Chem. Sci.* **2020**, *11*, 7182-7187.
48 See Chapter II.
49 See Chapter III.
50 See Chapter IV.

The presence of chiral OPE arrangements in both, covalent and supramolecular helical polymers, attracted our attention. We thought it possible to combine both families of helical polymers within a single helical structure to create the matryoshka-like helical materials.

To prepare a matryoshka helix based on POPEPAS modelling studies were carried out. To this end different helical structures were built up fulfilling the requirements of both, the PA and the supramolecular OPE helices. During these modelling studies it was found that to generate the desired POPEPA matryoshka-like helical material it is necessary to control the dihedral angle between conjugated double bonds (ω_1), which is directly related to the tilting degree adopted by the OPE units. Hence, if the POPEPA adopts a *cis-cisoidal* polyene scaffold ($\omega_1 < 90°$), the classical helix constituted by two coaxial helices will be formed (Figure 2a). In such helical scaffolds, the internal helix is defined by the polyene backbone (helix 1), while the external helix is defined by the helical array of the pendant groups (helix 2) (Figure 2a).[51,52] The tilting degree (Θ) between OPE units within these helical structures is high, describing a hand-fan shape array of OPE units. As a result, no evidence of matryoshka-like helical materials should be found in *cis-cisoidal* POPEPAs. However, it was found that if the POPEPA adopts an extended *cis-transoidal* helical structure ($\omega_1 > 160°$), the two classical internal and external helices found in PAs (helix 1 and helix 2) coexist with another two helical structures (helix 3 and 4), which correspond to a helical array of the achiral OPE units used as spacers between the chiral pendant and the polyene backbone (Figure 2b). These helical structures described by the OPE units within the helical polymer are coincident with those found in a OPE supramolecular helix (Figure 1b). Therefore, by using this approach we will look for the stabilization of a supramolecular helix within a covalent helical polymer.

[51] Fernández, B.; Rodríguez, R.; Quiñoá, E.; Riguera, R.; Freire, F. *ACS Omega* **2019**, *4*, 5233-5240.
[52] Fernández, B.; Rodríguez, R.; Rizzo, A.; Quiñoá, E.; Riguera, R.; Freire, F. *Angew. Chem. Int. Ed.* **2018**, *57*, 3666-3670.

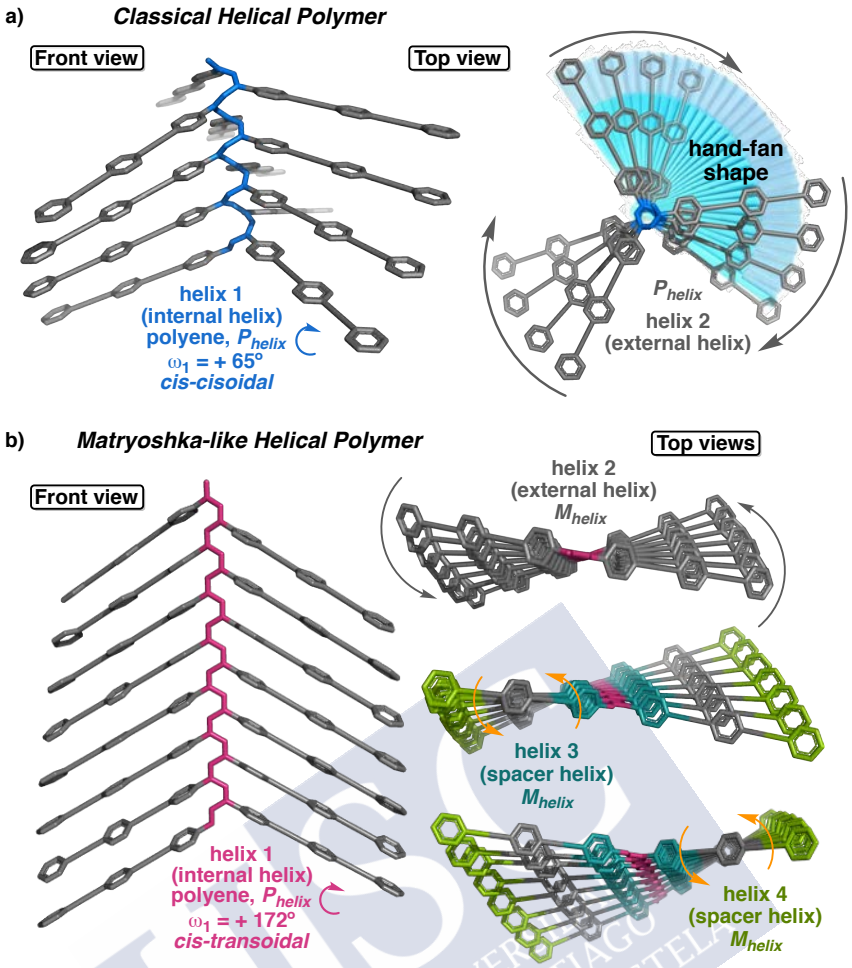

Figure 2. (a) POPEPA adopting a classical helical structure. (b) POPEPA showing a matryoshka-like helical scaffold.

To perform these studies, it is necessary to design and prepare a POPEPA that adopts a *cis-transoidal* helical scaffold. From literature, it is known that poly(phenylacetylene)s (PPAs) bearing benzamide connectors between the backbone and the pendant groups promote the formation of *cis-transoidal* structures.[53] Thus, as model compound we used the PPA that bears the benzamide of the (*L*)-decyl alaninate (poly-**1**), which adopts a stretched *cis-transoidal* (2/1) helix.[54,55]

Oligo[(*p*-phenyleneethynylene)$_n$]phenylacetylene monomers (n = 1, 2) containing the benzamide of the (*L*)-decyl alaninate —m-[**2**-**3**]— (Figure 3a) were prepared and further polymerized with a Rh (I) catalyst, which generates poly-[**2**-**3**] in good yield, low polydispersity and high content of *cis* double bonds (Figure 3b).

[53] Louzao, I.; Seco, J. M.; Quiñoá, E.; Riguera, R. *Angew. Chem. Int. Ed.* **2010**, *49*, 1430-1433.
[54] Okoshi, K.; Sakurai, S.; Ohsawa, S; Kumaki J.; Yashima, E. *Angew. Chem. Int. Ed.* **2006**, *45*, 8173-8176.
[55] Sakurai, S.; Okoshi, K.; Kumaki, J.; Yashima, E. *J. Am. Chem. Soc.* **2006**, *128*, 5650-5651.

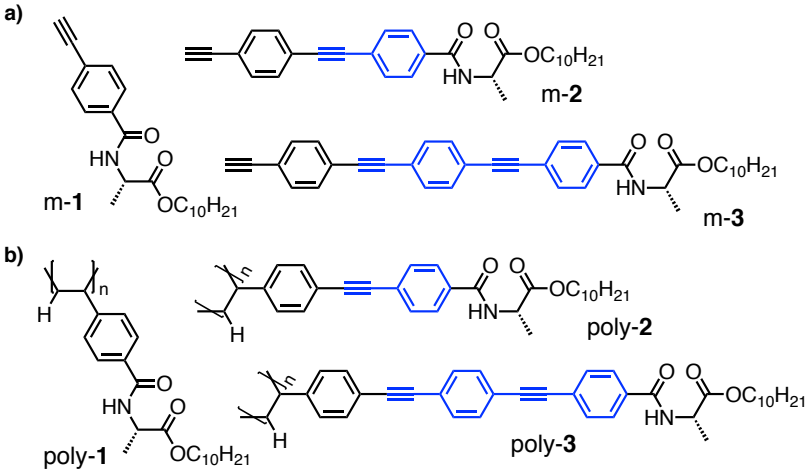

Figure 3. Chemical structures of (a) monomers —m-[**1**-**3**]— and (b) polymers — poly-[**1**-**3**]—.

Next, structural and dynamic behavior studies were carried out for poly-**2** and poly-**3**. CD studies of poly-**2** in different solvents such as $CHCl_3$, DCM, THF or DMF [(poly-**2**) = 0.44 mM] showed the classical ECD trace for a helical polymer, with three alternating Cotton effects. The first positive Cotton band, which corresponds to the polyene band, indicates the presence of a *P* internal helix (Figure 4a) and to obtain information related to the orientation of the external helix, AFM studies were performed. A 2D-crystal of poly-**2** was prepared from a chloroform solution by the Langmuir-Schaefer technique,[56] employing HOPG as substrate. The AFM studies revealed the presence of well-ordered monolayers, which allowed us to obtain high-resolution AFM images. From these images it was possible to extract the orientation of the external helix —*M* helix— and different structural parameters such as the helical pitch (4.6 nm) and the packing angle (80°) (Figure 4b). The combined information, extracted from the ECD and AFM studies, indicates that poly-**2** adopts a *cis-transoidal* scaffold (ω_1 ca., 165°), where the internal and the external helices rotate in opposite directions —P_{int} [$CD_{405\ nm}$ = (+)], M_{ext} (AFM)— (Figure 4b).

To corroborate the information extracted from the experimental data, computational studies [TD-DFT(CAM-B3LYP)/3-21G][57-59] were performed on a M_{ext} helix (with 8 monomer units) for poly-**2** —*cis-transoidal* skeleton (ω_1 = 165°)—. In this model, the chiral moiety was introduced into an *antiperiplanar* conformation, placing both carbonyl groups in opposite orientations, and in order to lower the computational demands, the long alkyl chain was replaced by a methyl group. The simulated ECD spectrum (Figure 4a and see Experimental Section Chapter V, Figure S10) is in good agreement with that experimentally obtained, which indicates that the proposed model is a good approximation to the structure adopted by poly-**2**.

---

56 Ulman, A. An Introduction to Ultrathin Organic Flims-From Langmuir-Blodget to Self-Assembly. Accademic Press, New York, 1991.
57 Runge, E.; Gross, E. K. U. Density-Functional Theory for Time-Dependent Systems. *Phys. Rev. Lett.* **1984**, *52*, 997-1000.
58 Yanai, Y.; Tew, D. P.; Handy, N. C. *Chem. Phys. Lett.* **2005**, *393*, 51-57.
59 Binkley, J. S.; Pople, J. A.; Hehre, W. J. *J. Am. Chem. Soc.* **1980**, 102, 939-947.

Interestingly, when poly-**2** is dissolved in low-polar solvents such as CCl_4 or Toluene, a yellow to red color change is produced, indicative of a helical stretching. UV-Vis studies confirm the elongation of the polyene chain due to a 100 nm bathochromic shift of the polyene band, from 425 ($CHCl_3$) to 525 nm (Toluene) (Figure 4c). Moreover, the solubility of the polymer decreases in these solvents due to the presence of a highly stretched, almost planar, helix. ECD studies of poly-**2** in these solvents revealed the disappearance of the classical ECD trace with three alternating Cotton effects, depicting a large bisignated (-/+) signal centered at 323 nm (Figure 4d). Interestingly, the ECD trace obtained for poly-**2** in CCl_4 or Toluene is coincident with the CD signature of an OPE supramolecular helix, where the -/+ sign of the CD trace is indicative of an *M* helical array of the OPE units within the POPEPA scaffold.[49,50]

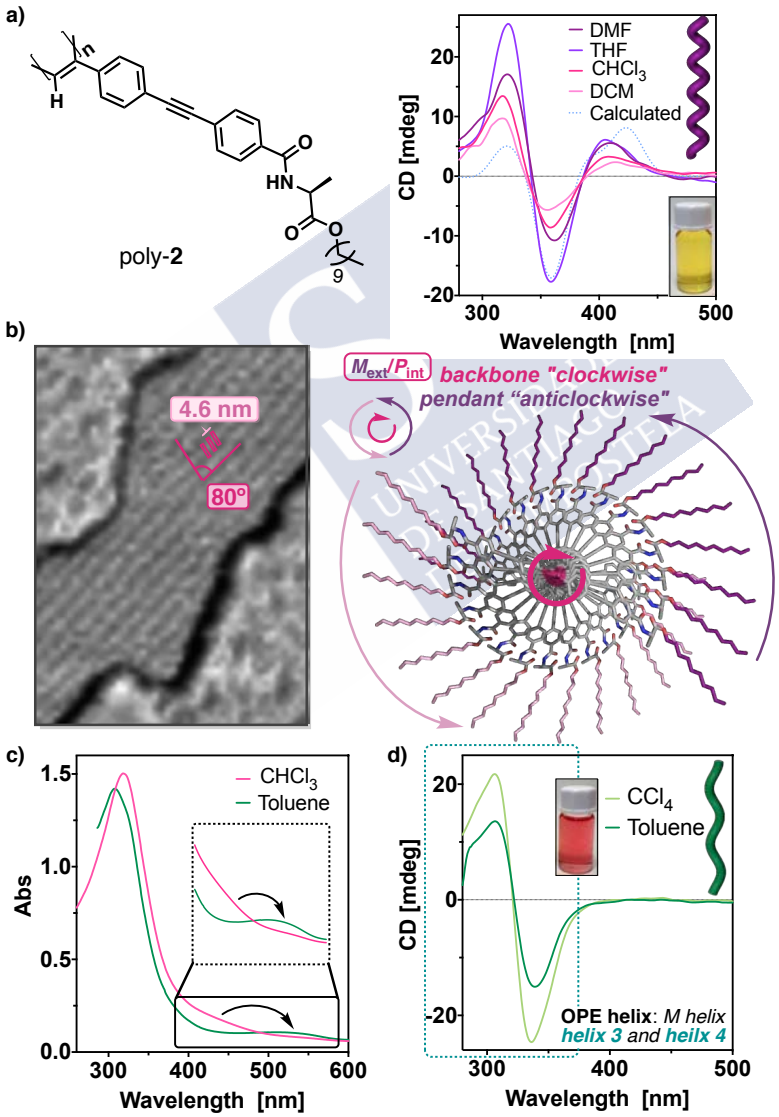

Figure 4. (a) Chemical structure for poly-**2** and ECD spectra recorded in different solvents compared to the simulated ECD (FWHM = 20 nm). (b) High-resolution AFM images and 3D-model of poly-**2** in polar solvents. (c) Comparison of the UV-Vis spectra obtained for poly-**2** in $CHCl_3$ and Toluene. (d) ECD spectra of poly-**2** in CCl_4 and Toluene.

[49] See Chapter III.
[50] See Chapter IV.

By using this information, a molecular model was built up for poly-**2** in low polar solvents using a large value for ω_1 (ca., 175°), which corresponds to an almost planar structure (Figure 5). By looking at this 3D-model, it is possible to visualize the two coaxial helices of a PPA; the first one described by the polyene backbone —P_{int} helix 1 (ω_1 = + 175°)— and the second one by the pendant groups —M_{ext} helix 2—. As expected, the presence of a *cis-transoidal* polyene skeleton makes that the internal and the external helices rotate in opposite directions (P_{int}/M_{ext}). In addition to these two coaxial helices, another two helices can be observed in this 3D-model structure. These latter helices are described by the OPE units used as spacers between the chiral pendant groups and the polyene backbone (Θ = 11°) —helix 3 and 4— and show a helical sense coincident with that described by the external helix —*M* helix—. Interestingly although this structure is formed by four helices —$P_1/M_2/M_3/M_4$— the resulting ECD spectrum is governed by the helical array of the OPE units and the chiroptical information of the polyene chain becomes negligible in the ECD spectrum [ECD null at ca. 525 nm but UV-Vis active] (Figure 4c, d).

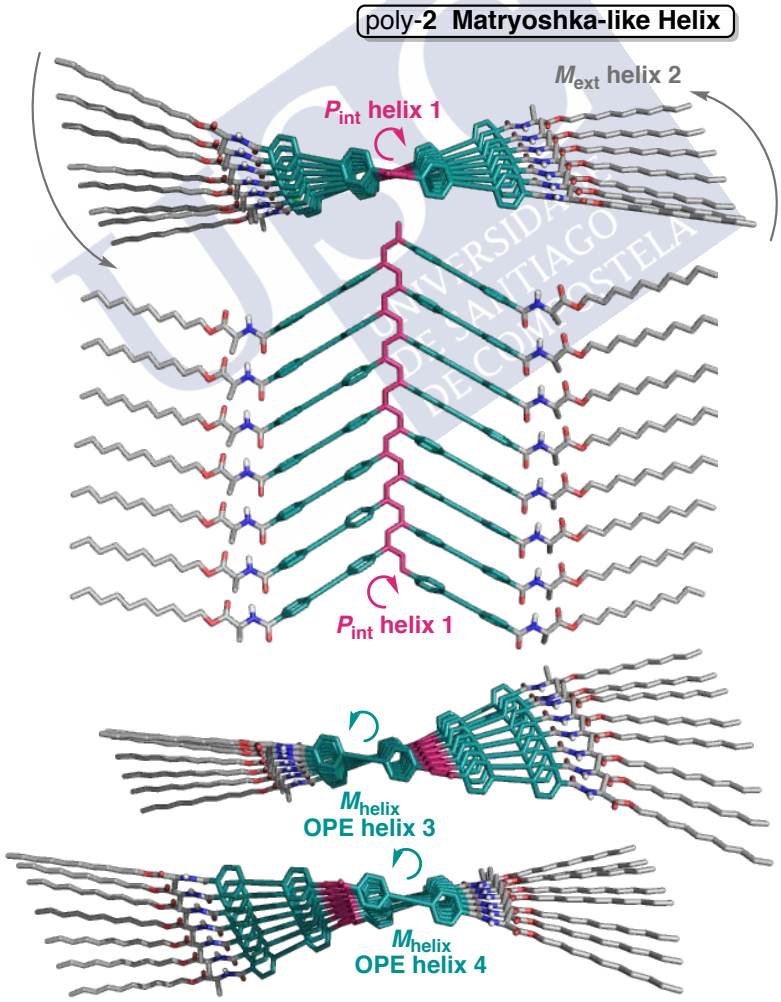

Figure 5. 3D-model for poly-**2** adopting a matryoshka-like helix.

Among the discovery of a matryoshka-like helical material, where four different helices coexist within the same material, another important finding was done during these studies. It was demonstrated that a supramolecular helix, such as an OPE supramolecular helical polymer can be stabilized within a covalent helical polymer. To show the versatility and robustness of our hypothesis and results, similar studies to those above were performed for poly-**3**, which has an extra OPE unit in the spacer (n = 2). To this end, solutions of poly-**3** ([poly-**3**] = 0.72 mM) were prepared in different solvents such as CCl_4, $CHCl_3$, THF, Toluene, ODCB, DCM or 1,2-DCE (Figure 6a and see Experimental Section Chapter V, Figure S7a and b). All these poly-**3** solutions showed a deep red color and a poor solubility, indicative of the presence of a highly stretched helix with a large hydrophobic surface and a high aggregation tendency.[25] UV-Vis studies of these poly-**3** solutions corroborate the presence of a stretched helix due to the presence of the polyene band at ca. 565 nm (Figure 6c and see Experimental Section Chapter V, Figure S7d).

In addition, ECD studies for poly-**3** do not show a Cotton band in the polyene region in all the tested solvents (Figure 6b and see Figure S7a and b), but a strong bisignated signal at shorter wavelengths (ca., 315 nm). The obtained CD trace resembles the one recorded for the supramolecular polymer helical arrangement (SP-**3**) of the monomer m-**3** (Figure 6d).[50] The bathochromic shift of the OPE band, observed in the CD spectrum when poly-**3** is compared to SP-**3**, is ascribed to the conjugation with the polyene backbone.

These data indicate that poly-**3** describes a matryoshka-like helix, where two novel helices show up due to the chiral arrangement of the OPE units. In this polymer four helical structures coexist; the internal helix, described by the polyene backbone (helix 1), the external helix, described by the pendant groups (helix 2), and the helical structures described by the OPE (n = 2) units employed as spacers (helix 3 and helix 4). These helices are interconnected and, by knowing the orientation of one of them it is possible to extract the orientation of the other helices (Figure 6e). Therefore, if poly-**3** shows a *P* orientation for helices 3 and 4 in DCM [CD (+/-)], then helix 2 rotates in the same *P* direction, whereas the internal helix 1 has to rotate in the opposite sense (*M*), according to the *cis-transoidal* configuration adopted by the polyene.

Computational studies [TD-DFT(CAM-B3LYP)/3-21G][57-59] have been performed on a M_{ext} helix (with 20 monomer units) for poly-**3** —*cis-transoidal* skeleton (ω_1 = 170°)— and, to reduce the computational demands, the chiral moiety has been removed from the pendants, keeping only the achiral spacer. This model simplification allowed us to create a 3D structure describing half a helix turn, necessary to observe the external helices described by the OPEs (helix 3 and helix 4). The calculated ECD spectrum is in full agreement with the experimental

[25] Rodríguez, R.; Quiñoá, E.; Riguera, R.; Freire F. *J. Am. Chem. Soc.* **2016**, *138*, 9620-9628.
[50] See Chapter IV.
[57] Runge, E.; Gross, E. K. U. Density-Functional Theory for Time-Dependent Systems. *Phys. Rev. Lett.* **1984**, *52*, 997-1000.
[58] Yanai, Y.; Tew, D. P.; Handy, N. C. *Chem. Phys. Lett.* **2005**, *393*, 51-57.
[59] Binkley, J. S.; Pople, J. A.; Hehre, W. J. *J. Am. Chem. Soc.* **1980**, 102, 939-947.

one obtained for DCM (Figure 6b), indicating that the proposed model is a good approximation to the *cis-transoidal* and highly stretched structure adopted in this solvent.

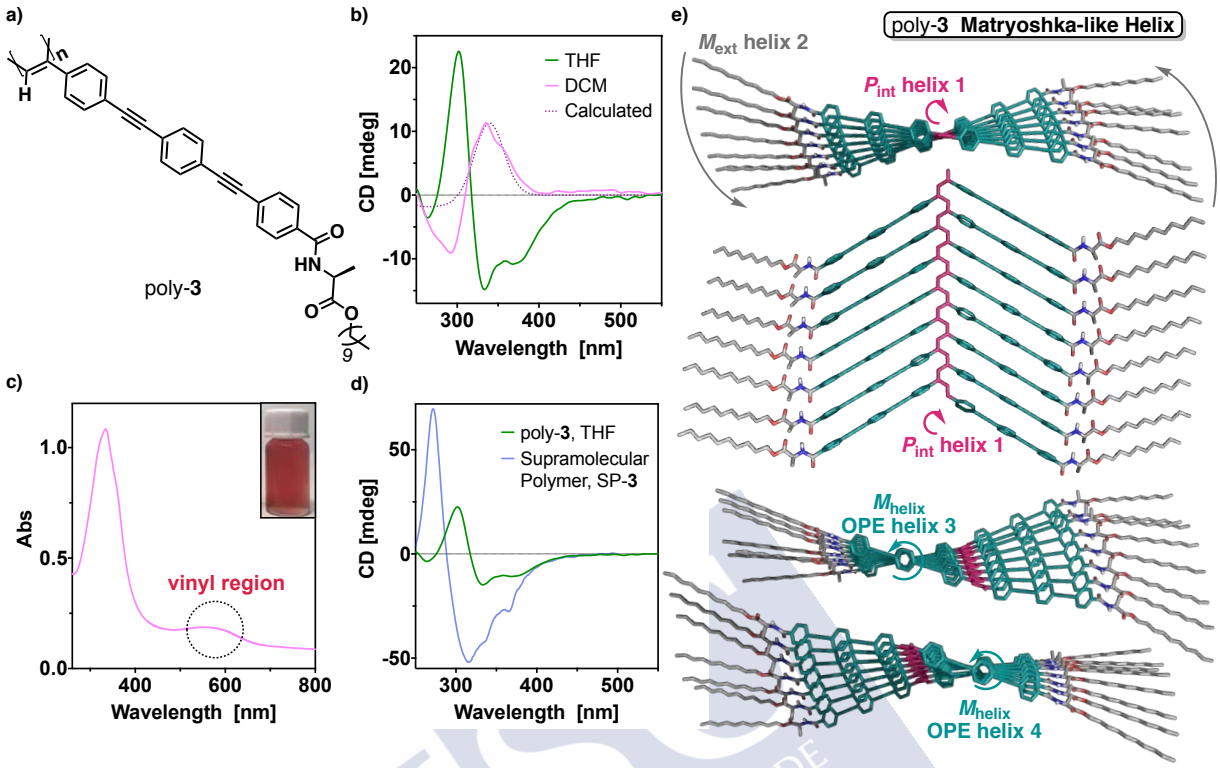

Figure 6. (a) Chemical structure for poly-**3**. (b) ECD spectra of poly-**3** in DCM and THF and comparison with the theoretically obtained ECD. Full Width at Half-Maximum (FWHM) equals 20 nm. (c) UV-Vis spectrum of poly-**3** in DCM. (d) Comparison of the ECD spectra obtained for poly-**3** and SP-**3**. (e) 3D-model for poly-**3** describing a matryoshka-like helix.

Moreover, CD studies indicate that the helical sense described by the OPE array in poly-**3** depends on the dielectric constant of the solvent (ε-1)/(ε+1). Therefore, poly-**3** is a dynamic helical polymer that can act as a chiroptical switch triggered by subtle variations of the polarity. On the one hand solvents with (ε-1)/(ε+1) > 0.8 (i.e., ODCB, DCM or 1,2-DCE) show a bisignated (+/-) CD signature, that corresponds to a *P* helix of the OPE array (helix 3 and 4) —$M_1/P_2/P_3/P_4$ matryoshka helix—. On the other hand, solvents with (ε-1)/(ε+1) < 0.8 (i.e., CCl_4, $CHCl_3$, THF or Toluene) produce an *M* orientation of the OPE helical array (helix 3 and 4) yielding a $P_1/M_2/M_3/M_4$ matryoshka helix (see Experimental Section Chapter V, Figure S7a-c).

USC
UNIVERSIDADE
DE SANTIAGO
DE COMPOSTELA

Conclusions

USC
UNIVERSIDADE
DE SANTIAGO
DE COMPOSTELA

Conclusions

The main conclusions obtained in the different chapters are summarized next.

Chapter I. Chiral Information Harvesting in Helical Poly(acetylene) Derivatives Using Oligo(*p*-phenyleneethynylene)s as Spacers

Herein, a novel chiral harvesting transmission mechanism has been described in poly(acetylene)s bearing oligo(*p*-phenylenethynylene)s as rigid spacers that place the chiral pendant group away from the polyene backbone, at a distance around 1.7 nm for poly-**2**, and 2.4 nm for poly-**3**. Hence, the disposition of the chiral moiety affects the stacking of the OPE units within the helical structure, inducing a specific positive or negative tilting degree, which is further harvested by the polyene backbone inducing either a *P* or *M* internal helix.

We believe that these results open new horizons in the development of novel helical structures by combining information from the helical polymers and supramolecular helical polymers fields, which leads to the formation of novel materials with applications in important fields such as asymmetric synthesis, chiral recognition or chiral stationary phases among others.

Chapter II. Aromatic Substitution Pattern Effects in Poly-[[oligo(phenylene ethynylene)]phenylacetylene]s: Modulation of the Helical Periphery Without Affecting the Folding of the Main Chain

In this chapter it has been demonstrated that while in PPAs the different aromatic substitution pattern affects largely to the elongation of the helical scaffold, in POPEPAs the modifications on the stretching of the polymer backbone are drastically reduced when the size of the achiral rigid OPE (n = 1, 2) spacer is increased. Therefore, for POPEPAS bearing an OPE spacer with n = 1, a variation in the helical elongation is still observed for the different aromatic substituted polymers. However, in the case of n = 2, no variation on the elongation of the internal helix is noticed. The synthesized POPEPAs —derivatized at the *ortho*-, *meta*- and *para*- positions of the external aryl group with the anilide of a chiral acid [(*S*)-MPA]— produce helical scaffolds with resembling internal helix but different external one, although the molecular structure or conformational composition of the chiral group remains unaffected. These studies open a new horizon for helical polymers with potential applications in fields such as chiral recognition, asymmetric synthesis or sensing, among others. By using these systems it is possible to explore the effect that the variations on the helical periphery can have over the efficiency of these smart materials.

Chapter III. Complex Supramolecular Polymerization Pathway of an Asymmetrical and Rigid OPE Derivative: The Role of the Supramolecular Polymerization Degree in the Aggregate Morphology

A complex aggregation pathway was demonstrated for a rigid chiral OPE derivative [(*S*)-**1**]. Dissolving this monomer into a MCH:DCM (99:1) solvent mixture results in an isodesmic off-pathway aggregation mechanism, which yields to the formation of a metastable aggregate (**Agg$_I$**). In this way, a short *P* twisted oligomer is obtained and self-assembles producing an in-plane aggregation that provides extended and slightly twisted sheets. Heating and cooling this sample (**Agg$_I$**) to 273 K results in an isodesmic on-pathway aggregation mechanism, generating the thermodynamic **Agg$_{II}$** aggregate. In this case, a supramolecular *M* helical polymer is obtained where the monomers self-assemble into a columnar helical aggregate. Furthermore, the metastable aggregate (**Agg$_I$**) can be kinetically trapped (isodesmic, off-pathway) if the sample preparation conditions are modified —MCH:Tol:DCM (97:2:1)—, observing that the obtained aggregate becomes stable over time.

These results constitute a significant example of a complex supramolecular polymerization pathway, where on- and off-aggregation pathways are described, being possible to trap the kinetic aggregate by changing the solvent mixture. Moreover, these studies also reveal how the size of the supramolecular aggregate affects the aggregate morphology. Thus, while the formation of short oligomers (off-pathway) produces in-plane aggregation to generate twisted sheets, the formation of large supramolecular helical polymers (on-pathway) provides the formation of columnar helical aggregates.

Chapter IV. Supramolecular Triangular Tessellation Produced by the Self-Assembly of Chiral Helical Oligomers Obtained from OPE Derivatives

In this project, we have been able to demonstrate the role of the long alkyl chain in the supramolecular polymerization process of asymmetric OPE derivatives. It was previously found that a complex isodesmic pathway governs the supramolecular polymerization of an OPE lacking the alkyl chain. Herein, we have shown how an OPE derivative bearing this structural motif follows a cooperative supramolecular polymerization process, with thermodynamic parameters similar to those found in BTAs. The helical structure of this SP was elucidated by ECD theoretical calculations and AFM studies. Moreover, the use of an asymmetric OPE in combination with two different flexible ends —one rigid (OPE), one bendable (alkyl chain)—, produces the tessellation of the HOPG by second order supramolecular self-assembly of OPE oligomers during the drop casting and solvent evaporation of the sample. As a result, a novel regular triangular lattice is obtained.

This work opens a new way in the creation of extended and regular 2D-supramolecular nanostructures based on supramolecular helical polymers or oligomers which can further

aggregate to form regular 3D structures, similar to those found in other materials such as MOFs or nanomaterials.

Chapter V. Matryoshka-like Helical Polymers: When Supramolecular and Covalent Helical Polymers are Mixed Up

We have proven that it is possible to stabilize a supramolecular helix embedded within a covalent helical polymer through two different examples —poly-**2** and poly-**3**—. To perform these studies, we have chosen as covalent polymer a poly(acetylene) derivative, while as supramolecular polymer an oligo(*p*-phenyleneethynylene) has been selected. From previous studies in both fields —covalent and supramolecular polymers— we know that both structures can fit in proper matryoshka helical scaffolds. In this special case —PA/OPE system—, the polyene should adopt an almost planar yet twisted helical structure (i.e., a *cis-transoidal* helix with ω_1 > 165º). This fact makes the pendant groups of the PA, in this case OPE derivatives, display a tilting degree between OPE units (Θ) close to 11º, similar to the one present in OPE supramolecular polymers. Thus, if we are able to induce an ω_1 > 165º in the PA, the matryoshka helix can be prepared, stabilizing a SP helix within a covalent helix. A perfect example is poly-**2** that bears an OPE with n = 1. This polymer in THF adopts a helical structure with ω_1 ca. 165º, which shows a CD signature with three alternating Cotton effects, as a classical PPA helix. On the other hand, in Toluene or CCl_4 poly-**2** adopts a helical scaffold with ω_1 > 170º, which produces a CD signature governed by the axial orientation of the OPE units, instead of being commanded by the helical orientation of the PPA chain. As a result, two novel helices emerge within this helical novel scaffold, where four different helices coexist in the helical material: the two coaxial helices —internal (helix 1) and external (helix 2)— and the two helices described by the OPE axial arrays (helices 3 and 4). These four helices are interconnected and, by identifying the orientation of one of them, it is possible to obtain the helical sense of the others. In this case two scenarios are possible $M_1/P_2/P_3/P_4$ or $P_1/M_2/M_3/M_4$.

In the second design, poly-**3** always generates a matryoshka-like helix with an axial array of the OPE units and the presence of four helices within a single polymer.

These results open a new horizon in helical polymer design, where the stabilization of supramolecular helices within covalent polymers will allow to use these structures in applications that were limited before, due to the difficulty of generate SP polymers in polar solvents.

USC
UNIVERSIDADE
DE SANTIAGO
DE COMPOSTELA

Resumo

USC
UNIVERSIDADE
DE SANTIAGO
DE COMPOSTELA

Resumo

Dende o seu nacemento, inspirado nos polímeros naturais, a estrutura dos polímeros sintéticos foi obxecto de estudo por parte da comunidade científica. A finalidade destas pescudas primitivas era a de imitar a estrutura observada nas hélices biolóxicas sen embargo, co paso do tempo, o estudo dos polímeros helicoidais sintéticos demostrou que estes materiais presentan propiedades únicas e funcionalidades específicas que non son observables nin alcanzables nos sistemas naturais. Desta maneira, a partir do século XX, a ciencia de polímeros emerxeu como unha das principais áreas na ciencia dos materiais e continúa séndoo a día de hoxe, facendo difícil imaxinar a vida actual sen a presenza destes materiais.

As propiedades que presentan estes materiais son comúns para os dous tipos de polímeros e son debidas ás estruturas que adoptan. Estes polímeros —covalentes e supramoleculares— diferéncianse principalmente no tipo de interaccións que unen os monómeros que os conforman. Por un lado, no caso dos polímeros covalentes a reacción de polimerización xera un material no que os monómeros se unen de maneira irreversible, mentres que os polímeros supramoleculares forman agregados só en condicións favorables, que se son modificadas resultan na perda da autoensamblaxe. Unha das propiedades máis interesantes destes materiais é a da amplificación de quiralidade, descrita por primeira vez para polímeros covalentes (i.e., poli(isocianato)s), e estendida hoxe en día a todo tipo de polímeros. Relacionado con este fenómeno atópanse outras propiedades como a indución da helicidade, a memoria da helicidade ou a autoclasificación quiral.

Esta tese titulada: “Polímeros Helicoidais Supramoleculares e Covalentes: o Albor dos Materiais Matrioshka”, inclúe cinco proxectos de investigación nos que se abordarán o estudo das estruturas e o comportamento de polímeros helicoidais tanto supramoleculares coma covalentes. Finalmente a información recadada nestas pescudas será combinada, xerando así un novo material no que os dous motivos estruturais —covalente e supramolecular— estean presentes. A continuación expoñeranse os resultados máis relevantes de cada capítulo.

Capítulo I. Extracción da Información Quiral en Derivados Helicoidais de Poli(acetileno)s Empregando Oligo(*p*-fenilenoetinileno)s como Espazadores

Controlar a estrutura helicoidal adoptada polo polímero é un dos grandes retos da comunidade científica hoxe en día. Para isto é necesario coñecer a estrutura secundaria así como o mecanismo de transmisión da información quiral do mesmo. Na bibliografía atópanse diferentes exemplos nos que se consigue controlar de maneira eficaz a hélice final adoptada polo polímero a través da aplicación de estímulos externos, obtendo así un sentido de xiro específico. A maioría destas estruturas descritas presentan o centro quiral próximo á cadea polimérica, de maneira que a información quiral é transmitida mediante teleindución, ou

separado da mesma a través dun espazador flexible, o cal é capaz de se organizar de xeito que poida transmitir a información quiral.

Neste capítulo descríbese un novo mecanismo de comunicación quiral en polímeros derivados de poli(acetileno)s (PPAs), nos cales o centro quiral atopase separado da cadea polimérica mediante un espazador de oligo(*p*-fenilenoetinileno)$_n$ (OPE; n = 1 ou 2). Este espazador ríxido e aquiral permite localizar o centro quiral a distancias da orde de 1.7 nm e de 2.4 nm para n = 1 e n = 2, respectivamente. A pesar desta distancia, o centro quiral é capaz de inducir un sentido de xiro preferente na cadea polimérica mediante a organización dos espazadores de OPE. Isto débese a que a conformación adoptada polo centro quiral ten efecto sobre o amontoamento dos espazadores aquirais, resultando nun ángulo positivo ou negativo. Dito ángulo é finalmente transmitido á cadea polimérica, inducindo un sentido de xiro na hélice interna (conformada polos dobres enlaces conxugados) positivo ou negativo. Este proceso polo cal o centro quiral que está nunha posición remota é capaz de inducir un sentido de xiro preferente sobre a hélice interna coñécese como extracción da información quiral.

Así mesmo, neste traballo estudouse tamén a estrutura secundaria dos polímeros sintetizados. A través da combinación de diversas técnicas como Microscopía de Forza Atómica (AFM), Calorimetría Diferencial de Varrido (DSC) ou cálculos computacionais, entre outras, foi posible determinar a hélice adoptada pola cadea polimérica. En ambos casos atopouse que os polímeros sintetizados adoptan unha conformación comprimida *cis*-*cisoide*. Ademais, o estudo con catións metálicos permitiu demostrar a diminución do carácter dinámico conforme aumenta a lonxitude do espazador. Así, mentres que o polímero con n = 1 presenta amplificación da quiralidade e inversión da helicidade, no caso de n = 2 a adición de catións metálicos non ten ningún efecto sobre a estrutura helicoidal.

Capítulo II. Efecto do Patrón de Substitución Aromática en Poli[[oligo(fenilenoetinileno)fenilacetileno)s: a Modulación da Periferia Helicoidal sen Afectar ó Pregamento da Cadea Principal

Recentemente no noso grupo de investigación describiuse o efecto que ten sobre a estrutura a variación do patrón de substitución no anel aromático no caso dos poli(feniacetileno)s (PPAs). Deste xeito, mediante a modificación da posición de substitución do anel de fenilacetileno (*orto*-, *meta*- ou *para*-), atopouse un método sinxelo para modificar a elongación da estrutura así como o comportamento helicoidal. De maneira xeral, os PPAs con substituíntes en posición *para*- presentan estruturas comprimidas e dinámicas, debido ó alto grao de liberdade conformacional e o impedimento estérico case nulo entre o centro quiral e o esqueleto poliénico. No caso dos polímeros con substituínte en *meta*- a liberdade conformacional vese reducida, non podendo modular o sentido de xiro do polímero, mentres que en disolución coexisten dúas estruturas, unha estirada e outra comprimida, en equilibrio.

Isto débese ó aumento do impedimento estérico ó aproximar o centro quiral ó esqueleto poliénico o cal chega ó seu máximo ó localizar o substituínte na posición *orto*-, xerando desta maneira unha estrutura totalmente estendida e case plana aínda que lixeiramente helicoidal.

Estes resultados leváronnos a analizar o efecto que tería esta modificación na posición de substitución no caso dos poli-[[oligo(fenilenoetinileno)fenilacetileno)s (POPEPAs), onde o centro quiral sitúase afastado da cadea polimérica mediante un espazador ríxido e aquiral. O estudo revelou que, a diferencia dos PPAs, no caso dos POPEPAs a modificación do patrón de substitución sobre o anel aromático non ten un efecto tan acusado xa que, ó afastar o centro quiral da cadea polimérica, o impedimento estérico vese reducido. Mentres que para os polímeros co espazador de oligo(*p*-fenilenoetinileno)$_n$ (OPE) de n = 1 dáse unha lixeira variación na elongación do polímero, no caso no que o OPE é n = 2, a estrutura helicoidal non se ve afectada. Isto débese a que para n = 1, no caso da posición *para*-, o espazador localiza o centro quiral o suficientemente afastado da cadea polimérica, mentres que para as posicións *meta*- e *orto*-, a estrutura sufre unha pequena elongación respecto á *para*-, podendo así aliviar a tensión estérica debido á proximidade entre o centro quiral e o esqueleto poliénico. Isto non ocorre no caso de n = 2, onde o centro quiral nunca se atopa preto da cadea polimérica. Polo tanto os POPEPAs presentarán un pregamento similar nas hélices dos diferentes polímeros sintetizados. A conformación adoptada pola cadea polimérica foi confirmada mediante estudos de UV-Vis ou DSC, entre outros. Por outro lado, para a mesma posición de substitución (*orto*- *meta*- ou *para*-) e ó aumentar a lonxitude do espazador OPE obsérvase, en todos os casos, a mesma indución helicoidal xa que se da o mesmo mecanismo de comunicación, a extracción da información quiral, introducido no Capítulo I. Polo tanto, nesta nova familia de polímeros puidemos xerar materiais helicoidais de estrutura similar —elongación semellante na hélice interna— pero cunha decoración diferente na periferia, debido á diferente localización dos centros quirais na hélice externa —substitución *orto*- *meta*- ou *para*-—.

Capítulo III. O Complexo Mecanismo de Polimerización Supramolecular dun Derivado de OPE Asimétrico e Ríxido: O Papel do Grao de Polimerización Supramolecular na Morfoloxía do Agregado

Os polímeros supramoleculares caracterízanse por posuír un carácter dinámico e reversible. Estas propiedades, inherentes a este tipo de polímeros, sonlle conferidas pola natureza non covalente dos enlaces que unen as unidades monoméricas, o que permite aplicalos en diversos campos científicos tales como a nanoelectrónica ou catálise. De maneira xeral, as unidades monoméricas adoitan estar compostas por núcleos π-conxugados, que permiten a formación de interaccións π-π, e cadeas alquílicas longas que facilitan a agregación. Outras das interaccións débiles que adoitan formar parte na estabilización destas estruturas son os enlaces de hidróxeno ou as interaccións de Van der Waals principalmente.

Para poder comprender o mecanismo de formación dos agregados os polímeros supramoleculares son analizados a través do rexistro dunha medida espectroscópica —Dicroísmo Circular (CD), UV-Vis ou fluorescencia— dependente da temperatura. O sinal espectroscópico obtido a unha lonxitude de onda determinada é normalizado e representado en función da temperatura, obtendo unha curva que permitirá determinar se a polimerización segue un proceso isodésmico ou cooperativo. Para levalo a cabo, a disolución de polímero quécese ata alcanzar unha temperatura na que se asegura a rotura dos enlaces non covalentes, quedando presentes en disolución só os monómeros sen agregar, isto tradúcese nunha linealidade na curva. Este quecemento vai seguido dun arrefriamento controlado que permita a formación do produto termodinámicamente máis favorable, obtendo así a curva de arrefriamento.

Neste traballo descríbese o mecanismo de polimerización supramolecular dun oligo(*p*-fenilenoetinileno) asimétrico, no cal un dos extremos está funcionalizado cun monómero derivado do ácido (*S*)-α-metoxi-α-fenilacético (MPA), mentres que no outro lado o alquino permanece inalterado. Os estudos revelan que cando este monómero se disolve nunha mestura MCH:DCM (99:1) fórmase un agregado metaestable (**Agg$_{I}$**) que evoluciona co tempo. Imaxes de AFM, en conxunto con cálculos computacionais, revelan que o monómero produce pequenos oligómeros con xiro a dereitas que agregan para dar nano-follas lixeiramente rotadas unhas sobre as outras. Para poder determinar o mecanismo de agregación, tal e como se indicou con anterioridade, o polímero someteuse a un proceso de quecemento/arrefriamento e, a partir da curva de arrefriamento obtida, determinouse que a polimerización que segue é de tipo isodésmica. De xeito curioso, estudos de UV-Vis suxiren a formación dunha nova especie, debido á aparición dunha nova banda de absorción, e medidas de CD revelan a formación dunha nova estrutura (**Agg$_{II}$**) cun sentido de xiro oposto ó de **Agg$_{I}$**. O descubrimento deste novo agregado, **Agg$_{II}$**, foi confirmado mediante AFM en cálculos computacionais, o que desvelou a formación de longas cadeas helicoidais con sentido de xiro á esquerda.

Adicionalmente, mediante unha lixeira modificación na polaridade do disolvente —MCH:Tolueno:DCM (97:2:1)—, fomos capaces de illar o agregado metaestable (**Agg$_{I}$**) e convertelo nun produto termodinámico e estable no tempo durante días. Desta maneira puidemos describir o complexo mecanismo de polimerización supramolecular dun OPE asimétrico.

Capítulo IV. Teselado Triangular Supramolecular Producido Mediante o Autoensamblaxe de Oligómeros Helicoidais Quirais Obtidos de Derivados de OPE

Estudos feitos con anterioridade revelaron que a introdución de cadeas alquílicas nos bloques de construción dos polímeros supramoleculares favorecen a agregación dos mesmos, ademais de incrementar a solubilidade en disolventes pouco polares. Animados polos

resultados recollidos no Capítulo III e tendo en conta os datos atopados na bibliografía, decidimos estudar o mecanismo de agregación dun OPE asimétrico substituído nun dos dous extremos cun monómero de decil-(*L*)-alaninato. O monómero disolveuse en MCH e someteuse a un proceso de quecemento/arrefriamento, monitorizado os cambios mediante CD a unha lonxitude de onda fixa, o que revelou que a formación do agregado segue un proceso cooperativo. As curvas de quecemento e arrefriamento obtidas presentan histérese entre elas, o que é indicativo da presenza de estados cinéticamente atrapados no proceso de arrefriamento polo que, ademais da estrutura termodinámicamente máis estable xerada, en disolución tamén haberá pequenos oligómeros. Co fin de poder observar o polímero supramolecular formado depositouse unha mostra do mesmo nun substrato de HOPG (grafito pirolítico altamente ordenado) e analizouse mediante AFM. Mediante esta técnica obtivéronse imaxes de alta resolución que indican que a hélice xira á esquerda, o que está en total acordo co observado mediante CD —onde se obtén un bisignato (-/+)— e cos cálculos computacionais levados a cabo sobre un oligómero de doce unidades monoméricas.

Ademais, de forma sorprendente, na mesma placa de HOPG onde se observaron as hélices supramoleculares, rexistráronse tamén zonas nas que aparece un teselado triangular. Este teselado non é regular e nalgúns puntos os triángulos presentan defectos ou non están formados de todo, posiblemente debido o proceso de evaporación da mostra que non permite a perfecta cristalización. Para poder explicar esta intrigante formación débese ter en conta a estrutura do monómero empregado, a cal está constituída por dous motivos de diferente flexibilidade, por un lado o OPE que é totalmente ríxido mentres que no outro atópase a cadea alquílica, a cal se pode pregar con gran facilidade. A partir de estudos computacionais sábese que durante a oligomerización do monómero todas as unidades OPE orientaranse dun lado, mentres que as cadeas alquílicas disporanse no outro para estabilizar o agregado. Así ó depositala mostra e evaporarse o disolvente producirase a interacción entre os pequenos oligómeros xerados no proceso de arrefriamento. A partir dos datos extraídos de AFM sábese que os devanditos oligómeros estarán formados pola unión de catro monómeros. Estes oligómeros interactuarán entre eles a través da cadea alquílica e a través dos OPE mediante interaccións alquino-π, xerando unha estrutura plano triangular. O crecemento desta estrutura plano triangular producirá, mediante interaccións non covalentes, un hexágono que pode continuar medrando ata a formación dunha estrutura composta pola fusión de cinco polígonos regulares e que recorda aos paneis das abellas. Cada unidade de cinco hexágonos describe un triángulo e a repetición desta estrutura leva á formación do teselado triangular observado mediante AFM. Os datos extraídos das imaxes de alta resolución, tales como o espesor ou a lonxitude dos motivos xeométricos, coinciden co modelo proposto para a formación deste entramado.

Capítulo V. Polímeros Helicoidais Tipo Matrioshka: a Mezcla dos Polímeros Supramoleculares e Covalentes

Os polímeros supramoleculares e covalentes posúen diversas características comúns, diferenciándose principalmente no tipo de enlaces que manteñen as unidades monoméricas que os conforman xuntas. En ambos os dous casos obsérvanse propiedades como a amplificación da quiralidade, a inversión da helicidade, o efecto Sarxento e Soldado ou o fenómeno da Regra da Maioría.

Como se mencionou con anterioridade, coñecer a estrutura secundaria destes polímeros é clave á hora de poder manipular a hélice polimérica. No caso dos polímeros supramoleculares a hélice está definida pola disposición non simétrica dos monómeros, polo que as unidades que conforman o polímero non covalente poden ou non ser quirais. Pola contra nos polímeros helicoidais covalentes (i.e., PPAs) sábese que a estrutura secundaria está conformada por dúas hélices coaxiais, a hélice interna (hélice 1), conformada polos dobres enlaces conxugados do polieno, e a hélice externa (hélice 2), descrita polos "pendant". Estas hélices poden rotar na mesma dirección, xerando unha estrutura *cis-cisoide* ($\omega_1 < 90^o$), ou en sentidos opostos, dando lugar á formación dunha estrutura *cis-transoide* ($\omega_1 > 90^o$). Este escenario dáse tamén no caso dos POPEPAs, sen embargo a análise dos modelos tridimensionais para un destes polímero con $\omega_1 > 165^o$ (*cis-transoide*) revelou que, ademais das dúas hélices clásicas (hélices 1 e 2), existen dúas hélices adicionais descritas polos espazadores (hélices 3 e 4). Isto é debido a que ó aumentar o ángulo da hélice interna (hélice 1) os espazadores derivados de OPE, localizados entre o centro quiral e o polieno, aproxímanse no espazo reducindo así o ángulo de desfase entre eles e describindo unha hélice similar á descrita nun polímero supramolecular. Tendo en conta esta información e os resultados obtidos nos capítulos anteriores, decidimos ir na procura dun novo material que combine ambos polímeros, o covalente e o supramolecular. Para levar a cabo esta idea empregamos o monómero descrito no Capítulo IV, onde demostramos que forma un agregado supramolecular de tipo helicoidal e porque é sabido que os compostos con conexión benzamida inducen a adopción dunha estrutura *cis-transoide*.

Polo tanto sintetizamos dous polímeros co espazador de oligo(*p*-fenilenoetinileno)$_n$ (OPE) de diferente lonxitude (n = 1 e 2). Estudos de CD para o POPEPA con n = 1 demostran que o polímero ó ser disolto en disolventes polares (e.g., DCM ou THF) presenta unha traza clásica con tres efectos Cotton alternantes. Imaxes de AFM para unha disolución do polímero indican que nestas condicións a hélice adopta unha estrutura *cis-transoide* con xiro a esquerdas. Esta conformación foi asegurada mediante estudos computacionais, no que os datos teóricos concordan cos experimentais. De xeito interesante no caso en que este POPEPA se solubilice en disolventes pouco polares obsérvase un claro estiramento helicoidal no UV-Vis que se da tamén a nivel macroscópico, puidendo visualizar un claro cambio de cor, de amarela a vermella. De estudos anteriores sábese que esta cor vermella é indicativa da adopción dunha

hélice estirada e case plana. O cambio na elongación da estrutura helioidal dáse tamén no CD, onde desaparece o espectro clásico e a traza pasa a ser un bisignato (-/+). Este CD alternante, no que o primeiro efecto Cotton é negativo, indica que a hélice presenta un xiro a esquerdas. Con esta información na mente modelamos unha estrutura tridimensional con unha hélice interna (hélice 1) positiva (ω_1 = 175º) e unha hélice externa (hélice 2) negativa, de acordo con a conformación *cis-transoide* adoptada polo polímero. Desta maneira é posible visualizar as hélices descritas polos espazadores (hélices 3 e 4), que xirarán no mesmo sentido que o descrito pola hélice externa (hélice 2).

No caso do POPEPA con n = 2 o polímero adopta unha estrutura moi estirada —*cis-transoide*—, o que se corrobora mediante medidas de UV-Vis e, ademais, todas as disolucións adoptan unha cor vermella escura. Este estiramento vese tamén nos estudos de CD, onde o bisignato (-/+) é coincidente coa traza de CD obtida para o polímero supramolecular do Capítulo IV, o que suxire a formación dunha hélice de xiro á esquerda. Esta hipótese foi confirmada mediante cálculos computacionais para un oligómero de 20 unidades xirando á esquerda, reproducindo desta maneira os datos obtidos experimentalmente. Así mesmo o sentido de xiro deste polímero é determinado pola constante dieléctrica do disolvente, polo que o devandito polímero actuará como un sensor quiroóptico da polaridade do medio. Así, no caso en que os disolventes presenten $(\varepsilon-1)/(\varepsilon+1) > 0.8$, na traza de CD observarase un bisignato (+/-) mentres que se $(\varepsilon-1)/(\varepsilon+1) < 0.8$, o espectro de CD será unha imaxe especular do anterior cun bisignato (-/+).

USC
UNIVERSIDADE
DE SANTIAGO
DE COMPOSTELA

Experimental Section

Chapter I

USC
UNIVERSIDADE
DE SANTIAGO
DE COMPOSTELA

1. Materials and Methods

CD measurements were done in a Jasco-720 and UV spectra were registered in a Jasco V-630. The amount of polymer used is indicated in the corresponding section. Measurements were performed in a 1mm quartz cell. The concentration of perchlorate salts used in the studies was 50 $mg \cdot mL^{-1}$ in THF. VT-CD measurements were performed in a Jasco-1100.

IR spectra were recorded in a Perkin Elmer FT-IR ATR Spectrum Two.

The optical rotation was measured in a Jasco P-2000.

Raman spectra were carried out in a Renishaw confocal Raman spectrometer (Invia Reflex model) equipped with a 785 nm diode laser and a 514 nm Ar laser.

DSC traces were obtained in a DSC Q200 Tzero Technology (TA Instruments, New Castle, UK) equipped with a refrigerated cooling system RCS90 (TA Instruments, New Castle, UK), using a Tzero low-mass aluminium pan.

TGA traces were obtained in a TGA Q5000 (TA Instruments, New Castle, UK) using a platinum pan.

Chiral HPLC experiments were carried out in a Waters System equipped with a Phenomenex Lux 5mm i-Amilose-1 column. The amount of monomer used was 0.5 $mg \cdot mL^{-1}$ and the mixture hexane:isopropanol (8:2) was used as eluent (flow rate: 0.5 $mL \cdot min^{-1}$).

GPC studies were carried out in a Waters Alliance equipped with Phenomenex GPC columns (10^3 Å, 10^4 Å and 10^5 Å). The amount of polymer used was 0.5 $mg \cdot mL^{-1}$. THF was used as eluent (flow rate: 1 $mL \cdot min^{-1}$) and as inner standard, polystyrene narrow standards (PSS) were used.

AFM measurements were performed in a Multimode V Scanning Probe Microscope (Veeco Instruments) in air at r.t., with standard silicon cantilevers and supersharp cantilevers in tapping mode using 12 mm and 1 mm scanners. Nanoscope processing software and WSxM 4.0 Beta 1.0 [4] (Nanotec Electrónica, S.L.) was used for image analysis. All measurements were performed at CACTI (Vigo University, Spain).

The monolayers were prepared by the Langmuir-Schaefer method in a rectangular shallow trough made of poly(tetrafluoroethylene) (36 cm x 11 cm x 1 cm). A Wilhelmy balance provided with a 20 mm wide filter paper was used as a plate to measure the surface pressure. The polymer solution [250 µL (0.1 $mg \cdot mL^{-1}$)] was spread drop by drop on the Milli-Q water surface. After fifteen minutes, time needed to allow the $CHCl_3$ evaporation as well as for the stabilization of the system, the barriers were gradually closed until reaching the target pressure (1 $mN \cdot m^{-1}$), indicative for the formation of a compact monolayer. This monolayer was recollected onto a freshly cleaved HOPG substrate (Telstar Instrumat, ZYH grade), with a dipper speed of $1mm \cdot s^{-1}$.

Spartan 10 (MMFF94) was used for molecular modelling.

PyMOL was used as a molecular visualization system.

2. Synthesis of Monomers

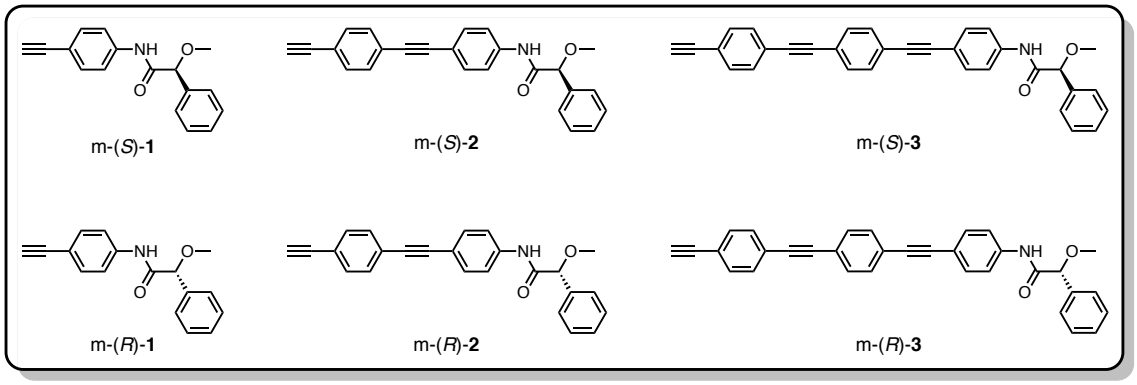

m-(*S*)-**1** and m-(*R*)-**1** were prepared according to the previously reported procedure.[S1]

[S1] F. Freire, J. M. Seco, E. Quiñoá and R. Riguera, *Angew. Chem. Int. Ed.* 2011, **50**, 11692-11696.

Synthesis of 4-((4-((trimethylsilyl)ethynyl)phenyl)ethynyl)aniline (**1**)

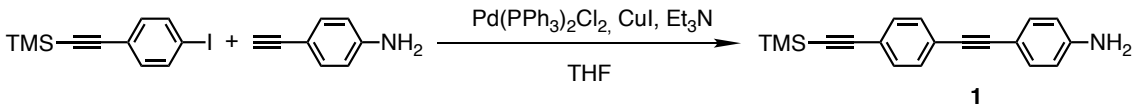

1

((4-iodophenyl)ethynyl)trimethylsilane (0.80 g, 2.66 mmol 1.00 equiv.), bis(triphenylphosphine)palladium(II) dichloride ($Pd(PPh_3)_2Cl_2$, 0.04 g, 0.05 mmol, 0.02 equiv.) and copper iodide (CuI, 0.01 g, 0.05 mmol, 0.02 equiv.) were dissolved in dry THF (30 mL). Next triethylamine (Et_3N, 15 mL) and 4-ethynylaniline (0.31 g, 2.66 mmol, 1 equiv.) were added and the mixture was stirred for three hours. After removing the solvent, the crude product was chromatographed on silica gel (70-230 mesh) with hexane/ethyl acetate (80:20) as eluent obtaining, after solvent removal, a pale-yellow solid (0.65 g, 84% of yield).

^{1}H NMR (300 MHz, $CDCl_3$) δ_H (ppm): 7.42 (s, 4H), 7.33 (d, 2H), 6.62 (d, 2H), 3.84 (s, 2H), 0.27 (s, 9H).

^{13}C NMR (75 MHz, $CDCl_3$) δ_C (ppm): 146.9, 133.0, 131.8, 131.1, 124.1, 122.1, 114.7, 112.2, 104.9, 95.9, 92.3, 87.1, 0.0.

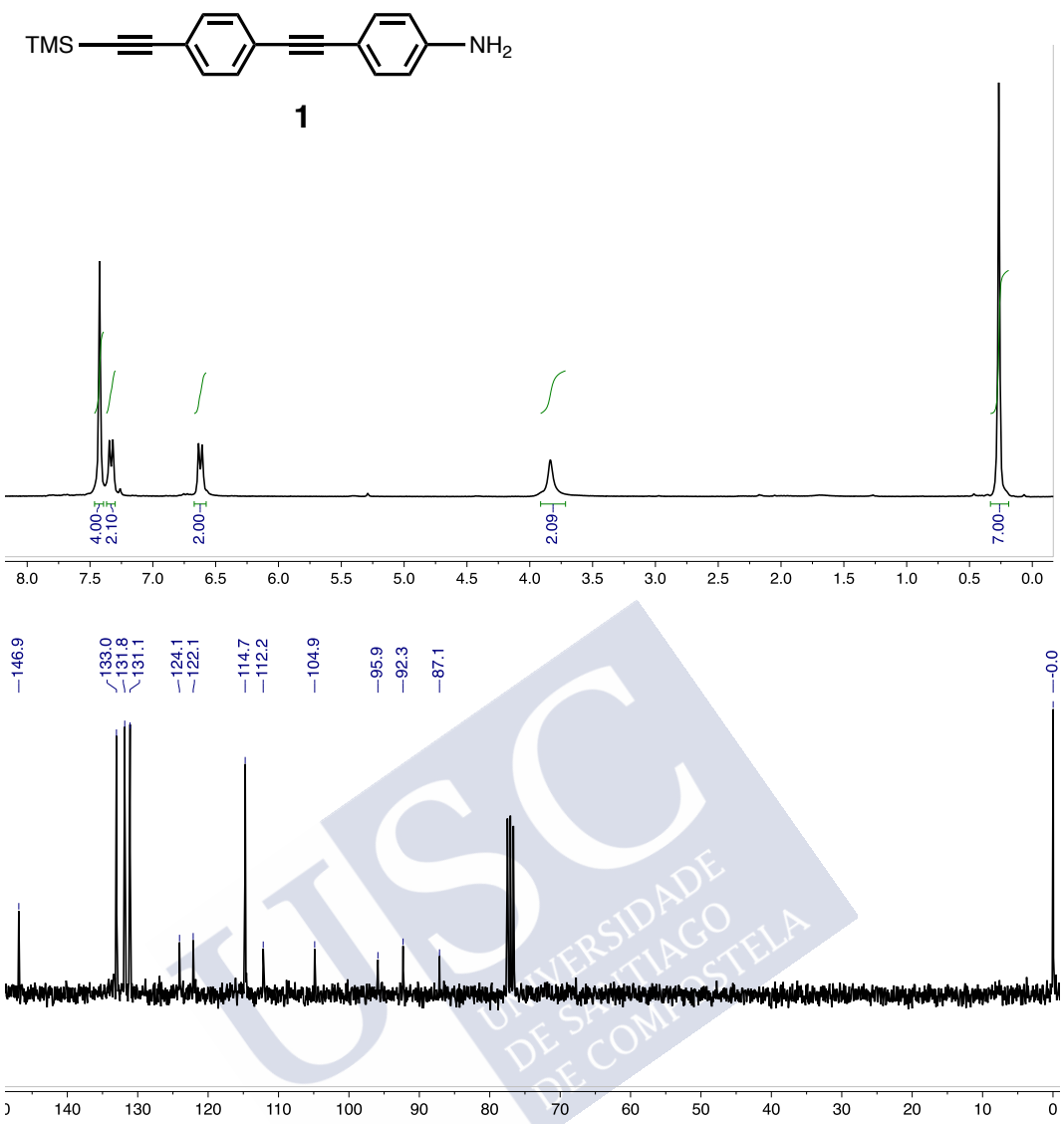

Figure S1. ^{1}H-NMR and ^{13}C-NMR of **1** in $CDCl_3$.

Synthesis of 4-((4-ethynylphenyl)ethynyl)aniline (**2**)

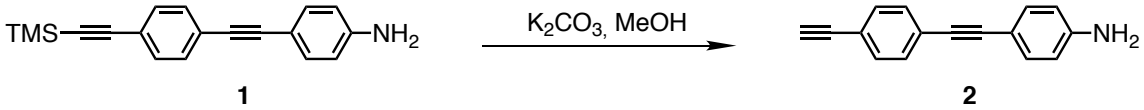

1 **2**

Once obtained the 4-((4-((trimethylsilyl)ethynyl)phenyl)ethynyl)aniline (**1**, 0.65 g, 2.24 mmol, 1.00 equiv.), it was dissolved in a mixture THF:MeOH (1:1) (10 mL) and potassium carbonate was added (K_2CO_3, 0.93 g, 931.10 mmol, 3.00 equiv.). After 15 minutes the organic layer was washed three times with water and dried over anhydrous $NaHCO_3$. The crude was chromatographed on silica gel (70-230 mesh) with hexane/ethyl acetate (70:30) as eluent (0.41 g, 70% of yield).

^{1}H NMR (300 MHz, $CHCl_3$) δ_H (ppm): 7.44 (s, 4H), 7.33 (d, 2H), 6.63 (d, 2H), 3.85 (s, 2H), 3.16 (s, 1 H).

^{13}C NMR (75 MHz, $CHCl_3$) δ_C (ppm): 146.9, 133.0, 132.0, 131.2, 124.5, 121.1, 114.7, 112.2, 92.3, 86.9, 83.5, 78.6.

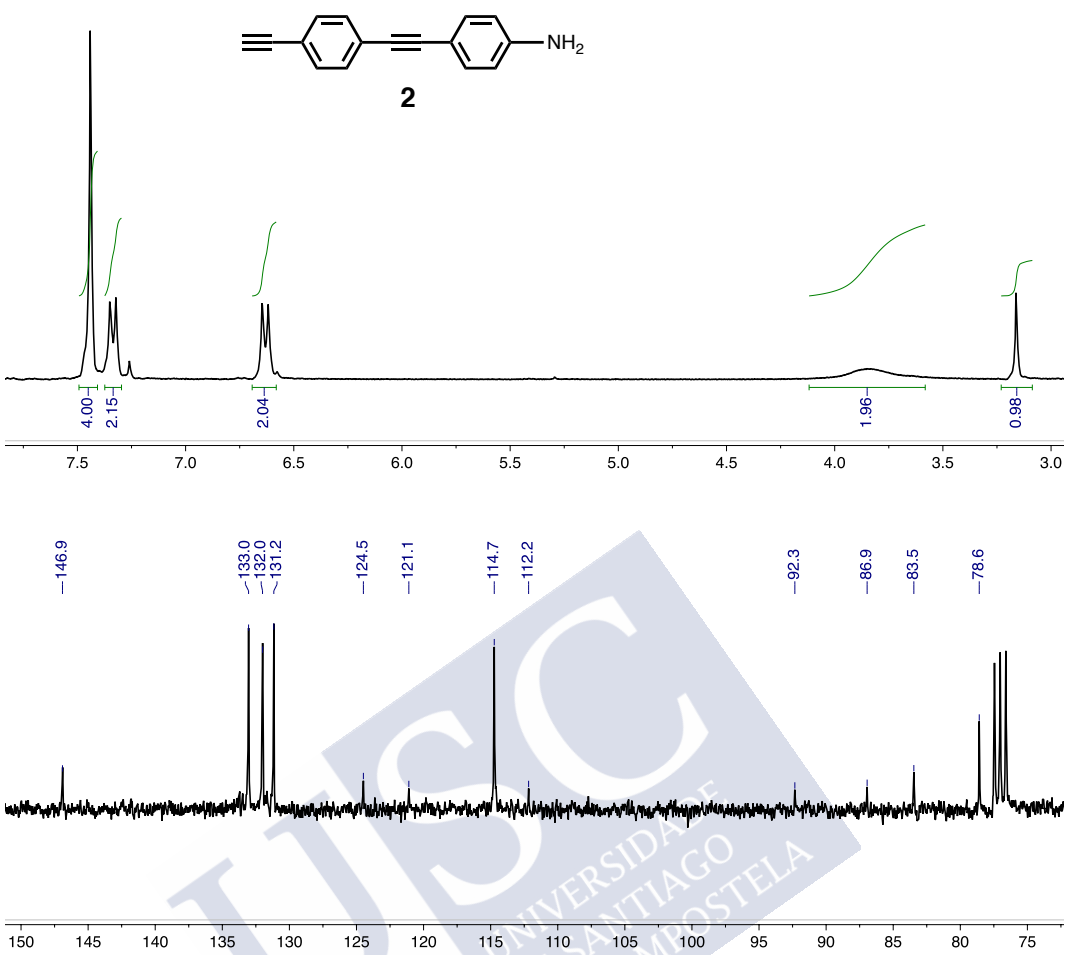

Figure S2. ^{1}H-NMR and ^{13}C-NMR of **2** in $CDCl_3$.

Synthesis of (*S*)- or (*R*)-*N*-(4-((4-ethynylphenyl)ethynyl)phenyl)-2-methoxy-2-phenylacetamide (m-(*S*)-**2** or m-(*R*)-**2**)

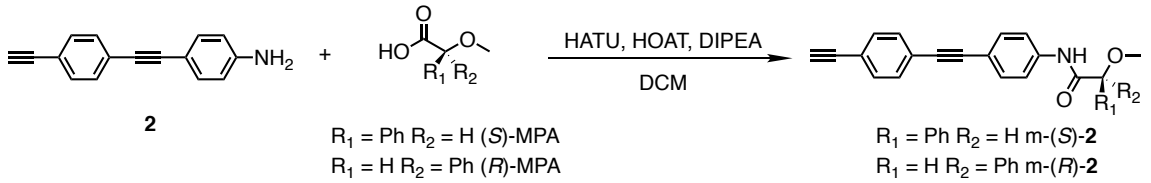

2

R_1 = Ph R_2 = H (*S*)-MPA
R_1 = H R_2 = Ph (*R*)-MPA

R_1 = Ph R_2 = H m-(*S*)-**2**
R_1 = H R_2 = Ph m-(*R*)-**2**

The corresponding (*S*) or (*R*)-α-methoxy-α-phenylacetic acid (0.28 g, 1.66 mmol, 1.20 equiv.), 2-(7-aza-1H-benzotriazole-1-yl)-1,1,3,3-tetramethyluronium (HATU, 0.63 g, 1.66 mmol, 1.20 equiv.), 1-hydroxy-7-azabenzotriazole (HOAT 0.23 g, 1.66 mmol, 1.20 equiv.) and diisopropyltriethylamine (DIPEA, 0.30 mL, 1.66 mmol, 1.20 equiv.) were dissolved in 20 mL of dry CH_2Cl_2. After 15 minutes, time needed to activate the acid, 4-((4-ethynylphenyl)ethynyl)aniline (0.30 g, 1.38 mmol, 1.00 equiv.) was added and the mixture was stirred overnight. The organic layer was washed three times with HCl 1M, a saturated solution of $NaHCO_3$ and brine. The combined organic layers were dried over anhydrous Na_2SO_4, filtered and evaporated at reduced pressure. The crude product was chromatographed on silica gel (70-230 mesh) with hexane/ethyl acetate (80:20) as eluent (0.60 g, 93% of yield).

^{1}H NMR (300 MHz, $CDCl_3$) δ_H (ppm): 8.65 (s, 1H), 7.62 (d, 2H), 7.55-7.43 (m, 8H), 7.39 (d, 3H), 4.75 (s, 1H), 3.45 (s, 3H), 3.18 (s, 1H).

^{13}C NMR (75 MHz, $CDCl_3$) δ_C (ppm): 168.6, 137.6, 136.4, 132.5, 132.1, 131.4, 128.7, 127.1, 123.8, 121.7, 119.4, 118.7, 91.2, 88.6, 83.3, 83.3, 78.9, 57.4.

HRMS (ESI) m/z calcd for $C_{25}H_{19}NO_2Na$ $[M+Na]^+$: 388.1308, found: 388.1308.

For m-(*S*)-**2**, α_D^{20} = +5.59 (c = 5 mg mL^{-1}, DCM)
For m-(*R*)-**2**, α_D^{20} = -4.94 (c = 5 mg mL^{-1}, DCM)

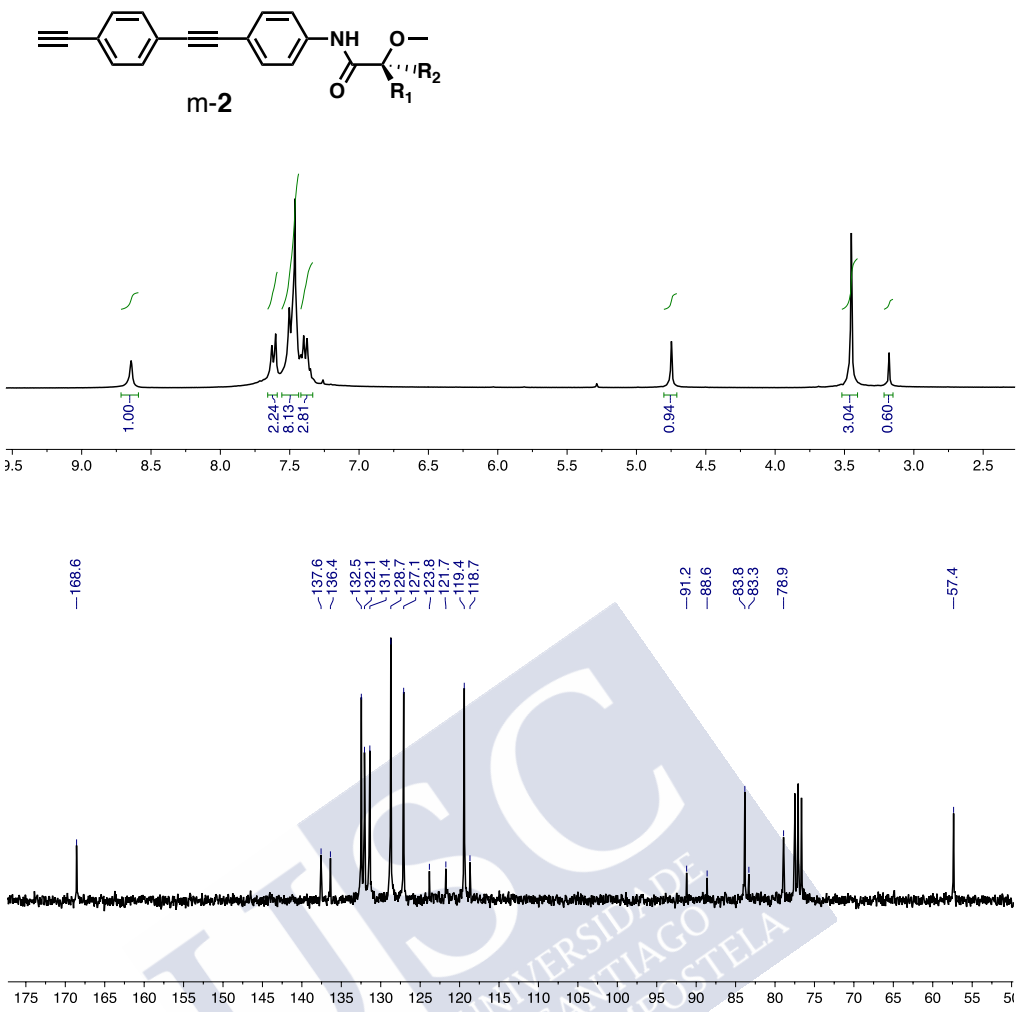

Figure S3. ^{1}H-NMR and ^{13}C-NMR of m-**2** in $CDCl_3$.

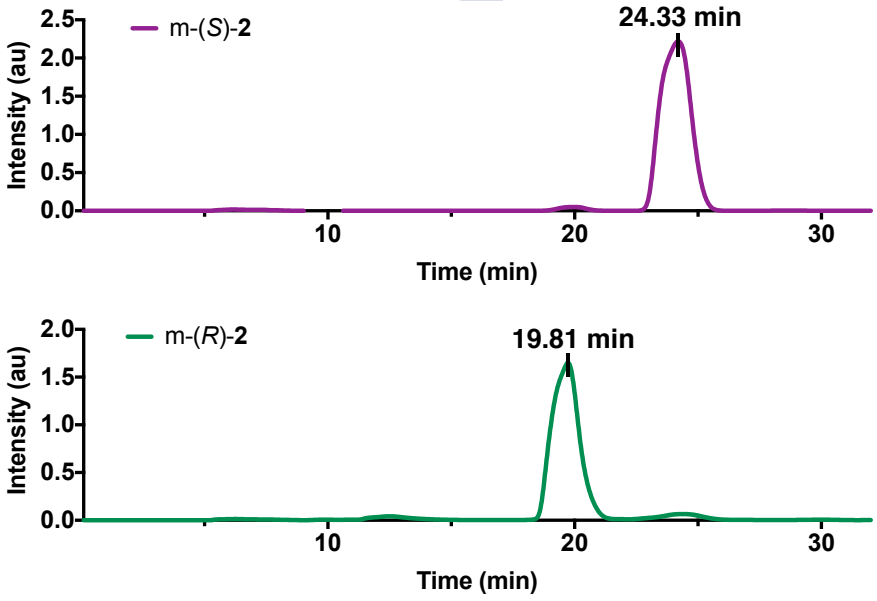

Figure S4. Chiral HPLC traces for m-(*S*)-**2** and m-(*R*)-**2** respectively.

Synthesis of (*S*)- or (*R*)-2-methoxy-2-phenyl-*N*-(4-((4-((4-((trimethylsilyl)ethynyl)phenyl)ethynyl)phenyl)ethynyl)phenyl)acetamide ((*S*)-**3** or (*R*)-**3**)

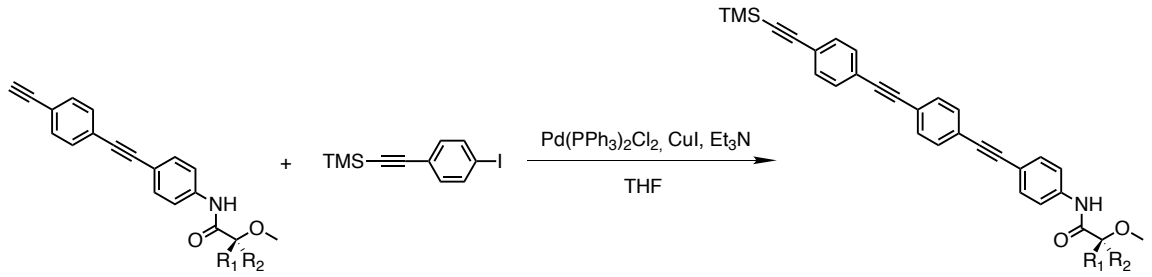

R_1=Ph R_2=H m-(*S*)-**2**
R_1=H R_2=Ph m-(*R*)-**2**

R_1=Ph R_2=H (*S*)-**3**
R_1=H R_2=Ph (*R*)-**3**

((4-iodophenyl)ethynyl)trimethylsilane (0.41 g, 1.36 mmol, 1.00 equiv.), bis(triphenylphosphine)palladium(II) dichloride ($Pd(PPh_3)_2Cl_2$, 0.02 g, 0.03 mmol, 0.02 equiv.) and copper iodide (CuI, 0.01 g, 0.03 mmol, 0.02 equiv.) were dissolved in dry THF (20 mL). Next triethylamine (Et_3N, 5 mL) and the corresponding (*S*)- or (*R*)-*N*-(4-((4-ethynylphenyl)ethynyl)phenyl)-2-methoxy-2-phenylacetamide (m-(*S*)-**2** or m-(*R*)-**2**, 0.50 g, 1.36 mmol, 1.00 equiv.) were added and the mixture was stirred at r.t. for three hours. After removing the solvent, the crude product was chromatographed on silica gel (70-230 mesh) with hexane/ethyl acetate (80:20) as eluent (0.42 g, 65% of yield).

^{1}H NMR (300 MHz, $CDCl_3$) δ_H (ppm): 8.64 (s, 1H), 7.62 (d, 2H), 7.54-7.44 (m, 12H), 7.40 (d, 3H), 4.75 (s, 1H), 3.45 (s, 3H), 0.27 (s, 9H).

^{13}C NMR (75 MHz, $CDCl_3$) δ_C (ppm): 168.5, 137.5, 136.4, 134.8, 132.4, 131.9, 131.5, 131.5, 131.4, 128.7, 127.1, 123.4, 123.1, 122.7, 119.4, 118.7, 104.6, 96.4, 91.3, 91.1, 90.9, 88.8, 83.8, 57.3, 0.0.

HRMS (ESI) m/z calcd for $C_{36}H_{32}NO_2Si$ $[M+H]^+$: 538.2124, found: 538.1308.

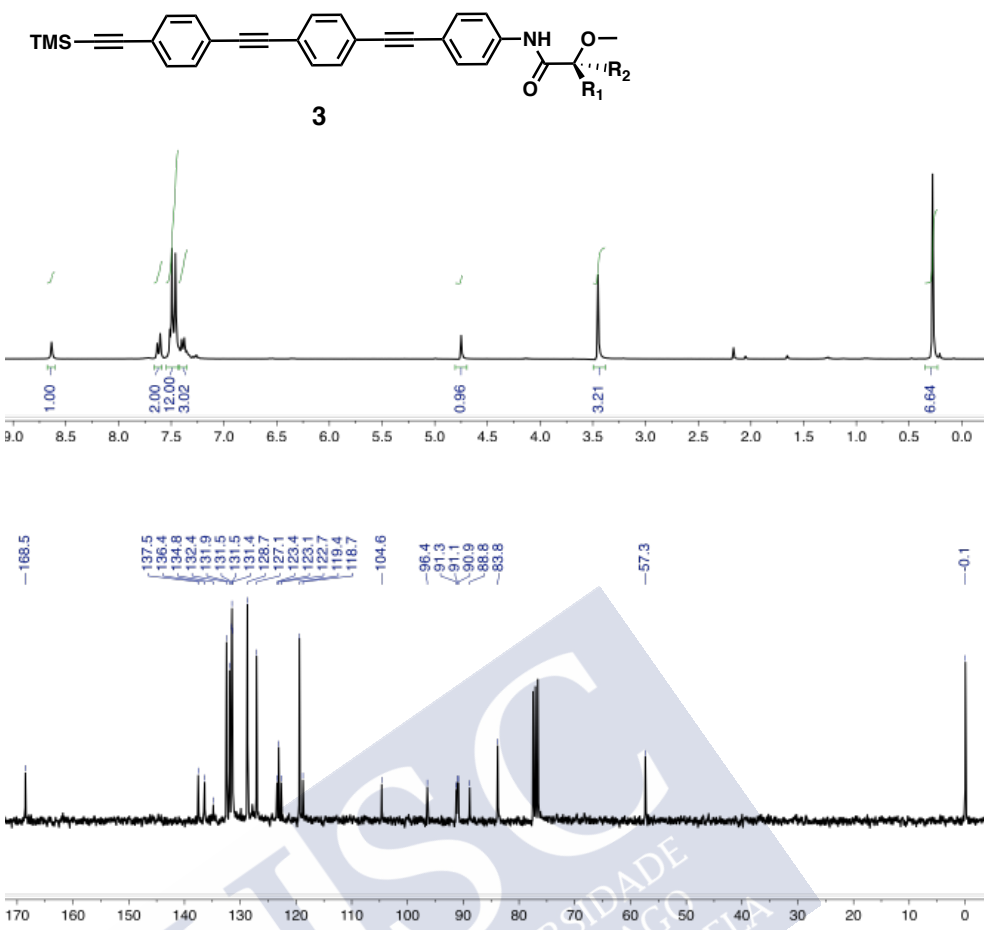

Figure S5. ^{1}H-NMR and ^{13}C-NMR of **3** in $CDCl_3$.

Synthesis of (*S*)- or (*R*)-*N*-(4-((4-((4-ethynylphenyl)ethynyl)phenyl)ethynyl)phenyl)-2-methoxy-2-phenylacetamide (m-(*S*)-**3** or m-(*R*)-**3**)

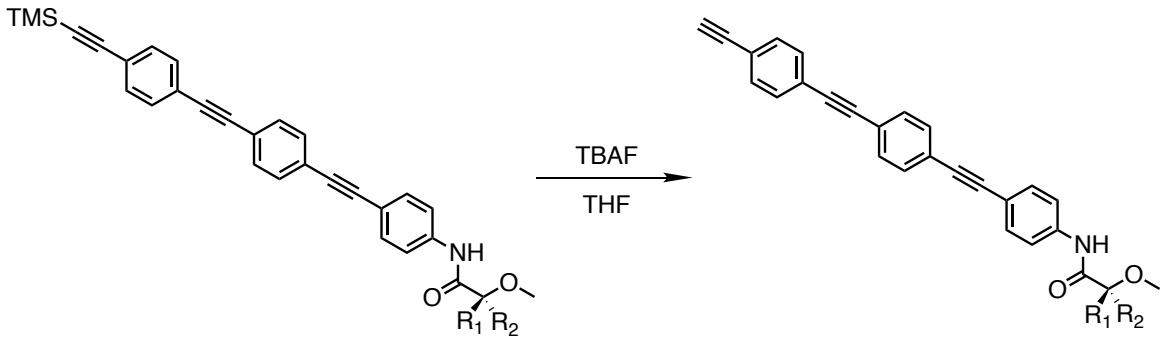

R_1=Ph R_2=H (*S*)-**3**
R_1=H R_2=Ph (*R*)-**3**

R_1=Ph R_2=H m-(*S*)-**3**
R_1=H R_2=Ph m-(*R*)-**3**

The corresponding (*S*)- or (*R*)-2-methoxy-2-phenyl-*N*-(4-((4-((4-((trimethylsilyl)ethynyl)phenyl)ethynyl)phenyl)ethynyl)phenyl)acetamide ((*S*)-**3** or (*R*)-**3**, 0.42 g, 0.74 mmol, 1.00 equiv.) was dissolved in THF (10 mL). Next TBAF was added (1M in hexane, 0.89 mL, 0.89 mmol, 1.20 equiv.) and the reaction was stirred at r.t. for 15 minutes. The crude was chromatographed on silica gel (70-230 mesh) with hexane/ethyl acetate (70:30) as eluent (0.45 g, 88% of yield).

^{1}H NMR (300 MHz, $CDCl_3$) δ_H (ppm): 8.62 (s, 1H), 7.60 (d, 2H), 7.53-7.34 (m, 15H), 4.75 (s, 1H), 3.47 (s, 3H), 3.18 (s, 1H).

^{13}C NMR (75 MHz, $CDCl_3$) δ_C (ppm): 168.5, 140.0, 137.5, 136.3, 132.4, 132.1, 131.5, 131.5, 128.7, 127.0, 123.5, 123.5, 122.6, 122.0, 119.4, 118.7, 100.3, 91.2, 91.1, 90.6, 88.8, 83.8, 83.2, 79.0, 57.4.

HRMS (ESI) m/z calcd for $C_{33}H_{24}NO_2$ $[M+H]^+$: 466.1829, found: 466.1802.

For m-(*S*)-**3**, α_D^{20} = +17.80 (c = 5 mg mL^{-1}, DCM)
For m-(*R*)-**3**, α_D^{20} = -15.14 (c = 5 mg mL^{-1}, DCM)

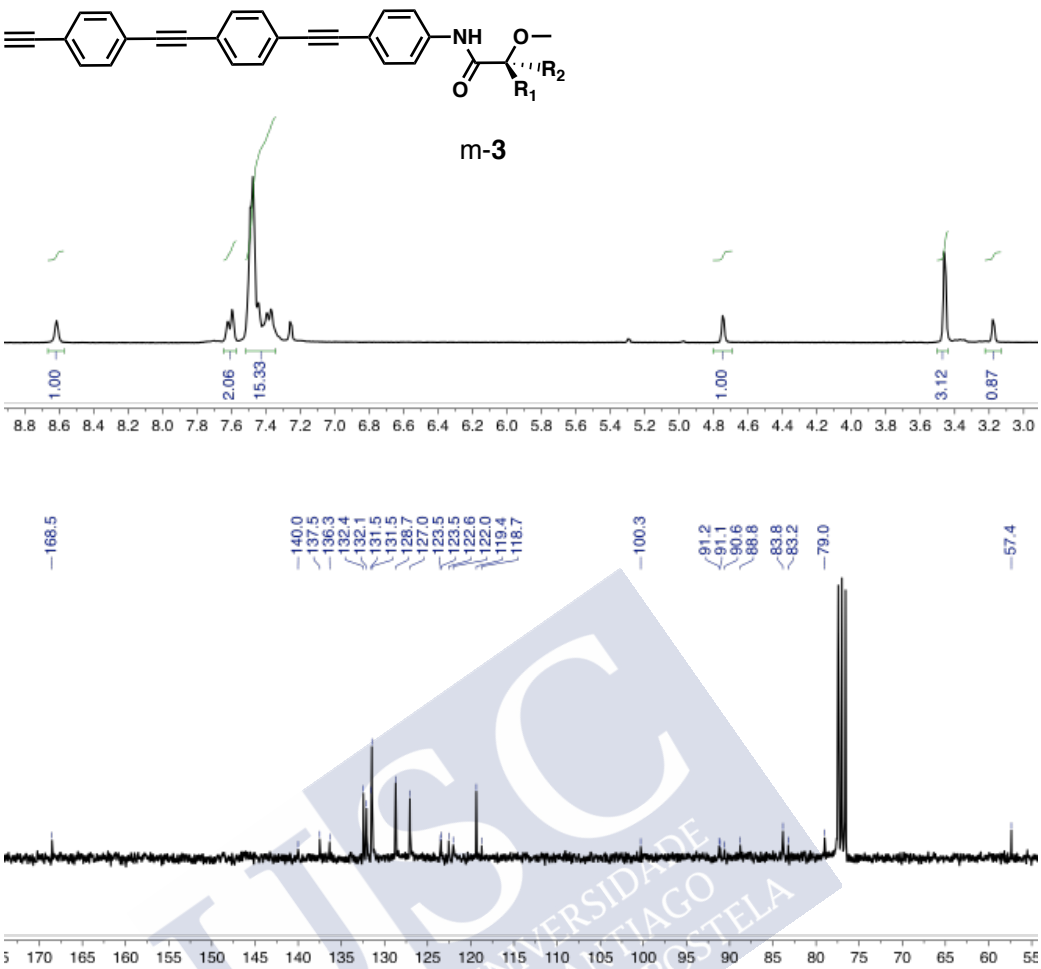

Figure S6. ^{1}H-NMR and ^{13}C-NMR of m-**3** in $CDCl_3$.

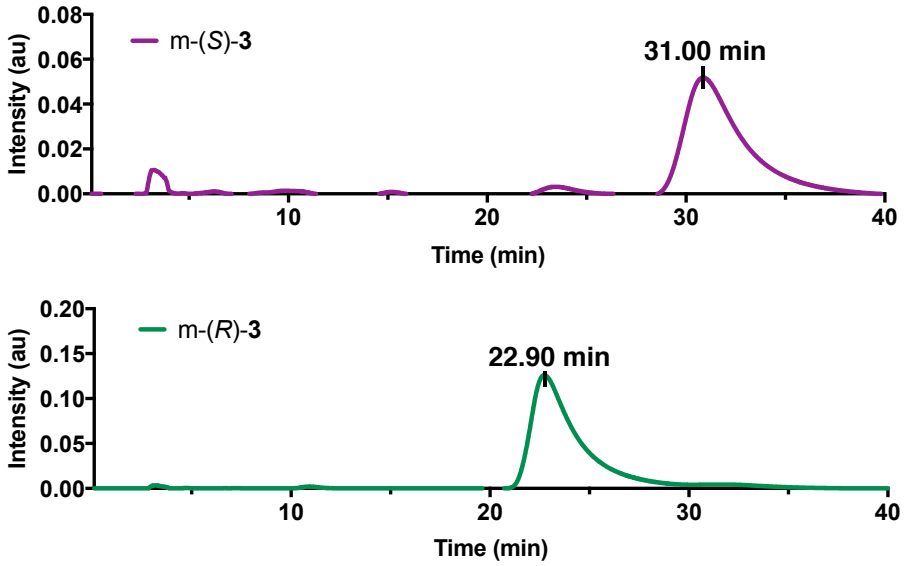

Figure S7. Chiral HPLC traces for m-(*S*)-**2** and m-(*R*)-**2** respectively.

3. Crystallographic Data

A summary of the crystallographic results is given bellow: Crystals of m-(*R*)-**2** and m-(*S*)-**3** for X-ray analysis were grown by slow evaporation from a 2:8 mixture of DCM/Hexane. A crystal was selected and mounted on a MiTeGen loop under oil and flash frozen at 100 K under a cold N_2 gas stream. X-ray diffraction data were collected on a Bruker X8 kappa APEX II CCD diffractometer.

Data collection: Bruker APEX2 software, [SAINT (version 8.34A), SADABS (version 2014/5), BrukerAXS Inc, Madison, Wisconsin, USA.)]; cell refinement: SAINT V8.34A integration software; absorption correction: SADABS2014/5 (Bruker (2014) APEX2 (Version 2014.11-0); data reduction: SORTAV3; program(s) used to solve structure: SHELXD2013/24 ; program used to refine structure: SHELXL2014/75 ; molecular graphics: ORTEP-3 for Windows 6 ; software used to prepare material for publication: WinGX publication routines.

Crystal data for m-(*R*)-**2**

Crystal data

$C_{25}H_{19}NO_2$
$M_r = 365.41$
Orthorhombic, $P2_12_12_1$
$a = 5.2753$ (2) Å
$b = 8.2287$ (2) Å
$c = 45.0822$ (11) Å
$V = 1956.97$ (10) Å^3
$Z = 4$
$F(000) = 768$

$D_x = 1.24$ Mg m^{-3}
Mo $K\alpha$ radiation, $\lambda = 0.71073$ Å
Cell parameters from 7950 reflections
$\theta = 2.5$–$27.0°$
$\mu = 0.08$ mm^{-1}
$T = 100$ K
Needle, colourless
0.52 × 0.09 × 0.05 mm

Data collection

Bruker APEX-II diffractometer
Radiation source: sealed x-ray tube
Graphite monochromator
φ or ω oscillation scans
Absorption correction: multi-scan
SADABS2014/5 - Bruker AXS area detector scaling and absorption correction
$T_{min} = 0.905$, $T_{max} = 0.991$

28768 measured reflections
4486 independent reflections
3752 reflections with $I > 2\sigma(I)$
$R_{int} = 0.041$
$\theta_{max} = 27.5°$, $\theta_{min} = 1.8°$
$h = -6 \rightarrow 6$
$k = -10 \rightarrow 10$
$l = -57 \rightarrow 58$

Refinement

Refinement on F^2
Least-squares matrix: full
$R[F^2 > 2\sigma(F^2)] = 0.041$
$wR(F^2) = 0.086$
$S = 1.04$
4486 reflections
258 parameters
0 restraints
0 constraints
Primary atom site location: other
Secondary atom site location: difference Fourier map
Hydrogen site location: mixed

H atoms treated by a mixture of independent and constrained refinement
$w = 1/[\sigma^2(F_o^2) + (0.0379P)^2 + 0.3837P]$ where $P = (F_o^2 + 2F_c^2)/3$
$(\Delta/\sigma)_{max} < 0.001$
$\Delta\rho_{max} = 0.19$ e Å^{-3}
$\Delta\rho_{min} = -0.20$ e Å^{-3}
Absolute structure: Flack x determined using 1346 quotients [(I+)-(I-)]/[(I+)+(I-)] (Parsons, Flack and Wagner, Acta Cryst. B69 (2013) 249-259).
Absolute structure parameter: −0.2 (5)

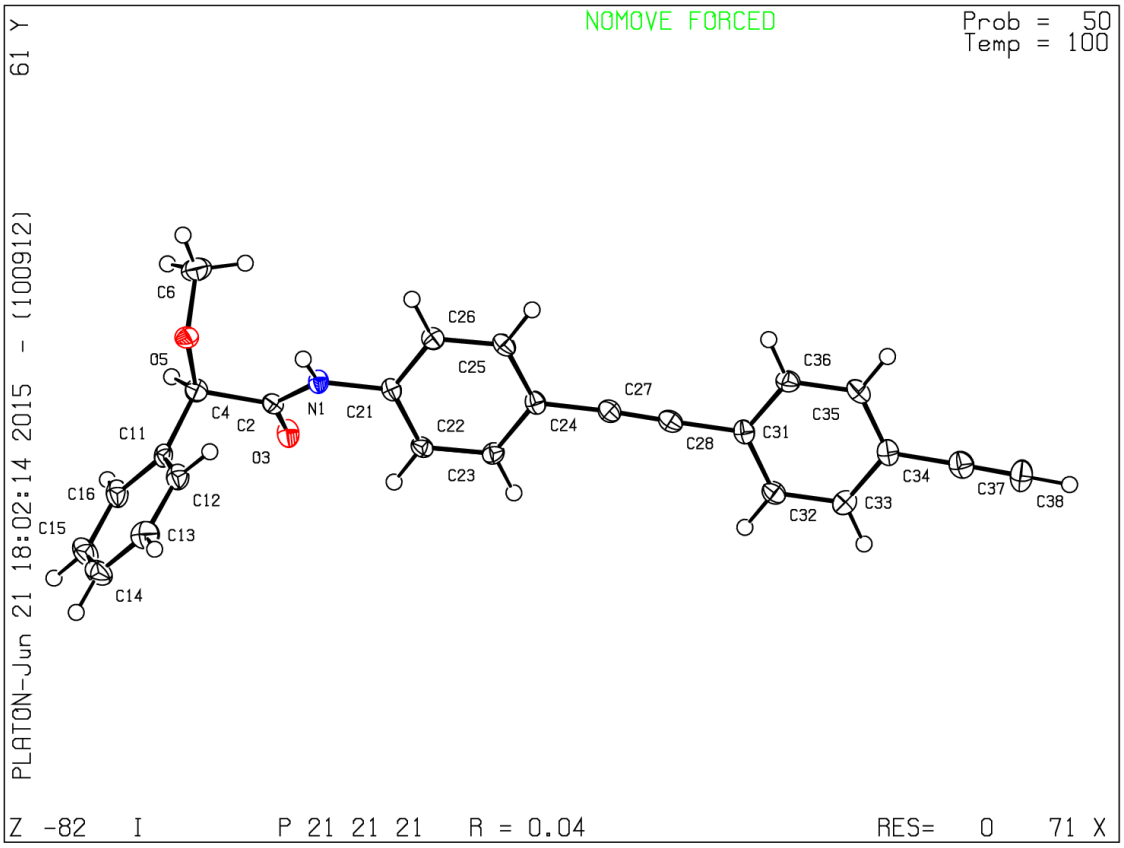

Figure S8. Crystal data and ORTEP view of the asymmetric unit content for m-(*R*)-**2**

Crystal data for m-(*S*)-**3**

Crystal data

$C_{33}H_{23}NO_2$
$M_r = 465.52$
Orthorhombic, $P2_12_12_1$
Hall symbol: P 2ac 2ab
$a = 5.3349\ (2)$ Å
$b = 8.0996\ (4)$ Å
$c = 58.179\ (2)$ Å
$V = 2513.94\ (18)$ Å^3
$Z = 4$

$F(000) = 976$
$D_x = 1.23$ Mg m^{-3}
Cu $K\alpha$ radiation, $\lambda = 1.54184$ Å
Cell parameters from 1556 reflections
$\theta = 3.0–74.1°$
$\mu = 0.60$ mm^{-1}
$T = 100$ K
Plate, colourless
0.09 × 0.08 × 0.02 mm

Data collection

Bruker D8 VENTURE PHOTON III-14 diffractometer
Radiation source: INCOATEC microfocus sealed tube, Incoatec IμS 3.0
Incoatec multilayer mirror monochromator
Detector resolution: 7.3910 pixels mm^{-1}
ω and phi scans
Absorption correction: multi-scan BRUKER *SADABS2016/2*

$T_{min} = 0.798$, $T_{max} = 0.971$
22404 measured reflections
5141 independent reflections
2954 reflections with $I > 2\sigma(I)$
$R_{int} = 0.138$
$\theta_{max} = 74.8°$, $\theta_{min} = 3.0°$
$h = -6\rightarrow4$
$k = -10\rightarrow10$
$l = -72\rightarrow70$

Refinement

Refinement on F^2
Least-squares matrix: full
$R[F^2 > 2\sigma(F^2)] = 0.076$
$wR(F^2) = 0.205$
$S = 1.00$
5141 reflections
334 parameters
0 restraints
0 constraints
Primary atom site location: dual
Secondary atom site location: dual
Hydrogen site location: mixed

H atoms treated by a mixture of independent and constrained refinement
$w = 1/[\sigma^2(F_o^2) + (0.092P)^2]$ where $P = (F_o^2 + 2F_c^2)/3$
$(\Delta/\sigma)_{max} < 0.001$
$\Delta\rho_{max} = 0.31$ e Å^{-3}
$\Delta\rho_{min} = -0.29$ e Å^{-3}
Absolute structure: Flack x determined using 792 quotients [(I+)-(I-)]/[(I+)+(I-)] (Parsons, Flack and Wagner, Acta Cryst. B69 (2013) 249-259).
Absolute structure parameter: 0.0 (6)

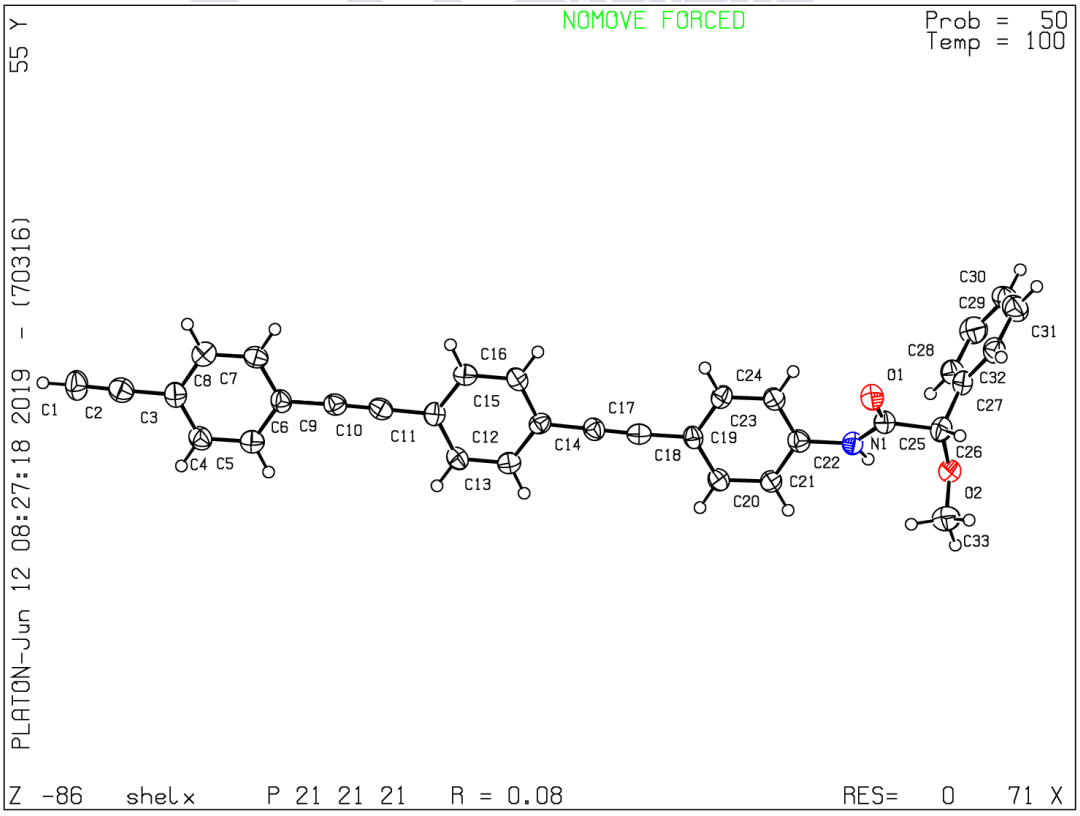

Figure S9. Crystal data and ORTEP view of the asymmetric unit content for m-(*S*)-**3**

4. Theoretical Calculations for Monomers

TD-DFT(CAM-B3LYP) calculations were performed, using the 3-21G basis set, for m-(*R*)-**2** and m-(*S*)-**3**. The data obtained are in good agreement with the experimental information obtained for the aforementioned monomers. This confirms the *ap* conformation adopted by the pendant.

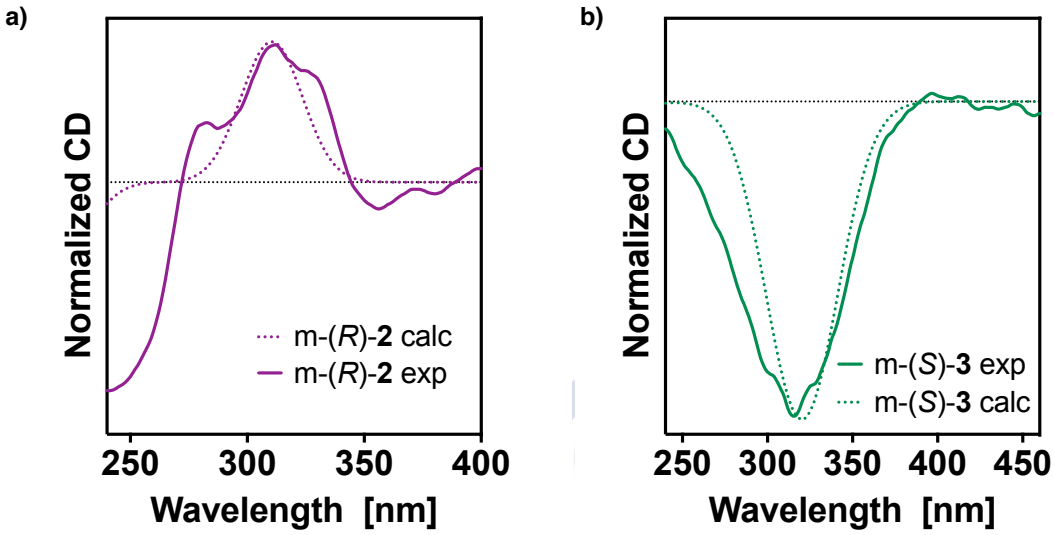

Figure S10. Comparison of the calculated and experimental CD spectra obtained for (a) m-(*R*)-**2** and (b) m-(*S*)-**3** (Full Width at Half-Maximum (FWHM) equals 20 nm).

5. Synthesis of Polymers

5.1. General Procedure for Polymerization

The polymers were synthesized in a flask (sealed ampoule) previously dried under vacuum and flushed with Ar for three times. The monomers were added as a solid and dissolved in dry THF. Next a solution of rhodium norbornadiene chloride dimer $[Rh(nbd)Cl]_2$ was added and the mixture was stirred overnight at 20 °C. The resulting polymers were diluted in CH_2Cl_2 and precipitated in a large amount of MeOH, centrifuged and reprecipitated in hexane and centrifuged again.

Table S1. Calculated amounts for the synthesis of the polymers.

Monomer	Mass (mg)	THF (mL)	Et_3N (mL)	Catalyst (mg)	Yield (%)
m-(*S*)-**2**	50	400	5	0.6	70
m-(*R*)-**2**	50	400	5	0.6	80
m-(*S*)-**3**	50	500	5	0.5	72
m-(*R*)-**3**	50	500	5	0.5	77

5.2. Low Temperature Polymerization

The general procedure was followed. Before the addition of the catalyst the corresponding monomer solution was cooled to 0 ºC. The polymerization was allowed to reach to room temperature and it was stirred overnight.

5.3. NMR and Raman Experiments

The *cis* configuration of the polyenic backbone was determined by ^{1}H NMR spectroscopy (vinylic protons resonate at δ = 5.7-5.8 ppm). The bands observed by Raman resonance confirmed the former configuration. The peak at highest wavelength corresponds to the C=C bond stretching and overlaps with that of the phenyl ring. The band at 1350-1340 cm^{-1} arises from the *cis* C-C bond coupled with the single bond connecting the main chain and the phenyl ring. The peak at lowest wavelength corresponds to the C-H bond of the *cis* form. The disappearance of the alkyne peak (ca. 2110 cm^{-1}) also confirms the formation of the polymer.

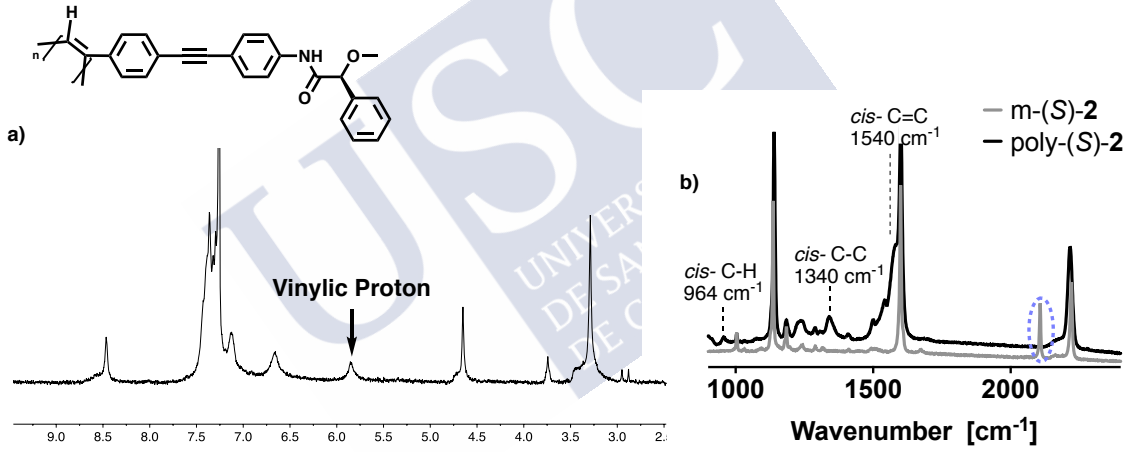

Figure S11. (a) ^{1}H-NMR for poly-**2** in $CDCl_3$ and (b) Raman spectra comparison.

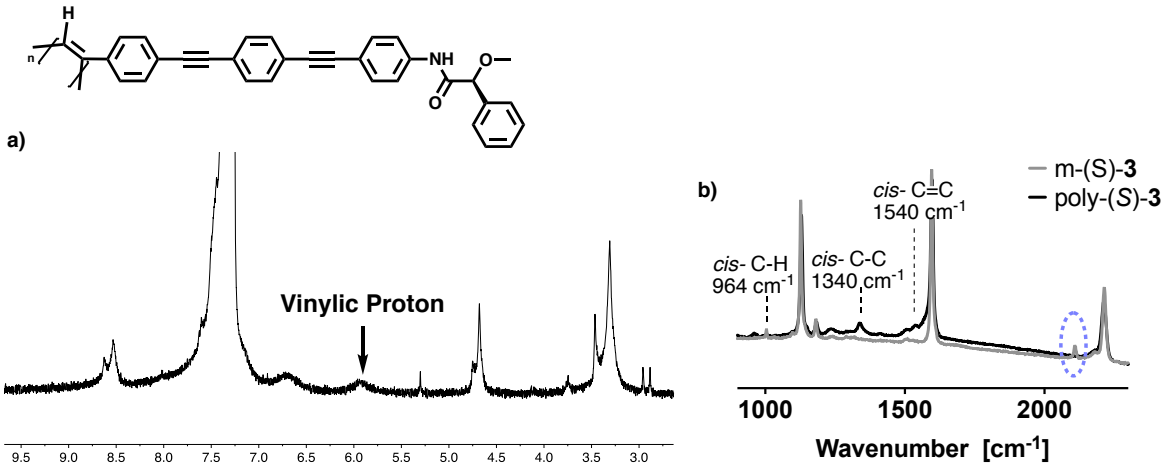

Figure S12. (a) ^{1}H-NMR for poly-**3** in $CDCl_3$ and (b) Raman spectra comparison.

6. GPC Studies

The molecular weight was estimated by GPC.

Table S2. GPC data for poly-**2**, poly-**3** and poly-**3** at 0 °C.

Polymer	Mn	Mw	Mz	PDI
Poly-**2**	22802	26941	33147	1.2
Poly-**3**	25383	67530	213386	2.7
Poly-**3** 0 °C	28286	60234	201811	2,1

7. Thermal Studies

7.1 DSC Studies

The geometry of the polymer was determined by DSC. As a general protocol, the polymer was placed in an aluminum pan up to 400 °C (heating rate: 10 °C·min^{-1}). The thermograms for poly-(*S*)-**2** and poly-(*S*)-**3** show a typical *c*-*c* trace with an exothermal peak, at 210 °C and 287 °C respectively, correspondent to a *t*-*t* transition. It is observed that the geometry of the polymer is kept despite the introduction of the spacer.

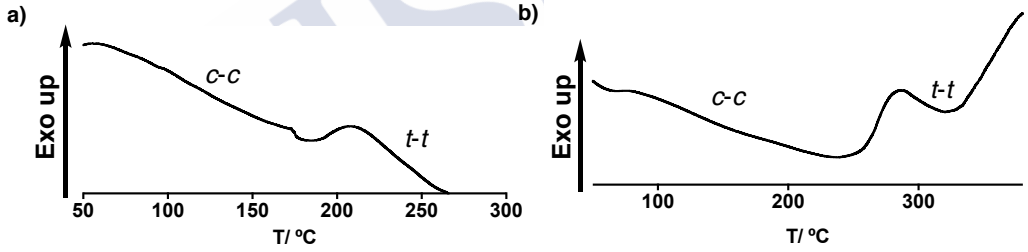

Figure S13. DSC studies for (a) poly-(*S*)-**2** and (b) poly-(*S*)-**3**.

7.2 TGA Studies

The thermal stability was evaluated by TGA. As a general protocol, the polymer sample was placed in a platinum pan and heated from 40°C to 800°C (heating rate: 10 °C min^{-1}). Poly-(*S*)-**2** starts to degrade at 300 °C while poly-(*S*)-**3** degradation initiates at 370 °C.

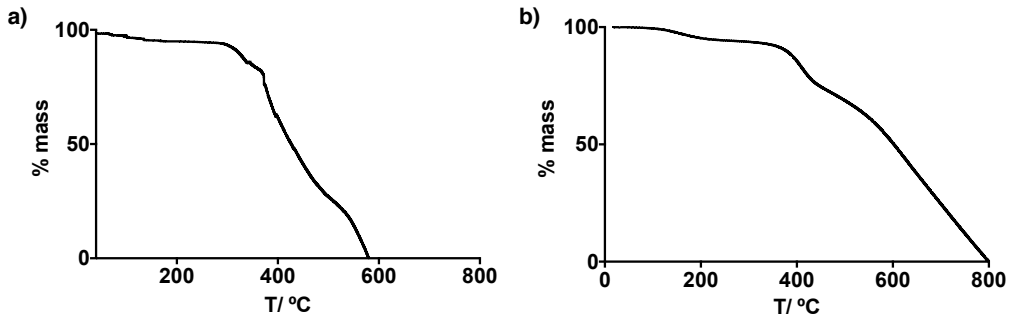

Figure S14. TGA thermograms (a) poly-(*S*)-**2** and (b) poly-(*S*)-**3**.

8. Conformational Studies

8.1 Solution Studies

Poly-(*S*)-**2** and poly-(*S*)-**3** (0.2 mg·mL^{-1}) were tested in different solvents. Poly-(*S*)-**2** shows a better folding in polar solvents, whereas poly-(*S*)-**3** exhibits almost the same CD intensity in all cases.

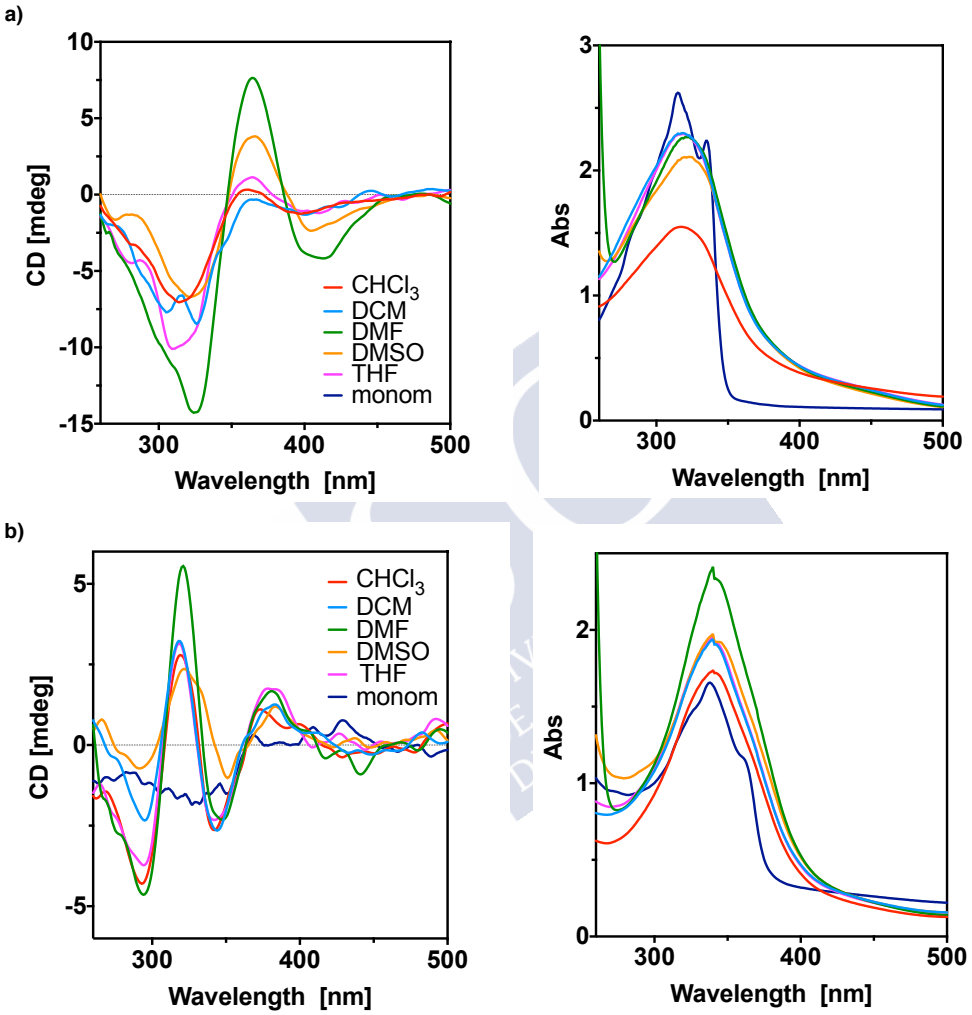

Figure S15. CD and UV-Vis spectra for (a) poly-(S)-**2** and (b) poly-(S)-**3** in different solvents.

8.2 Response to External Stimuli: Interaction with Metals

Both polymers were titrated with different divalent and monovalent perchlorates. Poly-(*S*)-**2** and poly-(*S*)-**3** were dissolved in $CHCl_3$ (0.1 mg·mL^{-1} and 0.2 mg·mL^{-1} respectively) and the correspondent metal salt solution (THF, 50 mg·mL^{-1}) was then added.

Poly-(*S*)-**2** shows a chiral enhancement for the case of Li^+, Ag^+, Na^+ (Figure S16a, b and c) and Ba^{2+} (Figure S17a). Interestingly for Ca^{2+}, a gradual inversion is observed in the monomeric region accompanied with a disappearance of the vinylic band (Figure S17b).

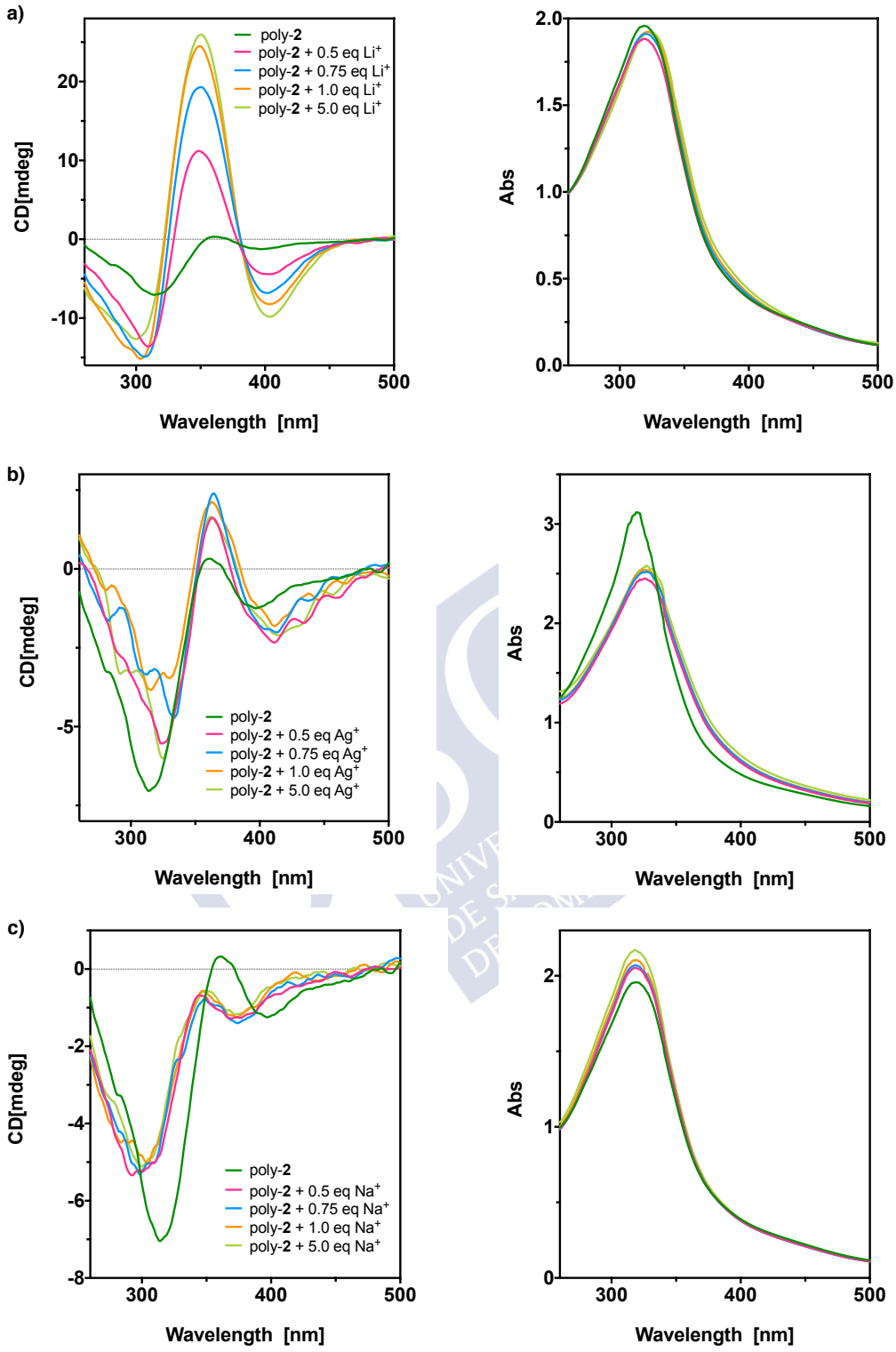

Figure S16. CD and UV-Vis spectra for poly-**2** ($CHCl_3$, 0.1 mg·mL^{-1}) titrated with different amounts of (a) $LiClO_4$, (b) $AgClO_4$ and (c) $NaClO_4$ (THF, 50 mg·mL^{-1}).

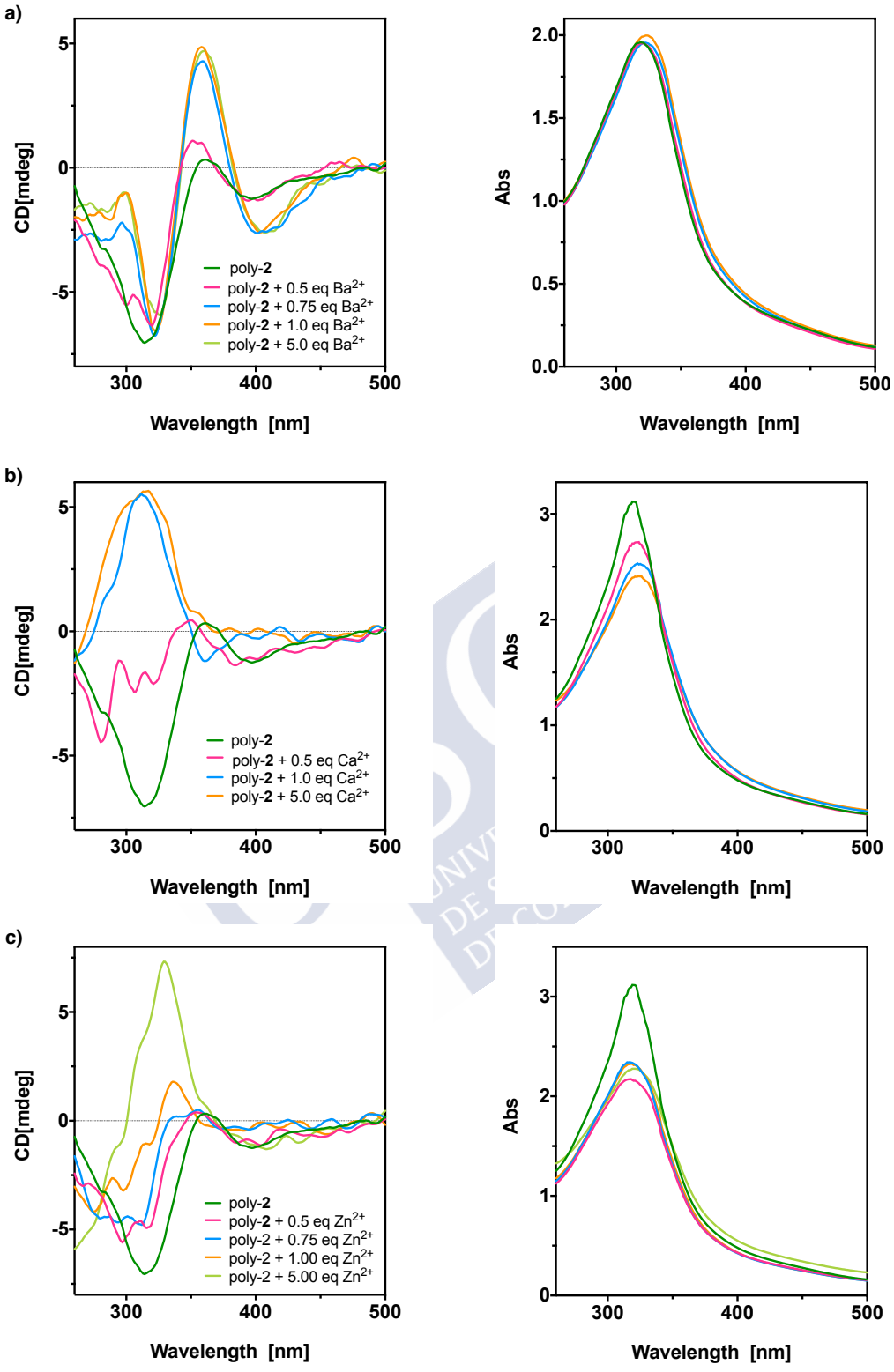

Figure S17. CD and UV-Vis spectra for poly-**2** ($CHCl_3$, 0.1 mg·mL^{-1}) titrated with different amounts of (a) $Ba(ClO_4)_2$ (b) $Ca(ClO_4)_2$ and (c) $Zn(ClO_4)_2$ (THF, 50 mg·mL^{-1}).

Similar experiments were performed for poly-**3**. Neither amplification of chirality nor inversion were observed.

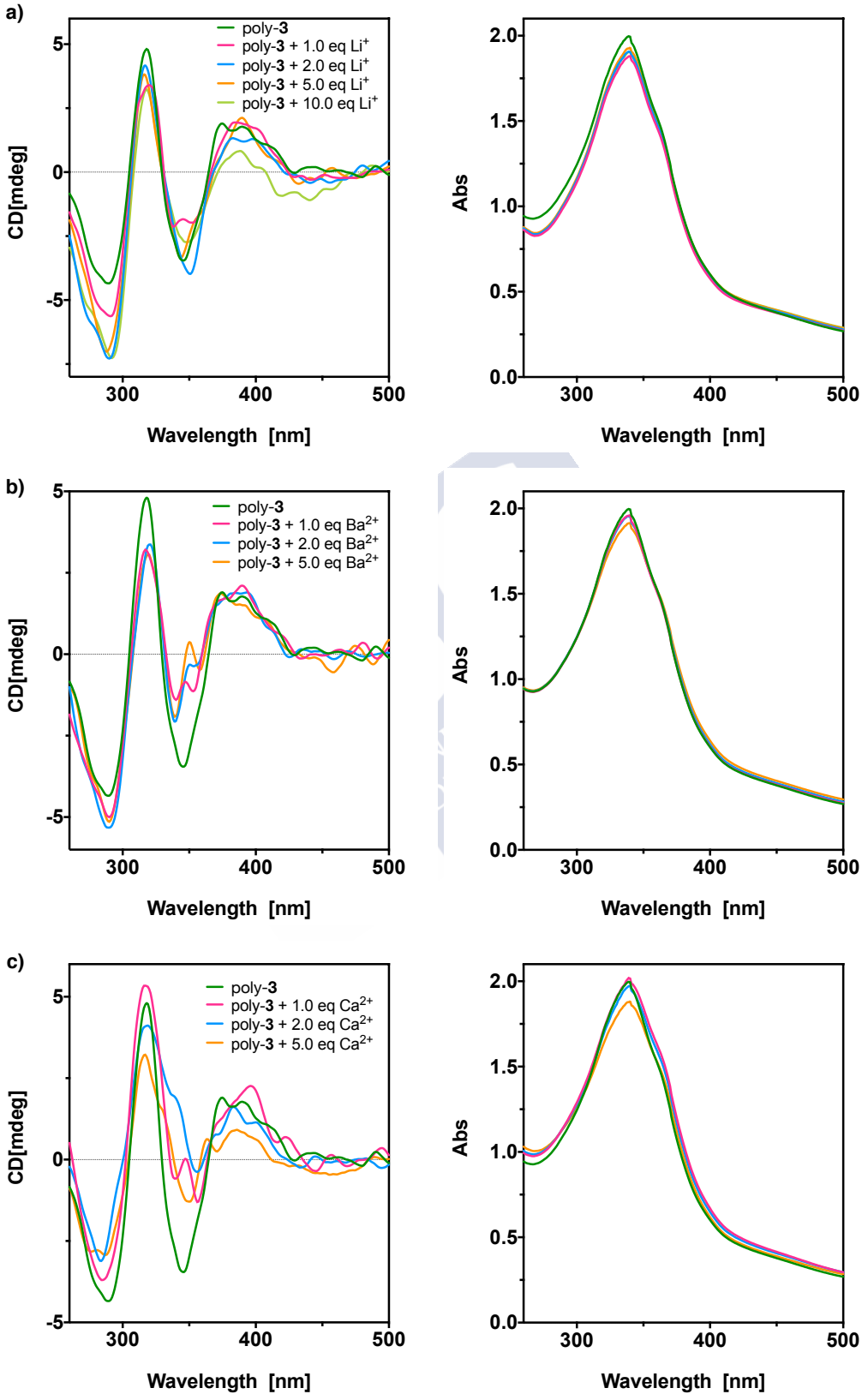

Figure S18. CD and UV-Vis spectra for poly-**3** ($CHCl_3$, 0.2 mg·mL^{-1}) titrated with different amounts of (a) $LiClO_4$ and (b) $BaClO_4$ and (c) $Ca(ClO_4)_2$ (THF, 50 mg·mL^{-1}).

9. ATR/FT-IR Studies

$M(ClO_4)_2$ or $MClO_4$ (THF, 50 mg·mL^{-1}) was added to a solution of poly-**2** ($CHCl_3$, 3 mg·mL^{-1}). The mixture was allowed to react for five minutes and analyzed by FT-IR.

In all cases, an increase of the degree of association is observed only for the carbonyl group —*ap* conformation—, except for Ca^{2+}, in which the degree of association is also increased in the methoxy group —*sp* conformation—. This is in full agreement with the CD studies.

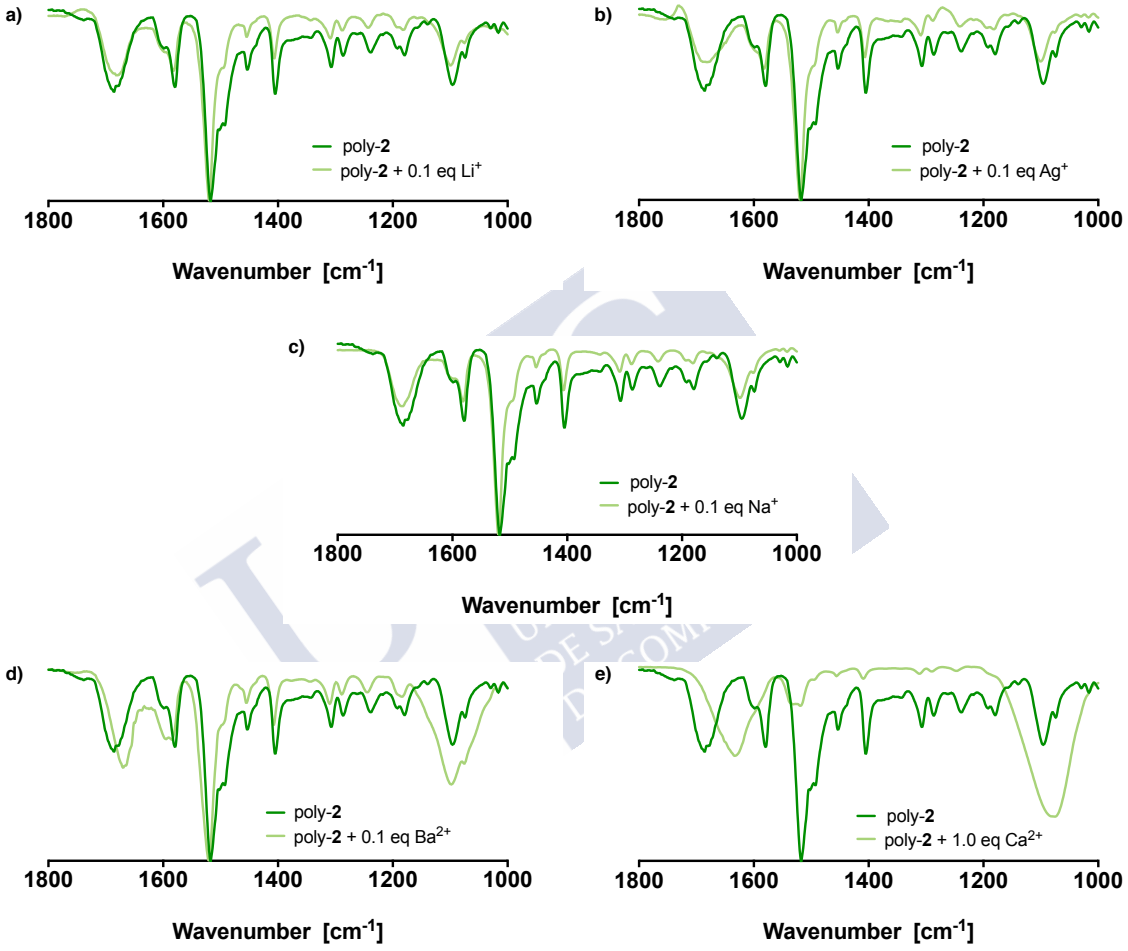

Figure S19. IR spectra of a solution of poly-**2** in $CHCl_3$ (3 mg·mL^{-1}) titrated with (a) $LiClO_4$ (THF, 50 mg·mL^{-1}), (b) $AgClO_4$ (THF, 50 mg·mL^{-1}), (c) $NaClO_4$ (THF, 50 mg·mL^{-1}), (d) $Ba(ClO_4)_2$ (THF, 50 mg·mL^{-1}) and (e) $Ca(ClO_4)_2$ (THF, 50 mg·mL^{-1}).

Table S3. FT-IR data of poly-**2** in solution.

	υ_{CO} (cm^{-1})	υ_{OMe} (cm^{-1})	$\Delta\upsilon_{CO}$ (cm^{-1})	$\Delta\upsilon_{OMe}$ (cm^{-1})
Poly-**2**	1685	1091	–	–
Poly-**2** + 0.1 eq Li^+	1675	1096	10	- 5
Poly-**2** + 0.1 eq Na^+	1679	1097	6	- 6
Poly-**2** + 0.1 eq Ag^+	1664	1094	21	- 3
Poly-**2** + 0.1 eq Ba^{2+}	1675	1096	10	- 5
Poly-**2** + 1.0 eq Ca^{2+}	1627	1070	58	-21

10. Cation-π Experiments

A solution of poly-**2** in $CDCl_3$ (3 mg·mL^{-1}) was titrated with 2.0 equivalents of $LiClO_4$ (10 mg·mL^{-1} in CD_3OD) and studied by ^7Li NMR spectroscopy. The shielding in the ^7Li chemical shift is indicative of a cation-π interaction, related to an *ap* conformation of the pendant group. This is in accordance with the information obtained from the CD and FT-IR experiments.

11. Low Temperature Polymerization

It was observed that when m-(*S*)-**3** is polymerized at low temperature, the resulting polymer presents a helical enhancement when compared to the polymer obtained at 20 °C. At 0 °C, the polymerization mechanism takes place at a lower rate, allowing the preorganization of the monomer and resulting in a better-folded polymer.

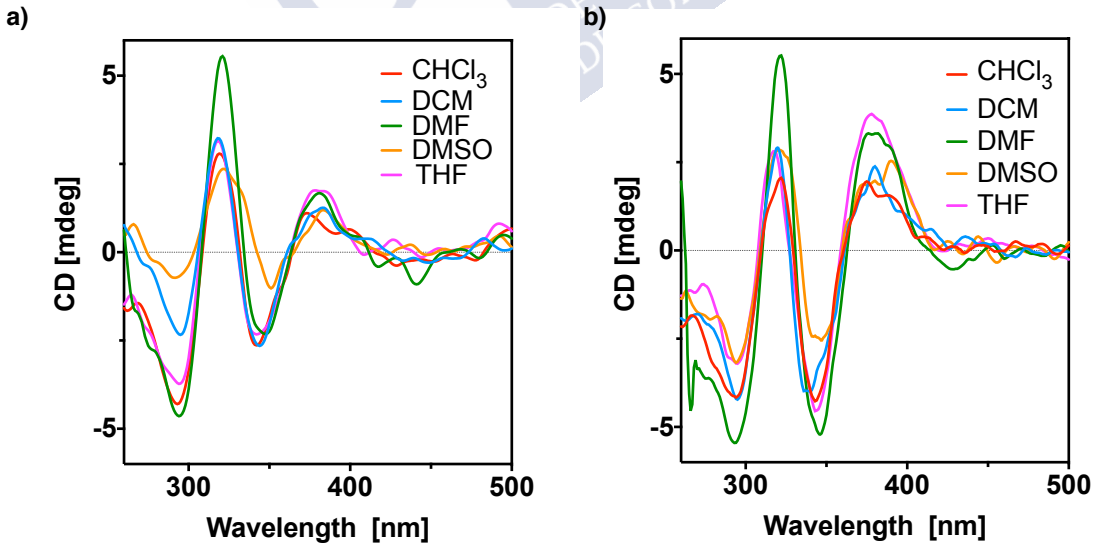

Figure S20. CD trace for poly-(*S*)-**3** in different solvents polymerized at (a) 25 °C and (b) 0 °C.

In order to get a better comparison between the CD traces, the data was normalized and the spectra was represented into the molar value.

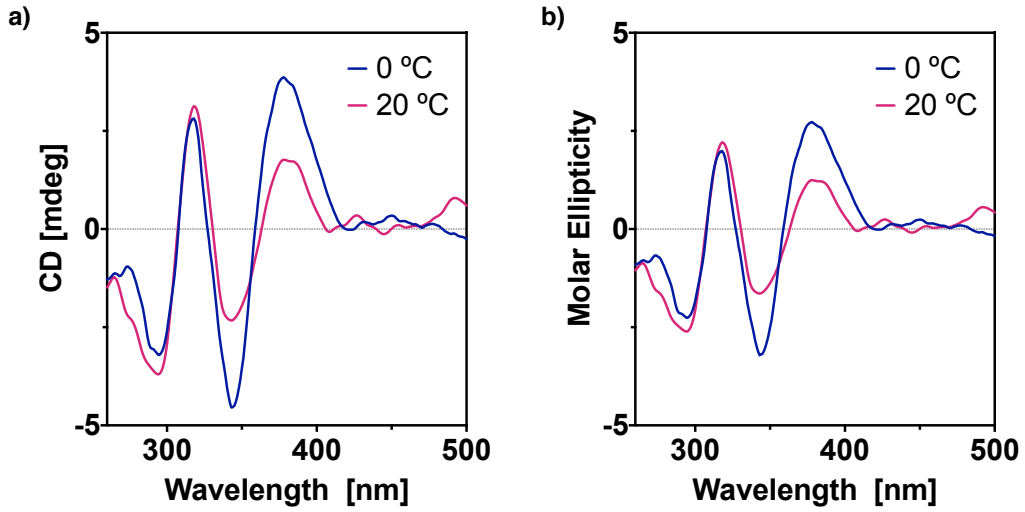

Figure S21. CD traces in THF polymerized at different temperatures and represented in (a) mdeg and (b) molar ellipticity.

12. VT-CD Experiments

Poly-(*S*)-**2** (0.2 mg·mL^{-1}, DMF) shows a decrease in the CD intensity when increasing the temperature. On the other hand, the CD trace of poly-(*S*)-**3** (0.2 mg·mL^{-1}, DMF) is slightly diminished when changing the temperature.

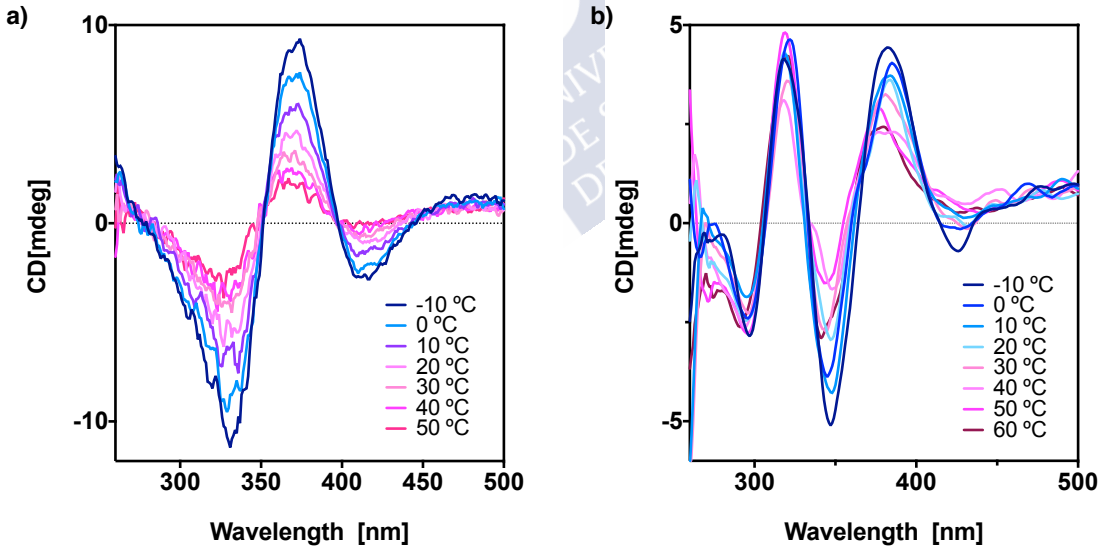

Figure S22. VT-CD of (a) poly-**2** and (b) poly-**3** heating rate 10 ºC·min^{-1}.

13. Atomic Force Microscopy (AFM) Measurements

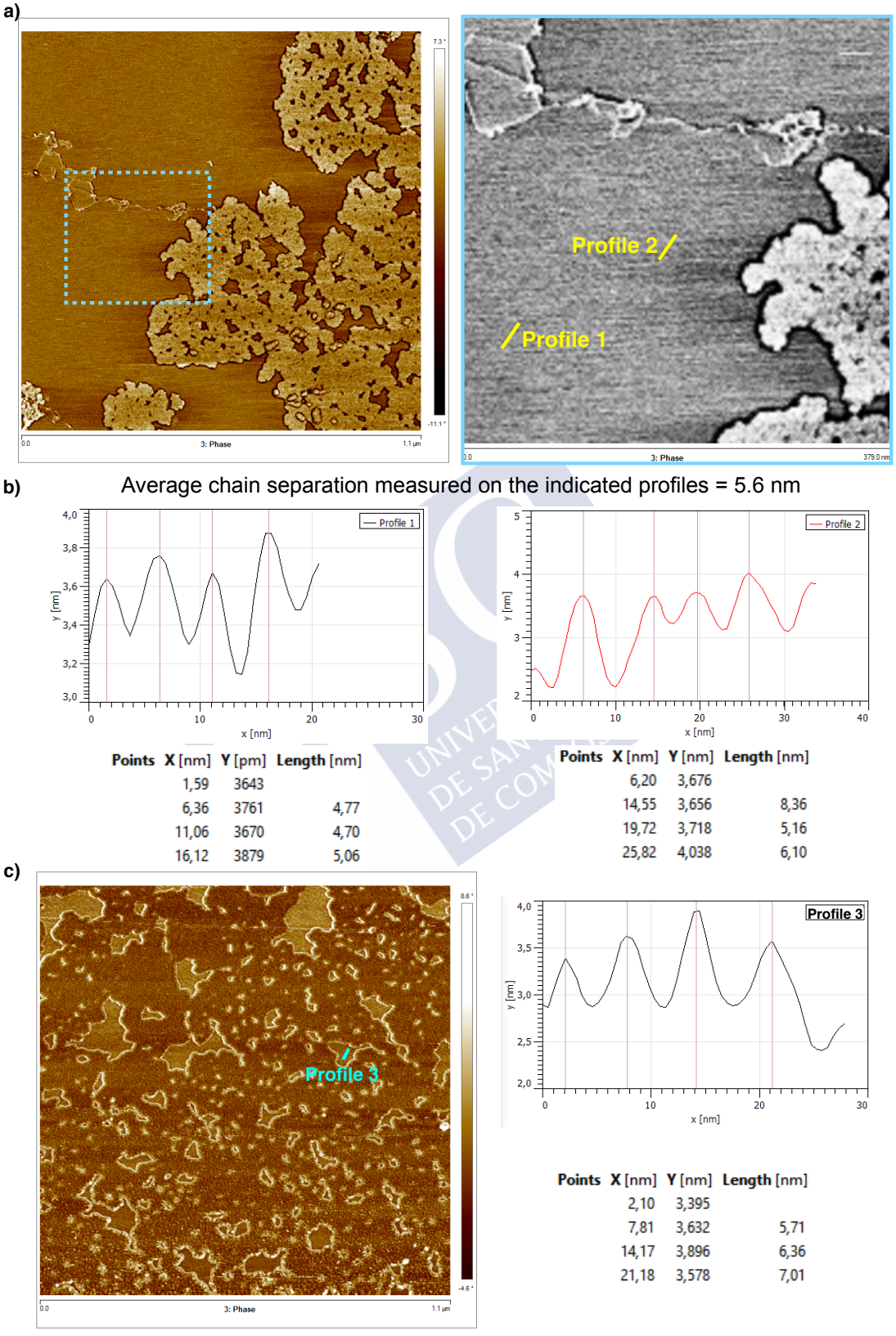

Figure S23. (a) AFM phase images for poly-(*S*)-**2**, from large scale image to magnification of the highlighted area. (b) Graphics showing the chain distribution profiles measured in the indicated zone. (c) Additional AFM phase image and the corresponding chain separation distribution.

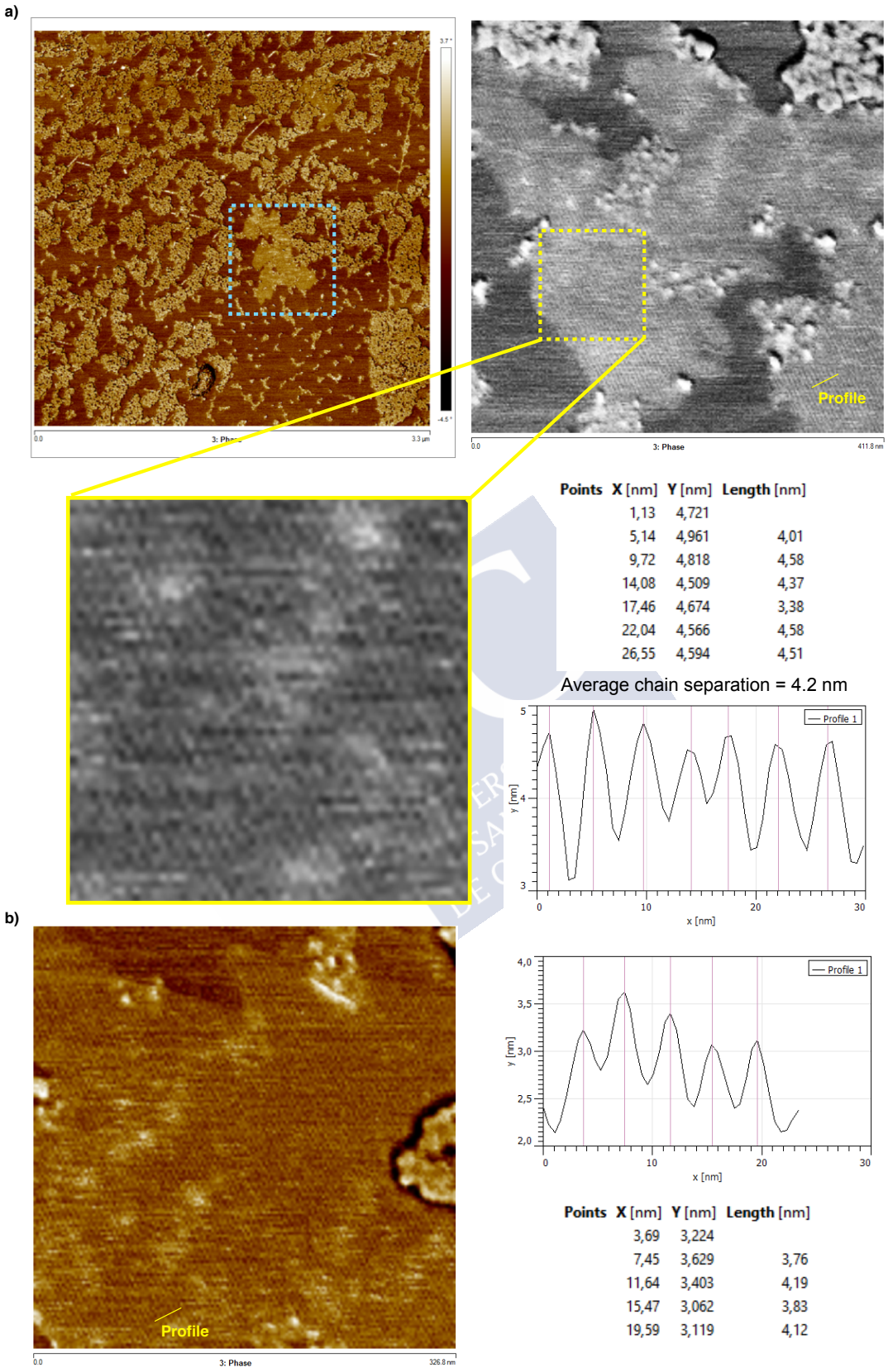

Figure S24. (a) AFM phase images for poly-(*S*)-**3**. From large scale images to magnification of the highlighted area showing the helical chains in detail. Graphic showing the chain distribution profile measured in the indicated zone. (b) Additional AFM phase image and the corresponding chain separation distribution.

14. Theoretical Calculations for Polymers

14.1 Computational Details

ECD spectroscopy is a powerful tool for the study of the absolute configuration and conformation of optically active molecules. From the computational point of view, the main quantity to be evaluated is the scalar rotational strength, that for a transition from the ground state of the molecule (0) to an excited state (*n*), can be calculated from the residue of the linear response function corresponding to the electric dipole-magnetic dipole polarizability tensor (R_{0n}^{LG}). In the length-gauge (LG) formalism, the residue is given by equation (1):

$$R_{0n}^{LG} = \sum_{\alpha} \lim_{\omega \to \omega_{0n}} (\omega - \omega_{0n}) \ll \mu_\alpha; m_\alpha \gg_\omega \qquad (1)$$

Where ω_{0n} is the frequency of the transition between 0 and the *n* state, μ_α is the α component of the electric dipole moment and m_α is the α component of the magnetic dipole moment of the molecule.[S2]

Considering the difficulties to carry out ECD theoretical calculations on large polymers, representative oligomers will be used —n = 9, where n denotes the number of monomer repeating units (m.r.u.)—.

The input structures used for ECD calculations were adjusted to the experimental data obtained from structural techniques such as DSC, AFM and UV-Vis spectroscopy, defining the four different dihedral angles needed to build up the helical scaffold (ω_1, ω_2, ω_3 and ω_4). Moreover, the pendant groups were introduced in *ap* conformation —confirmed by experimental studies—. 3-D structures of the oligomers for poly-**2** and poly-**3** were obtained and submitted for ECD calculations (Figure S25).

To evaluate the theoretical ECD time dependent density functional theory (TD-DFT)[S3] calculations, with the CAM-B3LYP functional[S4] and the 3-21G basis set,[S5] were carried out for the aforementioned oligomers using the ORCA program (80 excitations were included).[S6] The Gabedit[S7] code was used to plot the spectra. The obtained theoretical ECD spectra for these oligomers were compared to the experimental ones, observing that the results are in good agreement. For an efficient comparison and taking into account the tendency of the TD-DFT method to overestimate the excitation energies, the wavelength and intensity at the maximum/minimum corresponding to the first Cotton effect of the theoretical spectra were adjusted to the experimental spectra. Employing the same correction factors, the lambdas were shifted and the intensities rescaled (vide infra). In all cases the agreement was reasonable after the above-mentioned correction has been carried out (Figure S25).

[S2] Rizzo, A.; Coriani, S.; Ruud, K. *Computational Strategies for Spectroscopy. From Small Molecules to Nano Systems*, Barone, V. (Ed.) John Wiley & Sons, New Jersey **2012**.
[S3] Runge E.; Gross, E. K. U. *Phys. Rev. Lett*. **1984**, *52*, 997-1000.
[S4] Yanai, Y.; Tew, D. P.; Handy, N. C. A. *Chem. Phys. Lett.* **2005**, *393*, 51-57.
[S5] Binkley, J. S.; Pople, J. A.; Hehre, W. J. *J. Am. Chem. Soc.* **1980**, *102*, 939-947.
[S6] Neese, F. *WIREs Comput Mol Sci*. **2012**, *2*, 73-78.
[S7] A. R. Allouche *J. Comput. Chem.* **2011**, *32*, 174-182.

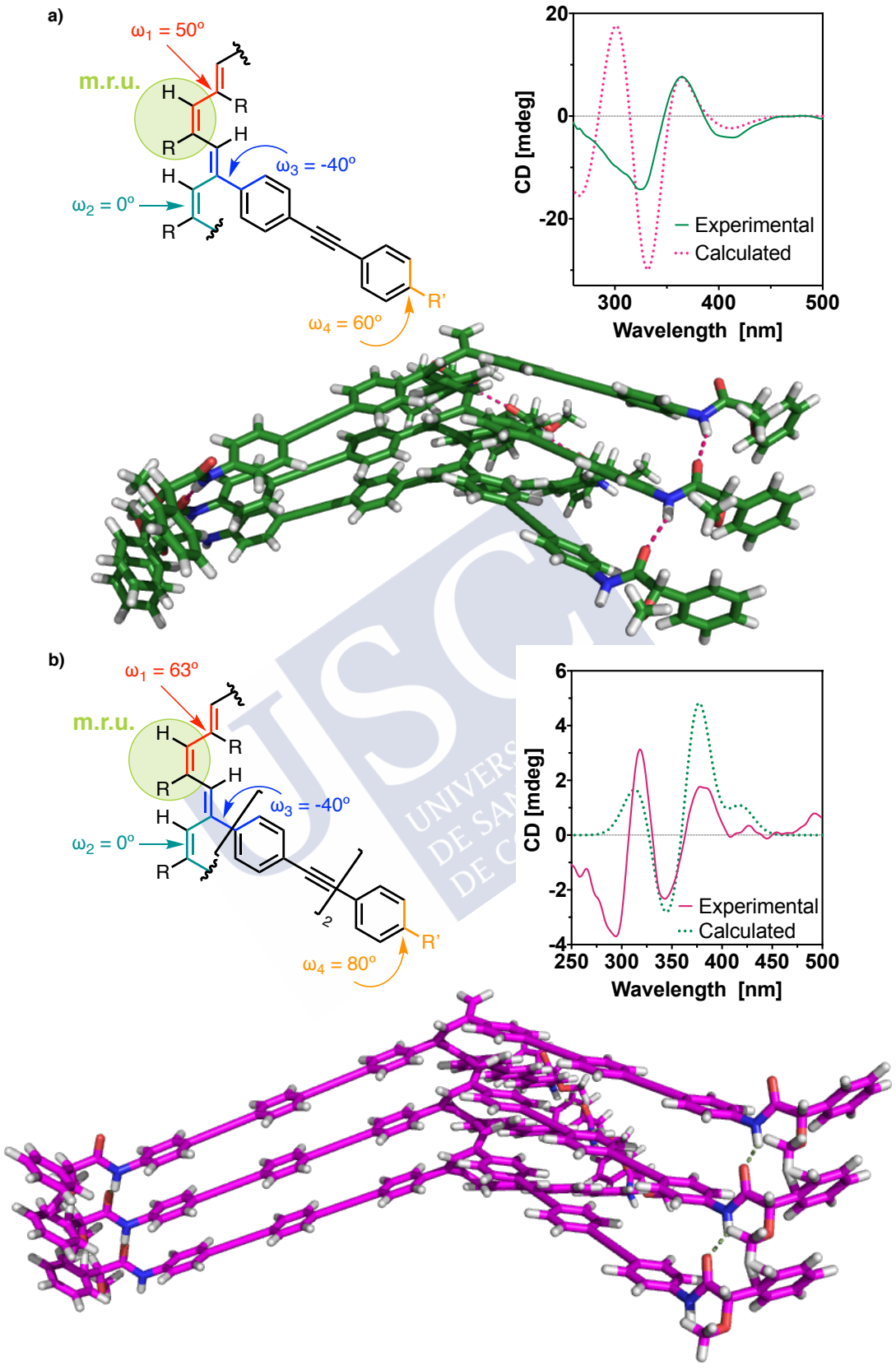

Figure S25. Dihedral angles used to build up the 3D model and the corresponding calculated CD (Full width at half-maximum (FWHM) equals 20 nm) for (a) poly-**2** and (b) poly-**3**.

14.2 Additional Computational Details

The methodology used to perform the theoretical calculations was selected according to the size of the polymers under investigation. Taking this into account, we selected the TD-DFT[S3] method and the CAM-B3LYP[S4] functional due to its a good performance in the evaluation of ECD spectra, as previously observed for theoretical calculations in PPAs.[48,49]

The 3-21G basis set was selected after performing a basis set selection study carried out on a PPA with n = 9, where this basis set proved to be a good choice to evaluate the spectra for larger polymers.

In order to compare the theoretical and experimental spectra, a correction factor was applied. The theoretical spectrum was adjusted to the experimental one by comparing the wavelength and intensity at the maximum/minimum corresponding to the first Cotton effect. We evaluated a correction factor for lambda as the difference between theoretical and experimental wavelengths (at first the maximum/minimum) and shifted the theoretical spectrum accordingly. Regarding the CD intensity, the theoretical values were rescaled in order to be able to compare them to the experimental ones.

Experimental Section

Chapter II

USC
UNIVERSIDADE
DE SANTIAGO
DE COMPOSTELA

1. Materials and Methods

CD measurements were done in a Jasco·720 and UV spectra were registered in a Jasco V·630. The amount of polymer used is indicated in the corresponding section.

VT·CD experiments were performed in a Jasco·1100.

Raman spectra were carried out in a Renishaw confocal Raman spectrometer (Invia Reflex model) equipped with a 785 nm diode laser and a 514 nm Ar laser.

DSC traces were obtained in a DSC Q200 Tzero Technology (TA Instruments, New Castle, UK), using a Tzero low·mass aluminium pan.

TGA traces were obtained in a TGA Q5000 (TA Instruments, New Castle, UK) using a platinum pan.

GPC studies were carried out in a Waters Alliance equipped with Phenomenex GPC columns (10^3 Å, 10^4 Å and 10^5 Å). The amount of polymer used was 0.5 mg·mL^{-1}. THF was used as eluent (flow rate: 1 mL·min^{-1}) and as inner standard, polystyrene narrow standards (PSS) were used.

PyMOL was used as a molecular visualization system.

2. Synthesis of Monomers

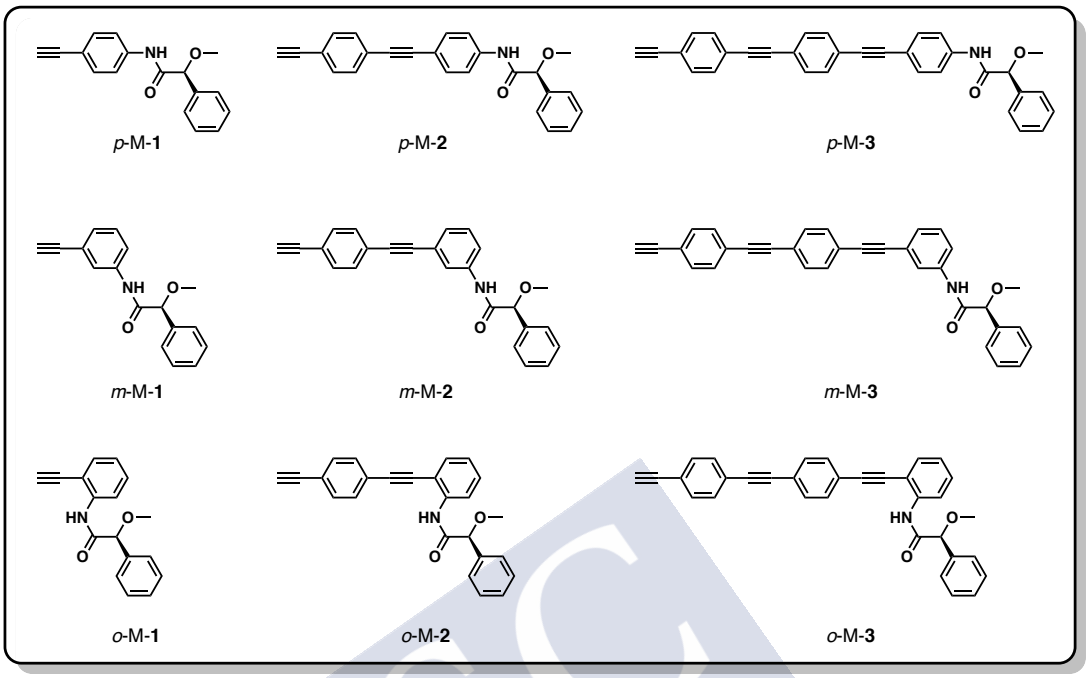

p-M-**1**, *m*-M-**1** and *o*-M-**1**[S1] were prepared according to a previously reported procedure, as well as *p*-M-**2** and *p*-M-**3**.[S2]

[S1] Rodríguez, R.; Quiñoá, E.; Riguera, R.; Freire F. *J. Am. Chem. Soc.* **2016**, *138*, 9620-9628.
[S2] Fernández, Z.; Fernández, B.; Quiñoá, E.; Riguera, R.; Freire, F. *Chem. Sci.* **2020**, *11*, 7182-7187.

Synthesis of 3-((4-((trimethylsilyl)ethynyl)phenyl)ethynyl)aniline (**1**)

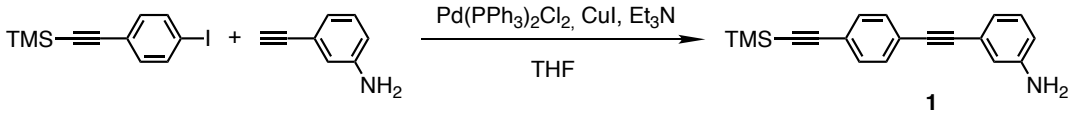

1

((4-iodophenyl)ethynyl)trimethylsilane (0.40 g, 1.33 mmol, 1.00 equiv.), bis(triphenylphosphine)palladium(II) dichloride ($Pd(PPh_3)_2Cl_2$, 0.02 g, 0.02 mmol, 0.02 equiv.) and copper iodide (CuI, 0.05 g, 0.02 mmol, 0.02 equiv.) were dissolved in dry THF (15 mL). Next triethylamine (Et_3N, 7.50 mL) and 3-ethynylaniline (0.15 g, 1.33 mmol, 1.00 equiv.) were added and the mixture was stirred for three hours. After removing the solvent the crude product was chromatographed on silica gel (70-230 mesh) with hexane/ethyl acetate (80:20) as eluent obtaining a pale yellow solid (0.34 g, 88% of yield).

^{1}H NMR (300 MHz, $CHCl_3$) δ_H (ppm): 7.45 (s, 4H), 7.12 (t, 1 H), 7.94 (d, 1 H), 6.84 (s, 1H), 6.65 (d, 1H), 3.68 (s, 2H), 0.29 (s, 6H).

^{13}C NMR (75 MHz, $CHCl_3$) δ_c (ppm): 146.4, 131.9, 131.4, 129.4, 123.6, 123.5, 122.8, 122.0, 118.3, 117.8, 116.8, 115.6, 104.7, 96.3, 91.7, 88.5, 0.0.

HRMS (ESI) m/z calcd for $C_{19}H_{19}NSi$ $[M+H]^+$: 290.1287, found: 290.1357.

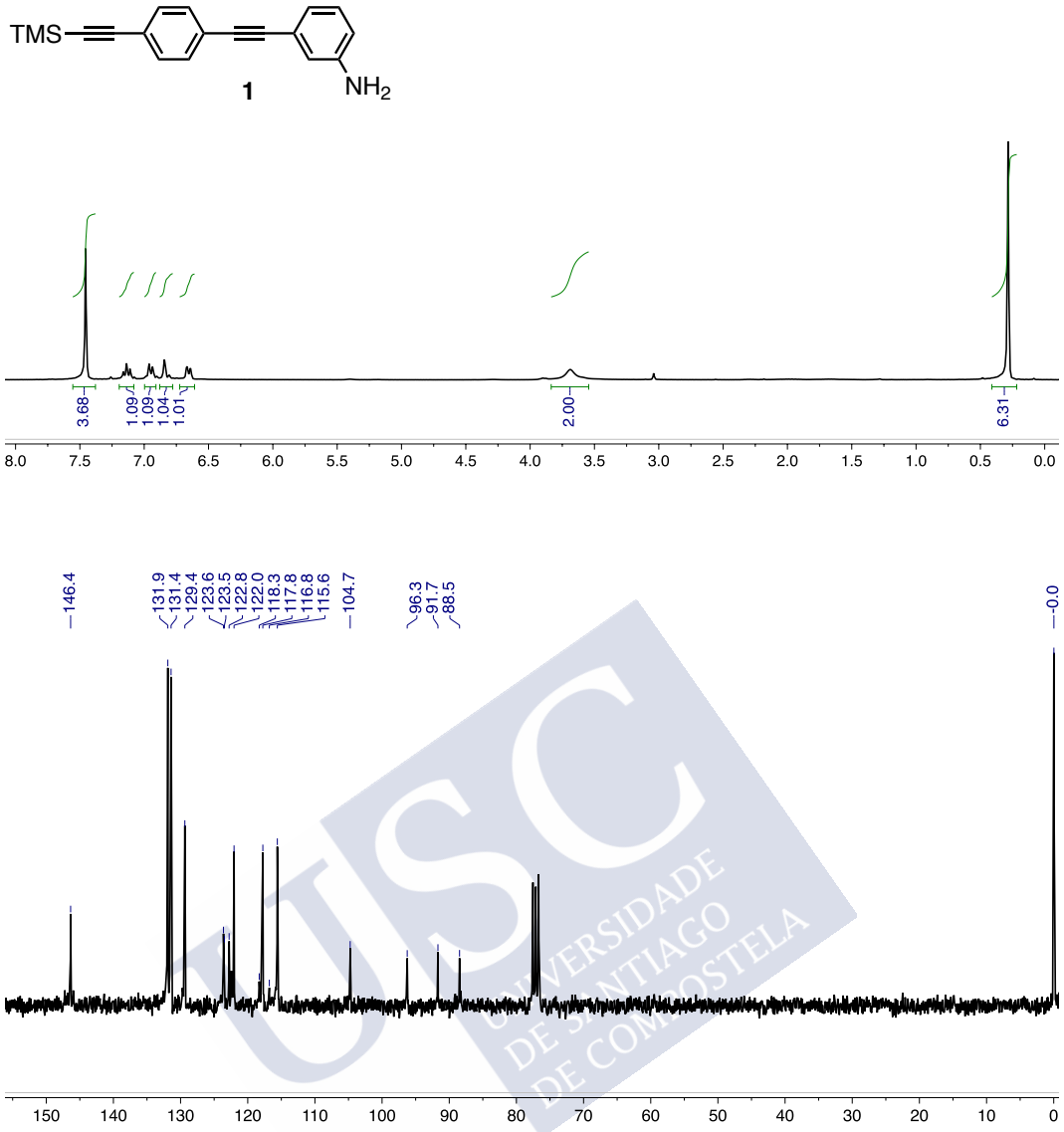

Figure S1. ^{1}H-NMR and ^{13}C for **1** in $CDCl_3$.

Synthesis of 3-((4-ethynylphenyl)ethynyl)aniline (**2**)

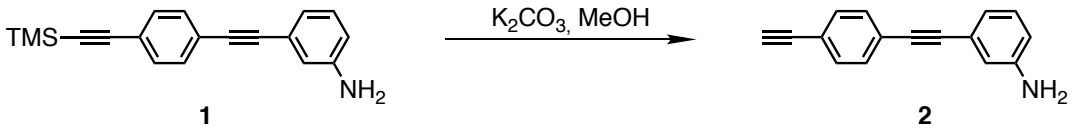

1 **2**

Once obtained the 3-((4-((trimethylsilyl)ethynyl)phenyl)ethynyl)aniline (**1**, 0.34 g, 1.16 mmol, 1.00 equiv.) it was disolved in MeOH (10 mL) and potassium carbonate was added (K_2CO_3, 0.48 g, 479.87 mmol, 3.00 equiv.). After 15 minutes the organic layer was washed three times with water and dried over anhydrous $NaHCO_3$. The crude was chromatographed on silica gel (70-230 mesh) with hexane/ethyl acetate (70:30) as eluent (0.25 g, 99% of yield).

^{1}H NMR (300 MHz, $CHCl_3$) δ_H (ppm): 7.46 (s, 4H), 7.14 (t, 1H), 7.94 (d, 1H), 6.85 (d, 1H), 6.66 (d, 1H), 3.70 (s, 2H), 3.19 (s, 1H).

^{13}C NMR (75 MHz, $CHCl_3$) δ_C (ppm): 146.3, 132.0, 131.5, 129.4, 123.9, 123.6, 122.1, 121.7, 117.8, 115.6, 91.7, 88.3, 83.3, 78.9.

HRMS (ESI) m/z calcd for $C_{16}H_{11}N$ $[M+H]^+$: 218.8901, found: 218.0963.

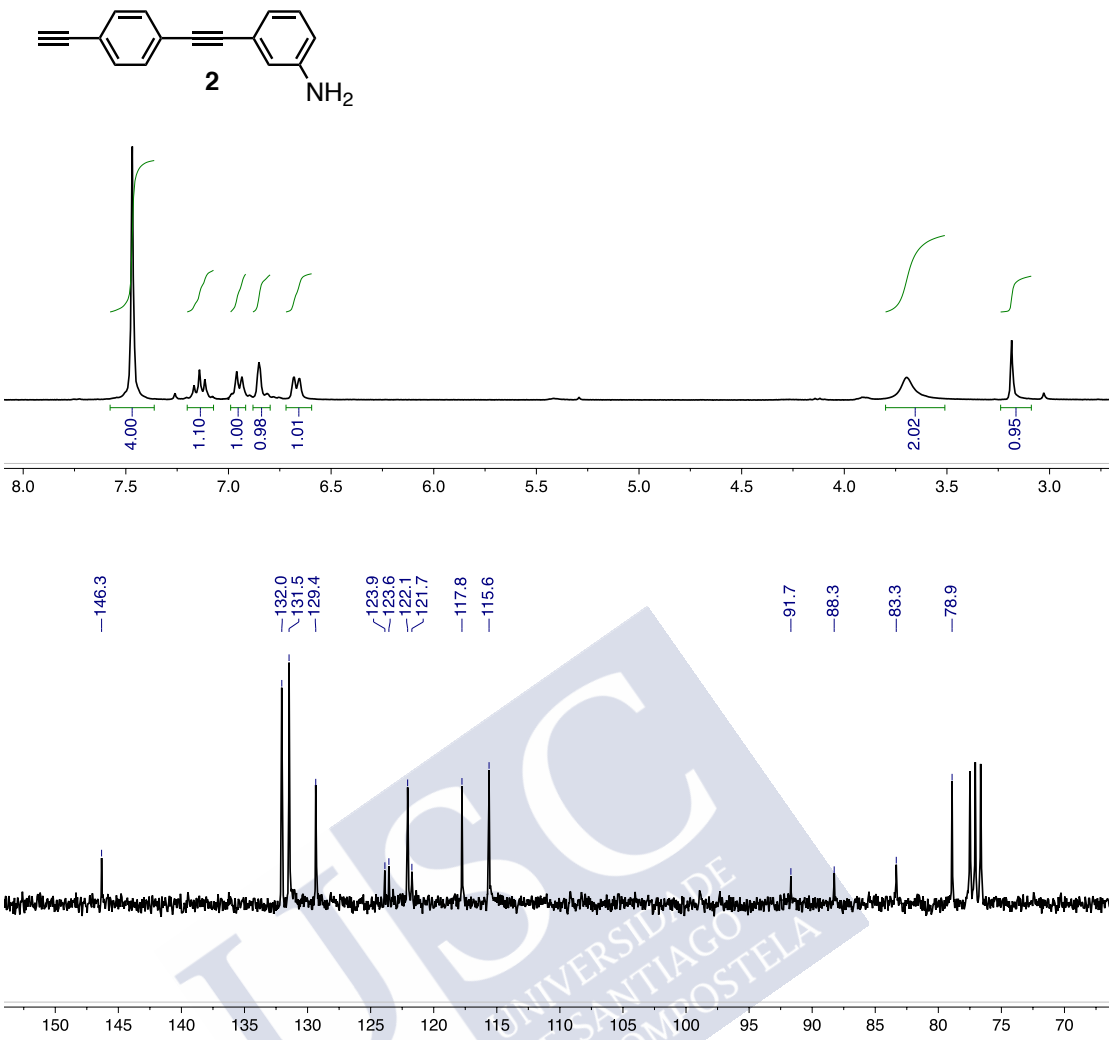

Figure S2. ^{1}H-NMR and ^{13}C for **2** in $CDCl_3$.

Synthesis of (*S*)-*N*-(3-((4-ethynylphenyl)ethynyl)phenyl)-2-methoxy-2-phenylacetamide (*m*-M-**2**)

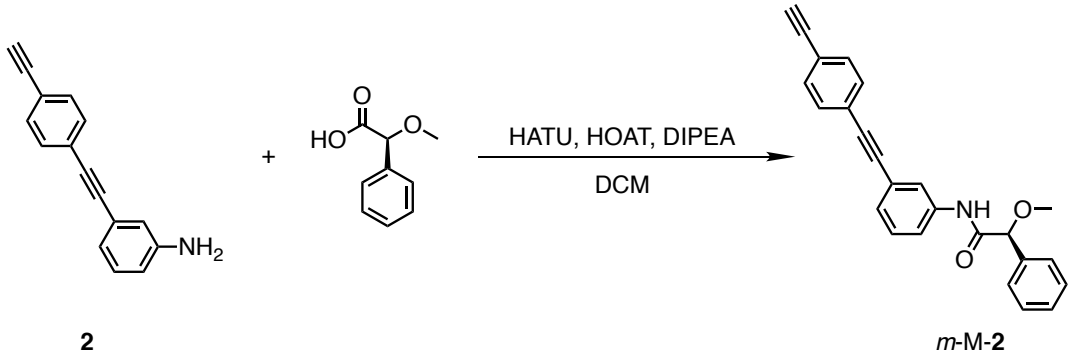

2 *m*-M-**2**

(*S*)-α-methoxy-α-phenylacetic acid (0.17 g, 0.99 mmol, 1.20 equiv.), 2-(7-Aza-1H-benzotriazole-1-yl)-1,1,3,3-tetramethyluronium (HATU, 0.38 g, 0.99 mmol, 1.20 equiv.), 1-hydroxy-7-azabenzotriazole (HOAT, 0.14 g, 0.99 mmol, 1.20 equiv.) and diisopropyltriethylamine (DIPEA, 0.17 mL, 1.20 equiv.) were dissolved in 10 mL of dry CH_2Cl_2. After 15 minutes, time needed to activate the acid, 3-((4-ethynylphenyl)ethynyl)aniline (**2**, 0.18 g, 0.83 mmol, 1.00 equiv.) was added and the mixture was stirred overnight. The organic layer was washed with HCl 1M, a saturated solution of $NaHCO_3$ and brine. The combined organic layers were dried over anhydrous Na_2SO_4, filtered and evaporated at reduced pressure. The crude product was chromatographed on silica gel (70-230 mesh) with hexane/ethyl acetate (80:20) as eluent (0.27 g, 72% of yield).

^{1}H NMR (300 MHz, $CHCl_3$) δ_H (ppm): 8.55 (s, 1H), 7.80 (s, 1H), 7.57 (d, 1H), 7.44 (s, 6H), 7.36 (d, 3H), 7.27 (d, 2H), 4.73 (s, 1H), 3.43 (s, 1H), 3.16 (s, 1H).

^{13}C NMR (75 MHz, $CHCl_3$) δ_c (ppm): 168.6, 137.5, 136.5, 132.0, 131.5, 129.0, 128.7, 127.6, 127.0, 123.7, 123.6, 122.7, 122.0, 119.9, 90.9, 89.1, 83.9, 83.3, 78.9, 57.3.

HRMS (ESI) m/z calcd for $C_{25}H_{19}NO_2Na$ $[M+Na]^+$: 388.1308, found: 388.1305.

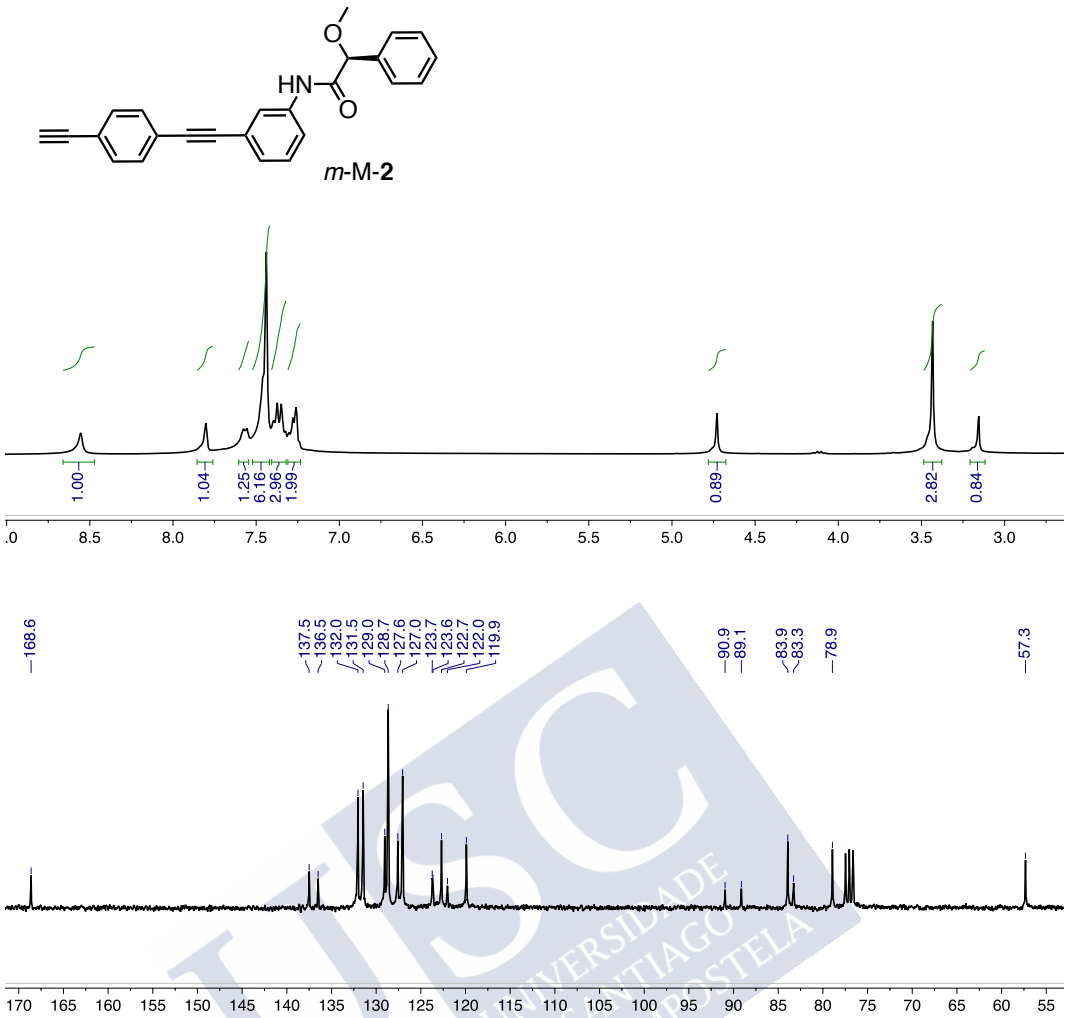

Figure S3. ^{1}H-NMR and ^{13}C for *m*-M-**2** in $CDCl_3$.

Synthesis of (*S*)-2-methoxy-2-phenyl-*N*-(3-((4-((4-((trimethylsilyl)ethynyl)phenyl)ethynyl)phenyl)ethynyl)phenyl)acetamide (**3**)

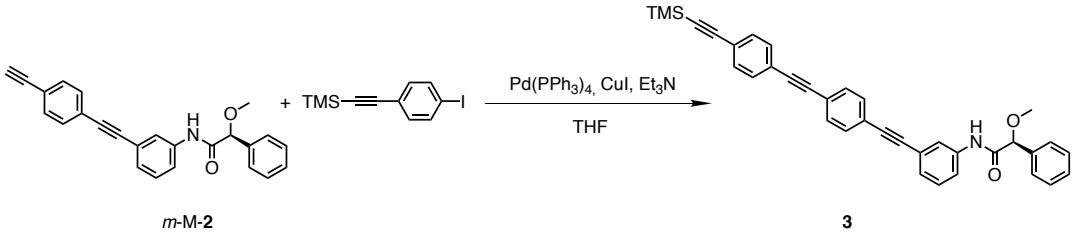

m-M-**2** **3**

((4-iodophenyl)ethynyl)trimethylsilane (0.20 g, 0.68 mmol, 1.00 equiv.), tetrakis(triphenylphosphine)palladium(0) ($Pd(PPh_3)_4$, 0.008 g, 0.06 mmol, 0.01 equiv.) and copper iodide (CuI, 0.002 g, 0.06 mmol, 0.01 equiv.) were dissolved in dry Et_3N (20 mL). Next (*S*)-*N*-(3-((4-ethynylphenyl)ethynyl)phenyl)-2-methoxy-2-phenylacetamide (*m*-M-**2**, 0.25 g, 0.68 mmol, 1.00 equiv.) was added and the mixture was stirred at r.t. for three hours. After removing the solvent the crude product was chromatographed on silica gel (70-230 mesh) with hexane/ethyl acetate (80:20) as eluent (0.38 g, 97% of yield).

^{1}H NMR (300 MHz, $CDCl_3$) δ_H (ppm): 8.59 (s, 1H), 7.83 (s, 1H), 7.63-7.58 (m, 1H), 7.49 (s, 4H), 7.46 (s, 5H), 7.41-7.36 (m, 3H), 7.32-7.27 (m, 2H), 4.75 (s, 1H), 3.46 (s, 3H), 0.27 (s, 7H).

^{13}C NMR (75 MHz, $CDCl_3$) δ_C (ppm) 168.6, 137.4, 136.4, 131.9, 131.6, 131.4, 129.1, 128.7, 127.6, 127.0, 123.8, 123.1, 122.9, 122.6, 119.8, 104.6, 96.4, 91.0, 90.9, 89.3, 83.8, 57.3, -0.1.

HRMS (ESI) m/z calcd for $C_{36}H_{32}NO_2Si$ $[M+H]^+$: 538.2124, found: 538.2198.

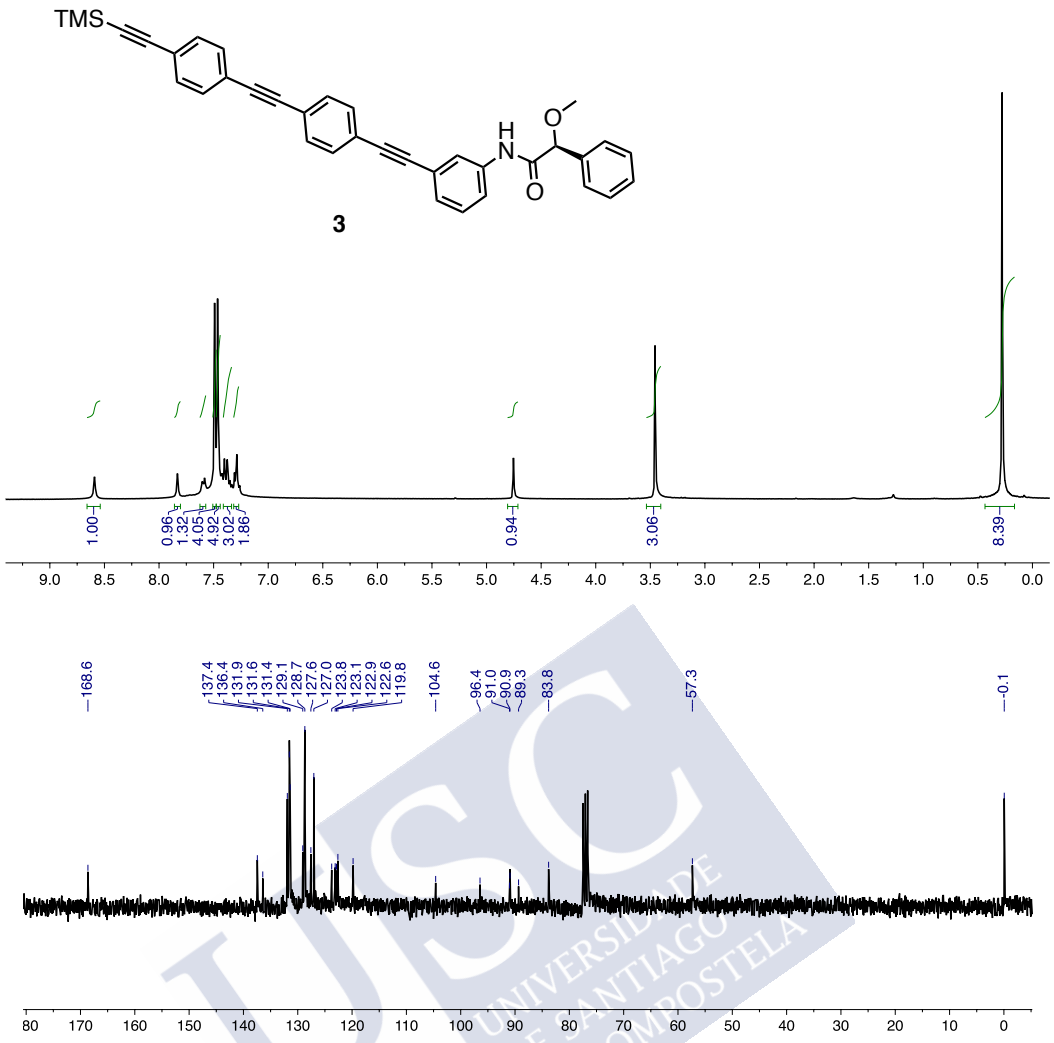

Figure S4. ^{1}H-NMR and ^{13}C for **3** in $CDCl_3$.

Synthesis of (*S*)-*N*-(3-((4-((4-ethynylphenyl)ethynyl)phenyl)ethynyl)phenyl)-2-methoxy-2-phenylacetamide (*m*-M-**3**)

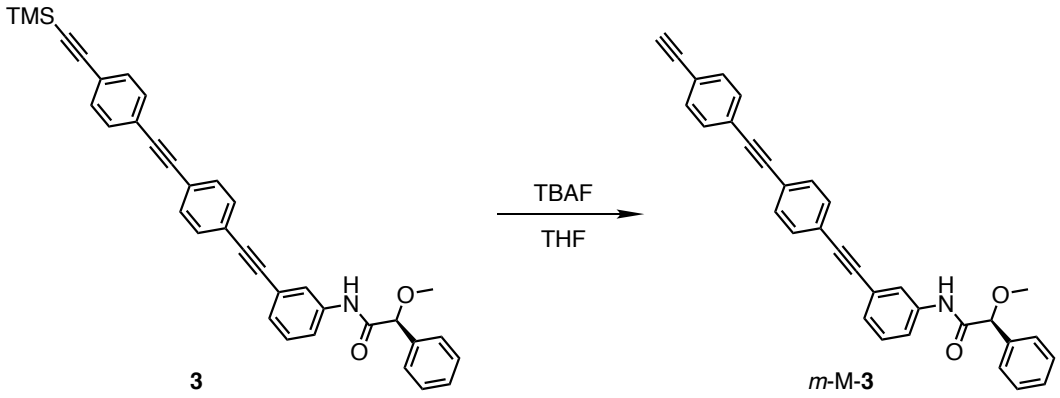

(*S*)-2-methoxy-2-phenyl-*N*-(3-((4-((4-((trimethylsilyl)ethynyl)phenyl)ethynyl)phenyl)ethynyl)phenyl)acetamide (**3**, 0.30 g, 0.31 mmol, 1.00 equiv.) was dissolved in THF (8 mL). Next TBAF was added (1M in THF, 0.64 mL, 0.64 mmol, 1.20 equiv.) and the reaction was stirred at r.t. for 15 minutes. After that time Milli-Q water was added to the reaction mixture and the product was extracted with DCM. The solvent was evaporated and the solid dissolved in $CHCl_3$:Milli-Q water (1:1) and washed twice with NH_4Cl 1M to remove the TBAF salts. After removing the solvent the crude was chromatographed on silica gel (70-230 mesh) with hexane/ethyl acetate (70:30) as eluent (0.22 g, 89% of yield).

^{1}H NMR (300 MHz, $CDCl_3$) δ_H (ppm): 8.58 (s, 1H), 7.82 (s, 1H), 7.60 (d, 1H), 7.52-7.43 (m, 9H), 7.41-7.34 (m, 3H), 7.33-3.25 (m, 2H), 4.75 (s, 1H), 3.46 (s, 3H), 3.19 (s, 1H).

^{13}C NMR (75 MHz, $CDCl_3$) δ_C (ppm) 168.6, 137.4, 136.4, 132.1, 131.6, 131.5, 129.1, 128.7, 127.6, 127.0, 123.7, 123.5, 123.2, 122.8, 122.6, 119.8, 91.1, 90.9, 89.3, 83.8, 83.2, 79.0, 57.4.

HRMS (ESI) m/z calcd for $C_{36}H_{32}NO_2Si$ $[M+H]^+$: 466.5520, found: 466.1796.

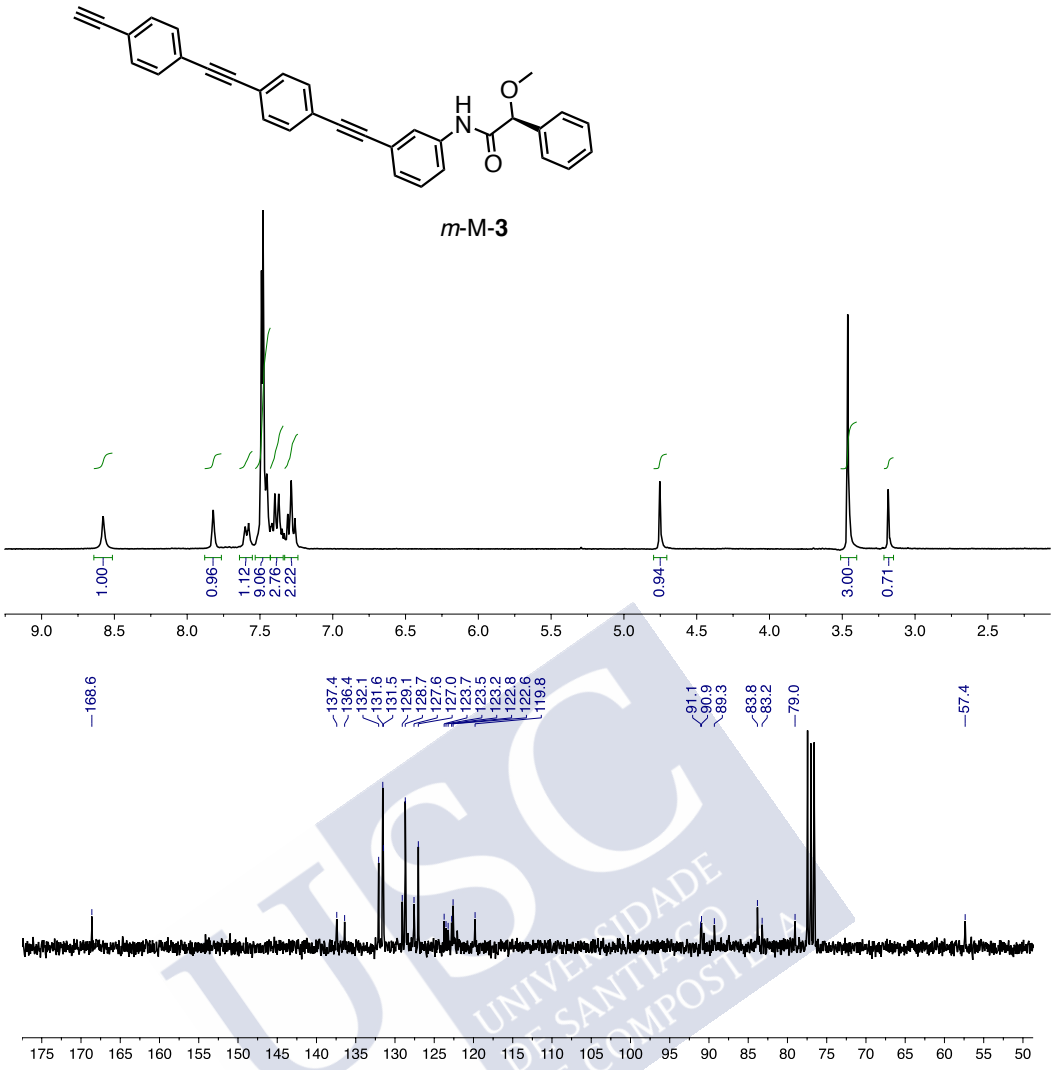

Figure S5. ^{1}H-NMR and ^{13}C for *m*-M-**3** in $CDCl_3$.

Synthesis of 2-((4-((trimethylsilyl)ethynyl)phenyl)ethynyl)aniline (**4**)

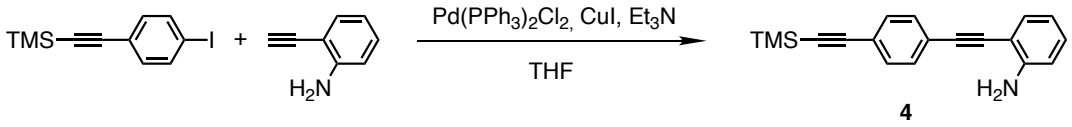

4

((4-iodophenyl)ethynyl)trimethylsilane (0.40 g, 1.33 mmol, 1.00 equiv.), bis(triphenylphosphine)palladium(II) dichloride ($Pd(PPh_3)_2Cl_2$, 0.02 g, 0.02 mmol, 0.02 equiv.) and copper iodide (CuI, 0.05 g, 0.02 mmol, 0.02 equiv.) were dissolved in dry THF (15 mL). Next triethylamine (Et_3N, 7.5 mL) and 2-ethynylaniline (0.15 g, 1.33 mmol, 1.00 equiv.) were added and the mixture was stirred for three hours. After removing the solvent the crude product was chromatographed on silica gel (70-230 mesh) with hexane/ethyl acetate (80:20) as eluent (0.34 g, 89% of yield).

^{1}H NMR (300 MHz, $CHCl_3$) δ_H (ppm): 7.45 (s, 4H), 7.36 (d, 1H), 7.15 (t, 1H), 6.85-6.82 (m, 2H), 4.27 (s, 2H), 0.28 (s, 8H).

^{13}C NMR (75 MHz, $CHCl_3$) δ_C (ppm): 147.8, 132.2, 131.9, 131.2, 130.0, 123.4, 122.8, 118.0, 114.4, 107.6, 104.6, 96.3, 94.4, 87.9, 0.0.

HRMS (ESI) m/z calcd for $C_{19}H_{19}NSi$ $[M+H]^+$: 290.1287, found: 290.1358.

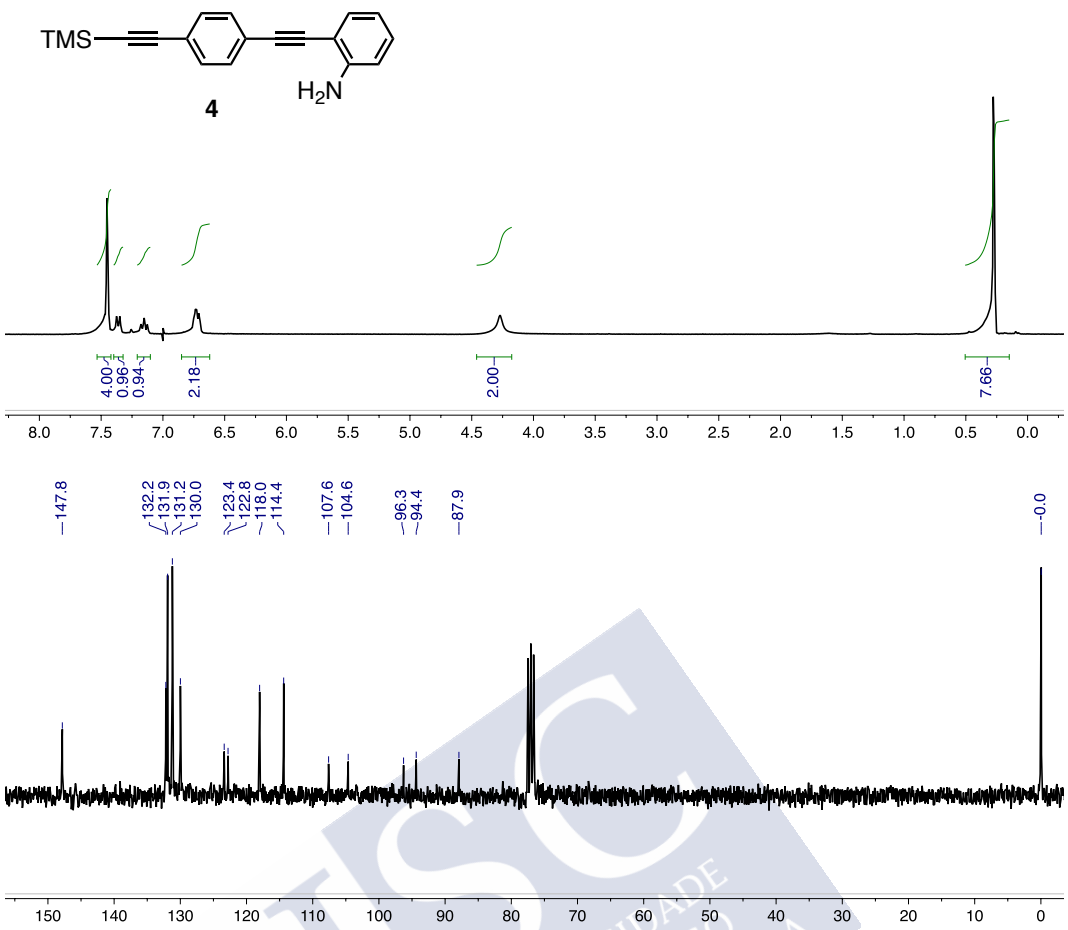

Figure S6. ^{1}H-NMR and ^{13}C for **4** in $CDCl_3$.

Synthesis of 2-((4-ethynylphenyl)ethynyl)aniline (**5**)

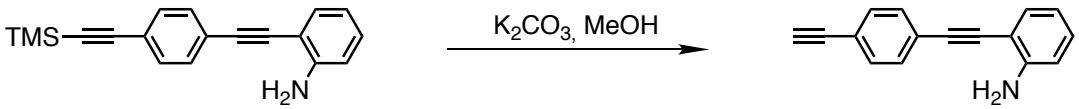

4 **5**

Once obtained the 2-((4-((trimethylsilyl)ethynyl)phenyl)ethynyl)aniline (0.34 g, 1.17 mmol, 1.00 equiv.) it was disolved in MeOH (10 mL) and potassium carbonate was added (K_2CO_3, 0.76 g, 3.52 mmol, 3.00 equiv.). After 15 minutes the organic layer was washed three times with water and dried over anhydrous $NaHCO_3$. The crude was chromatographed on silica gel (70-230 mesh) with hexane/ethyl acetate (70:30) as eluent (0.23 g, 90% of yield).

^{1}H NMR (300 MHz, $CHCl_3$) δ_H (ppm): 7.48 (s, 4H), 7.36 (d, 1H), 7.16 (t, 1H), 6.79-6.75 (m, 2H), 4.27 (s, 2H), 3.19 (s, 1H).

^{13}C NMR (75 MHz, $CHCl_3$) δ_C (ppm): 147.8, 132.2, 132.1, 131.3, 130.1, 123.8, 121.8, 118.0, 114.4, 107.5, 94.2, 88.0, 83.3, 79.0.

HRMS (ESI) m/z calcd for $C_{16}H_{11}N$ $[M+H]^+$: 218.0891, found: 218.0966.

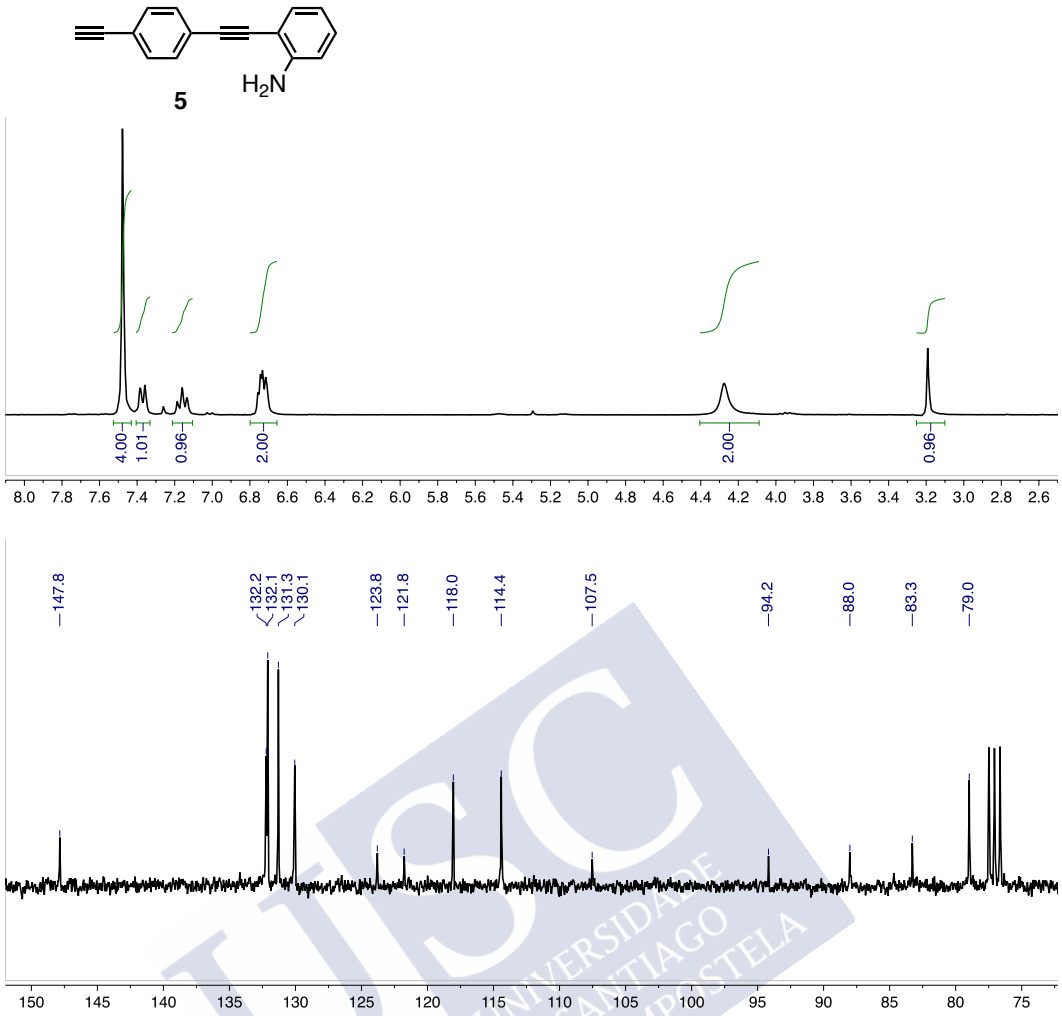

Figure S7. ^{1}H-NMR and ^{13}C for **5** in $CDCl_3$.

Synthesis of (*S*)-*N*-(2-((4-ethynylphenyl)ethynyl)phenyl)-2-methoxy-2-phenylacetamide (*o*-M-**2**)

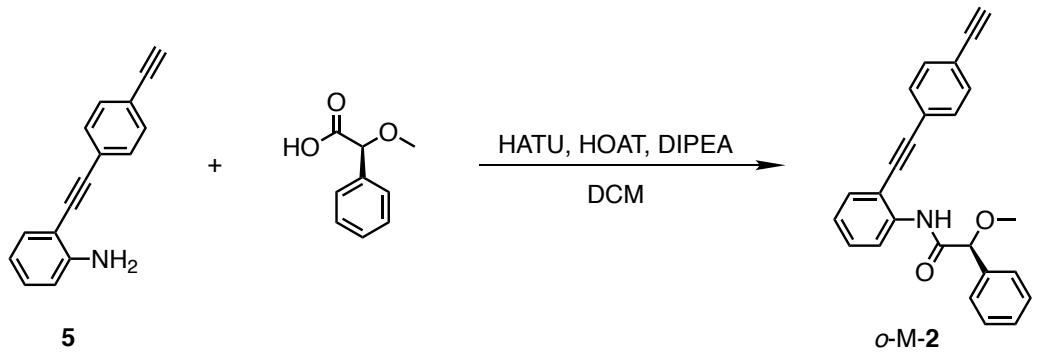

5 *o*-M-**2**

(*S*)-α-methoxy-α-phenylacetic acid (0.17 g, 0.99 mmol, 1.20 equiv.), 2-(7-Aza-1H-benzotriazole-1-yl)-1,1,3,3-tetramethyluronium (HATU, 0.38 g, 0.99 mmol, 1.20 equiv.), 1-hydroxy-7-azabenzotriazole (HOAT, 0.13 g, 0.99 mmol, 1.20 equiv.) and diisopropyltriethylamine (DIPEA, 0.17 mL, 0.99 mmol, 1.20 equiv.) were dissolved in 10 mL of dry CH_2Cl_2. After 15 minutes, time needed to activate the acid, 2-((4-ethynylphenyl)ethynyl)aniline (**5**, 0.18 g, 0.83 mmol, 1.00 equiv.) was added and the mixture was stirred overnight. The organic layer was washed with HCl 1M, a saturated solution of $NaHCO_3$ and brine. The combined organic layers were dried over anhydrous Na_2SO_4, filtered and evaporated at reduced pressure. The crude product was chromatographed on silica gel (70-230 mesh) with hexane/ethyl acetate (8/2) as eluent (0.25 g, 65% of yield).

^{1}H NMR (300 MHz, $CDCl_3$) δ_H (ppm): 9.59 (s, 1H), 8.44 (d, 1H), 7.64-7.45 (m, 7H), 7.40-7.30 (m, 4H), 7.09 (t, 1H), 4.80 (s, 1H), 3.47 (s, 1H), 3.21 (s, 1H).

^{13}C NMR (75 MHz, $CDCl_3$) δ_C (ppm): 168.6, 138.6, 136.6, 132.2, 131.4, 131.3, 130.0, 128.7, 127.0, 123.6, 123.0, 119.2, 112.2, 96.0, 86.3, 84.4, 83.0, 79.3, 57.5.

HRMS (ESI) m/z calcd for $C_{25}H_{19}NO_2Na$ $[M+Na]^+$: 388.1308, found: 388.1303.

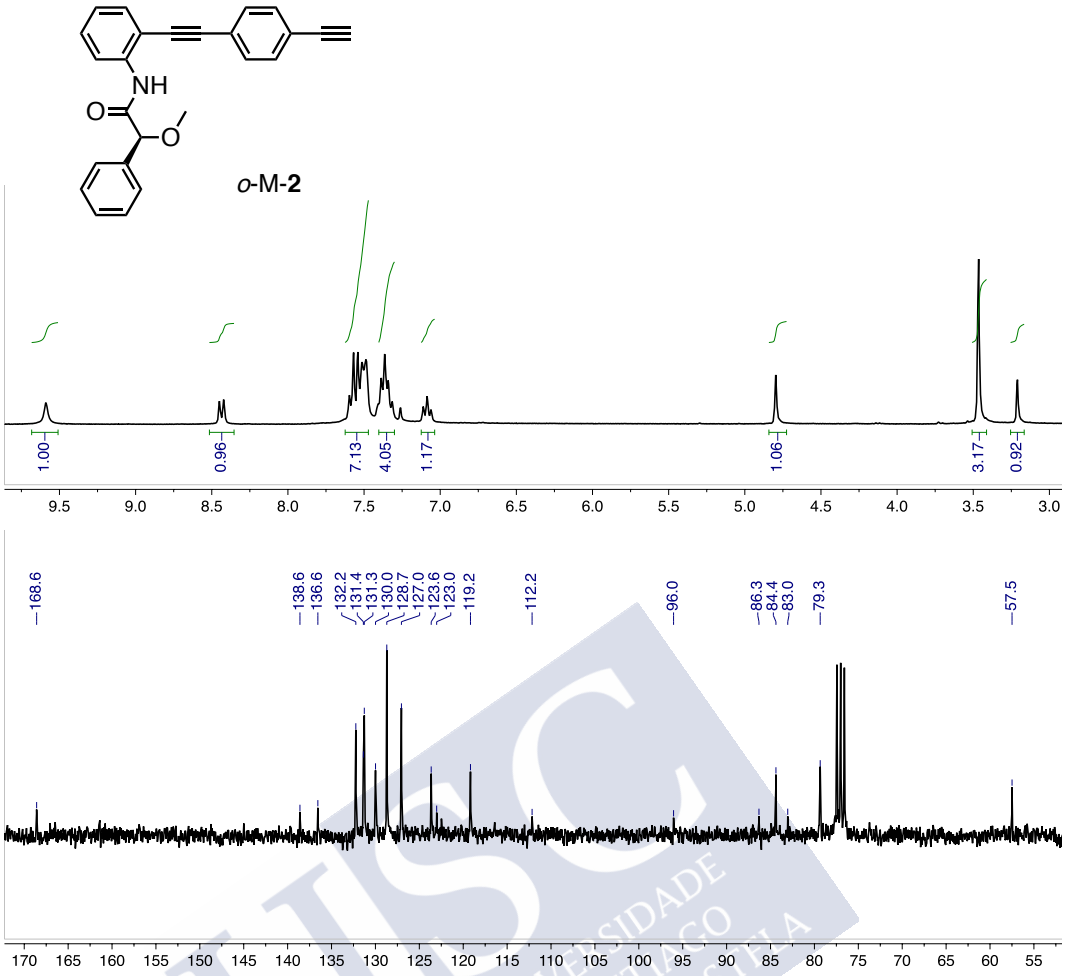

Figure S8. ^{1}H-NMR and ^{13}C for *o*-M-**2** in $CDCl_3$.

Synthesis of (*S*)-2-methoxy-2-phenyl-*N*-(2-((4-((4-((trimethylsilyl)ethynyl)phenyl)ethynyl)phenyl)ethynyl)phenyl)acetamide (**6**)

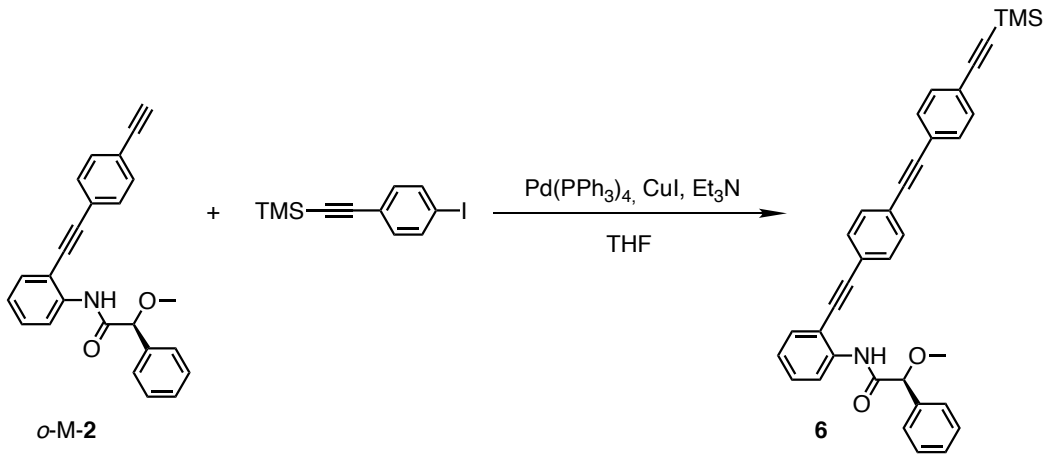

o-M-**2** **6**

((4-iodophenyl)ethynyl)trimethylsilane (0.21 g, 0.68 mmol, 1.00 equiv.), tetrakis(triphenylphosphine)palladium(0) ($Pd(PPh_3)_4$, 0.008 g, 0.06 mmol, 0.01 equiv.) and copper iodide (CuI, 0.002 g, 0.06 mmol, 0.01 equiv.) were dissolved in dry Et_3N (20 mL). Next (*S*)-*N*-(3-((4-ethynylphenyl)ethynyl)phenyl)-2-methoxy-2-phenylacetamide (0.25 g, 0.68 mmol, 1.00 equiv.) was added and the mixture was stirred at r.t. for three hours. After removing the solvent the crude product was chromatographed on silica gel (70-230 mesh) with hexane/ethyl acetate (80:20) as eluent (0.38 g, 98% of yield).

^{1}H NMR (300 MHz, $CDCl_3$) δ_H (ppm): 9.63 (s, 1H), 8.48 (d, 2H), 7.69-7.48 (m, 12H), 7.44-7.31 (m, 4H), 7.09 (t, 1H), 4.82 (s, 1H), 3.48 (s, 3H), 0.28 (s, 7H).

^{13}C NMR (75 MHz, $CDCl_3$) δ_C (ppm): 168.6, 138.6, 136.6, 132.0, 131.7, 131.4, 131.4, 130.0, 128.8, 127.9, 127.1, 123.7, 123.4, 123.3, 122.9, 122.6, 119.2, 112.2, 104.6, 96.6, 96.3, 91.3, 90.8, 86.4, 84.4, 57.5, 0.

HRMS (ESI) m/z calcd for $C_{36}H_{32}NO_2Si$ $[M+H]^+$: 538.2124, found: 538.1308.

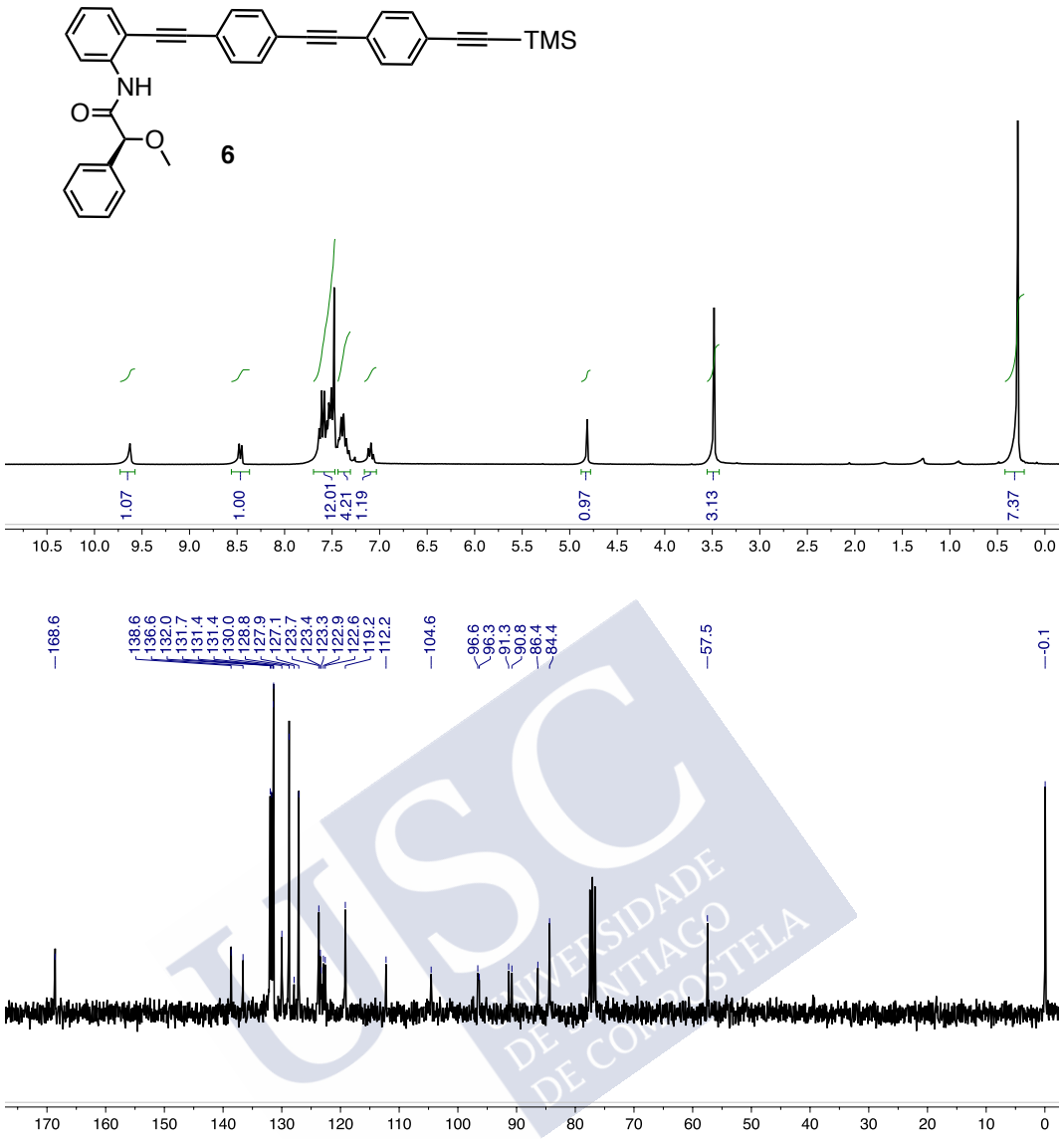

Figure S9. ^{1}H-NMR and ^{13}C for **6** in $CDCl_3$.

Synthesis of (*S*)-*N*-(2-((4-((4-ethynylphenyl)ethynyl)phenyl)ethynyl)phenyl)-2-methoxy-2-phenylacetamide (*o*-M-**3**)

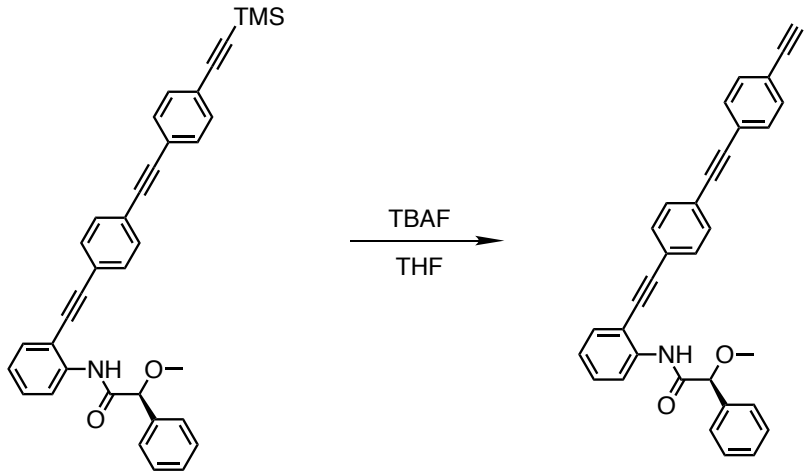

6 *o*-M-**3**

(*S*)-2-methoxy-2-phenyl-*N*-(3-((4-((4-((trimethylsilyl)ethynyl)phenyl)ethynyl)phenyl)ethynyl)phenyl)acetamide (0.30 g, 0.31 mmol, 1.00 equiv.) was dissolved in THF (8 mL). Next TBAF was added (1M in THF, 0.64 mL, 0.64 mmol, 1.20 equiv.) and the reaction was stirred at r.t. for 15 minutes. After that time Milli-Q water was added to the reaction mixture and the product was extracted with DCM. The solvent was evaporated and the solid dissolved in $CHCl_3$:Milli-Q water (1:1) and washed twice with NH_4Cl 1M to remove the TBAF salts. After removing the solvent the crude was chromatographed on silica gel (70-230 mesh) with hexane/ethyl acetate (70:30) as eluent (0.23 g, 94% of yield).

^{1}H NMR (300 MHz, $CDCl_3$) δ_H (ppm): 9.60 (s, 1H), 8.44 (d, 1H), 7.70-7.47 (m, 12H), 7.43-7.31 (m, 4H), 7.09 (t, 1H), 4.80 (s, 1H), 3.48 (s, 3H), 3.20 (s, 1H).

^{13}C NMR (75 MHz, $CDCl_3$) δ_C (ppm): 168.6, 138.6, 136.6, 132.1, 131.7, 131.5, 131.4, 130.0, 128.7, 127.1, 123.7, 123.3, 123.3, 122.7, 122.2, 119.2, 112.2, 91.1, 90.8, 86.4, 84.4, 83.2, 79.2, 57.5.

HRMS (ESI) m/z calcd for $C_{36}H_{32}NO_2Si$ $[M+H]^+$: 466.5520, found: 466.1802.

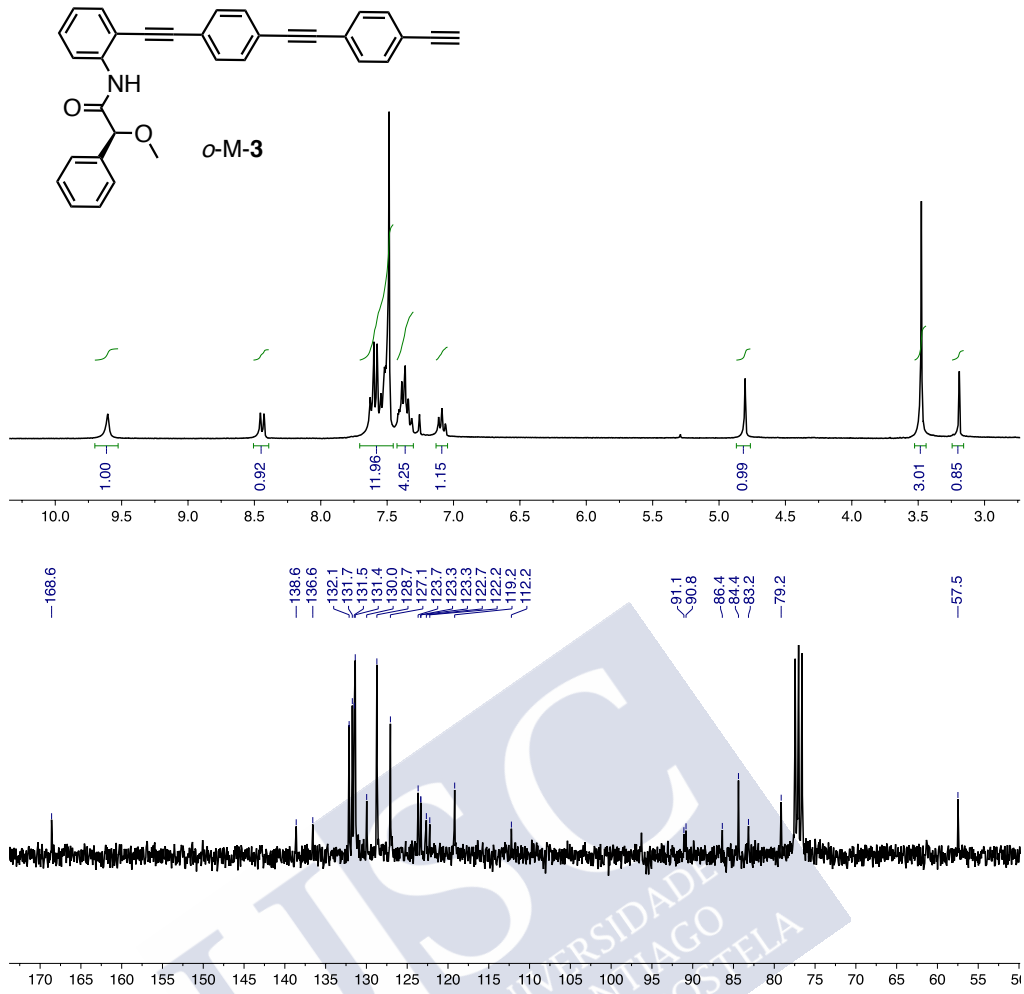

Figure S10. ^{1}H-NMR and ^{13}C for *o*-M-**3** in $CDCl_3$.

3. Synthesis of Polymers

3.1 General Procedure for Polymerization

The polymers were synthesized in a flask (sealed ampoule) previously dried under vacuum and flushed with Ar for three times. The monomers were added as a solid and dissolved in dry THF. Next a solution of rhodium norbadiene chloride dimer $[Rh(nbd)Cl]_2$ was added and the mixture was stirred overnight. The resulting polymers were diluted in CH_2Cl_2 and precipitated in a large amount of MeOH, centrifuged (twice) and reprecipitated in hexane and centrifuged again.

Table S1. Calculated amounts for the polymers synthesis.

Monomer	Mass (mg)	THF (mL)	Et_3N (mL)	Catalyst (mg)	Yield (%)
m-poly-**2**	50	400	5	0.6	82
m-poly-**3**	50	400	5	0.5	78
o-poly-**2**	50	400	5	0.6	75
o-poly-**3**	50	400	5	0.5	80

3.2 NMR and Raman Experiments

The *cis*- configuration of the polyenic backbone was determined by ^1H NMR spectroscopy; vinylic protons resonate at δ = 5.7-5.8 ppm.

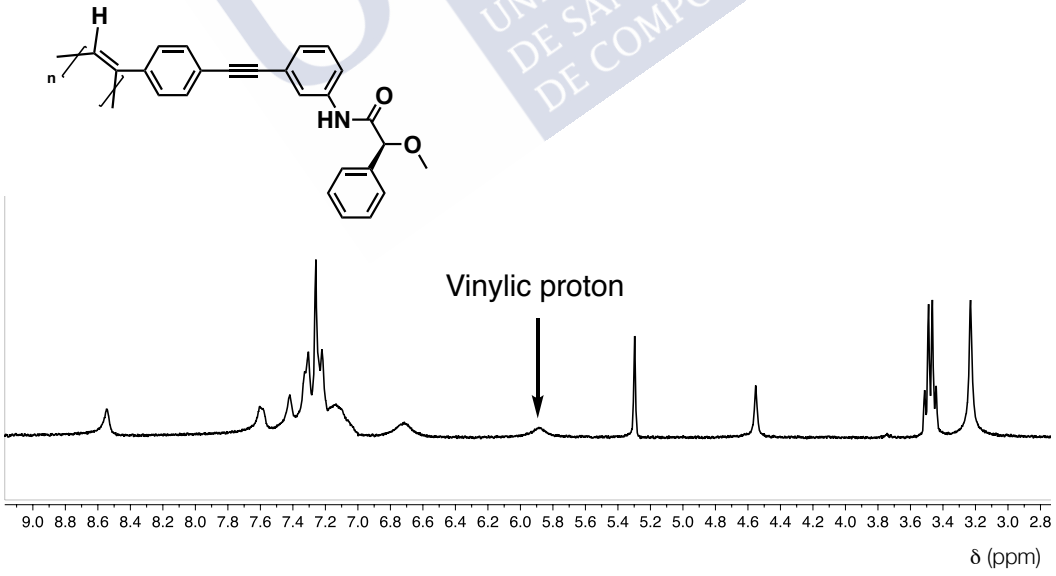

Figure S11. ^1H-NMR for *m*-poly-**2** in $CDCl_3$.

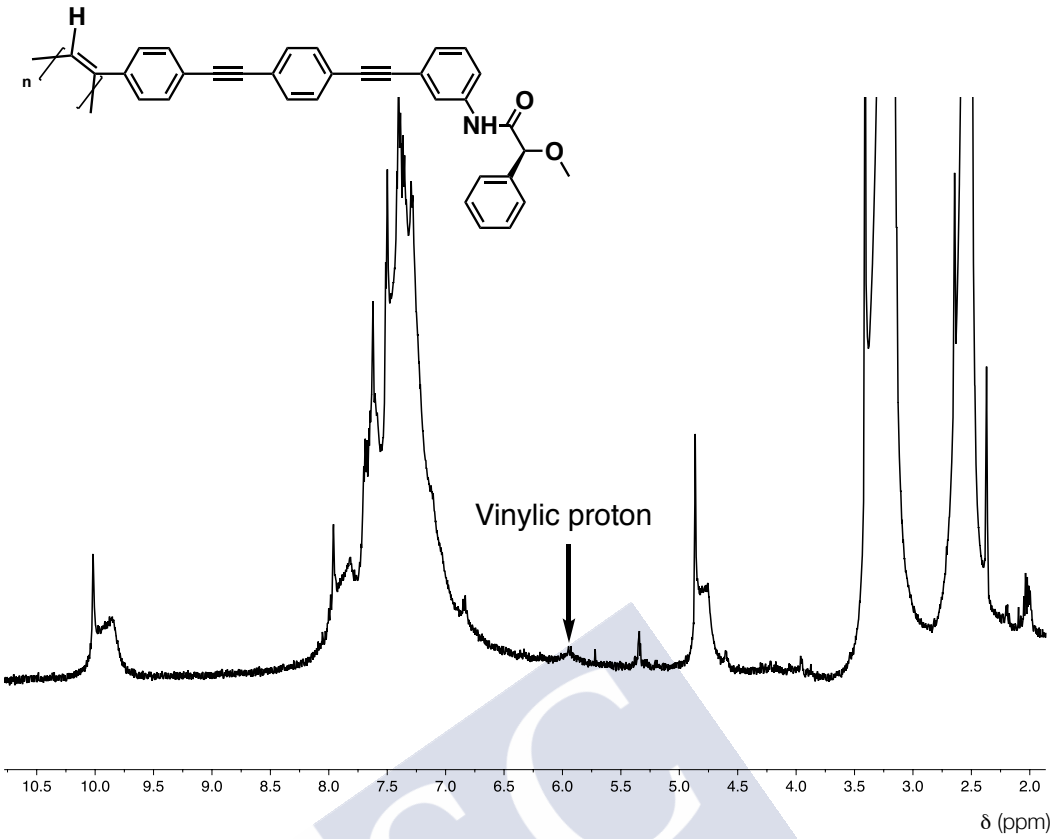

Figure S12. ^{1}H-NMR for *m*-poly-**3** in DMSO-d_6.

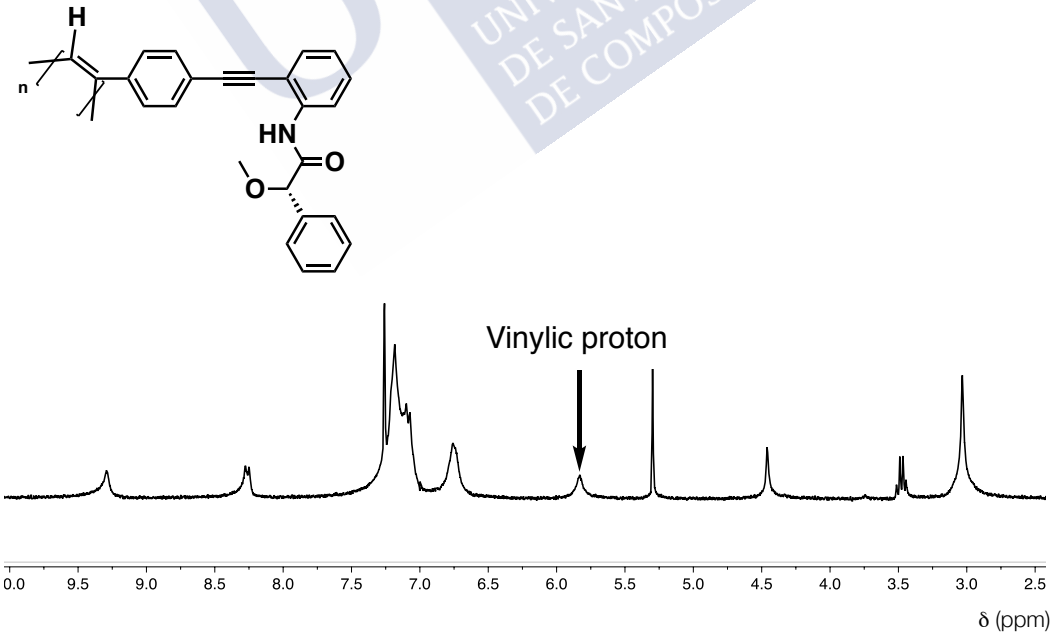

Figure S13. ^{1}H-NMR for *o*-poly-**2** in $CDCl_3$.

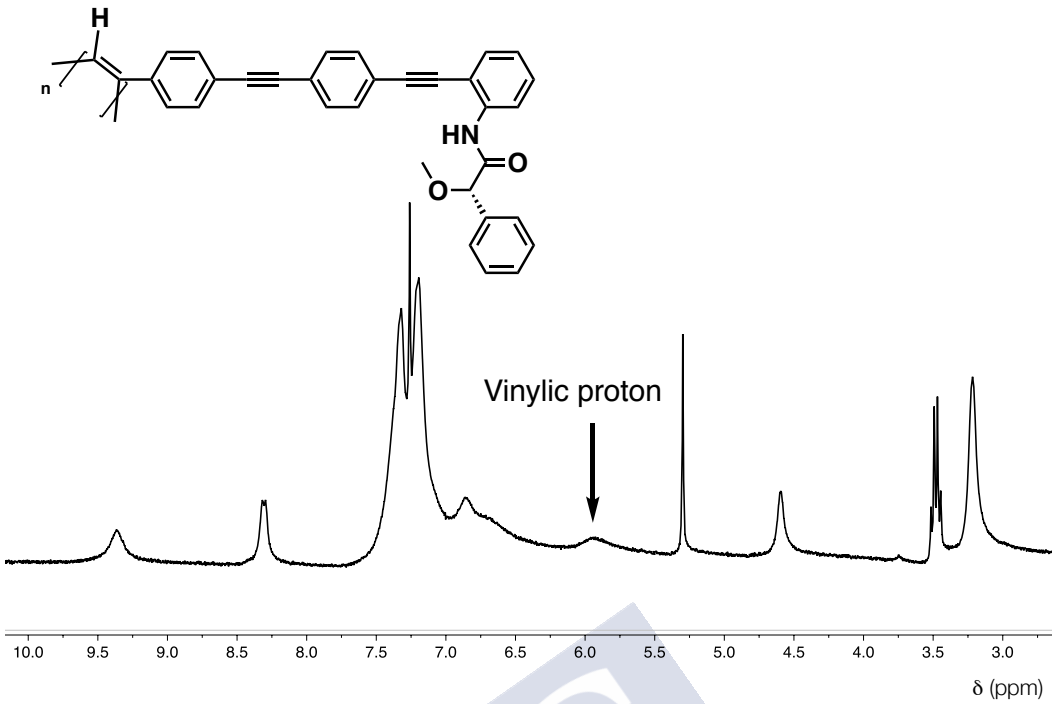

Figure S14. ^{1}H-NMR for *o*-poly-**3** in $CDCl_3$.

The bands observed by Raman resonance confirmed the former configuration. The peak at highest wavelength corresponds to the C=C bond stretching and overlaps with that of the phenyl ring. The band at 1350-1340 cm^{-1} is arisen from the *cis* C-C bond coupled with the single bond connecting the main chain and the phenyl ring. The peak at lowest wavelength corresponds to the C-H bond of the *cis* form. The disappearance of the alkyne band (ca. 2110 cm^{-1}) confirms the formation of the conjugated double bonds of the polymer backbone.

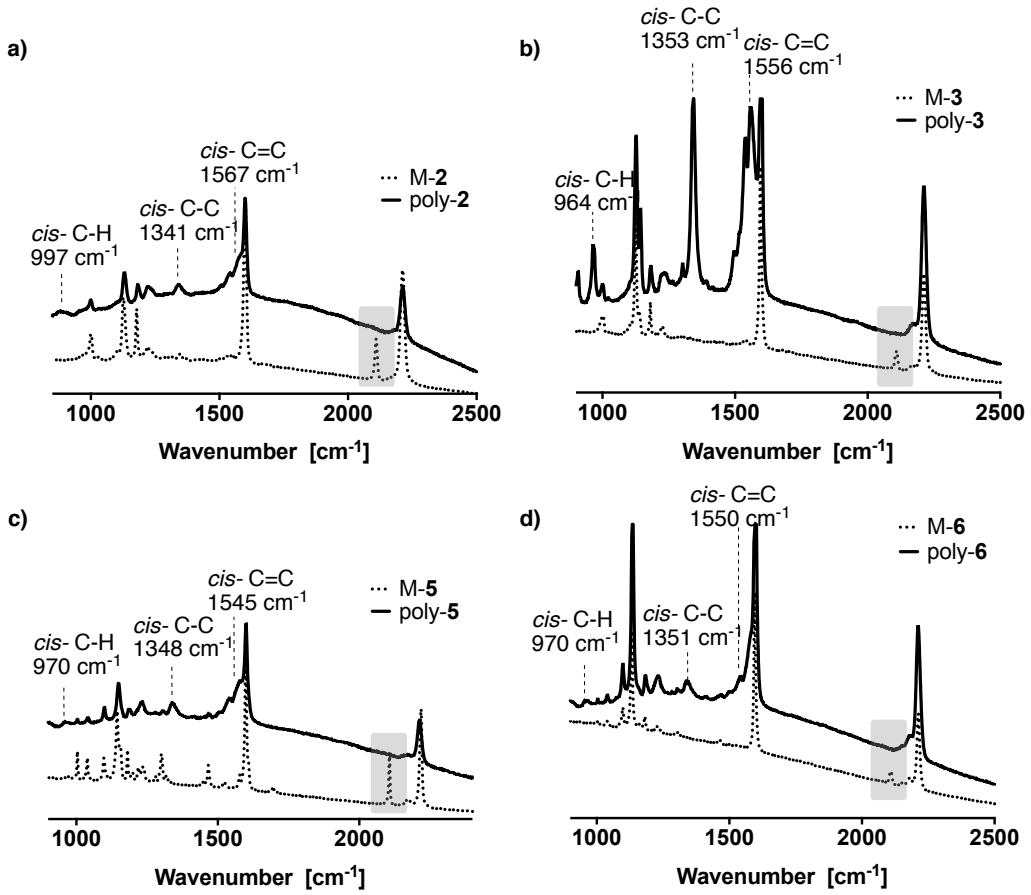

Figure S15. Raman spectra for (a) *m*-poly-**2**, (b) *o*-poly-**2**, (c) *m*-poly-**3** and (d) *o*-poly-**3**.

4. GPC Studies

The molecular weight was estimated by GPC using THF (flow rate: 1 mL·min^{-1}) as eluent and polystyrene narrow standards (PSS) as calibrants.

Table S2. GPC data for the synthesized polymers.

Polymer	Mn	Mw	Mz	PDI
m-poly-**2**	6029	15902	76416	2.64
m-poly-**3**	10387	23031	71395	2.13
o-poly-**2**	13328	27604	58162	2.07
o-poly-**3**	9650	23898	60616	2.48

5. Thermal studies

5.1. DSC Studies

The geometry of the polymer was determined by DSC studies. The thermograms for *m*-poly-**2** and *m*-poly**-3** are related to a *c*-*t* backbone, where the two exothermal peaks observed are arised from the *c*-*t* to *c*-*c* and *c*-*c* to *t*-*t* transitions respectively. The

thermograms for *o*-poly-**2** and *o*-poly-**3** show a typical *c*-*c* trace with an exothermal peak around 200-210 °C, corresponding to a *t*-*t* transition.

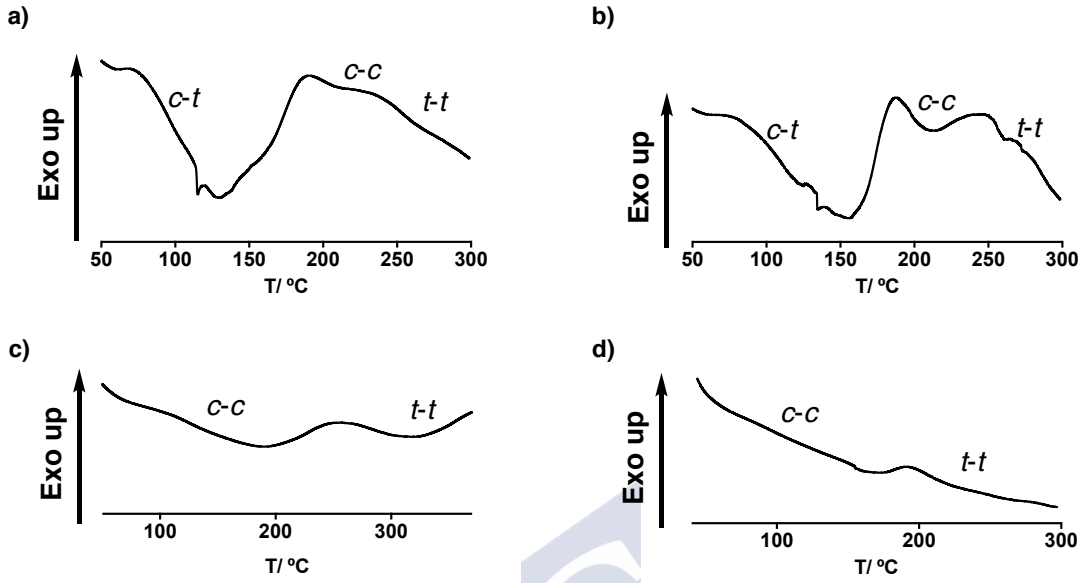

Figure S16. DSC thermograms for (a) *m*-poly-**2**, (b) *o*-poly-**2**, (c) *m*-poly-**3** and (d) *o*-poly-**3**.

5.2. TGA Studies

The thermal stability was evaluated by TGA studies. It varies between 300-350 °C.

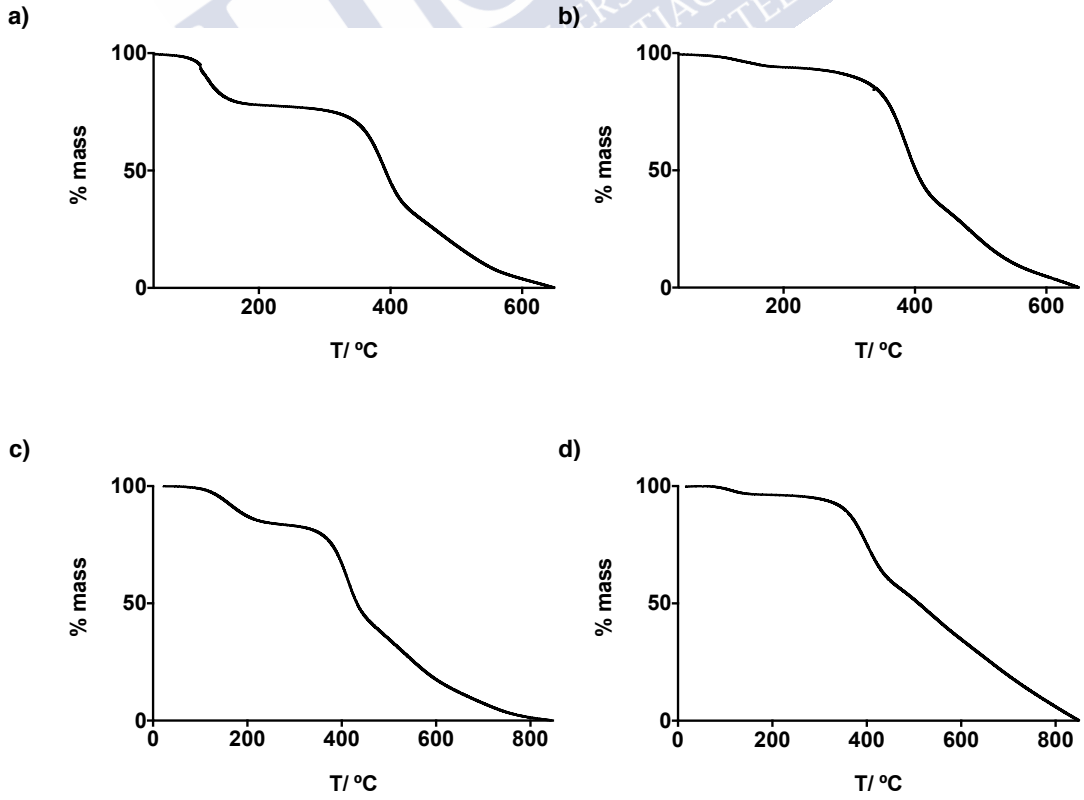

Figure S17. TGA traces for (a) *m*-poly-**2**, (b) *o*-poly-**2**, (c) *m*-poly-**3** and (d) *o*-poly-**3**.

6. Behaviour in Solution

All polymers were tested in different solvents. In any case the polarity affects the helical sense of the polymer.

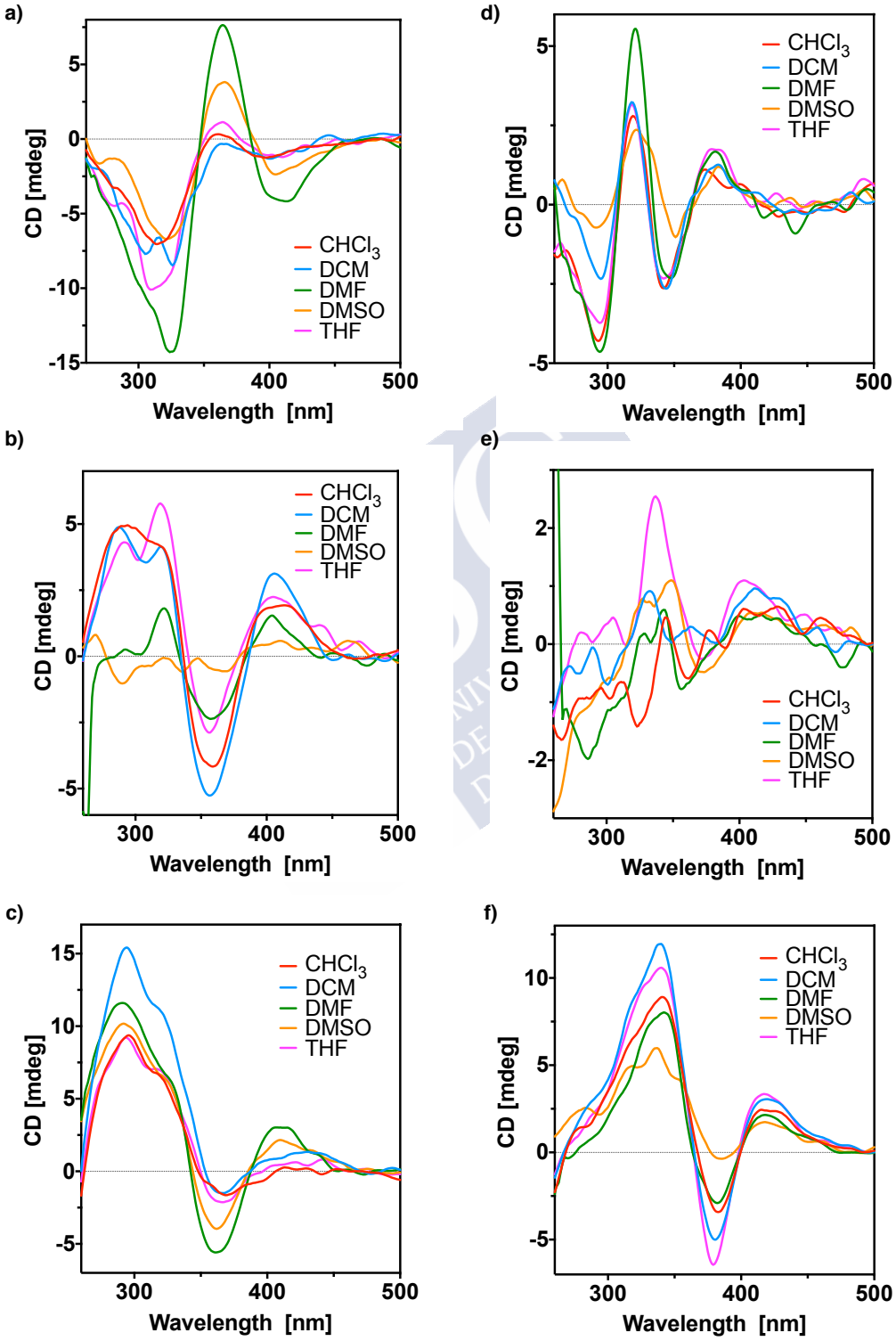

Figure S18. CD spectra for (a) *p*-poly-**2** (0.2 mg·mL^{-1}), (b) *m*-poly-**2** 0.2 mg·mL^{-1}), (c) *o*-poly-**2** (0.2 mg·mL^{-1}), (d) *p*-poly-**3** (0.2 mg·mL^{-1}), (e) *m*-poly-**3** (0.2 mg·mL^{-1}) and (f) *o*-poly-**3** (0.1 mg·mL^{-1}) evaluated in different solvents.

7. VT-CD experiments

In all cases a decrease of the CD intensity is observed when increasing the temperature.

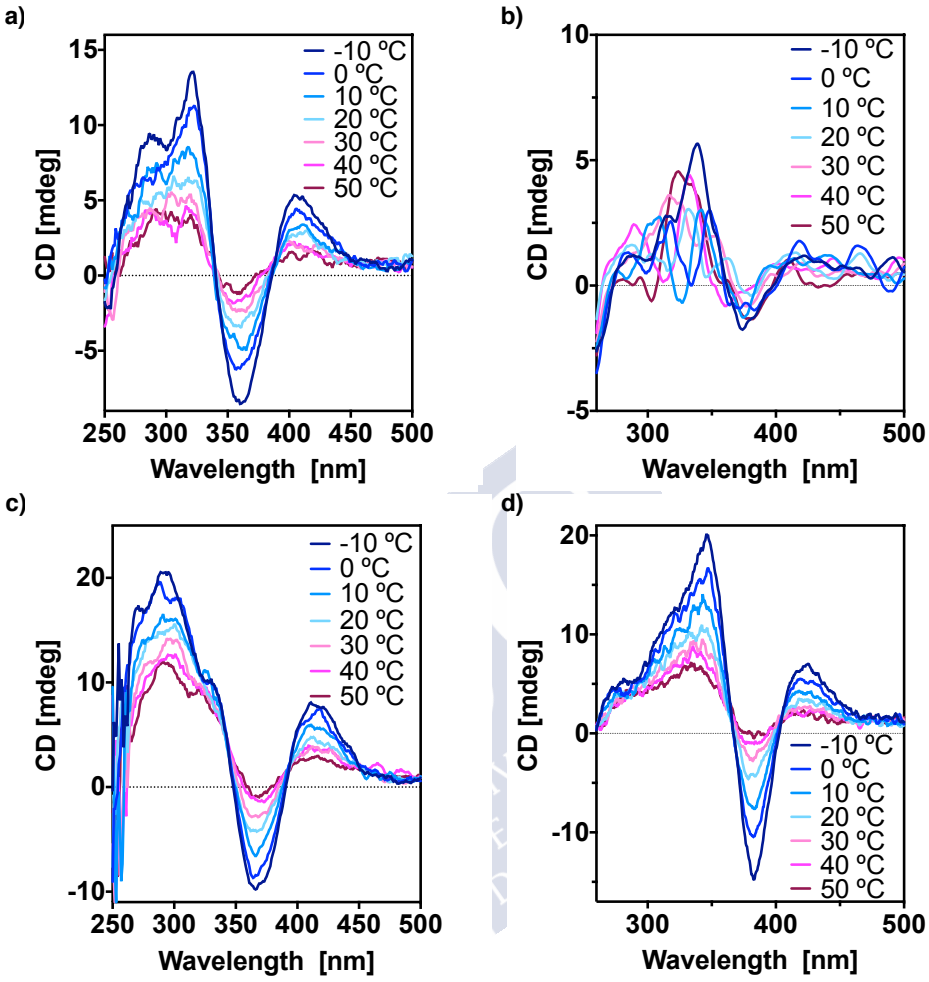

Figure S19. VT-CD for (a) *m*-poly-**2** (DCM), (b) *m*-poly-**3** (THF) (c) *o*-poly-**5** (DMF) and (d) *o*-poly-**6** (DCM). Heating rate 10 °C·min^{-1}.

USC
UNIVERSIDADE
DE SANTIAGO
DE COMPOSTELA

Experimental Section

Chapter III

USC
UNIVERSIDADE
DE SANTIAGO
DE COMPOSTELA

1. Materials and Methods

CD measurements were done in a Jasco-1100 and UV spectra were registered in a Jasco V-630. These measurements were performed in a 1mm quartz. The concentration of the supramolecular polymer used is indicated in the corresponding section.

VT-CD was measured in a Jasco-1100 using a 1mm quartz cuvette.

VT-UV was measured in a Jasco V-630.

AFM measurements were performed in a Multimode V Scanning Probe Microscope (Veeco Instruments) in air at r.t., with standard silicon cantilevers and supersharp cantilevers in tapping mode using 12 mm and 1 mm scanners. Nanoscope processing software and WSxM 4.0 Beta 1.0 [4] (Nanotec Electrónica, S.L.) were used for image analysis. All measurements were performed at CACTI (Vigo University, Spain).

PyMOL was used as a molecular visualization system.

2. Synthesis of the Monomer

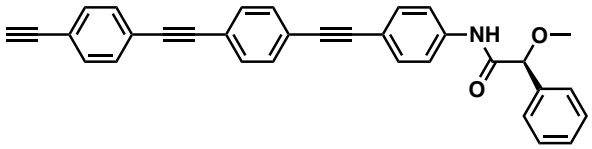

1

Compound **1** was prepared according to a previously reported procedure.[S1]

[S1] Fernández, Z.; Fernández, B.; Quiñoá, E.; Riguera, R.; Freire, F. *Chem. Commun.* **2020**, *11*, 7182-7187.

3. Stability Studies for Agg_{II}

The stability of the **Agg_{II}** was also evaluated over time. The CD trace obtained after keeping the solution of **Agg_{II}** for two days at r.t. is almost the same as the one acquired for the freshly prepared solution. The slight decrease in the CD over time is concomitant with a modification in the UV spectra.

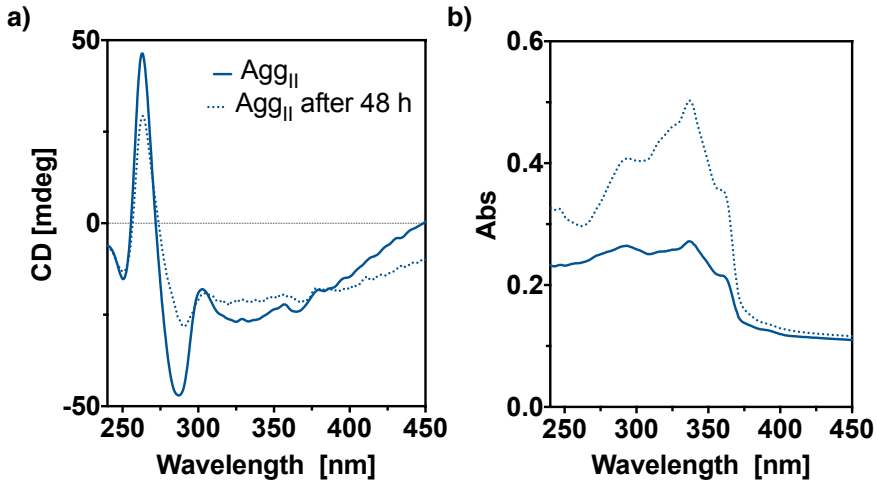

Figure S1. (a) CD and (b) UV-Vis for the **Agg_{II}** comparing the freshly prepared solution with the same solution after two days.

4. Cooling curve 97% MCH:2% Toluene:1% DCM

Measuring the disassemble and assemble processes for **1** in these conditions —100 μM, 1 K min^{-1}— results in a large difference between the disassembly (T_e) and assembly (T_e') temperatures.

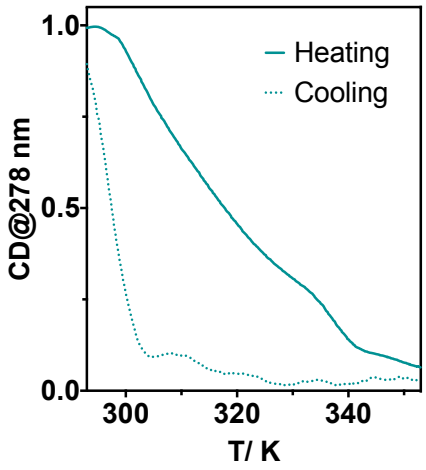

Figure S2. Heating and cooling curves for **1**.

5. Atomic Force Microscopy (AFM) Measurements

5.1. AFM Images obtained for Agg_I

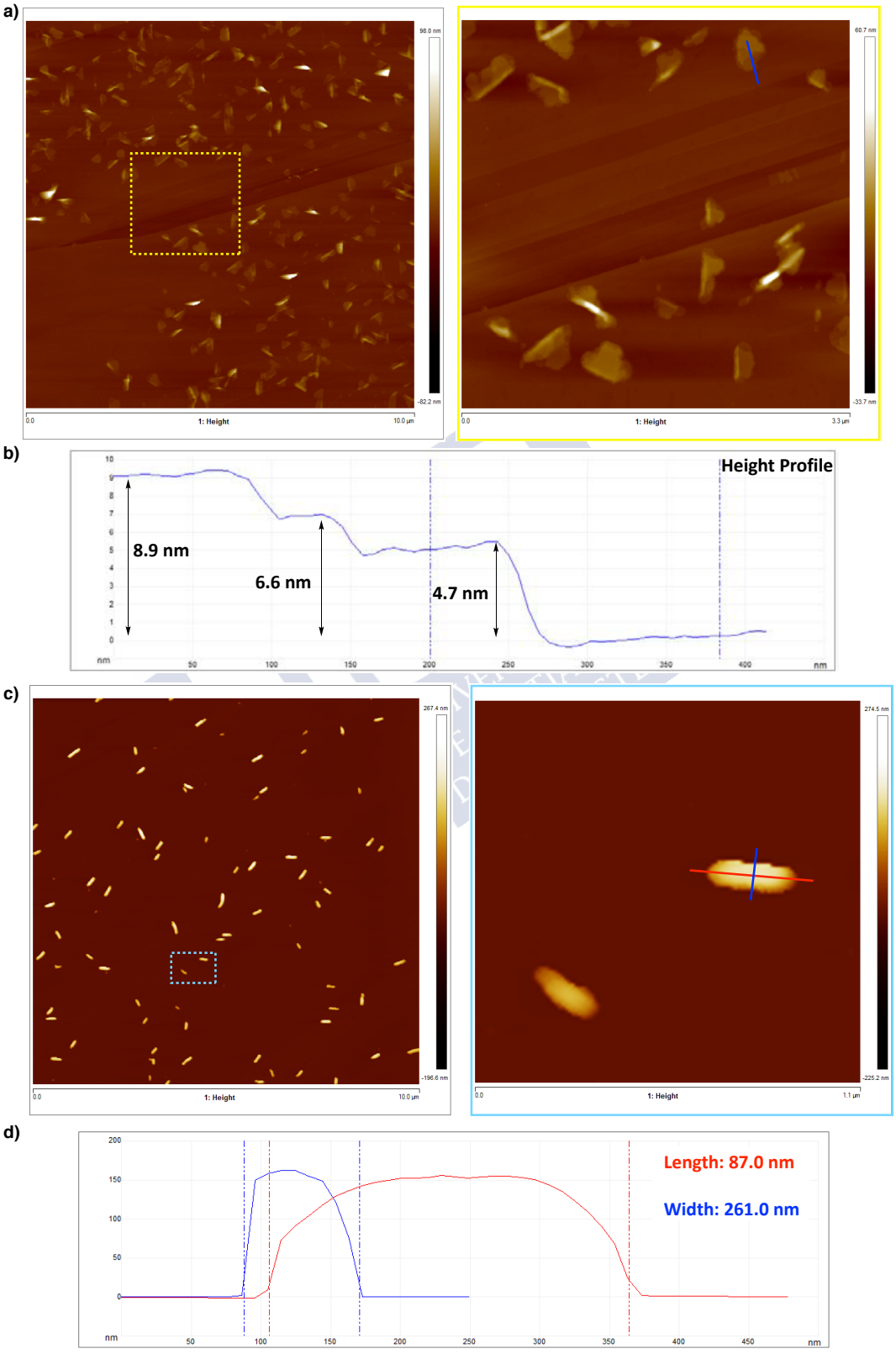

Figure S3. (a) AFM image and magnification. (b) Height profile of the sheet-like nanostructures. a) AFM image and magnification. (b) Height profile depicting the length and width of the brick-like nanostructure.

5.2. AFM Images obtained for Agg_{II}

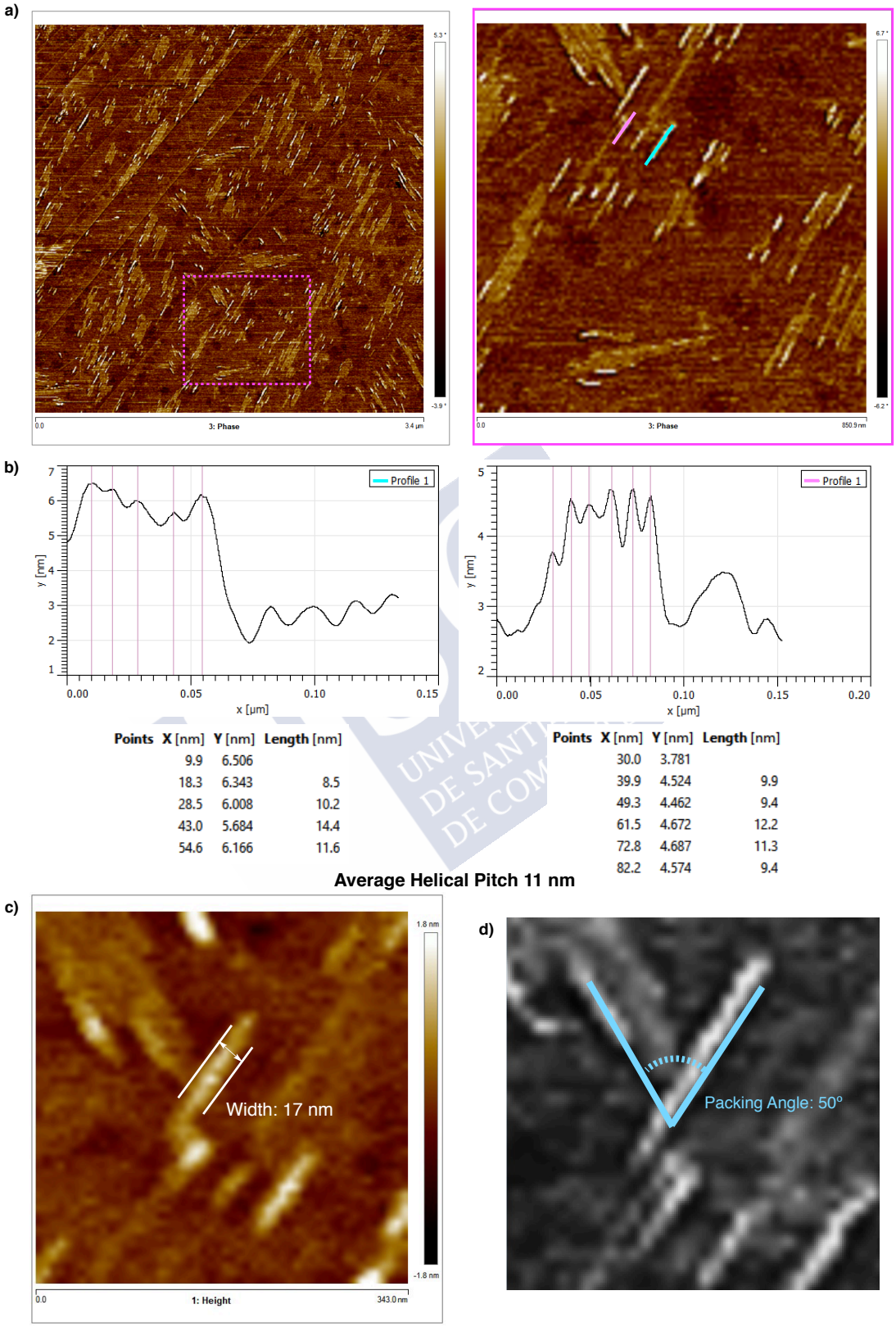

Figure S4. (a) AFM image and magnification of the highlighted area. (b) Profile depicting the helical pitch. (c) AFM image showing the helix width. (d). Packing angle obtained from the microscopy measurements.

6. Theoretical Studies

Considering the difficulties to carry out ECD theoretical calculations on large polymers, representative oligomers, interacting through π·π stacking and hydrogen bonding for stabilization, were used —n = 8 and 12, where n denotes the number of monomer repeating units (m.r.u.)—.

This selection of n is supported by the results of previous work,[S1-S3] where we evaluated the spectra for a series of oligomers obtained through systematic increase of monomer units. From these experiments we concluded that 8-10 (12) monomers were enough to describe the n+2 (n+3) polymers studied.

In order to get the n = 8 and 12 geometries, we started from the monomer and systematically added monomer units to it, obtaining the corresponding dimers, tetramers, octamers, and dodecamers.

The input structures used for the ECD calculations were simulated either with the chiral moieties stacked one on top of another (head-to-head, hh-geometry) or in an alternate fashion (head-to-tail, ht-geometry) and the pendant groups were introduced in the most stable (*ap*) conformation. For n up to 4 we used the CREST molecular dynamics program[S2] —to obtain the most convenient conformers in terms of stacking— and, thereafter, we optimized the geometries of those with significant populations at room temperature using DFT(B3LYP-D3)/6-31G** methodology. In this way, for the dimer two main conformers resulted, hh and ht, and the former was obtained as the most stable one, with an energy difference with respect to the latter of 6.7 kcal·mol^{-1}. This large energy gap implies a significant difference in population with respect to the ht-stacking at room temperature, indicating a negligible contribution of the ht-conformer to the spectra. Additionally, using the counterpoise correction, we evaluate DFT(B3LYP-D3)/6-31G** interaction energies for the hh and ht dimers, getting values of -24.7, and -11.7 kcal·mol^{-1}, respectively, which shows that the hh dimer is considerably more stable than the ht.

From the optimized dimers starting geometries for the 4-mers were constructed and following the same methodology, the most suitable conformers were obtained and optimized. From the final 4-mers we constructed the 8- and 12-mer structures. In all steps of the geometry assembly visual inspection of the conformers was mandatory in order to select the units that were adequate for an increase in oligomer size; hence, conformers with lack of order and monomers located at the edges of the oligomer needed to be disregarded. This resulted in the n = 8 **Agg$_{I}$** and n = 12 **Agg$_{II}$** geometries displayed in Figure S5. In the case of **Agg$_{II}$** (n = 12) and in order to lower the computational demands, we replaced the pendants by -NH-COH groups.

S1 Fernández, Z.; Fernández, B.; Quiñoá, E.; Riguera, R.; Freire, F. *Chem. Commun.* **2020**, *11*, 7182-7187.
S2 Fernández, B.; Rodríguez, R.; Rizzo, A.; Quiñoá, E.; Riguera, R.; Freire, F. *Angew. Chem. Int. Ed.* **2018**, *57*, 3666-3670.
S3 Fernández, B.; Rodríguez, R.; Quiñoá, E.; Riguera, R.; Freire, F. *ACS Omega* **2019**, *4*, 5233-5240.

The ECD computational methodology was selected according to the size of the polymers under investigation. Taking this into account, to evaluate the theoretical spectra we used time dependent density functional theory (TD-DFT),[S3] together with the CAM-B3LYP[S4] functional, and the 3-21G basis set.[S4] In previous work,[S5-S7] where we carried out systematic density functional and basis set selection studies for the evaluation of ECD spectra in poly(phenylacetylene)s (PPAs), this method-basis set combination proved to be a good choice to evaluate the spectra for long polymers.

Taking into account the tendency of the TD-DFT method to overestimate excitation energies, once the theoretical ECD spectra for the above mentioned oligomers were obtained and in order to carry out an efficient comparison to experiment, we applied the following correction. The theoretical spectra were adjusted to the experimental ones by comparing the wavelength and intensity at the maximum/minimum corresponding to the first Cotton effect. In this way, we evaluated a correction factor for lambda as the difference between theoretical and experimental wavelengths (at the first maximum/minimum) and shifted the theoretical spectrum accordingly. Regarding ECD intensity, the theoretical values were rescaled in order to be able to compare them to the experimental ones.

The resulting theoretical ECD spectra are in good agreement with their experimental counterparts. Both, for **Agg$_I$** and **Agg$_{II}$**, the spectra are dominated by two bands. By way of example, **Agg$_I$** displays a positive band at ca. 299 nm (dominated by the S_0 to S_7 excitation) and a negative one around 278 nm (dominated by the S_0 to S_9 transition). To get more insight into these spectral bands, the electron density difference for the corresponding transitions at the TD-DFT(CAM-B3LYP)/3-21G level of theory (isovalue = 0.0002) was evaluated (Figure S5).

S3 Fernández, B.; Rodríguez, R.; Quiñoá, E.; Riguera, R.; Freire, F. *ACS Omega* **2019**, *4*, 5233-5240.
S4 Grimme, S. *J. Chem. Theor. Comput.* **2019**, *15*, 2847-2862.
S5 Runge, E.; Gross, E. K. U. *Phys. Rev. Lett.* **1984**, *52*, 997-1000.
S6 Yanai, Y.; Tew, D. P.; Handy, N. C. *Chem. Phys. Lett.* **2005**, 393, 51-57.
S7 Binkley, J. S.; Pople, J. A.; Hehre, W. J. *J. Am. Chem. Soc.* 1980, 102, 939-947.

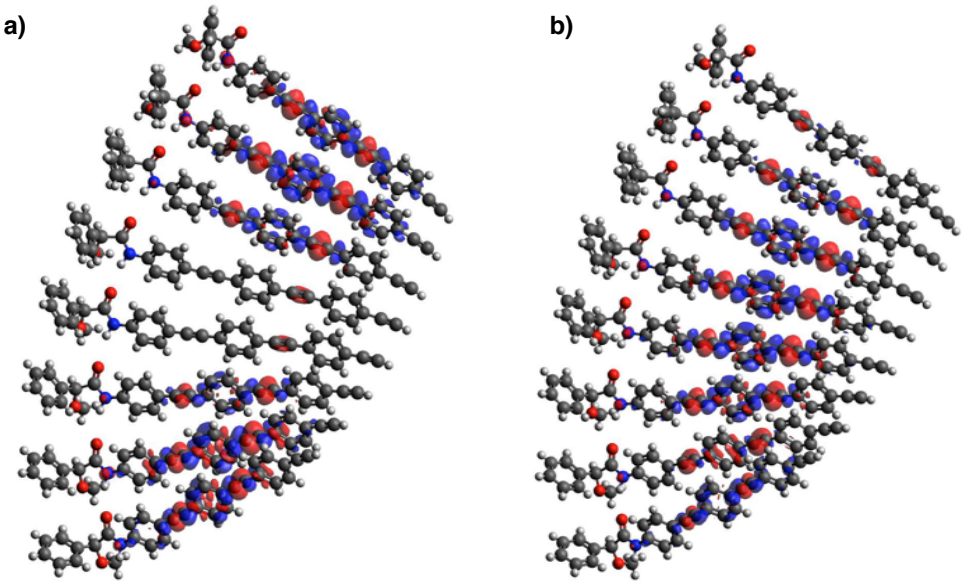

Figure S5. TD-DFT (CAM-B3LYP)/3-21G (a) S0 → S7 and (b) S0 → S9 electron density differences for the modeled p3SMPA-hh 8-mer: with the rotation axis passing through the extreme rings.

We carried out the ECD calculations with the ORCA program (80 excitations were included).[S8] To plot the spectra we used the Gabedit[S9] code and for the density differences Avogadro.[S10] We selected a Full-Width at Half Height (FWHM) of 20.0 nm and gaussian curves for the ECD plots.

[S8] Neese, F. *WIREs Comput Mol Sci*. **2012**, *2*, 73-78.
[S9] Allouche, A. R. *J. Comput. Chem.* **2011**, *32*, 174-182.
[S10] Hanwell, M. D.; Curtis, D. E.; Lonie, D. C.; Vandermeersch, T.; Zurek, E.; Hutchison, G. R. *Journal of Cheminformatics* **2012**, *4*, 17.

Experimental Section

Chapter IV

USC
UNIVERSIDADE
DE SANTIAGO
DE COMPOSTELA

1. Materials and Methods

Polymer solutions were prepared by weighting the monomer and adding the necessary ammount of MCH to obtain the desired concentration. To completetly solubilize the monomer the mixture was heated up to 80 ºC for two hours.

CD measurements were done in a Jasco-720 and UV spectra were registered in a Jasco V-630.

VT-CD were measured in a Jasco-1100.

VT-UV-Vis studies were performes in a Jasco-620.

PyMOL was used as a molecular visualization system.

2. Synthesis of Monomers

Synthesis of heptyl-4-iodobenzoate (**1**)

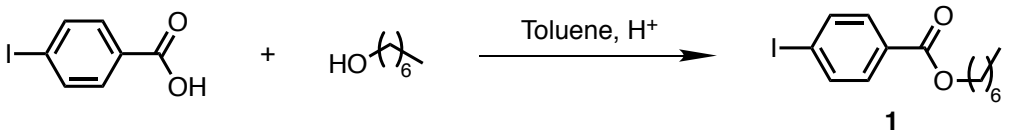

1

4-iodobenzoic acid (6.00 g, 24.19 mmol, 1 equiv.), 1-heptanol (6.50 mL, 45.96 mmol, 1.90 equiv.), toluene (50 mL) and a catalytic amount of H_2SO_4 (0.10 mL) were introduced in a round bottom flask fitted with a Dean-Stark. The mixture was heated at reflux temperature overnight. The organic phase was washed twice with Milli-Q water and brine. The crude product was chromatographed on silica gel (70-230 mesh) using hexane as eluent, obtaining **1** an orange oil (8.60 g, 97% of yield).

^{1}H NMR (300 MHz, $CDCl_3$) δ_H (ppm): 7.79 (d, 2H), 7.73 (d, 2H), 4.29 (t, 2H), 1.84-1.67 (m, 2H), 1.50-1.17 (m, 8H), 0.88 (t, 3H).

^{13}C NMR (75 MHz, $CDCl_3$) δ_C (ppm): 166.1, 137.6, 131.0, 130.0, 100.5, 65.4, 31.7, 28.9, 28.7, 26.0, 22.6, 14.1.

HRMS (APCI) m/z calcd for $C_{14}H_{19}IO_2$ $[M+H]^+$: 347.0430, found: 347.0500.

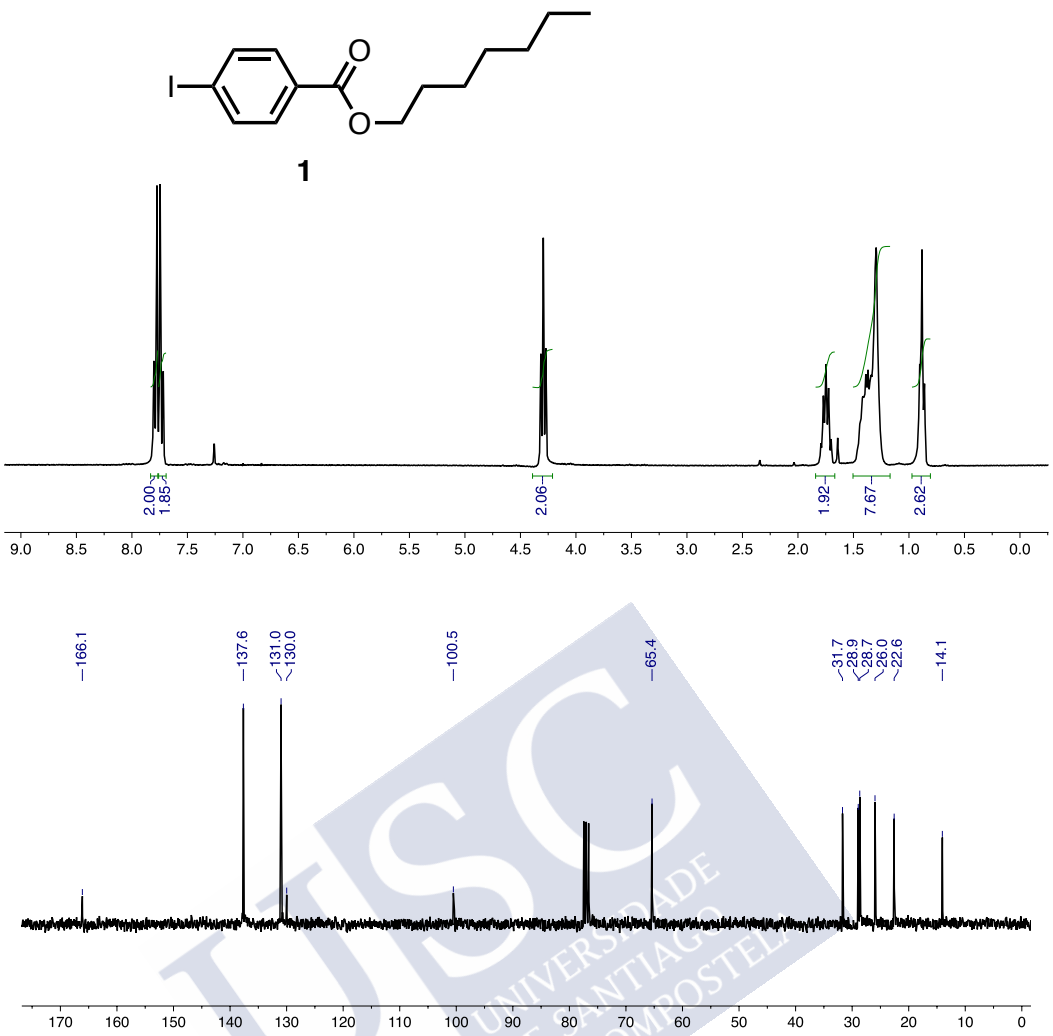

Figure S1. ^{1}H·NMR and ^{13}C·NMR of **1** in $CDCl_3$.

Syntesis of heptyl 4-((trimethylsilyl)ethynyl)benzoate (**2**)

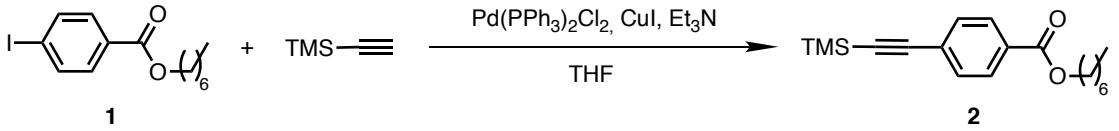

Heptyl-4-iodobenzoate (8.00 g, 23.10 mmol, 1.00 equiv.), bis(triphenylphosphine)palladium(II) dichloride ($Pd(PPh_3)_2Cl_2$, 0.32 g, 0.46 mmol, 0.02 equiv.) and copper iodide (CuI, 0.09 g, 0.46 mmol, 0.02 equiv.) were dissolved in dry THF (50 mL). Next triethylamine (Et_3N, 15 mL) and ethynyltrimethylsilane (3.20 mL, 23.10 mmol, 1.00 equiv.) were added and the mixture was stirred for three hours at room temperature. After removing the solvent, the crude product was chromatographed on silica gel (70-230 mesh) using hexane as eluent (7.00 g, 96% of yield).

^{1}H NMR (300 MHz, $CDCl_3$) δ_H (ppm): 7.96 (d, 2H), 7.73 (d, 2H), 4.29 (t, 2H), 1.84-1.66 (m, 2H), 1.47-1.18 (m, 8H), 0.88 (t, 3H), 0.26 (s, 7H).

^{13}C NMR (75 MHz, $CDCl_3$) δ_C (ppm): 166.0, 131.8, 130.1, 129.3, 127.6, 104.1, 97.5, 65.3, 31.7, 28.9, 28.7, 26.0, 22.6, 14.0, -0.2.

HRMS (APCI) m/z calcd for $C_{19}H_{29}O_2Si$ $[M+H]^+$: 317.1859, found: 317.1928.

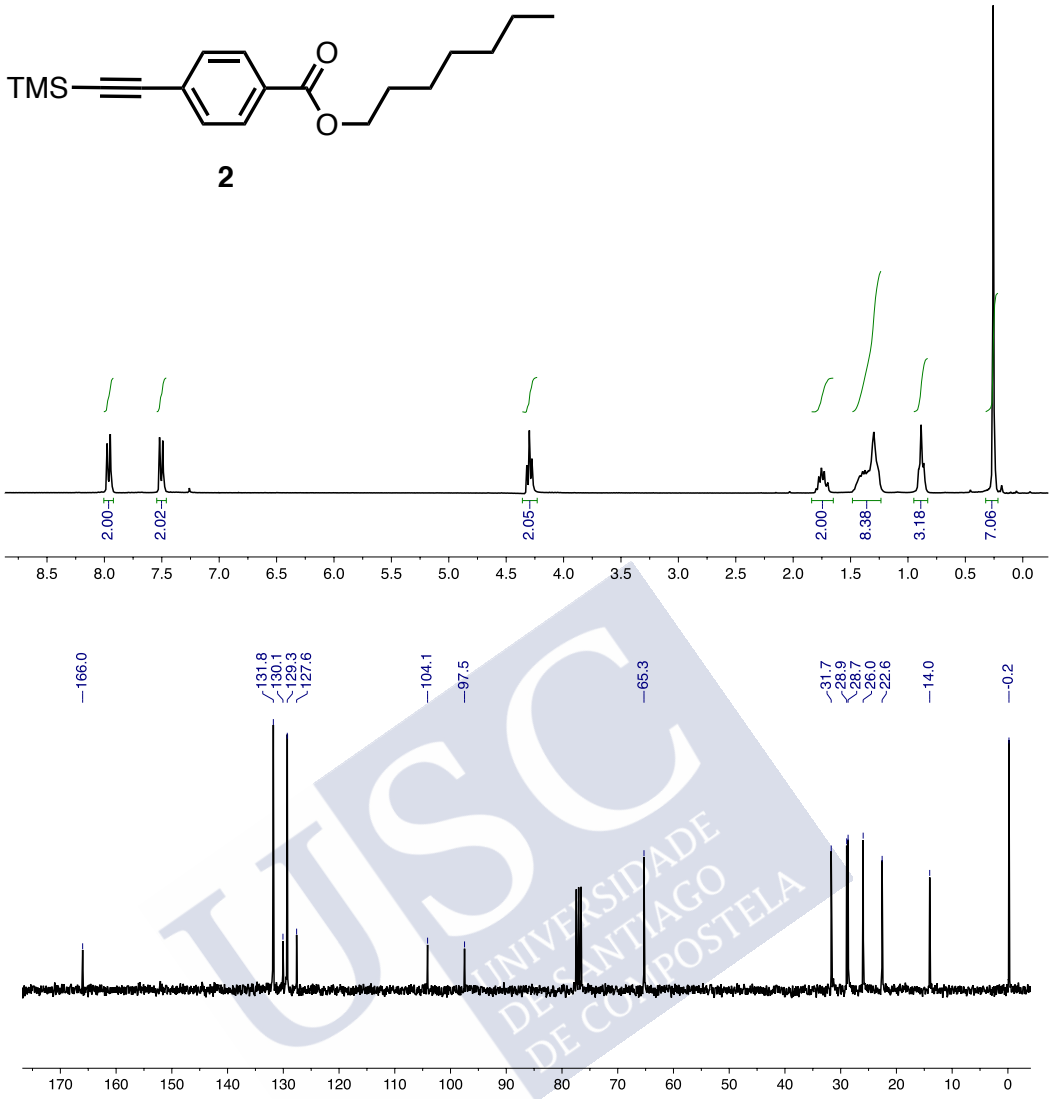

Figure S2. ^{1}H-NMR and ^{13}C-NMR of **2** in $CDCl_3$.

Synthesis of heptyl 4-ethynylbenzoate (**3**)

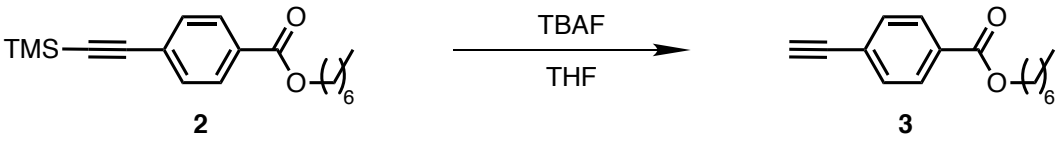

2 **3**

Heptyl 4-((trimethylsilyl)ethynyl)benzoate (7.00 g, 22.11 mmol, 1.00 equiv.) was dissolved in THF (50 mL). Next TBAF (1M in hexane, 26.54 mL, 26,54 mmol, 1.20 equiv.) was added and the reaction was stirred at r.t. for 15 minutes. After this time the organic solvent was removed and the crude was chromatographed on silica gel (70-230 mesh) with hexane/ethyl acetate (80:20) as eluent (4.21 g, 77% of yield).

^{1}H NMR (300 MHz, $CDCl_3$) δ_H (ppm): 7.85 (d, 2H), 7.53 (d, 2H), 4.30 (t, 2H), 3.22 (s, 1H), 1.89-1.66 (m, 2H), 1.51-1.20 (m, 8H), 0.88 (t, 3H).

^{13}C NMR (75 MHz, $CDCl_3$) δ_C (ppm): 165.9, 132.0, 130.5, 129.4, 126.6, 82.8, 79.9, 65.4, 31.7, 28.9, 28.7, 26.0, 22.6, 14.0.

HRMS (APCI) m/z calcd for $C_{16}H_{22}O_2$ $[M+H]^+$: 245.1463, found: 245.1535.

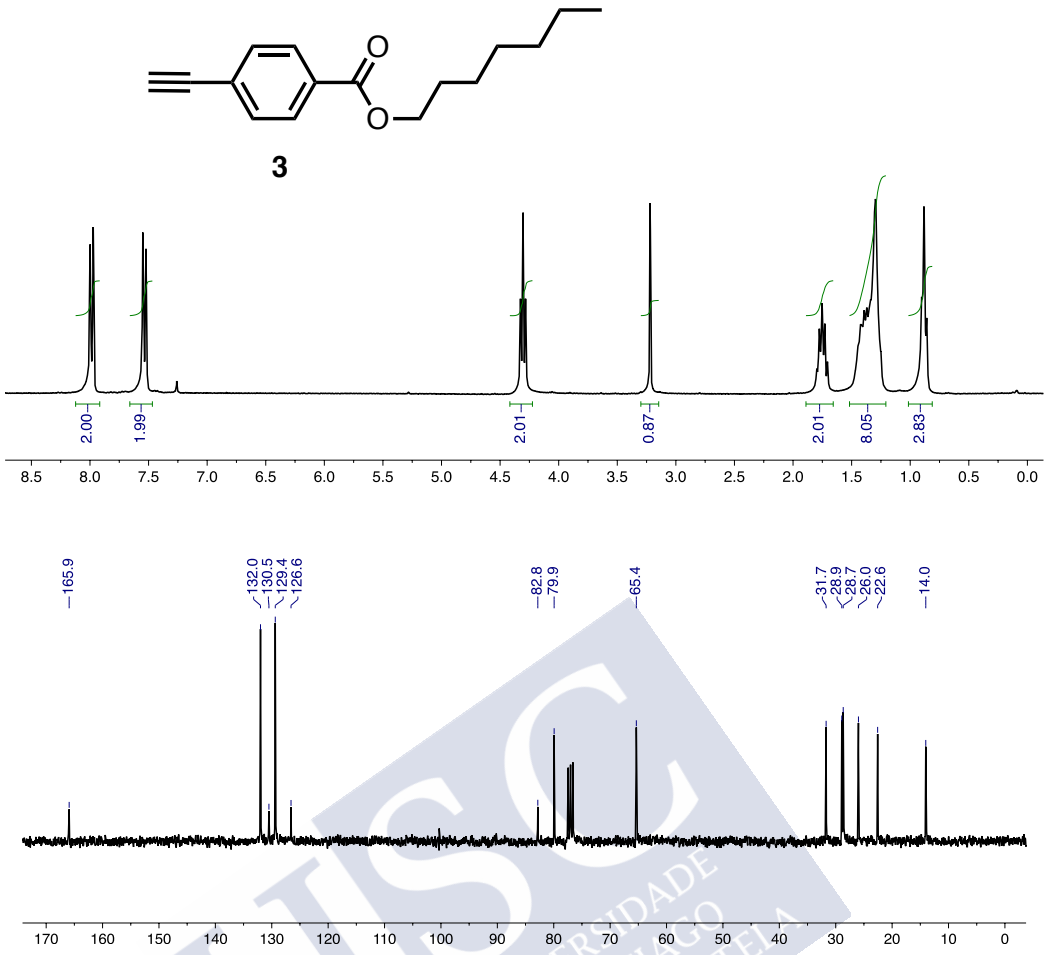

Figure S3. ^{1}H-NMR and ^{13}C-NMR of **3** in $CDCl_3$.

Synthesis of heptyl 4-((4-((trimethylsilyl)ethynyl)phenyl)ethynyl)benzoate (**4**)

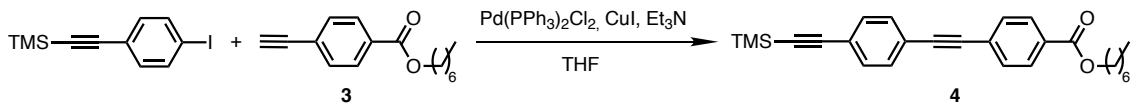

((4-iodophenyl)ethynyl)trimethylsilane (3.68 g, 12.27 mmol, 1.00 equiv.), bis(triphenylphosphine)palladium(II) dichloride ($Pd(PPh_3)_4$, 0.85 g, 0.73 mmol, 0.02 equiv.) and copper iodide (CuI, 0.14 g, 0.73 mmol, 0.02 equiv.) were dissolved in dry Et_3N (40 mL). Next heptyl 4-ethynylbenzoate (3.68 g, 12.27 mmol, 1.00 equiv.) was dissolved in $CHCl_3$ and added to the reaction. The mixture was stirred at 40 °C for three hours. After removing the solvent the crude product was chromatographed on silica gel (70-230 mesh) with hexane/dichloromethane (90:10) as eluent (4.02 g, 78% of yield).

^{1}H NMR (300 MHz, $CDCl_3$) δ_H (ppm): 8.02 (d, 2H), 7.57 (d, 2H), 7.46 (s, 4H), 4.32 (t, 2H), 1.84-1.65 (m, 2H), 1.50-1.18 (m, 8H), 0.90 (t, 3H), 0.25 (s, 7H).

^{13}C NMR (75 MHz, $CDCl_3$) δ_C (ppm): 166.0, 131.9, 131.5, 131.5, 130.0, 129.5, 127.5, 123.4, 122.7, 104.5, 96.6, 91.8, 90.5, 65.3, 31.7, 28.9, 28.7, 26.0, 22.6, 14.1, -0.1.

HRMS (ESI) m/z calcd for $C_{27}H_{32}O_2Si$ $[M+H]^+$: 417.2172, found: 417.2242.

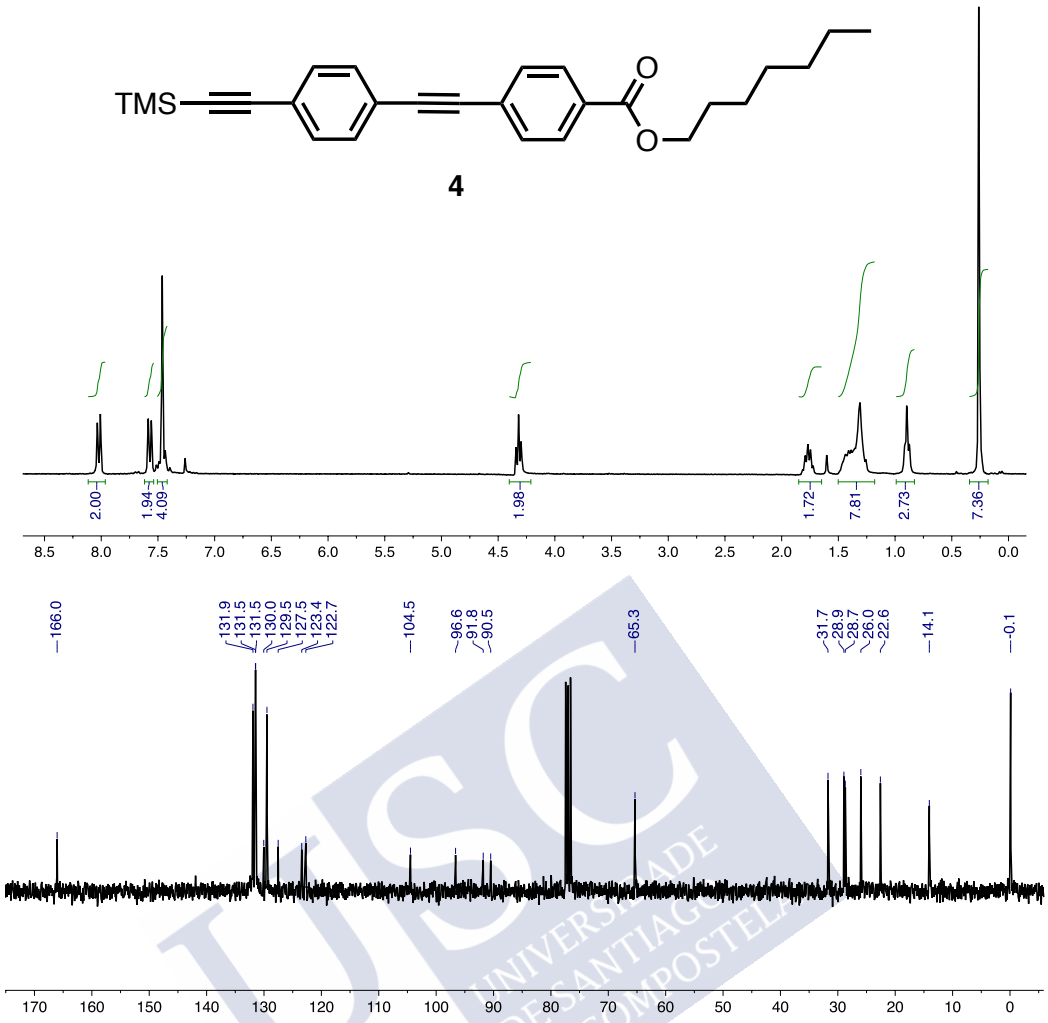

Figure S4. ^{1}H-NMR and ^{13}C-NMR of **4** in $CDCl_3$.

Synthesis of 4-((4-ethynylphenyl)ethynyl)benzoic acid (**5**)

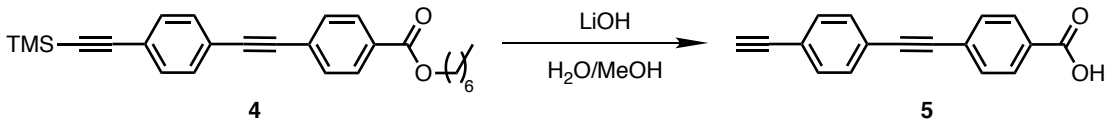

4 **5**

Heptyl 4-((4-((trimethylsilyl)ethynyl)phenyl)ethynyl)benzoate (4.00 g, 9.60 mmol, 1.00 equiv.) was dissolved in MeOH (50 mL). Then Milli-Q water (30 mL) and LiOH (1.15 g, 48.00 mmol, 5.00 equiv.) were added to the solution and the mixture was stirred at 60 °C. Upon completion of the reaction the solvent was removed under reduced preassure. The residue was redisolved in a small amount of water and acidified to pH = 1. After extracting with ethyl acetate (4 times), the solution was dried over Na_2SO_4. Next, the organic solvent was removed obtaining the product as an orange solid (2.00 g, 85% of yield).

^{1}H NMR (300 MHz, DMSO) δ_H (ppm): 13.18 (s, 1H), 7.96 (d, 2H), 7.66 (d, 2H), 7.58 (d, 2H), 7.52 (d, 2H), 4.37 (s, 1H).

^{13}C NMR (75 MHz, DMSO) δ_C (ppm): 171.8, 137.3, 137.0, 136.8, 136.0, 134.8, 131.4, 127.6, 127.4, 96.4, 95.7, 88.3.

HRMS (ESI) m/z calcd for $C_{17}H_{10}O_2$ $[M+H]^+$: 247.0681 , found: 247.0752.

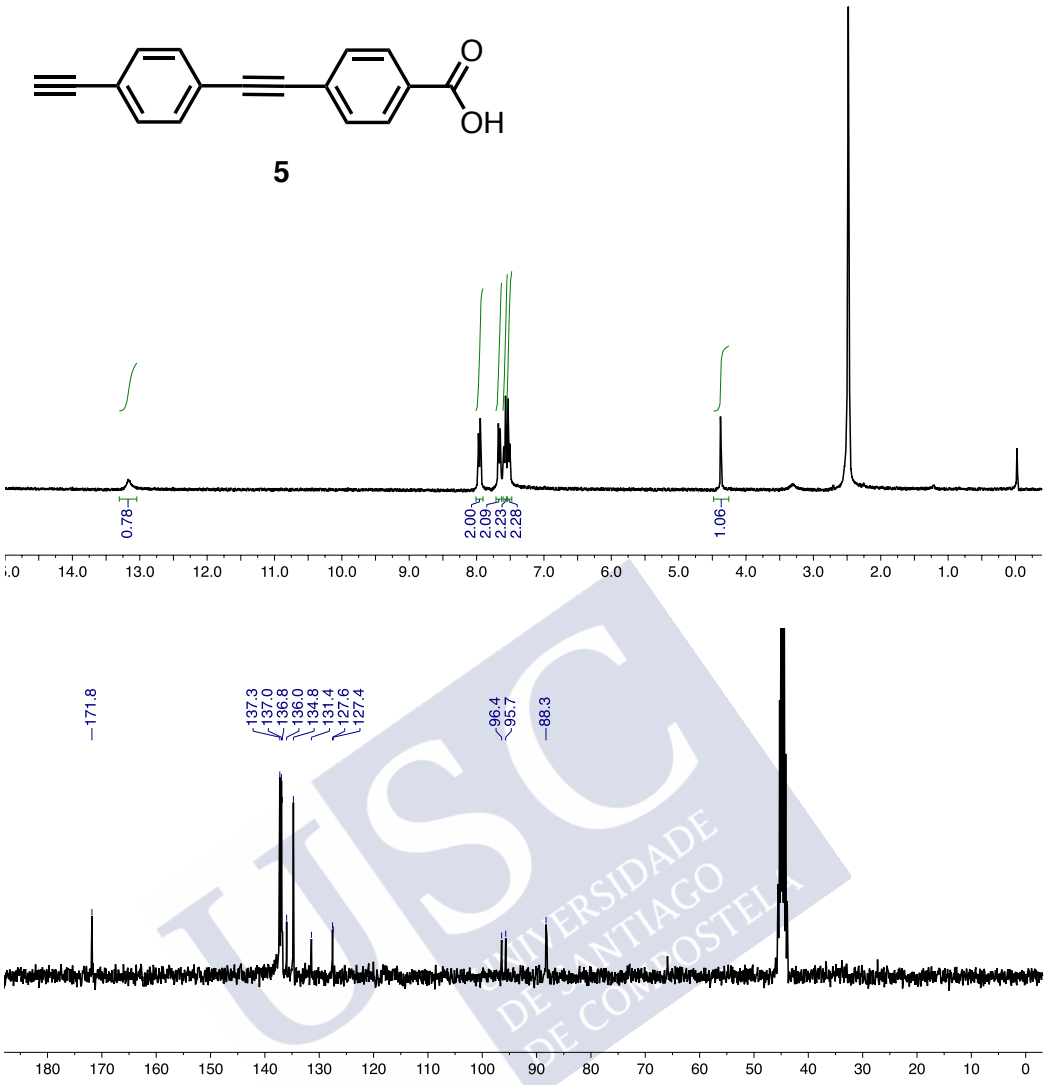

Figure S5. ^{1}H-NMR and ^{13}C-NMR of **5** in DMSO-d_6.

Synthesis of decyl (*tert*-butoxycarbonyl)-*L*-alaninate (**6**)

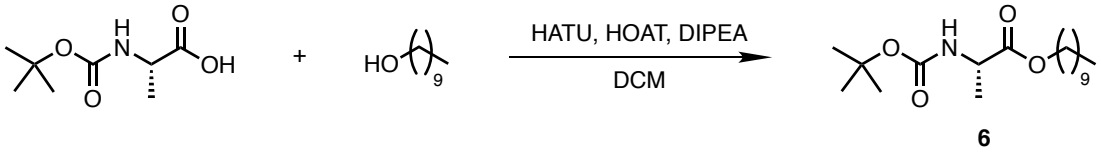

6

N-(tert-Butoxycarbonyl)-*L*-alanine (2.00 g, 10.60 mmol, 1.00 equiv.), 2-(7-Aza-1H-benzotriazole-1-yl)-1,1,3,3-tetramethyluronium (HATU, 4.22 g, 11.10 mmol, 1.05 equiv.), 1-hydroxy-7-azabenzotriazole (HOAt, 1.51 g, 11.10 mmol, 1.05 equiv.) and diisopropyltriethylamine (DIPEA, 2.22 mL, 12.68 mmol, 1.20 equiv.) were dissolved in 50 mL of dry CH_2Cl_2. After 15 minutes, time needed to activate the acid, 1-decanol (2.00 mL, 10.60 mmol, 1.00 equiv.) was added and the mixture was stirred overnight. The crude product was chromatographed on silica gel (70-230 mesh) with hexane/ethyl acetate (90:10) as eluent (1.48 g, 43% of yield).

^{1}H NMR (300 MHz, $CDCl_3$) δ_H (ppm): 5.11 (s, 1H), 4.25 (s, 1H), 2.20 (s, 2H), 1.65-1.52 (m, 2H), 1.48-1.16 (m, 26H), 0.98-0.76 (t, 3H).

^{13}C NMR (75 MHz, $CDCl_3$) δ_C (ppm): 173.4, 155.0, 79.6, 65.4, 49.2, 31.8, 29.4, 29.2, 29.1, 28.5, 28.3, 25.7, 22.6, 18.7, 14.0.

HRMS (ESI) m/z calcd for $C_{18}H_{36}NO_4$ $[M+H]^+$: 330.2566, found: 330.2638; calcd for $C_{18}H_{35}NO_3Na$ $[M+Na]^+$: 352.2566, found: 352.2462.

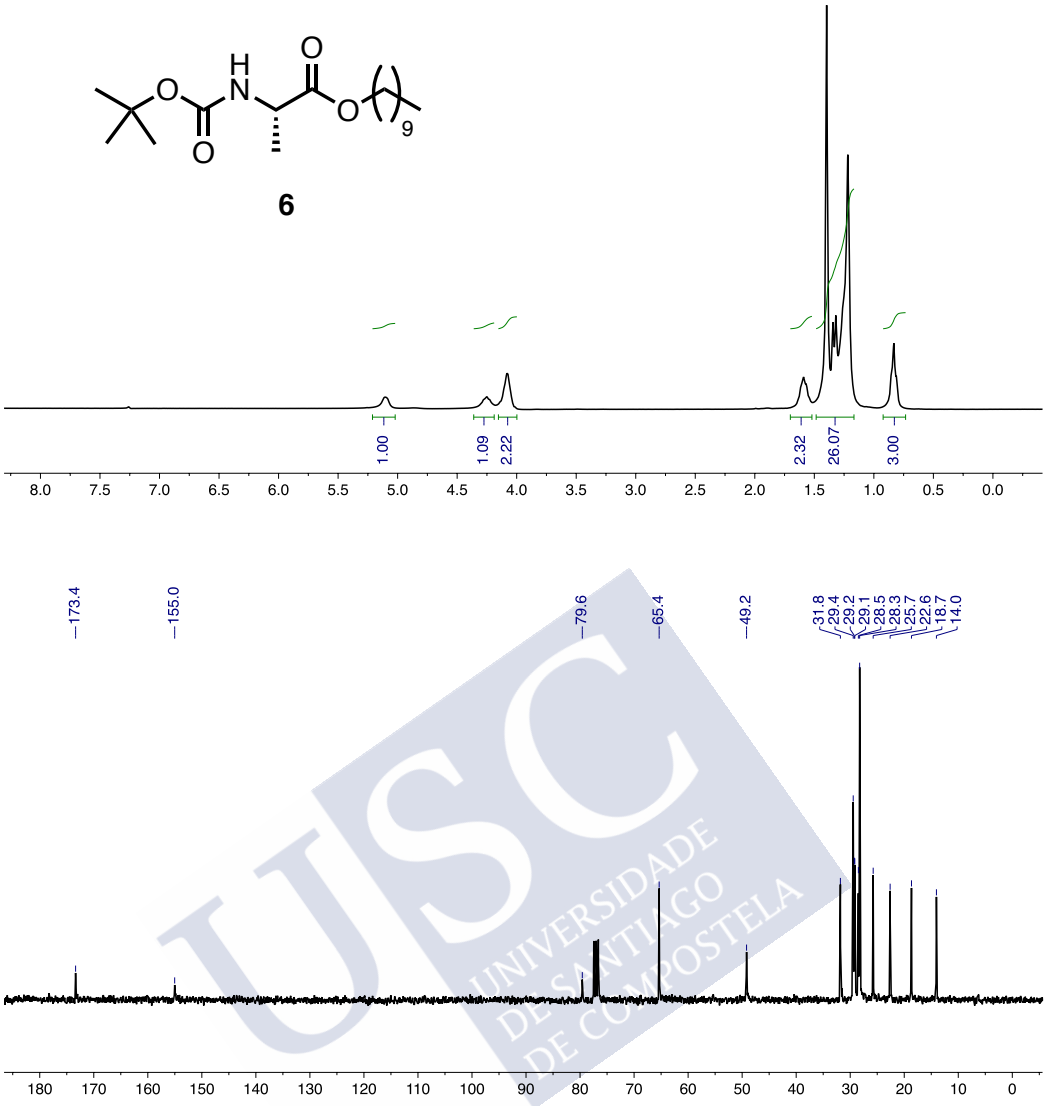

Figure S6. ^{1}H-NMR and ^{13}C-NMR of **6** in $CDCl_3$.

Synthesis of decyl (4-((4-ethynylphenyl)ethynyl)benzoyl)-*L*-alaninate (**7**)

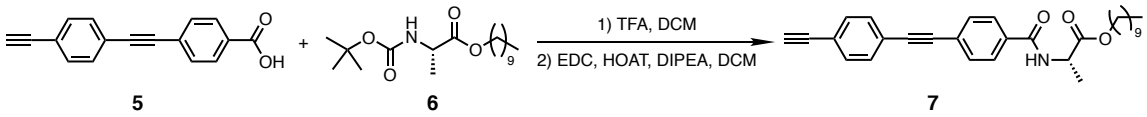

5 **6** **7**

Decyl (*tert*-butoxycarbonyl)-*L*-alaninate was disolved in DCM:TFA (7:3). After the completion of the reaction, the solvent was removed and the crude was washed twice with MeCN. Decyl *L*-alaninate was obtained as a colourless liquid.

4-((4-ethynylphenyl)ethynyl)benzoic acid (0.70 g, 2.84 mmol, 1.00 equiv.), *N*-(3-dimethylaminopropyl)-*N'*-ethylcarbodiimide hydrochloride (EDC, 0.57 g, 2.98 mmol, 1.05 equiv.), 1-hydroxy-7-azabenzotriazole (HOAt, 0.41 g, 2.98 mmol, 1.05 equiv.) and diisopropyltriethylamine (DIEA, 0.60 mL, 3.41 mmol, 1.20 equiv.) were dissolved in 30 mL of dry CH_2Cl_2. After 15 minutes, time needed to activate the acid, decyl (*L*)-alaninate (0.94 g, 2.84 mmol, 1.00 equiv.) was added and the mixture was stirred overnight. The organic layer was washed three times with HCl 1M, a saturated solution of $NaHCO_3$ and brine. The combined organic layers were dried over anhydrous Na_2SO_4, filtered and evaporated at reduced pressure. The crude product was chromatographed on silica gel (70-230 mesh) with hexane/ethyl acetate (80:20) as eluent (0.25 g, 78% of yield).

^{1}H NMR (300 MHz, $CDCl_3$) δ_H (ppm): 7.82 (d, 2H), 7.59 (d, 2H), 7.50 (s, 4H), 6.86 (d, 1H), 4.88-4.73 (q, 1H), 4.26-4.14 (m, 2H), 3.20 (s, 1H), 1.78-1.63 (m, 2H), 1.54 (d, 3H), 1.42-1.24 (m, 14H), 0.93-0.85 (t, 3H).

^{13}C NMR (75 MHz, $CDCl_3$) δ_C (ppm): 173.3, 166.0, 133.4, 132.1, 131.7, 131.6, 127.1, 126.4, 123.2, 122.3, 91.2, 90.5, 83.2, 79.3, 65.8, 48.7, 31.9, 29.5, 29.3, 29.2, 28.5, 25.8, 22.7, 18.6, 14.1.

HRMS (ESI) m/z calcd for $C_{30}H_{35}NO_3$ $[M+H]^+$: 458.2717, found: 458.2688.

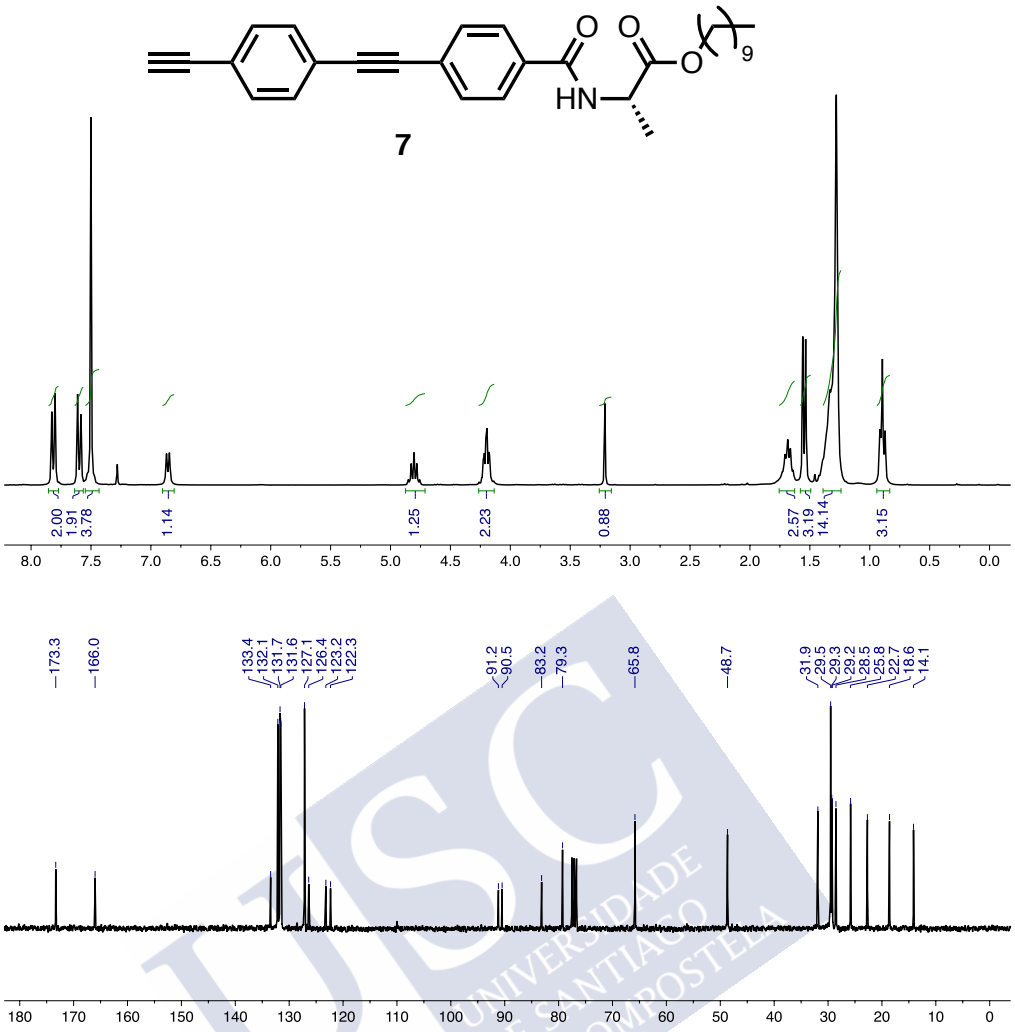

Figure S7. ^{1}H-NMR and ^{13}C-NMR of **7** in $CDCl_3$.

Synthesis of decyl (4-((4-((4-((trimethylsilyl)ethynyl)phenyl)ethynyl)phenyl)ethynyl)benzoyl)-*L*-alaninate (**8**)

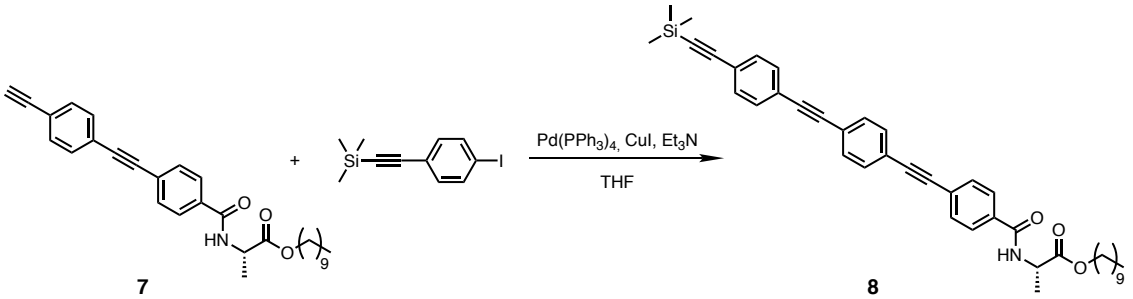

((4-iodophenyl)ethynyl)trimethylsilane (0.13 g, 0.44 mmol, 1.00 equiv.), tetrakis(triphenylphosphine)palladium(0) ($Pd(PPh_3)_4$, 0.01 g, 0.01 mmol, 0.02 equiv.) and copper iodide (CuI, 0.01 g, 0.01 mmol, 0.02 equiv.) were dissolved in dry THF (10 mL). Next triethylamine (Et_3N, 5 mL) and decyl (4-((4-ethynylphenyl)ethynyl)benzoyl)-*L*-alaninate (**7**, 0.20 g, 0.44 mmol, 1.00 equiv.) were added and the mixture was stirred at 40 °C overnight. After removing the solvent the crude product was chromatographed on silica gel (70-230 mesh) with hexane/ethyl acetate (60:40) as eluent (0.17 g, 63% of yield).

^{1}H NMR (300 MHz, $CDCl_3$) δ_H (ppm): 7.79 (d, 2H), 7.56 (d, 2H), 7.50 (s, 4H), 7.44 (s, 4H), 6.89 (d, 1H), 4.84-4.70 (q, 1H), 4.23-4.12 (m, 2H), 1.78-1.60 (m, 2H), 1.52 (d, 2H), 1.39-1.19 (m, 14H), 0.98-0.79 (m, 3H), 0.25 (s, 7H).

^{13}C NMR (75 MHz, $CDCl_3$) δ_C (ppm): 173.3, 166.0, 133.4, 131.9, 131.7, 131.7, 131.6, 131.4, 127.1, 126.5, 123.2, 123.2, 123.0, 122.7, 96.5, 91.4, 91.1, 90.9, 90.5, 65.8, 48.6, 31.9, 29.5, 29.3, 29.2, 28.5, 25.8, 22.7, 18.7, 14.1, 0.

HRMS (ESI) m/z calcd for $C_{41}H_{47}NO_3Si$ $[M+H]^+$: 630.3325, found: 630.3399.

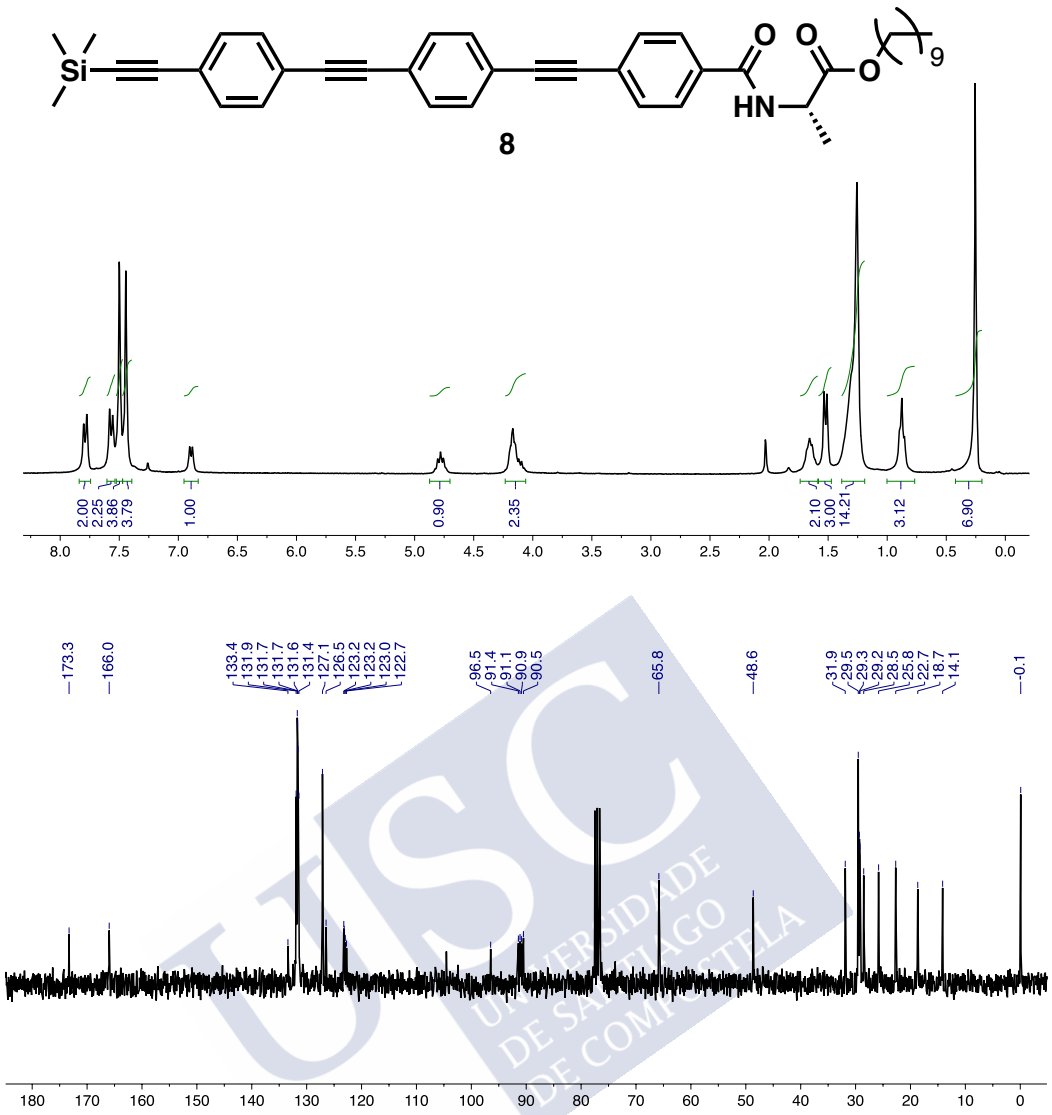

Figure S8. ^{1}H-NMR and ^{13}C-NMR of **8** in $CDCl_3$.

Synthesis of decyl (4-((4-((4-ethynylphenyl)ethynyl)phenyl)ethynyl)benzoyl)-*L*-alaninate ((*L*)-**1**)

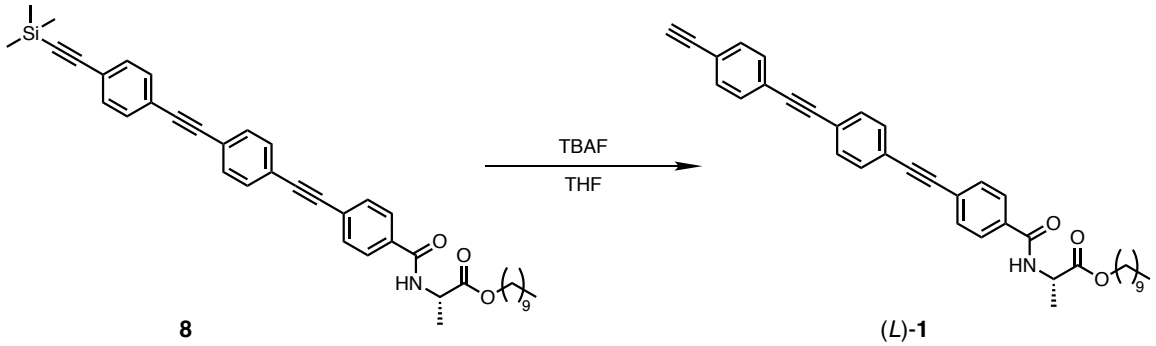

8 (*L*)-**1**

Decyl (4-((4-((4-((trimethylsilyl)ethynyl)phenyl)ethynyl)phenyl)ethynyl)benzoyl)-*L*-alaninate (**8**, 0.17 g, 0.27 mmol, 1.00 equiv.) was dissolved in THF (5 mL). Next TBAF was added (1M in hexane, 0.32 mL, 0.32 mmol, 1.20 equiv.) and the reaction was stirred at r.t. for 15 minutes. The crude was chromatographed on silica gel (70-230 mesh) with chloroform/ethyl acetate (90:10) as eluent (0.10 g, 70% of yield).

^{1}H NMR (300 MHz, $CDCl_3$) δ_H (ppm): 7.80 (d, 2H), 7.58 (d, 2H), 7.52 (s, 4H), 7.74 (s, 4H), 6.83 (d, 1H), 4.85-4.75 (q, 1H), 4.24-4.12 (m, 2H), 3.18 (s, 1H), 1.74-1.62 (m, 2H), 1.54 (d, 3H), 1.36-1.23 (m, 14H), 0.92-0.83 (t, 3H).

^{13}C NMR (75 MHz, $CDCl_3$) δ_C (ppm): 173.3, 165.9, 133.5, 132.1, 131.7, 131.7, 131.6, 131.5, 127.1, 126.5, 123.4, 123.2, 122.8, 122.2, 91.4, 90.9, 90.5, 87.5, 83.2, 79.1, 65.9, 48.6, 31.9, 29.5, 29.3, 29.2, 28.5, 25.8, 22.7, 18.7, 14.1.

HRMS (APCI) m/z calcd for $C_{29}H_{23}NO_3$ $[M+H]^+$: 558.2930, found: 558.3005.

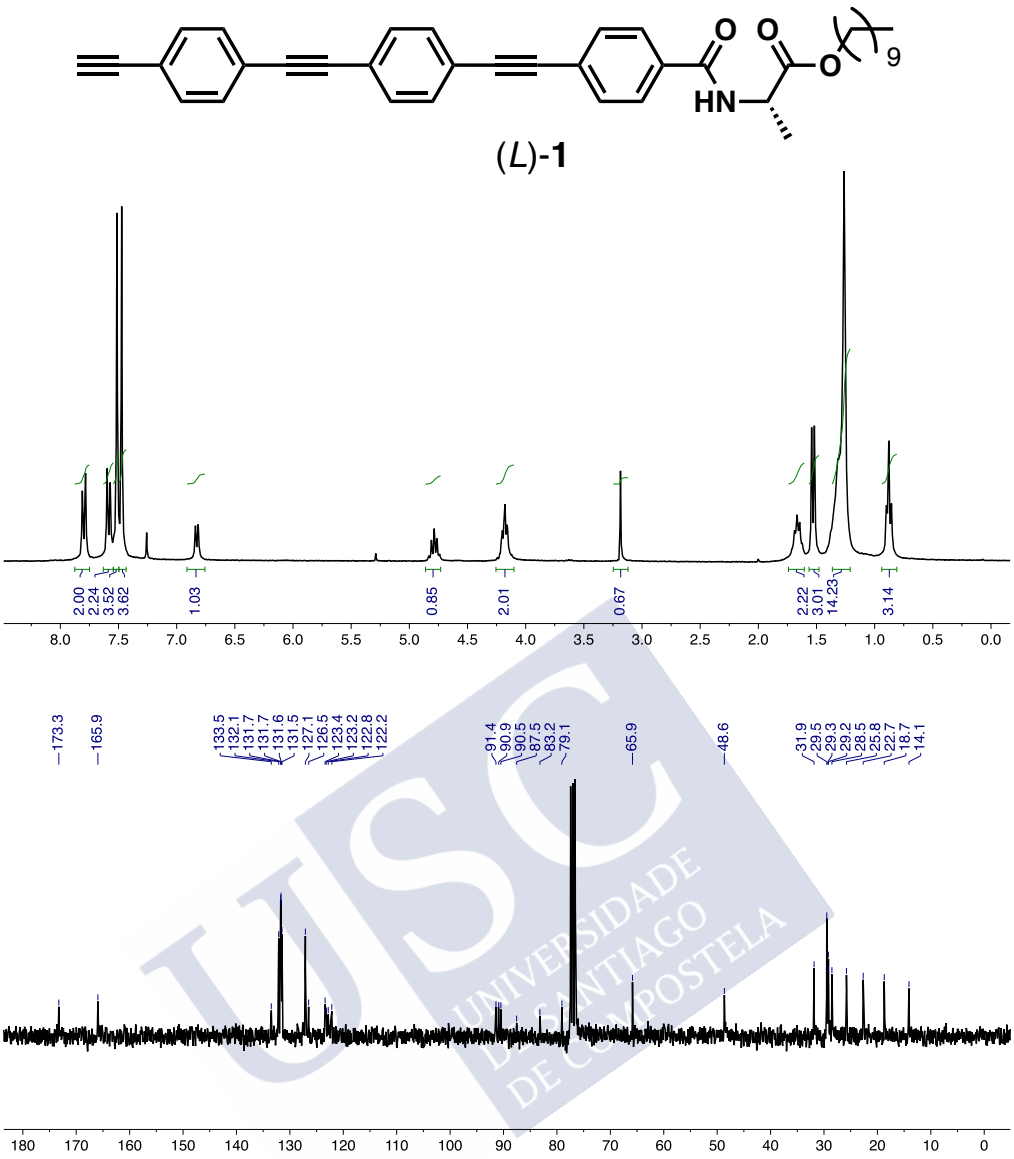

Figure S9. ^{1}H-NMR and ^{13}C-NMR of (*L*)-**1** in $CDCl_3$.

3. Atomic Force Microscopy (AFM) Measurements

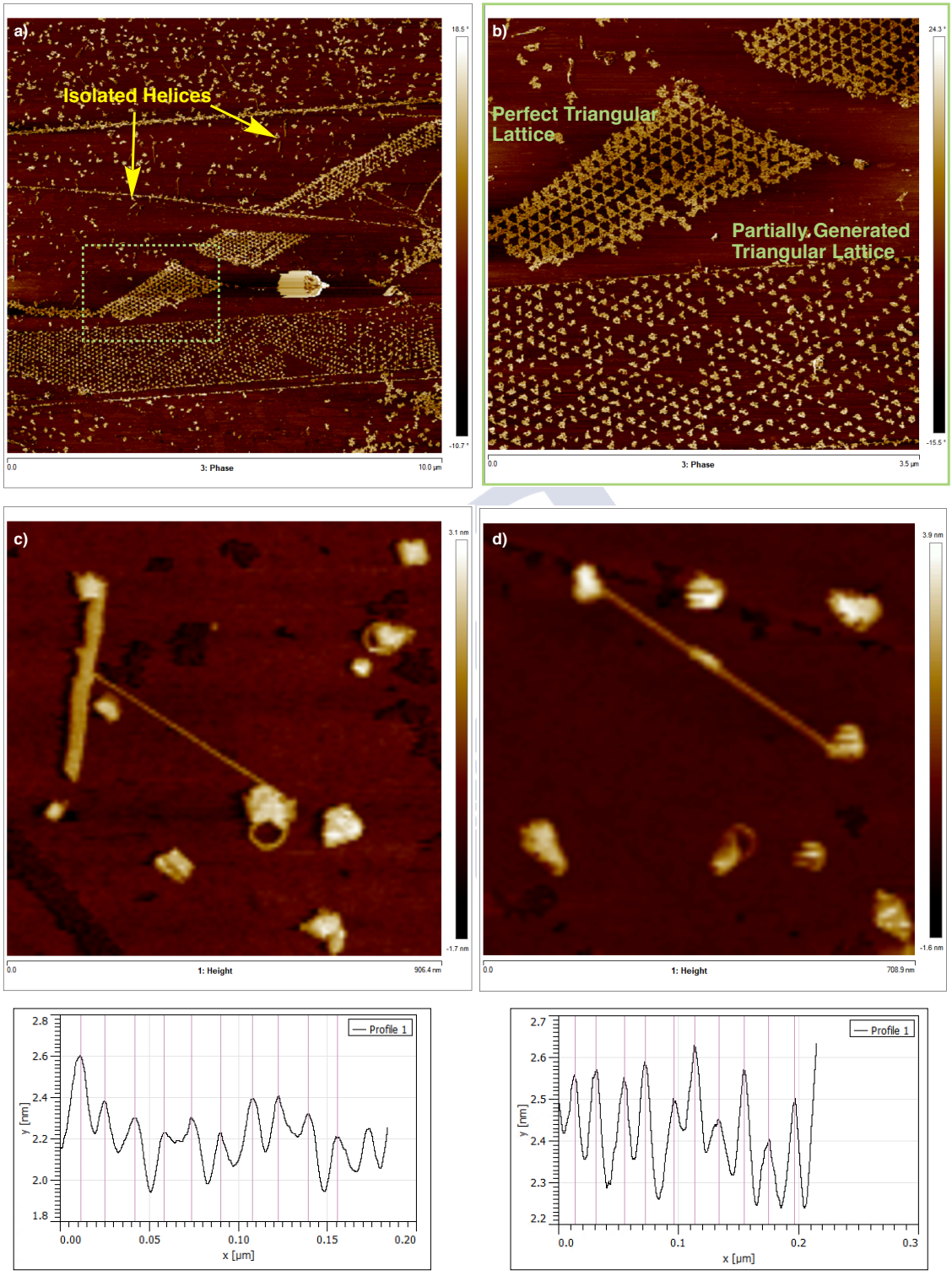

Figure S10. (a) AFM image depicting the two different morphologies obtained: long isolated helices and the triangular tessellation. (b) Zoomed area showing the triangular lattice with and without defects. (c), (d) Isolated helices and their corresponding profiles for the helical pitch measurement.

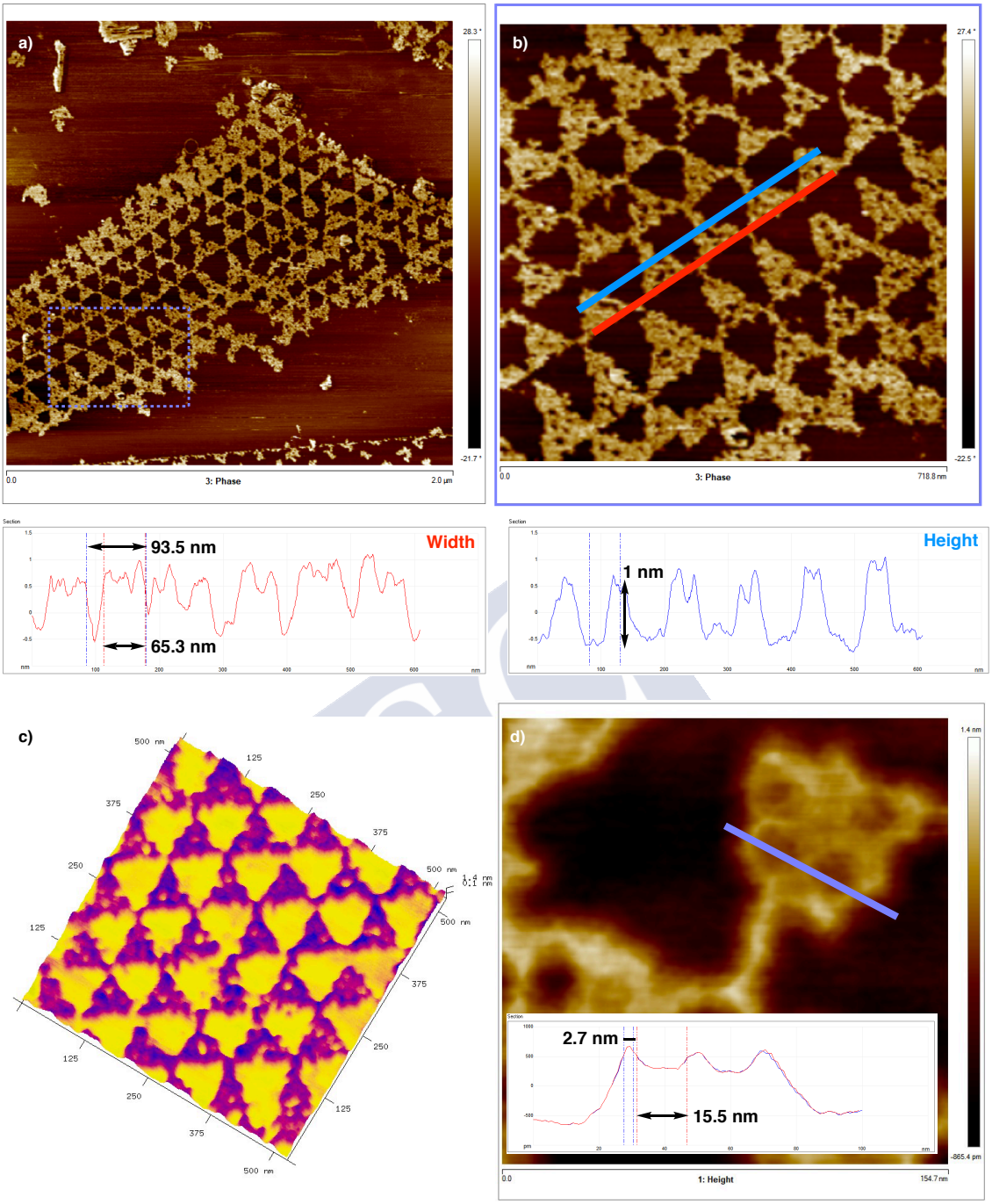

Figure S11. (a) AFM image for the triangular tessellation. (b) AFM image showing the triangles obtained, where the straight lines correspond to the cross-section width (red) and height (blue) profiles. (c) 3D-projection image for (b). (d) Zoomed image for a triangle where the hexagons can be easily observed with the corresponding width profile.

USC
UNIVERSIDADE
DE SANTIAGO
DE COMPOSTELA

Experimental Section

Chapter V

USC
UNIVERSIDADE
DE SANTIAGO
DE COMPOSTELA

1. Materials and Methods

CD measurements were done in a Jasco-720 and UV spectra were registered in a Jasco V-630. The amount of polymer used is indicated in the corresponding section.

VT-CD measurements were performed in a Jasco-1100.

Raman spectra were carried out in a Renishaw confocal Raman spectrometer (Invia Reflex model) equipped with a 785 nm diode laser and a 514 nm Ar laser.

DSC traces were obtained in a DSC Q200 Tzero Technology (TA Instruments, New Castle, UK), using a Tzero low-mass aluminium pan.

TGA traces were obtained in a TGA Q5000 (TA Instruments, New Castle, UK) using a platinium pan.

GPC studies were carried out in a Waters Alliance equipped with Phenomenex GPC columns (10^3 Å, 10^4 Å and 10^5 Å). The amount of polymer used was 0.5 mg·mL^{-1}. THF was used as eluent (flow rate: 1 mL·min^{-1}) and as inner standard, polystyrene narrow standards (PSS) were used.

PyMOL was used as a molecular visualization system.

2. Synthesis of Monomers

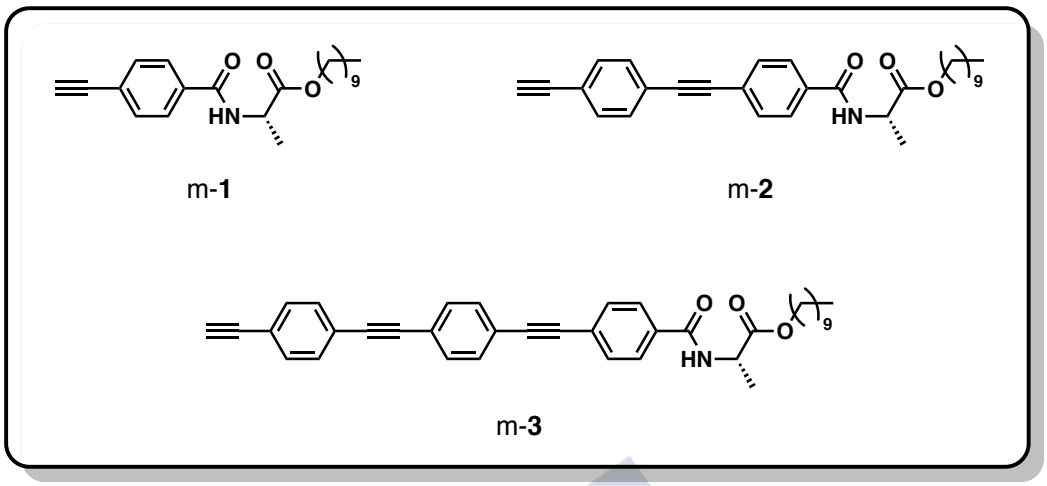

The monomers were synthesized according to previously reported procedures (m-**1**;[S1] m-**2** and m-**3**[S2])

[S1] Okoshi, K.; Sakajiri, K.; Kumaki, J.; Yashima, E. *Macromolecules* **2005**, *38*, 4061-4064.
[S2] Chapter IV.

3. Synthesis of Polymers

3.1 General Procedure for Polymerization

The polymers were synthesized in a flask (sealed ampoule) previously dried under vacuum and flushed with Ar for three times. The monomers were added as a solid and dissolved in dry THF. Next a solution of rhodium norbadiene chloride dimer $[Rh(nbd)Cl]_2$ was added and the mixture was stirred overnight. The resulting polymers were diluted in CH_2Cl_2 and precipitated in a large amount of MeOH, centrifuged (twice) and reprecipitated in hexane and centrifuged again.

Table S1. Calculated amounts for the polymers synthesis.

Monomer	Mass (mg)	THF (mL)	Et_3N (mL)	Catalyst (mg)	Yield (%)
poly-**2**	50	218	10	0.5	89
poly-**3**	50	300	10	0.4	91

3.2 NMR Experiments

The *cis*- configuration of the polyenic backbone was determined by ^1H NMR spectroscopy (vinylic protons, δ_H = 5.7-5.8 ppm) for poly-**2**.

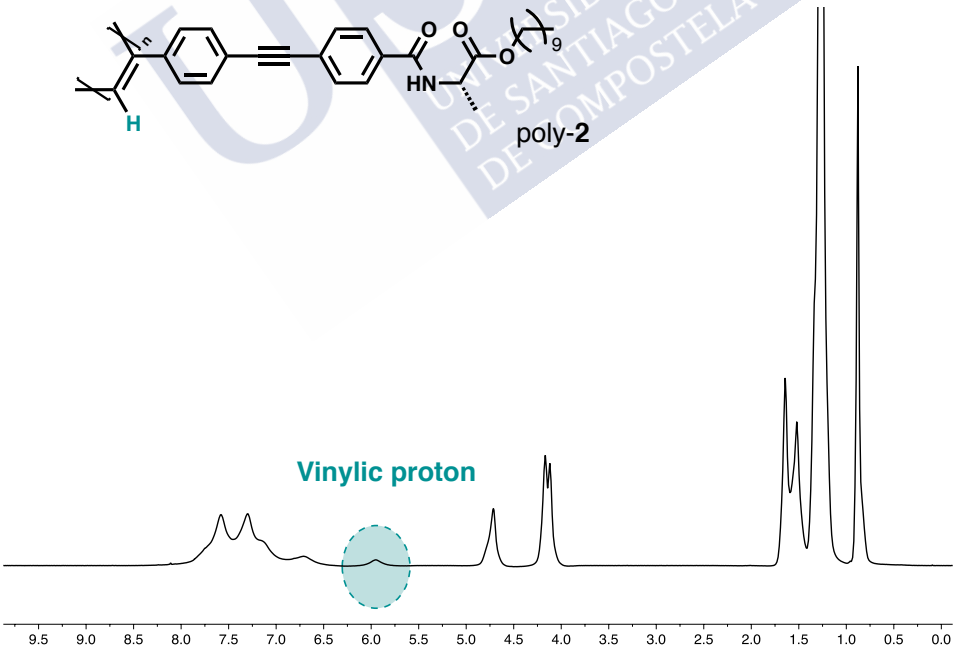

Figure S1. ^1H-NMR for poly-**2** in DMSO.

The highly stretched scaffold adopted by poly-**3** results into the disappearance of the vinylic signal, which is shifted towards the aromatic region. This is confirmed by applying a 1D ^1H-NMR singlet filter[S3] to a solution of poly-**3** in DMSO at 40 °C (Figure S2 bottom).

[S3] Martin-Pastor, M. *J. Agric. Food Chem.* **2014**, *62*, 1190-1197.

This filter allows the visualization of only the singlet signals, removing the remaining signals from the spectra.

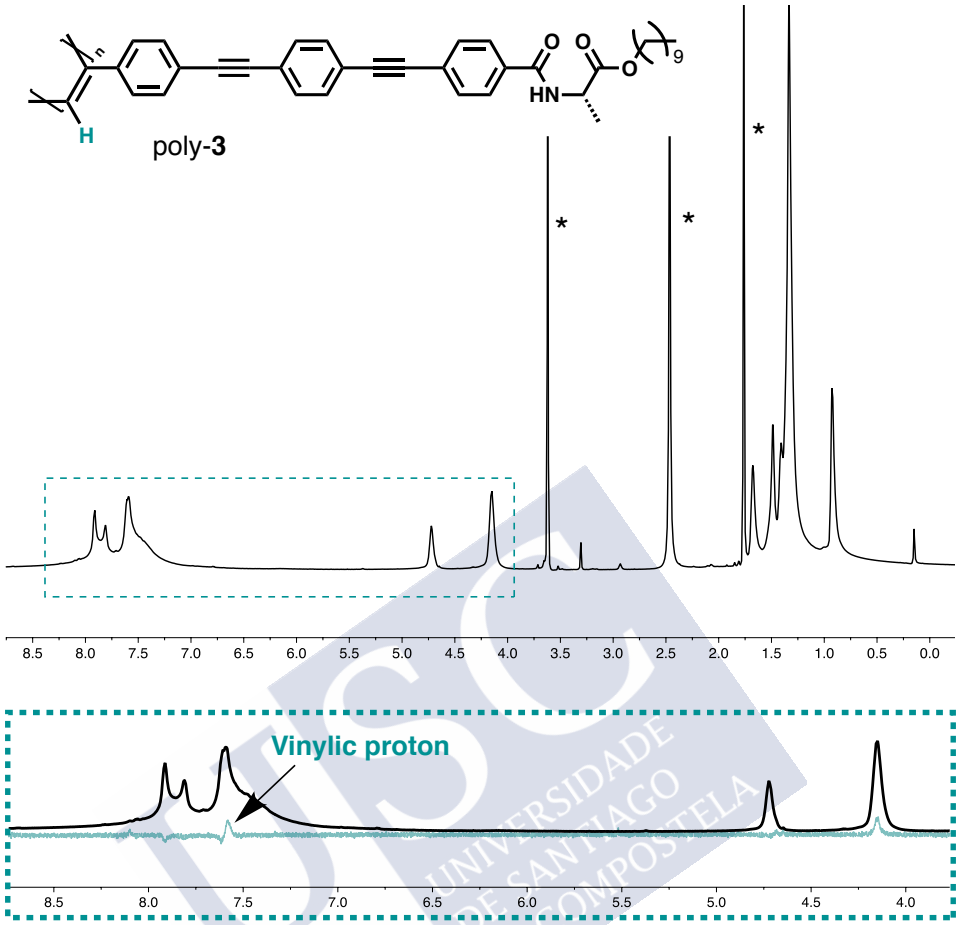

Figure S2. ^{1}H-NMR for poly-**3** in DMSO at 40 °C (top) and zoomed area comparing the 1H-NMR with the 1D 1H-NMR single filter (bottom). The singlets observed at 7.59 ppm and 4.16 ppm correspond to the vinylic signal and to the terminal methyl group of the long alkyl chain, respectively.

3.3 Raman experiments

The bands observed by Raman resonance confirmed the *cis*- configuration. The peak at highest wavelength corresponds to the C=C bond stretching and overlaps with that of the phenyl ring. The band at 1350-1340 cm^{-1} is arisen from the *cis* C-C bond coupled with the single bond connecting the main chain and the phenyl ring. The peak at lowest wavelength corresponds to the C-H bond of the *cis* form. The disappearance of the alkyne band (ca. 2110 cm^{-1}) confirms the formation of the conjugated double bonds of the polymer backbone.

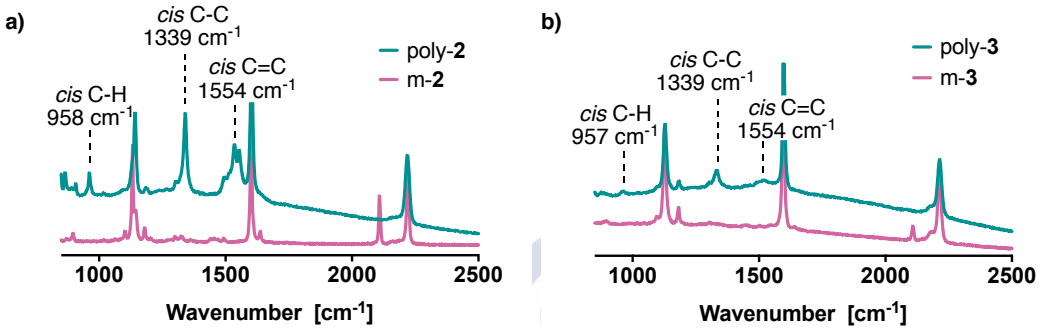

Figure S3. (a) Overlay of the Raman spectra obtained for m-**2** and poly-**2**. (b) Comparision of the Raman spectra for m-**3** and poly-**3**.

4. GPC Studies

The molecular weight was estimated by GPC using THF (flow rate: 1 mL/min) as eluent and polystyrene narrow standards (PSS) as calibrants.

Table S2. GPC data for the synthesized polymers.

Polymer	Mn	Mw	Mz	PDI
poly-**2**	10143	13015	16113	1.28
poly-**3**	8827	10899	13275	1.23

5. TGA Studies

The thermal stability was evaluated by TGA. The degradation starts at 300 °C for poly-**2** and for poly-**3** at 310 °C.

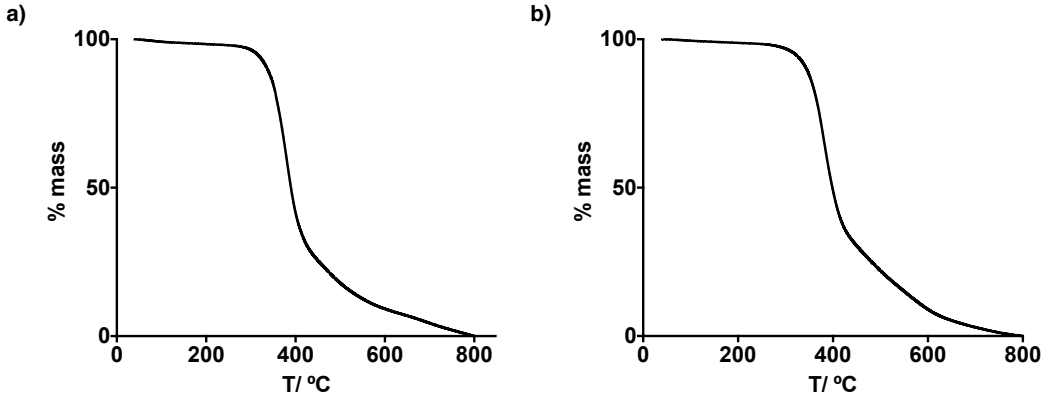

Figure S4. TGA traces for (a) poly-**2** and (b) poly-**3**.

6. Analysis in Different Solvents

6.1 Studies for poly-2

CD spectra for poly-**2** in different solvents. The different scaffolds adopted — classical *c*-*t* helix, ω_1 =165°, and matryoshka-like helix, ω_1 = 170°— can easily be tracked by UV-Vis as well as by CD spectroscopy.

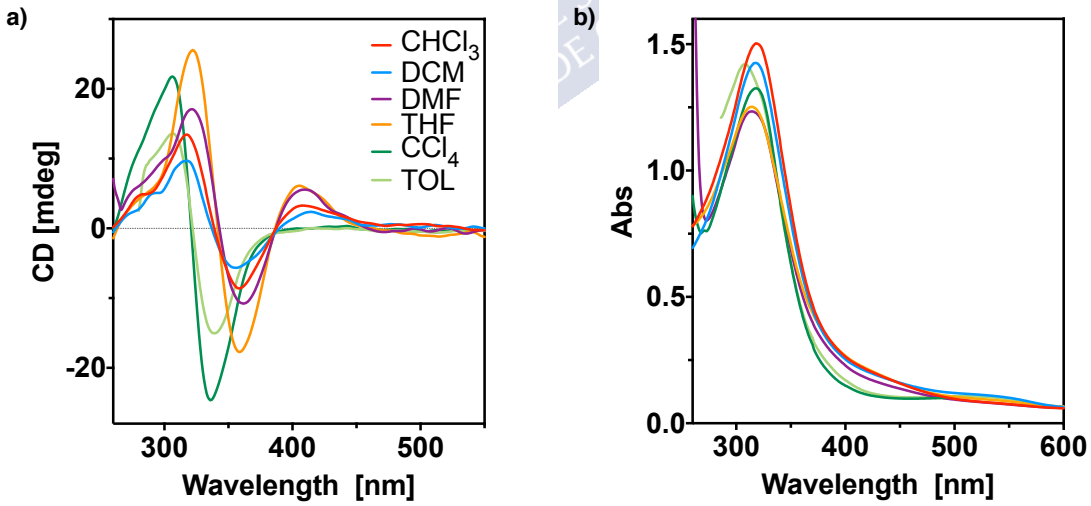

Figure S5. (a) CD and (b) UV-vis spectra for poly-**2** (0.2 mg mL^{-1}) in different solvents.

The stretching observed by UV-Vis for low-polar solvents is confirmed by Raman spectroscopy. If poly-**2** is dissolved in $CHCl_3$ and in CCl_4 (elongated polymer), a shift of 7 nm in the vibrational band associated to the cis C-H stretching (ca., 1000 nm^{-1}) is observed.

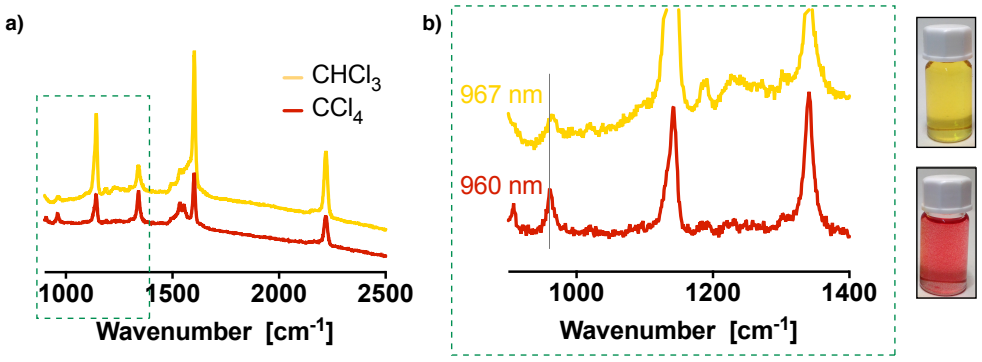

Figure S6. (a) Raman spectra obtained when poly-**2** is dissolved in $CHCl_3$ and CCl_4. (b) Magnification of the 900 to 1400 cm^{-1} area highlighted in (a) and vials depicting visual change in the colour solution, arisen by the different helical scaffolds adopted by poly-**2**.

6.2 Studies for poly-3

To prepare the polymer samples, due to the difficulty of solubilizing the polymer, small ammounts of poly-**3** are weighted and dissolved into the corresponding solvent at the desired concentration. The resulting mixture is heated overnight at 40 °C while being magnetically stirred.

Depending on the dielectric constant of the solvent in which poly-**3** is dissolved, the polymer will adopt a *M* or *P* helix. The change in the conformation of the chiral moiety is produced when (ε-1)/(ε+1) > 0.8.

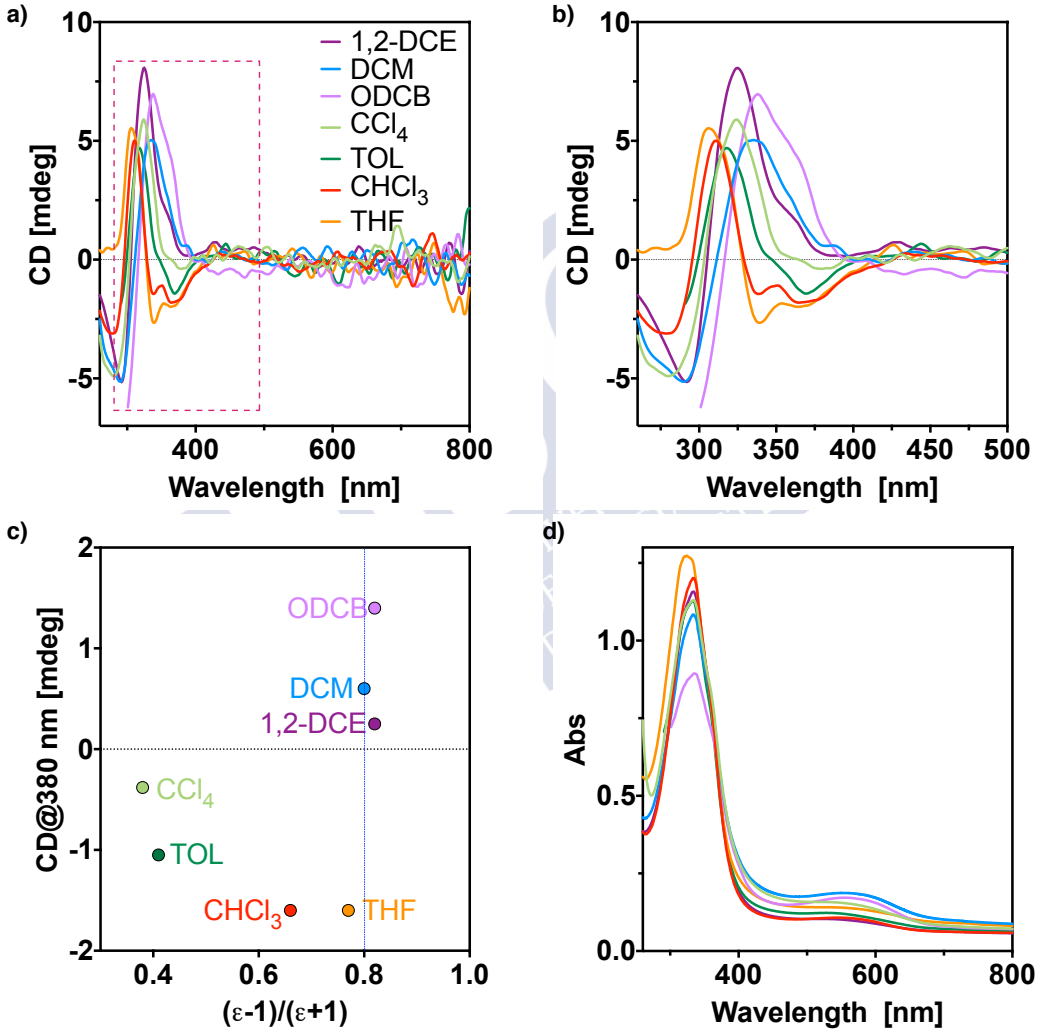

Figure S7. CD spectra (a) and magnification of the same (b) for poly-**3** (0.2 mg·mL^{-1}) evaluated in different solvents. (c) Plot of the CD intensity of poly-**3** at 380 nm as a function of the dielectric constant of the different solvents. (d) UV-Vis trace for poly-**3** in diferent solvents where a large absorption in the 600 nm region is recorded due to the large stretching of the helical scaffold.

7. Atomic Force Microscopy (AFM) Measurements

AFM images for poly-**2**.

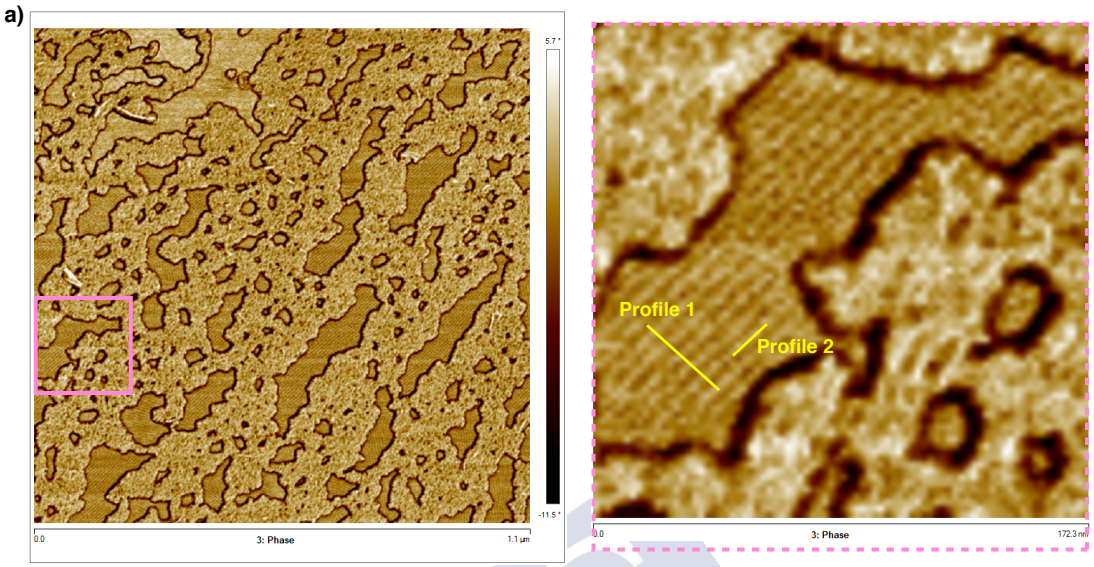

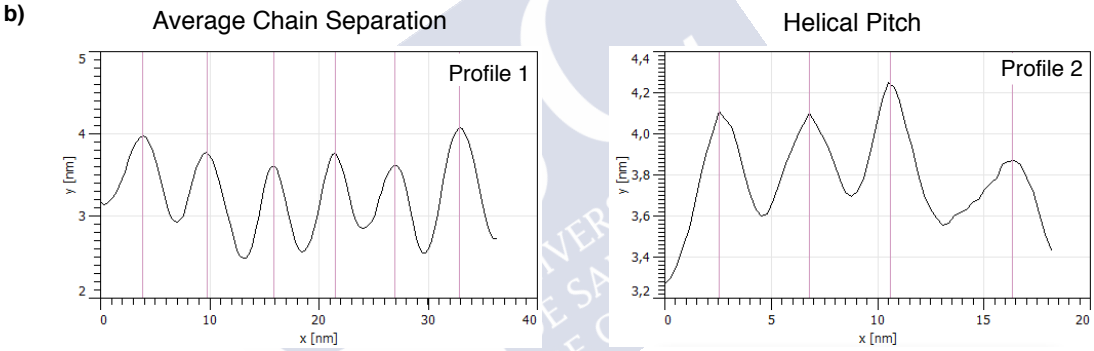

Points	X [nm]	Y [nm]	Length [nm]
	3,85	3,978	
	9,77	3,771	5,92
	15,87	3,619	6,10
	21,50	3,774	5,63
	26,95	3,635	5,45
	32,86	4,092	5,92

Points	X [nm]	Y [pm]	Length [nm]
	2,55	4113	
	6,80	4105	4,24
	10,60	4244	3,81
	16,34	3873	5,73

Figure S8. (a) AFM image for poly-**2**, from large scale image to magnification of the highlighted area. (b) Graphics depicting the chain distribution and the helical pitch measured in the indicated zones.

8. Theoretical Calculations

Considering the difficulties to carry out ECD theoretical calculations on large polymers, representative oligomers were used.

On the one hand, in the case of poly-**2** an oligomer with n = 8 —where n denotes the number of monomer repeating units (m.r.u.)— was employed and, in order to reduce the computational demands, the long alkyl chains were replaced by methyl groups. The number of monomer units was selected considering the results of previous studies,[S4-S6] where we evaluated the spectra for a series of poly(phenylacetylene) oligomers obtained through systematic increase of monomer units, and concluded that 8-10 monomers were enough to describe the n+2 polymer ECD spectra. The starting structure of poly-**2** was built through adjustment to the experimental data obtained from structural techniques, such as AFM and UV-Vis spectroscopy, defining the four different dihedral angles needed to build up the helical scaffold (ω_1, ω_2, ω_3 and ω_4; see Figure S9). Additionally, the pendant groups were introduced in the most stable conformation (*ap*). The oligomer geometry was optimized using the DFT method[S7] together with the B3LYP-D3 functional[S8] and the 6-31G** basis set.[S9]

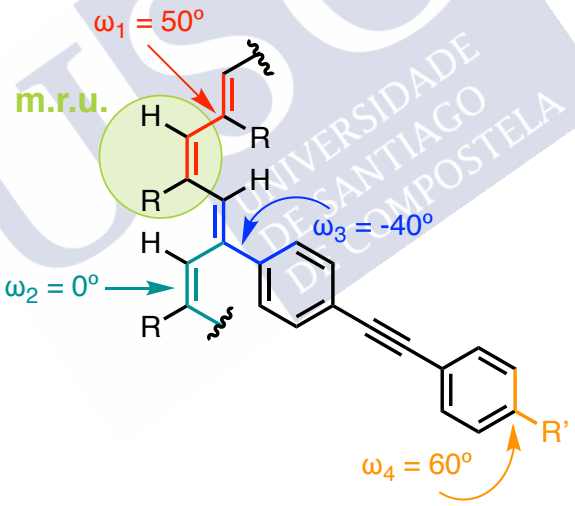

Figure S9. Main dihedral angles involved in the helical structure for poly(phenylacetilene)s and derivatives.

On the other hand, for poly-**3** the chiral moiety was removed from the pendant units in order to achieve a longer oligomer (n = 20, 504 atoms). In this case the length of the oligomer is essential to visualize the helices described by the OPE pendants (helix 3 and helix 4).

S4 Fernández, B.; Rodríguez, R.; Rizzo, A.; Quiñoá, E.; Riguera, R.; Freire, F. *Angew. Chem. Int. Ed.* **2018**, *57*, 3666-3670.
S5 Fernández, B.; Rodríguez, R.; Quiñoá, E.; Riguera, R.; Freire, F. *ACS Omega* **2019**, *4*, 5233-5240.
S6 Fernández, Z.; Fernández, B.; Quiñoá, E.; Riguera, R.; Freire, F. *Chem. Commun.* **2020**, *11*, 7182-7187.
S7 Hohenberg, P.; Walter, K. *Physical Review* **1964**, *136*, B864-B871.
S8 Grimme, S. *WIREs Computational Molecular Science* **2011**, *1*, 211-228.
S9 (a) Hariharan, P. C.; Pople, J. A. *Theor. Chim. Acta* **1973**, *28*, 213-222. (b) Hehre, W. J.; Ditchfield, R.; Pople, J. A. *J. Chem. Phys.* **1972**, *56*, 2257-2261.

The ECD computational methodology was selected according to the size of polymers under investigation. Taking this into account, to evaluate the theoretical spectra time dependent density functional theory (TD-DFT),[S10] in combination with the CAM-B3LYP functional[S11] and the 3-21G basis set,[S12] have been used. The ECD calculations were performed with the ORCA program (including 80 excitations).[S13] The Gabedit[S14] code was used to plot the spectra and the density differences were displayed with Avogadro.[S15] Furthermore, the full width at half height (FWHM) was fixed to 20.0 nm and the ECD were plotted with Gaussian curves.

For an efficient comparison and taking into account the tendency of the TD-DFT method to overestimate the excitation energies, the wavelength and intensity at the maximum/minimum Cotton effect correspondent to the polyene backbone in the theoretical spectra were adjusted to the experimental spectra. Employing the same correction factors, the lambdas were shifted and the intensities rescaled. The resulting ECD spectra are in good agreement with the experimental ones.

Poly-**2** (ω_1 ca. 165°) displays a classical ECD trace with a positive Cotton effect at ca. 405 nm, dominated by the S_0 to S_1 excitation and ascribed to the polyenic backbone. It is observed that the excited states mostly contribute to the first Cotton bands (Figure S10).

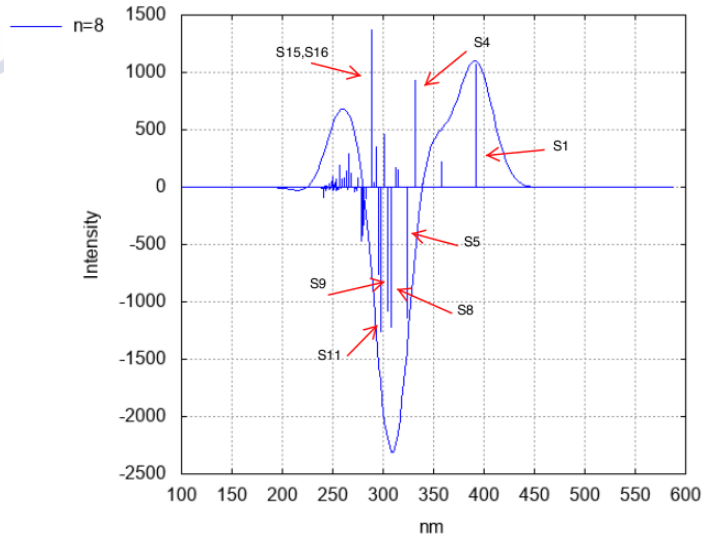

Figure S10. TD-DFT (CAM-B3LYP)/3-21G ECD poly-**2** spectra evaluated at the DFT(B3LYP-D3)/6-31G** geometries showing the excited states that most contribute to the first Cotton bands.

[S10] Runge, E.; Gross, E. K. U. *Phys. Rev. Lett.* **1984**, *52*, 997-1000.
[S11] Yanai, Y.; Tew, D. P.; Handy, N. C. A. *Chem. Phys. Lett.* 2005, 393, 51-57.
[S12] Binkley, J. S.; Pople, J. A.; Hehre, W. J. *J. Am. Chem. Soc.* 1980, 102, 939-947.
[S13] Neese, F. *WIREs Comput Mol Sci.* **2012**, *2*, 73-78.
[S14] Allouche, A. R. *J. Comput. Chem.* **2011**, *32*, 174-182.
[S15] Hanwell, M. D.; Curtis, D. E.; Lonie, D. C.; Vandermeersch, T.; Zurek, E.; Hutchison, G. R. *Journal of Cheminformatics* **2012**, *4*,17.

To get more insight into these spectral bands, the electron density differences for the corresponding transitions were evaluated at the same level of theory (Figure S11).

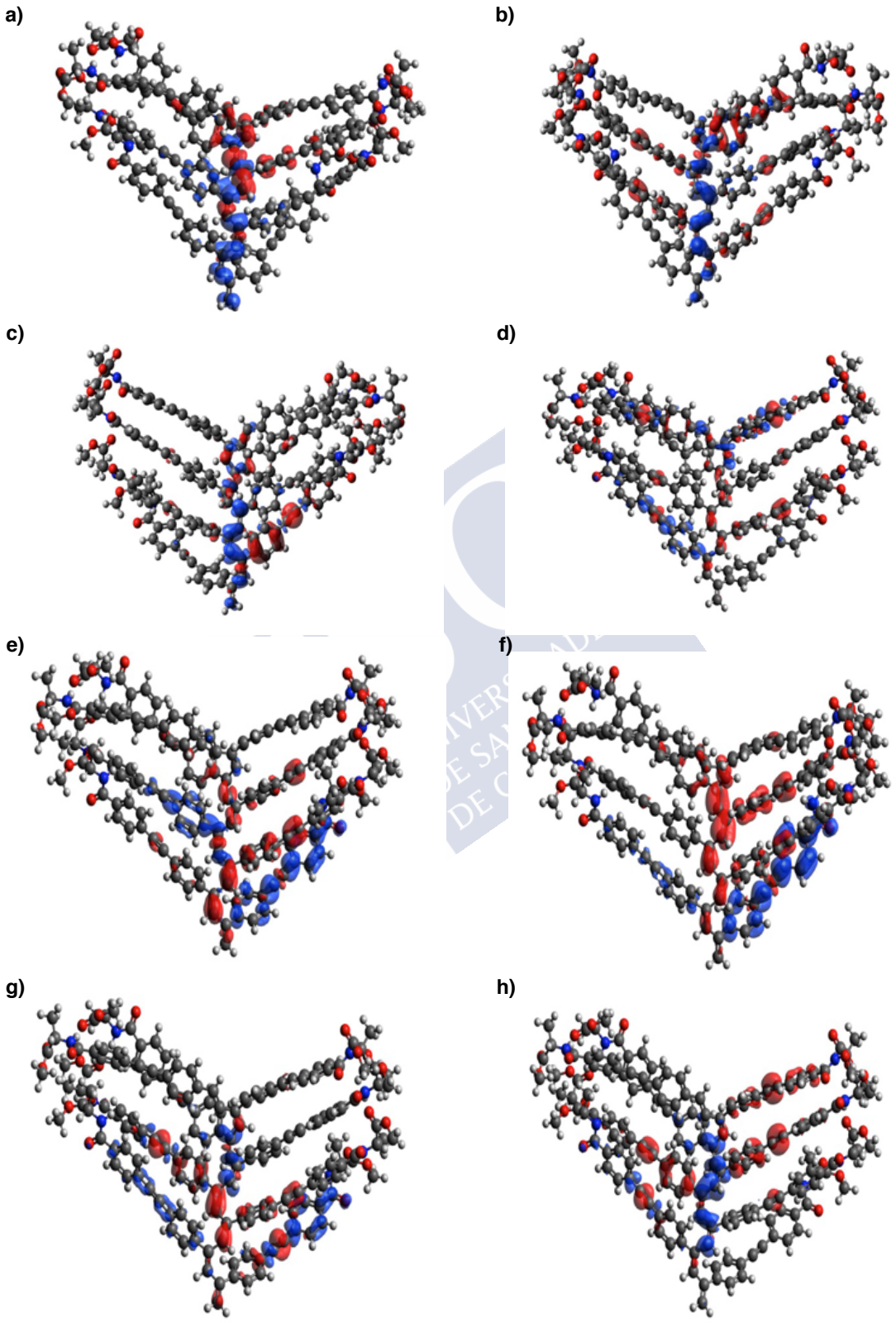

Figure S11. Poly-**2** electron density differences with respect to the ground state for the states shown in Figure S10: (a) S0 to S1, (b) S0 to S4, (c) S0 to S5, (d) S0 to S8, (e) S0 to S9, (f) S0 to S11, (g) S0 to S15 and (h) S0 to S16. An isovalue of 0.0005 was selected.

Poly-**3** (ω_1 ca. 170°) ECD shows a highly intense positive Cotton effect at ca. 340 nm, dominated by the S_0 to S_1 excitation and ascribed to the polyenic backbone. The excited states mostly contribute to the Cotton bands (Figure S11).

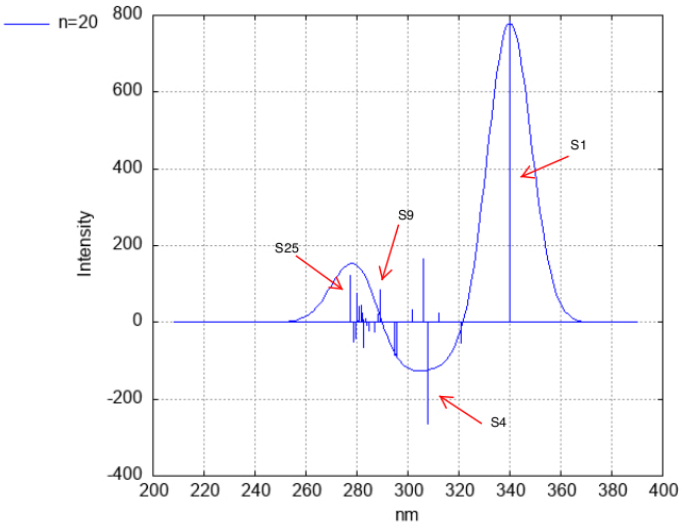

Figure S11. TD-DFT (CAM-B3LYP)/3-21G ECD poly-**3** spectrum evaluated at the DFT(B3LYP-D3)/6-31G** geometries showing the excited states that most contribute to the first Cotton bands.